JOURNAL OF THE AERONAUTICAL SCIENCES

VOLUME 12 JANUARY, 1945 NUMBER 1

CONTENTS

Three-Dimensional Analysis of Engine Mount Rings by a Strain Energy Method . . . . . CHARLES E. MACK, JR. 1

Wing Flaps in Light Aircraft Design . . . . . MAURICE A. GARBELL 14

A Note on Bending Beyond the Proportional Limit . . . . . M. YACHTER 21

Mechanical Properties of Magnesium-Alloy Tubing . . . . . R. T. SCHWARTZ AND G. M. MARTELL 31

Motogliders—A Natural Link Between Gliders and Light Planes . . . . . WIESLAW Z. STEPNIEWSKI 39

A Graphic Solution for Strains and Stresses from Strain Rosette Data . . . . . ROBERTO CONTINI 47

Investigation of the Wing-Wake Frequency with Application of the Strouhal Number . . . . . M. ZBIGNIEW KRZYWOBLOCKI 51

Analytic Investigation of Problems Concerning the Flow of Cooling Air in Light Airplane Engine Installations . . . . . JOHN R. WESKE 63

Bearing Strength in Airplane Design . . . . . ALBERT EPSTEIN 67

Lag Determination of Altimeter Systems . . . . . RICHARD M. HEAD 85

The Influence of Structural Deformation on Airplane Characteristics . . . . . ALEXANDER H. FLAX 94

A Simplified Analysis of Hollow Beams with Longitudinal Webs Subjected to Torsional Loads . . . . . ERYK KOSKO 103

Vibrations of Composite Structures . . . . . H. SERBIN 108

Airfoil Theory for Flows of Variable Velocity . . . . . RUFUS ISAACS 113

Calculated Gust Loads for Tailless Airplanes . . . . . RAYMOND F. ANDERSON 118

Letters to the Editor 107, 122, 123

Copyright, 1945, by the

INSTITUTE OF THE AERONAUTICAL SCIENCES, INC.

JOURNAL OF THE AERONAUTICAL SCIENCES

VOL. 12 JANUARY, 1945 NO. 1

PUBLISHED QUARTERLY BY THE INSTITUTE OF THE AERONAUTICAL SCIENCES, INC.

Chairman of the Editorial Board: HUGH L. DRYDEN, *Chief of Mechanics and Sound Division, National Bureau of Standards*

Editor: ROBERT R. DEXTER *Manager:* JOSEPH J. MAITAN

The Institute of the Aeronautical Sciences publishes the JOURNAL OF THE AERONAUTICAL SCIENCES quarterly, in January, April, July, and October, and the AERONAUTICAL ENGINEERING REVIEW monthly.

The JOURNAL OF THE AERONAUTICAL SCIENCES prints papers of scientific and technical interest to Institute members and subscribers. In general, it provides an opportunity for specialists to publish articles disclosing new knowledge and new applications in the field of the aeronautical sciences. The JOURNAL restricts itself to the aeronautical aspects of advances in science and engineering, and papers printed have either been submitted directly to the JOURNAL or have been previously presented at a meeting of the Institute.

The AERONAUTICAL ENGINEERING REVIEW keeps members and subscribers informed regarding the contents of new books and current periodicals in the field of aeronautics. It reviews new developments in the aircraft industry and reports on progress from house organs and catalogues published by aircraft and engine manufacturers and other companies engaged in aeronautical activities. It publishes papers on applied engineering and aircraft production. News of Institute activities is published in the REVIEW.

Statements and opinions expressed in the JOURNAL are to be understood as individual expressions of the authors and not those of the Institute.

SUBSCRIPTION RATES

Journal of the Aeronautical Sciences
Published Quarterly

United States and Possessions		Foreign Countries Including Canada (American Currency Rates)	
1 Year	$7.00	1 Year	$9.00
Single Copies	2.00	Single Copies	2.50

Aeronautical Engineering Review
Published Monthly

United States and Possessions		Foreign Countries Including Canada (American Currency Rates)	
1 Year	$3.00	1 Year	$3.50
Single Copies	0.30	Single Copies	0.35

Notices of change of address should be sent to the Institute at least 30 days prior to actual change of address.

Manuscripts for publication, proofs, and all correspondence should be addressed to the Editorial Office of the JOURNAL.

Correspondence regarding subscriptions may be addressed to Publication Office, 20th and Northampton Sts., Easton, Pa., or to the Editorial Office of the JOURNAL OF THE AERONAUTICAL SCIENCES, 1505 RCA Building West, 30 Rockefeller Plaza, New York 20, New York.

Entered as Second-Class Matter at the Post Office, Easton, Pa., May 1, 1937 Acceptance for mailing at a special rate of Postage provided for in the Act of August 24, 1912. Authorized April 29, 1937.

JOURNAL OF THE AERONAUTICAL SCIENCES

VOLUME 12 JANUARY, 1945 NUMBER 1

Three-Dimensional Analysis of Engine Mount Rings by a Strain Energy Method

CHARLES E. MACK, JR.*

Grumman Aircraft Engineering Corporation

SUMMARY

A strain energy method for the determination of bending and torsional moments in a circular engine mount ring is presented. The analysis given is for the three-dimensional case in which bending normal to the plane of the ring, bending in the plane of the ring, and torsion of the ring occur simultaneously. The known external loads on the system consist of vertical, side and drag forces together with yawing, pitching, and rolling moments

The method is based on the fact that the total elastic energy stored in the system of engine, ring, and mounting tubes must be a minimum. The equations of static equilibrium are first written down. The energy in the mounting tubes and in the rubber of the engine supports is then calculated. To determine the energy in the ring, the bending and torsional moments are developed in general terms. Through the use of these expressions, the minimization of the total energy is shown to lead to a set of equations, linear in the unknown forces and moments, which contain just 14 characteristic integrals associated with the ring itself. The component parts of these equations can be listed by rule as soon as the geometry of the structure to be analyzed is known.

The paper attempts to develop equations sufficiently general to be readily adaptable to any closed circular ring, under non-distributed loads, which is capable of taking bending. The possibilities for further extension, as well as for specialization of the analysis, are briefly considered.

SYMBOLS AND SIGN CONVENTIONS

i, j, k	= as subscripts—station numbers on ring
t, s	= as superscripts—type of force, moment, or energy
P_i^t	= external force on ring of type t at station i defined in Table 1. Positive directions shown in Figs. 3 and 5
Y_θ^t, X_θ^t	= internal force and moment, respectively, of type t at cut in ring defined in Table 2. Positive directions shown in Fig. 4
R	= as multiplier—mean radius of ring
R	= as superscript—quantity associated with right side of ring
L	= as superscript—quantity associated with left side of ring
L_j	= length of mount tube at station j
A_j	= area of mount tube at station j
k_2	= spring constant of rubber mounts associated with radial engine force
k_3	= spring constant of rubber mounts associated with tangential engine force
D, S, V	= external forces at c.g. of engine in direction of OD, OS, OV axes, respectively. Positive directions shown in Fig. 6
M_D, M_S, M_V	= external moments on system about OD, OS, OV axes, respectively. Positive as shown in Fig. 6
α_i	= fixed angle measured from cut in ring to station i ($\alpha_i \leqq 180°$)
θ	= variable angle measured from cut to any arbitrary position on ring ($\theta \leqq 180°$)
l_i^1, m_i^1, n_i^1	= direction cosines of mount tubes with respect to OD, OS, OV axes
U^s	= internal energy of type s in system defined in Table 2
U	= total internal energy of the system
$X_{i\theta}^s$	= portion of bending moment of type s at station θ due to forces and moments at station i. Positive directions shown in Fig. 8
K_{jk}^s, L_{kj}^s	= trigonometric integrals used in evaluation of elastic equations for the ring, defined by Eqs. (18)
a_i^t, b_i^t	= direction constants associated with bending normal to plane of ring, defined by Eqs. (11)
c_i^t, d_i^t, f_i^t	= direction constants associated with bending in plane of ring, defined by Eqs. (13)
h_i^t, q_i^t	= direction constants associated with torsional moment of ring, defined by Eqs. (15)
A_j, B_j	= column numbers associated with elastic Eq. (22) for bending normal to plane, defined by Eqs. (20)
C_j, D_j, F_j	= column numbers associated with elastic Eq. (24) for bending in plane of ring, defined by Eqs. (23)
H_j, Q_j	= column numbers associated with elastic Eq. (26) for torsion on the ring, defined by Eqs. (25)

Condensed version of paper presented at the Structures Session, Twelfth Annual Meeting, I.A.S., New York, January 25–27, 1944.

* Research Engineer

L629.05.1
J82

$R', \gamma, \mu, \eta, \xi, \lambda$ = distances occurring in equilibrium equations, defined by Fig. 7
ρ = distance from centerline of ring to line of action of radial engine force
c_s = constant factor for elastic equations of the ring, $c_1 = c_2 = 1$, $c_3 = EI/GJ$
φ = angle between radial forces and OD axis
EI = bending rigidity of ring
GJ = torsional rigidity of ring

Introduction

THE OBJECT OF THIS PAPER is to develop a general method for the determination of bending and torsional moments in a circular engine mount ring of circular cross section loaded as specified below. The aim is to so formalize the procedure that a great part of the solution may be carried through by rule.

A typical ring with its mounting tubes is shown in Fig. 1. The points of attachment of the mounting tubes to the airplane are considered fixed. The external loads on the system can be resolved into three orthogonal forces and three orthogonal moments acting at the center of mass of the engine group. The loads in the mounting tubes, as well as the loads applied to the ring by the engine, are unknowns to be determined.

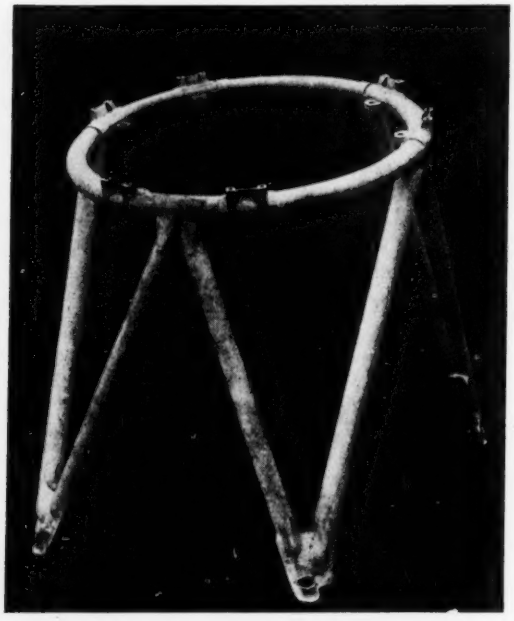

FIG. 1. Photograph of typical engine mount.

The engine is attached to the ring through rubber mountings in such a way that the forces applied by the engine are of known directions but of unknown magnitudes. The mounting tubes themselves are taken as pinned at each end. This is a matter of practical rather than theoretic necessity. The ring itself is considered to have no distributed loads acting on it. The lines of action of the forces supplied by the mount tubes are considered to pass through the centerline of the ring, but the engine forces in general apply moments to the ring.

A ring assembly will hereafter be referred to as symmetrical if it is symmetrical with respect to any plane perpendicular to the plane of the ring passing through the center of the ring. An external load is called symmetrical if it causes the loads in the structure to be equal at corresponding points on each side of the plane of symmetry; otherwise the load is said to be unsymmetrical.

Outline of Method to Be Used

Problems involving closed rings capable of taking bending are, in general, statically indeterminate internally. In order to find the moments, some reference point must be chosen and a "cut" made in the ring. In addition to being indeterminate internally, the ring may also be indeterminate externally and therefore the number of unknowns in a problem of this sort may be large.

The method selected for the solution of this problem is based upon Castigliano's Second Theorem, which states that a loaded structure must deform in such a way that, at equilibrium, the total elastic energy stored within it must be a minimum. The mathematical condition that the internal energy be a minimum (the possibility of a maximum may be excluded) is that the partial derivative of this energy with respect to each redundant force or moment be equal to zero.

The forces and moments existing at the cut in the ring are always redundant. Which of the remaining forces are redundant is somewhat arbitrary, the criterion being that the structure must be statically determinate when the forces selected as redundants have been removed.

The total energy of the system is the sum of several parts. The only energy in the ring that will be considered is that due to bending and twisting. The energy in the ring itself is divided into three parts: energy due to bending of the ring normal to its plane, energy due to bending in the plane of the ring, and energy due to torsion of the ring. The remainder of the elastic energy is stored in the supporting tubes and rubber mounts. The energy in each part of the system is expressed in terms of all the forces and moments as they occur, and after differentiation with respect to one of the redundants the results are added and equated to zero. This process is repeated for each of the redundants, and the statically determinate forces are eliminated from the resulting equations. Instead of integrating completely around the ring, much labor is saved by dividing the structure in half as explained in the following section.

For the present purpose the problem may be considered solved when the equations that determine the redundants have been written down. In actual practice,

it is necessary to solve a set of simultaneous equations to obtain the redundants. The remaining unknowns are determined by means of the equations of static equilibrium. The moments on the ring are then found by substitution of the loads into general expressions for the bending and torsional moments developed later.

Loads Acting on Ring and Notation to Be Used

In order to write equations applicable to any ring, a generalized notation involving a system of superscripts and subscripts has been developed and found convenient in practice.

It is first necessary to decide where the "cut" is to be made in the ring. This cut should be so located that a plane through the center of the ring and the cut, perpendicular to the plane of the ring, will divide the entire structure so that most of the component parts are symmetrically placed. For convenience, this plane is henceforth referred to as the "plane of maximum symmetry." It is shown at the bottom of the ring in all figures and may always be brought into that position by simply rotating the entire assembly.

After the cut is located, "station numbers" should be attached to the ring as shown in Fig. 2. Each point on the ring where a load enters is assigned a number, the cut itself being zero. Superscripts R and L are used to distinguish between the halves. If there are more load points on one side than the other, "dummy" stations should be introduced so that the two sides correspond. This is done for reasons of symmetry.

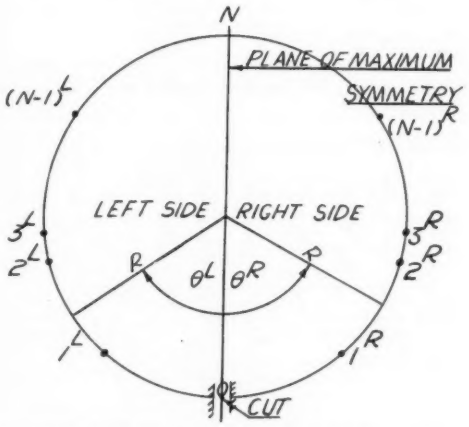

Fig. 2. Method of labeling a ring of n stations (front view looking aft).

The forces applied to the ring from the engine are shown in Fig. 3. The "Dynamic Suspension Mounts,"[1] through which the engine is attached to the ring, can be considered to supply two forces perpendicular to each other. The lines of action of one type of force converge to a point in front of the ring. These forces are called "radial." The other type of force exerted on the ring by the engine is called "tangential"; these

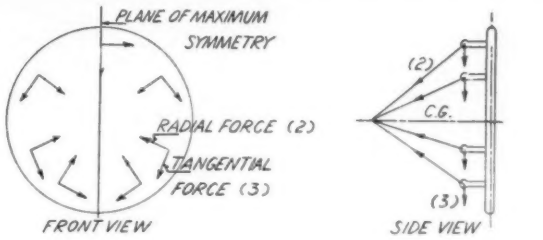

Fig. 3. Forces supplied by typical engine installation to mounting ring.

forces lie in a plane parallel to the ring. Both types of force in general apply moments to the ring.

The loads applied to the ring by the mount tubes are directed along the mount tubes, the lines of action passing through the centerline of the ring.

These three types of forces will be denoted by P_i^t, where t represents the type and i the station number, according to Table 1. The positive directions of these

Table 1

Notation for Mount Tubes and Engine Forces

t	Force	Description
1	P_i^1	Mount tube force at station i
2	P_i^2	Radial engine force at station i
3	P_i^3	Tangential engine force at station i

forces are shown in Figs. 3 and 5. If two or more mount tubes join the ring at one point, they are distinguished one from the other by using double subscripts—viz., P_{21}^1, P_{22}^1 for two tubes at station 2.

At the cut in the ring, there are, in general, three components of force and three components of moment. To differentiate these internal forces from the external forces on the ring, they are denoted by Y_0^t with appropriate values for t. Similarly, the three moments are denoted by X_0^t. Table 2 will make the notation clear.

Table 2

Notation for Forces and Moments at Cut

t	Redundant	Description
1	X_0^1	Moment tending to bend ring normal to its plane
2	X_0^2	Moment tending to bend ring in its plane
3	X_0^3	Moment tending to twist ring about its center line
4	Y_0^4	Force perpendicular to plane of ring
5	Y_0^5	Force tangential to circumference at cut (in plane of ring)
6	Y_0^6	Force perpendicular to circumference at cut (in plane of ring)

The forces and moments in Table 2 are shown in Fig. 4. To distinguish between the two halves, the R and L superscripts are used. In Fig. 4 the forces and moments are shown in such a sense that all bending and twisting moment expressions will be identical in form for both

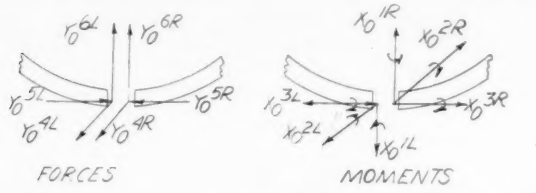

FIG. 4. Forces and moments at cut in an unsymmetrical loading condition.

the right and left sides of the ring under the conventions adopted. For equilibrium, it is necessary that

$$\begin{aligned} X_0^{1R} &= X_0^{1L} & Y_0^{4R} &= -Y_0^{4L} \\ X_0^{2R} &= X_0^{2L} & Y_0^{5R} &= Y_0^{5L} \\ X_0^{3R} &= -X_0^{3L} & Y_0^{6R} &= -Y_0^{6L} \end{aligned} \qquad (1)$$

The moments for both sides of the ring cannot be the same unless X_0^3, Y_0^4, and Y_0^6 are zero. It is only when the structure or the loading is unsymmetrical that X_0^3, Y_0^4, and Y_0^6 have values other than zero, and, accordingly, these three may be called "unsymmetrical redundants."

When attachment is made to the ring at station *o* or *n*, the following conventions may conveniently be adopted:

(1) If an engine support joins the ring at either of these two stations, the forces will be assigned to the right side.

(2) If an even number of mount tubes join the ring at *o* or *n*, half will be assigned to the right side and half to the left.

(3) If an odd number of tubes join the ring at these stations, the extra tube is assigned to the right side unless it is symmetrically placed, when it may be treated as in (2). This means the tube is considered as split in two.

Equilibrium Equations for the System

Two independent sets of equilibrium equations can be written, one set containing mount tube forces and the other containing only engine forces. This may be seen by inspection of Fig. 5. The portion of the structure to the left of the plane AA must be held in equilibrium by the engine forces only. Likewise, considering the portion of the structure to the left of plane BB, it is evident that only the mount tube forces will enter the equations.

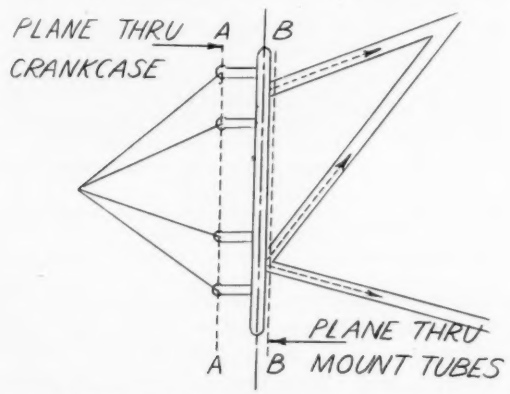

FIG. 5. Method of dividing structure for equilibrium equations.

The external loads (D, S, V, M_D, M_S, M_V) on the system are shown in Fig. 6. The equations for the mount tubes will be obtained first. If l_i^1, m_i^1, n_i^1 are the direction cosines of the tubes with reference to the OD, OS, OV axes, respectively, the components of the P_i^1 forces in these directions will be $l_i^1 P_i^1$, $m_i^1 P_i^1$, and $n_i^1 P_i^1$. These must be summed over all stations. Thus, the three force equations are:

$$\sum_i (l_i^{1R} P_i^{1R} + l_i^{1L} P_i^{1L}) + D = 0 \qquad (2a)$$

$$\sum_i (m_i^{1R} P_i^{1R} + m_i^{1L} P_i^{1L}) + S = 0 \qquad (2b)$$

$$\sum_i (n_i^{1R} P_i^{1R} + n_i^{1L} P_i^{1L}) + V = 0 \qquad (2c)$$

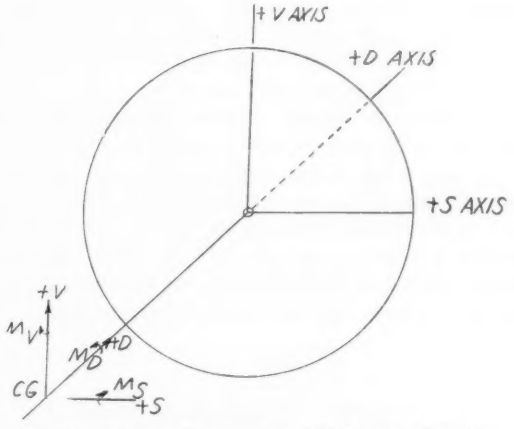

FIG. 6. Forces and moments applied to c.g. of engine.

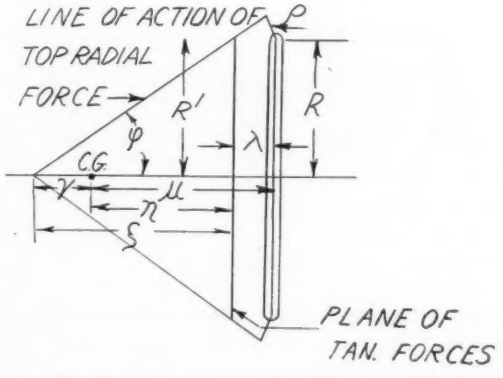

FIG. 7. Definition of quantities appearing in equilibrium and moment equations.

To obtain the moment equations, reference should be made to Fig. 7, which shows the distance of the c.g. from the reference planes. The drag component of the P_i^1 forces produces moments about the OS and OV axes. Summing up all moments about OS gives:

$$\sum_i (l_i^{1R} \cos \alpha_i^R P_i^{1R} + l_i^{1L} \cos \alpha_i^L P_i^{1L}) - (\mu V/R) - (M_S/R) = 0 \quad (2d)$$

Similarly, for moments about OV, it is evident that

$$\sum_i (l_i^{1R} \sin \alpha_i^R P_i^{1R} + l_i^{1L} \sin \alpha_i^L P_i^{1L}) + (\mu S/R) - (M_V/R) = 0 \quad (2e)$$

In these equations α_i is the angle from the cut to the mount tube in question.

For the moment equation about OD, it is convenient to resolve the components of P_i^1 in the plane of the ring, $m_i^1 P_i^1$ and $n_i^1 P_i^1$, in a tangential direction. The positive directions of these components are taken parallel to the OS and OV axes, and the positive direction of the tangent is taken in the direction of decreasing α_i. Thus, for the right side, tangential component of

$$P_i^{1R} = -(m_i^{1R} \cos \alpha_i^R + n_i^{1R} \sin \alpha_i^R) P_i^{1R}$$

For the left side, in a similar manner, tangential component of

$$P_i^{1L} = (m_i^{1L} \cos \alpha_i^L - n_i^{1L} \sin \alpha_i^L) P_i^{1L}$$

The two expressions are identical, as they should be, for symmetrically placed tubes, for then $m_i^{1L} = -m_i^{1R}$. The moment equation can now be written down, the arm being simply R.

$$\sum_i [(m_i^{1R} \cos \alpha_i^R + n_i^{1R} \sin \alpha_i^R) P_i^{1R} + (m_i^{1L} \cos \alpha_i^L - n_i^{1L} \sin \alpha_i^L) P_i^{1L}] + (M_D/R) = 0 \quad (2f)$$

The equations for the engine are obtained in a similar way. It is necessary to remember that Fig. 3 shows the forces acting on the ring from the engine; the forces acting across the plane AA from the ring to the engine must be reversed from those of Fig. 3. With this in mind, the force equations may be written by resolving the radial and tangential forces in the direction of the axes and summing over all stations. This gives, for the OD, OS, and OV directions in order,

$$\sum_i (P_i^{2R} + P_i^{2L}) + (D/\cos \varphi) = 0 \quad (3a)$$

$$\sin \varphi \sum_i (P_i^{2R} \sin \alpha_i^R - P_i^{2L} \sin \alpha_i^L) + \sum_i (P_i^{3R} \cos \alpha_i^R - P_i^{3L} \cos \alpha_i^L) + S = 0 \quad (3bb)$$

$$-\sin \varphi \sum_i (P_i^{2R} \cos \alpha_i^R + P_i^{2L} \cos \alpha_i^L) + \sum_i (P_i^{3R} \sin \alpha_i^R + P_i^{3L} \sin \alpha_i^L) + V = 0 \quad (3cc)$$

The simplest form of the moment equations results if the moments are taken about a set of axes $O'D$, $O'S'$, $O'V'$, which are parallel to the OD, OS, OV axes, respectively, and whose origin O' is at the point of intersection of the radial loads on OD extended. With this set of axes no P_i^2 forces will appear in the moment equations. The moment arms for this set of axes are shown in Fig. 7. The three moment equations for equilibrium about $O'D$ (or OD, which is coincident with $O'D$), $O'S'$, and $O'V'$, respectively, are seen to be:

$$\sum_i (P_i^{3R} - P_i^{3L}) + (M_D/R') = 0 \quad (3d)$$

$$\sum_i (P_i^{3R} \sin \alpha_i^R + P_i^{3L} \sin \alpha_i^L) + \frac{V\gamma}{\xi} - \frac{M_S}{\xi} = 0 \quad (3e)$$

$$\sum_i (P_i^{3R} \cos \alpha_i^R - P_i^{3L} \sin \alpha_i^L) + \frac{S\gamma}{\xi} + \frac{M_V}{\xi} = 0 \quad (3f)$$

By means of the last two moment equations, the remaining equilibrium equations, which contain both tangential and radial forces, may be freed of the tangential forces. If this is done, Eqs. (3bb) and (3cc) become

$$\sum_i (P_i^{2R} \sin \alpha_i^R - P_i^{2L} \sin \alpha_i^L) + (S\eta/\xi \sin \varphi) - (M_V/\xi \sin \varphi) = 0 \quad (3b)$$

$$\sum_i (P_i^{2R} \cos \alpha_i^R + P_i^{2L} \cos \alpha_i^L) - (V\eta/\xi \sin \varphi) - (M_S/\xi \sin \varphi) = 0 \quad (3c)$$

This gives two subsets of three equations each for the engine and shows the statical independence of the two types of engine forces. In a numerical calculation, the equilibrium equations should be written down and solved once and for all for the dependent forces in terms of the redundants, which are considered as known quantities in these operations.

Development of the Elastic Equations

The internal energy of the system, U^s, may be divided into five main parts. This division is shown in Table 3. It is convenient, in view of the complicated nature of the first three components, to subdivide these into energy stored in the right or left sides. Then the total energy U is:

$$U = (U^{1R} + U^{1L}) + (U^{2R} + U^{2L}) + (U^{3R} + U^{3L}) + U^4 + U^5$$

For a minimum, if P_i^t is considered as one of the redundant forces, it follows that

$$\frac{\partial U}{\partial P_i^t} = \left(\frac{\partial U^{1R}}{\partial P_i^t} + \frac{\partial U^{1L}}{\partial P_i^t}\right) + \left(\frac{\partial U^{2R}}{\partial P_i^t} + \frac{\partial U^{2L}}{\partial P_i^t}\right) + \left(\frac{\partial U^{3R}}{\partial P_i^t} + \frac{\partial U^{3L}}{\partial P_i^t}\right) + \frac{\partial U^4}{\partial P_i^t} + \frac{\partial U^5}{\partial P_i^t} = 0 \quad (4)$$

Table 3

Components of Energy in the System

s	Type	Description
1	U^1	Energy stored in ring due to bending out of the plane of the ring
2	U^2	Energy stored in ring due to bending in the plane of the ring
3	U^3	Energy stored in ring due to torsion of the ring
4	U^4	Energy stored in the mount tubes
5	U^5	Energy stored in the rubber of the engine supports

It is understood that P_i^t in Eq. (4) is to be replaced by Y_0^t and X_0^t in order to obtain the equations for the internal redundants at the cut.

The expressions for the partial derivatives in Eq. (4) must be developed in more general terms. The terms involving U^4 and U^5 will be considered first, since these are the simplest.

The energy in any mount tube at station j (either half of the ring) is:

$$(P_j^1)^2 L_j / 2\bar{A}_j E$$

The total energy in all the tubes is therefore

$$U^4 = \sum_j \left\{ [(P_j^{1R})^2 L_j^R / 2\bar{A}_j^R E] + [(P_j^{1L})^2 L_j^L / 2\bar{A}_j^L E] \right\}$$

Differentiation gives

$$\frac{\partial U^4}{\partial P_i^t} = \sum_j \left[\left(\frac{L_j^R P_j^{1R}}{\bar{A}_j^R E} \right) \left(\frac{\partial P_j^{1R}}{\partial P_i^t} \right) + \left(\frac{L_j^L P_j^{1L}}{\bar{A}_j^L E} \right) \left(\frac{\partial P_j^{1L}}{\partial P_i^t} \right) \right] \quad (5)$$

which is the required expression. Its value will be zero unless the redundant P_i^t is the force in one of the mount tubes.

In a similar way, if k_2 and k_3 are the spring constants in the radial and tangential directions, the total energy in the rubber is:

$$U^5 = \frac{1}{2k_2} \sum_j [(P_j^{2R})^2 + (P_j^{2L})^2] + \frac{1}{2k_3} \sum_j [(P_j^{3R})^2 + (P_j^{3L})^2]$$

Differentiating this with respect to P_i^t results in

$$\frac{\partial U^5}{\partial P_i^t} = \frac{1}{k_2} \sum_j \left[P_j^{2R} \left(\frac{\partial P_j^{2R}}{\partial P_i^t} \right) + P_j^{2L} \left(\frac{\partial P_j^{2L}}{\partial P_i^t} \right) \right] + \frac{1}{k_3} \sum_j \left[P_j^{3R} \left(\frac{\partial P_j^{3R}}{\partial P_i^t} \right) + P_j^{3L} \left(\frac{\partial P_j^{3L}}{\partial P_i^t} \right) \right] \quad (6)$$

This expression will have a nonzero value only when the redundant P_i^t is one of the engine forces.

For the ring itself, one expression can be used—namely, $\partial U^s / \partial P_i^t$, where s has the value 1, 2, or 3. The R and L superscripts may be inserted later. The energy stored in either half of the ring, U^s, is equal to the sum of the energy in the ring between adjacent stations.

If $X_{i\theta}^s$ is the portion of the moment at any angular distance θ due to the action of loads at station $i (\alpha_i \leq \theta \leq \alpha_{i+1})$, then the energy may be written as follows:

$$U^s = \int_{\alpha_0}^{\alpha_1} \frac{(X_{0\theta}^s)^2 c_s R}{2EI} d\theta + \int_{\alpha_1}^{\alpha_2} \frac{(X_{0\theta}^s + X_{1\theta}^s)^2 c_s R}{2EI} d\theta + \cdots\cdots \int_{\alpha_{n-1}}^{\alpha_n} \frac{(X_{0\theta}^s + X_{1\theta}^s + \cdots\cdots X_{(n-1)\theta}^s)^2 c_s R}{2EI} d\theta \quad (7)$$

The factor c_s is 1 for $s = 1, 2$ and is EI/GJ for $s = 3$, to take care of the torsional case. Differentiating with respect to any redundant P_i^t, it follows that

$$\left(\frac{EI}{Rc_s} \right) \left(\frac{\partial U^s}{\partial P_i^t} \right) = \int_{\alpha_0}^{\alpha_1} X_{0\theta}^s \left(\frac{\partial X_{0\theta}^s}{\partial P_i^t} \right) d\theta + \int_{\alpha_1}^{\alpha_2} (X_{0\theta}^s + X_{1\theta}^s) \left(\frac{\partial X_{0\theta}^s}{\partial P_i^t} + \frac{\partial X_{1\theta}^s}{\partial P_i^t} \right) d\theta + \cdots\cdots \int_{\alpha_{n-1}}^{\alpha_n} (X_{0\theta}^s + \cdots\cdots X_{(n-1)\theta}^s) \times \left(\frac{\partial X_{0\theta}^s}{\partial P_i^t} + \cdots\cdots \frac{\partial X_{(n-1)\theta}^s}{\partial P_i^t} \right) d\theta \quad (8)$$

If this is rearranged so that all those integrals having the same integrand but different limits are collected into a single integral whose upper limit is α_n or π, it may be reduced to the following form:

$$\frac{EI}{Rc_s} \frac{\partial U^s}{\partial P_i^t} = \begin{bmatrix} \int_{\alpha_0}^{\pi} X_{0\theta}^s \left(\frac{\partial X_{0\theta}^s}{\partial P_i^t} \right) d\theta + \int_{\alpha_1}^{\pi} X_{0\theta}^s \left(\frac{\partial X_{1\theta}^s}{\partial P_i^t} \right) d\theta + \cdots\cdots \int_{\alpha_{n-1}}^{\pi} X_{0\theta}^s \left(\frac{\partial X_{(n-1)\theta}^s}{\partial P_i^t} \right) d\theta \\ + \int_{\alpha_1}^{\pi} X_{1\theta}^s \left(\frac{\partial X_{0\theta}^s}{\partial P_i^t} \right) d\theta + \int_{\alpha_1}^{\pi} X_{1\theta}^s \left(\frac{\partial X_{1\theta}^s}{\partial P_i^t} \right) d\theta + \cdots\cdots \int_{\alpha_{n-1}}^{\pi} X_{1\theta}^s \left(\frac{\partial X_{(n-1)\theta}^s}{\partial P_i^t} \right) d\theta \\ \cdots\cdots\cdots\

on the partial derivative than on the other factor of the integrand. The L-integrals that lie below the diagonal have a lower subscript on the partial derivative than on the remaining factor. Omitting the superscripts (here a general characterization is all that is desired), the K-integrals may be described by a double subscript notation:

$$K_{jk} = \int_{\alpha_j}^{\pi} X_{k\theta} \left(\frac{\partial X_{j\theta}}{\partial P_i^{\,t}}\right) d\theta \qquad k \leq j$$

Thus, in the K-integrals (1) the first subscript on K indicates both the lower limit on the integral and the subscript on the partial derivative, while (2) the second subscript on K is equal to the subscript associated with the moment $X_{k\theta}$. In a similar way, the L-integrals may be represented by

$$L_{kj} = \int_{\alpha_j}^{\pi} X_{j\theta} \left(\frac{\partial X_{k\theta}}{\partial P_i^{\,t}}\right) d\theta \qquad k < j$$

Therefore, in the L-integrals (1) the first subscript on L is that of the partial derivative, and (2) the second subscript on L indicates the lower limit of the integral and the subscript of the moment $X_{j\theta}$.

Every subintegral arising in connection with the energy in the ring itself will be shown to be one of these two types. These subintegrals cannot be defined until after the moment expressions have been developed.

Bending and Torsional Moments in the Ring

In order to obtain the moment expressions for the ring, a vectorial representation is desirable. The positive directions for these vectors are shown in Fig. 8. With the ring cut at the bottom, these conventions imply that bending normal to the plane of the ring puts compression on the front fibers; bending in the plane of the ring puts compression on the inside fibers. The positive torsional moment indicates rotation in a clockwise direction on the right side when looking along the centerline from the bottom toward the top, and it indicates rotation in a counterclockwise direction on the left side if the view is from bottom to top.

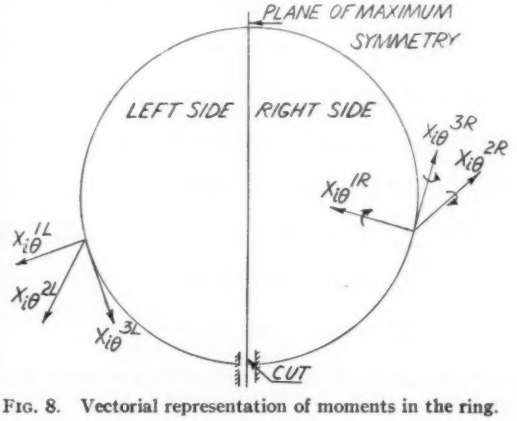

Fig. 8. Vectorial representation of moments in the ring.

With these conventions, the moments would be identical for both halves of the ring if the loading were symmetrical. In what follows, the right side will be considered and the superscript R omitted. The corresponding form for the left side will be identical with the right side except where explicitly mentioned.

Bending moments normal to the plane of the ring will first be considered. Since the axis about which this bending takes place lies in the plane of the ring, the only forces that can cause such bending must have components perpendicular to the plane of the ring. Any moment that is applied to the ring (by the engine forces or the moments at the cut) whose vector representation has a component in the plane of the ring will, in general, cause bending out of the plane. A torsional moment applied to the ring at one station will cause bending normal to the plane of the ring at another point.

A detailed consideration of the effect of the various forces and moments, which cannot be given here because of space limitations, indicates that the required expression is a linear function of $\sin(\theta - \alpha_i)$ and $\cos(\theta - \alpha_i)$. The complete expression is

$$R^{-1}X_{i\theta}^{\,1} = (\sum a_i^{\,1}P_i^{\,1} + a_i^{\,2}P_i^{\,2} + a_i^{\,4}Y_i^{\,4} + a_i^{\,3}X_i^{\,3}) \times \sin(\theta - \alpha_i) + (b_i^{\,3}P_i^{\,3} + b_i^{\,1}X_i^{\,1})\cos(\theta - \alpha_i) \quad (10)$$

where

$$\left.\begin{aligned} a_i^{\,1} &= -\,l_i^{\,1} & a_i^{\,4} &= +1 \\ a_i^{\,2} &= \cos\varphi + (\rho/R) & b_i^{\,1} &= +\,1/R \\ a_i^{\,3} &= -\,1/R & b_i^{\,3} &= -\,\lambda/R \end{aligned}\right\} \quad (11)$$

The convenience of this notation will become evident later. The a's and b's are all known numbers, determinable at the outset. The only quantity that varies from station to station is $a_i^{\,1}$, which will be different for the two halves of the ring if symmetry is lacking. The $\sum$-sign is written in front of the $P_i^{\,1}$ terms to call attention to the fact that, if two or more mount tubes join the ring at one point, the drag component of each force must be taken into account.

The next moment to be considered is $X_{i\theta}^{\,2}$, the bending in the plane of the ring due to forces and moments at station i. Only forces that have components in or parallel to the plane of the ring can contribute to this moment.

At the cut, for example, there are two forces, $Y_0^{\,5}$ and $Y_0^{\,6}$, which cause moments at any angle θ equal to $Y_0^{\,5}R$ vers $(\theta - \alpha_0)$ and $Y_0^{\,6}R \sin(\theta - \alpha_0)$. The other forces and moments must each be examined separately. The final result of combining all the terms is

$$R^{-1}X_{i\theta}^{\,2} = (\sum c_i^{\,1}P_i^{\,1} + c_i^{\,2}P_i^{\,2} + c_i^{\,6}Y_i^{\,6}) \times \sin(\theta - \alpha_i) + (\sum d_i^{\,1}P_i^{\,1} + d_i^{\,3}P_i^{\,3} + d_i^{\,5}Y_i^{\,5}) \times \operatorname{vers}(\theta - \alpha_i) + (f_i^{\,3}P_i^{\,3} + f_i^{\,2}X_i^{\,2}) \quad (12)$$

where

$$\left.\begin{aligned} c_i^1 &= n_i^1 \cos\alpha_i - m_i^1 \sin\alpha_i & d_i^3 &= +1 \\ c_i^2 &= \sin\varphi & d_i^5 &= +1 \\ c_i^6 &= +1 & f_i^2 &= 1/R \\ d_i^1 &= -(m_i^1 \cos\alpha_i + n_i^1 \sin\alpha_i) & f_i^3 &= \frac{-(R-R')}{R} \end{aligned}\right\} \quad (13)$$

The c_i^1 and d_i^1 parameters arise from the resolution of the mount tube forces into radial and tangential components. Eq. (12) stands just as it is written for either the right or left sides by adding R or L to the symbols. Eqs. (13) apply to the right half by adding superscript R. The left side may be derived from the right by replacing R by L throughout and replacing m_i^{1R} by $-m_i^{1L}$. This difference arises because the resolution of the mount tube forces into radial and tangential components is different for the two sides.

The torsional moment, $X_{i\theta}^3$, is much the same as the moment normal to the plane of the ring, $X_{i\theta}^1$, in that the same forces and moments occur. These quantities are in general multiplied by different functions of $(\theta - \alpha_i)$ than in the expression for $X_{i\theta}^1$. The required expression will contain sine, cosine, and versine terms and is

$$\begin{aligned} R^{-1}X_{i\theta}^3 = {} & (b_i^3 P_i^3 + b_i^1 X_i^1)\sin(\theta-\alpha_i) + \\ & (h_i^2 P_i^2 + h_i^3 X_i^3)\cos(\theta-\alpha_i) + \\ & (\textstyle\sum q_i^1 P_i^1 + q_i^2 P_i^2 + q_i^4 Y_i^4)\,\mathrm{vers}(\theta-\alpha_i) \end{aligned} \quad (14)$$

where (the b's have already been defined),

$$\left.\begin{aligned} h_i^2 &= -\rho/R & q_i^2 &= \cos\varphi \\ h_i^3 &= +1/R \\ q_i^1 &= -l_i^1 & q_i^4 &= +1 \end{aligned}\right\} \quad (15)$$

By comparing these with Eqs. (11), it will be noted that the two sets of parameters are identical if $\rho = 0$, which is an important case in practice.

The Fundamental Intregals for the Ring

Using the expressions above, it is now possible to determine the subintegrals that arise in the expansion of Eq. (9). In the case of moments normal to the plane of the ring, the K-integrals are given by

$$\int_{\alpha_j}^{\pi} X_{k\theta}^1 \left(\frac{\partial X_{j\theta}^1}{\partial P_i^t}\right) d\theta \qquad k \le j$$

Since $X_{k\theta}^1$ and $\partial X_{j\theta}^1/\partial P_i^t$ are linear functions of the sine and cosine, it is clear that four types of integrals will arise when these expresions are substituted in the above. These four integrals represent all the possible products, two at a time, of the functions $\sin(\theta - \alpha_k)$, $\cos(\theta - \alpha_k)$ with the functions $\sin(\theta - \alpha_j)$, $\cos(\theta - \alpha_j)$.

Writing the function that refers to the moment first under the integral sign and then the function that refers to the derivative, the integrals may be represented by

$$K_{jk}^1 = \int_{\alpha_j}^{\pi} \sin(\theta-\alpha_k)\sin(\theta-\alpha_j)d\theta \quad (16a)$$

$$K_{jk}^2 = \int_{\alpha_j}^{\pi} \cos(\theta-\alpha_k)\cos(\theta-\alpha_j)d\theta \quad (16b)$$

$$K_{jk}^3 = \int_{\alpha_j}^{\pi} \sin(\theta-\alpha_k)\cos(\theta-\alpha_j)d\theta \quad (16c)$$

$$K_{jk}^4 = \int_{\alpha_j}^{\pi} \cos(\theta-\alpha_k)\sin(\theta-\alpha_j)d\theta \quad (16d)$$

The L-integrals are given by

$$\int_{\alpha_j}^{\pi} X_{j\theta}^1 (\partial X_{k\theta}^1/\partial P_i^t)d\theta$$

These integrals may be obtained by direct substitution or, more simply, by merely reversing the k's and j's that occur inside the integral sign of the K-integrals but making no change in the lower limit. If this is done in order, replacing each K_{jk} by an L_{kj} while maintaining the superscripts, four L-integrals will be formed, which will be duplicates of the K-integrals as follows:

$$K_{jk}^1 = L_{kj}^1 \quad (17a) \qquad K_{jk}^3 = L_{kj}^4 \quad (17c)$$

$$K_{jk}^2 = L_{kj}^2 \quad (17b) \qquad K_{jk}^4 = L_{kj}^3 \quad (17d)$$

The utility of using the L-integrals will be made clear when the expansion of Eq. (9) is taken up.

For bending in the plane of the ring, the moments and partial derivatives are linear functions of the sine, versine, and a constant term, thus:

$$X_{k\theta}^2 = [\ \ ]\sin(\theta-\alpha_k) + [\ \ ]\,\mathrm{vers}(\theta-\alpha_k) + [\ \ ]$$

where the brackets are independent of θ and α. Of the eight new integrals that arise, some of them will not be a product of two trigonometric functions because one of the brackets [ ] above is not multiplied by such a function. Since for symmetry it is desirable to have all the integrals represented by two subscripts, "dummy" subscripts are used in such cases. Retaining the order of the factors and using (1) where a factor does not contain a variable, these eight integrals may be written as follows:

$$K_{jk}^5 = \int_{\alpha_j}^{\pi} \mathrm{vers}(\theta-\alpha_k)\sin(\theta-\alpha_j)d\theta \quad (16e)$$

$$K_{jk}^6 = \int_{\alpha_j}^{\pi} (1)\sin(\theta-\alpha_j)d\theta \quad (16f)$$

$$K_{jk}^7 = \int_{\alpha_j}^{\pi} \sin(\theta-\alpha_k)\,\mathrm{vers}(\theta-\alpha_j)d\theta \quad (16g)$$

$$K_{jk}^8 = \int_{\alpha_j}^{\pi} \mathrm{vers}(\theta-\alpha_k)\,\mathrm{vers}(\theta-\alpha_j)d\theta \quad (16h)$$

$$K_{jk}^9 = \int_{\alpha_j}^{\pi} (1)\,\mathrm{vers}(\theta-\alpha_j)d\theta \quad (16i)$$

$$K_{jk}^{10} = \int_{\alpha_j}^{\pi} (1)(1)\,d\theta \quad (16j)$$

$$K_{jk}^{11} = \int_{\alpha_j}^{\pi} \sin(\theta-\alpha_k)(1)\,d\theta \quad (16k)$$

$$K_{jk}^{12} = \int_{\alpha_j}^{\pi} \mathrm{vers}(\theta-\alpha_k)(1)\,d\theta \quad (16l)$$

The L-integrals may be obtained in the same way as previously, and it will be found that

$$K_{jk}^{5} = L_{kj}^{7} \quad (17e) \qquad K_{jk}^{9} = L_{kj}^{12} \quad (17i) \qquad K_{jk}^{10} = L_{kj}^{10} = \pi - \alpha_j \quad (18j)$$

$$K_{jk}^{6} = L_{kj}^{11} \quad (17f) \qquad K_{jk}^{10} = L_{kj}^{10} \quad (17j) \qquad K_{jk}^{11} = L_{kj}^{6} = \cos\alpha_k + \cos(\alpha_j - \alpha_k) \quad (18k)$$

$$K_{jk}^{7} = L_{kj}^{5} \quad (17g) \qquad K_{jk}^{11} = L_{kj}^{6} \quad (17k) \qquad K_{jk}^{12} = L_{kj}^{9} = (\pi - \alpha_j) - \sin\alpha_k + \sin(\alpha_j - \alpha_k) \quad (18l)$$

$$K_{jk}^{8} = L_{kj}^{8} \quad (17h) \qquad K_{jk}^{12} = L_{kj}^{9} \quad (17l)$$

Two new integrals arise when the torsion of the ring is considered:

$$K_{jk}^{13} = \int_{\alpha_j}^{\pi} \cos(\theta - \alpha_k)\,\mathrm{vers}\,(\theta - \alpha_j)d\theta \quad (16m)$$

$$K_{jk}^{14} = \int_{\alpha_j}^{\pi} \mathrm{vers}\,(\theta - \alpha_k)\cos(\theta - \alpha_j)d\theta \quad (16n)$$

and for the L-integrals:

$$K_{jk}^{13} = L_{kj}^{14} \quad (17m) \qquad K_{jk}^{14} = L_{kj}^{13} \quad (17n)$$

The way in which integrals containing dummy subscripts may be handled is best explained by an example. Suppose that during the substitution into Eq. (9) the integration was from α_2 to π, a term in the moment had a factor f_3, and a term in the partial derivative had a factor f_2 (the corresponding loads and superscripts are of no interest). Then the integral arising from the product would be

$$\int_{\alpha_2}^{\pi} f_3 f_2 d\theta = f_3 f_2 \int_{\alpha_2}^{\pi} (1)(1)\,d\theta = f_3 f_2 K_{23}^{10}$$

Thus, where dummy subscripts occur, there will always be f-constants in the brackets outside the integral sign with which to match up the subscripts.

In order to determine whether the integrals are K- or L-integrals, it is essential to know which of the two factors occurring refers to the moment and which to the partial derivative. It is for this reason that a strict order has been maintained in the definition of the integrals, although, of course, the numerical value is unchanged by alteration of the orders of the factors.

The values of the 14 different integrals are easily obtained. The results are:

$$K_{jk}^{1} = L_{kj}^{1} = \tfrac{1}{2}[(\pi - \alpha_j)\cos(\alpha_j - \alpha_k) + \sin\alpha_j\cos\alpha_k] \quad (18a)$$

$$K_{jk}^{2} = L_{kj}^{2} = \tfrac{1}{2}[(\pi - \alpha_j)\cos(\alpha_j - \alpha_k) - \sin\alpha_j\cos\alpha_k] \quad (18b)$$

$$K_{jk}^{3} = L_{kj}^{4} = \tfrac{1}{2}[\sin\alpha_j\sin\alpha_k + (\pi - \alpha_j)\sin(\alpha_j - \alpha_k)] \quad (18c)$$

$$K_{jk}^{4} = L_{kj}^{3} = \tfrac{1}{2}[\sin\alpha_j\sin\alpha_k - (\pi - \alpha_j)\sin(\alpha_j - \alpha_k)] \quad (18d)$$

$$K_{jk}^{5} = L_{kj}^{7} = 1 + \cos\alpha_j - K_{jk}^{4} \quad (18e)$$

$$K_{jk}^{6} = L_{kj}^{11} = 1 + \cos\alpha_j \quad (18f)$$

$$K_{jk}^{7} = L_{kj}^{5} = \cos\alpha_k + \cos(\alpha_j - \alpha_k) - K_{jk}^{3} \quad (18g)$$

$$K_{jk}^{8} = L_{kj}^{8} = (\pi - \alpha_j) + \sin(\alpha_j - \alpha_k) - \sin\alpha_j - \sin\alpha_k + K_{jk}^{2} \quad (18h)$$

$$K_{jk}^{9} = L_{kj}^{12} = (\pi - \alpha_j) - \sin\alpha_j \quad (18i)$$

$$K_{jk}^{13} = L_{kj}^{14} = \sin\alpha_k - \sin(\alpha_j - \alpha_k) - K_{jk}^{2} \quad (18m)$$

$$K_{jk}^{14} = L_{kj}^{13} = \sin\alpha_j - K_{jk}^{2} \quad (18n)$$

The numerical evaluation of the foregoing integrals is most conveniently done in tabular form. It will be observed that the number of types of integrals could be greatly reduced by replacing vers $(\theta - \alpha)$ by its equal $1 - \cos(\theta - \alpha)$, but this turns out to be inconvenient in practice.

General Expansion of the Elastic Equation for the Ring

It is now possible to expand Eq. (9) in full and thereby deduce, from the symmetry of the expansion, rules by which any particular case may be handled.

Consider first the case of bending normal to the plane of the ring. The terms above and including the diagonal of Eq. (9) are given by

$$\int_{\alpha_j}^{\pi} X_{k\theta}^{1}(\partial X_{j\theta}^{1}/\partial P_i^{t})d\theta$$

where

$$R^{-1}X_{k\theta}^{1} = (\sum a_k^{1}P_k^{1} + a_k^{2}P_k^{2} + a_k^{4}Y_k^{4} + a_k^{3}X_k^{3}) \times \sin(\theta - \alpha_k) + (b_k^{3}P_k^{3} + b_k^{1}X_k^{1})\cos(\theta - \alpha_k)$$

and

$$R^{-1}\left(\frac{\partial X_{j\theta}^{1}}{\partial P_i^{t}}\right) = \left[\sum a_j^{1}\left(\frac{\partial P_j^{1}}{\partial P_i^{t}}\right) + a_j^{2}\left(\frac{\partial P_j^{2}}{\partial P_i^{t}}\right) + a_j^{4}\left(\frac{\partial Y_j^{4}}{\partial P_i^{t}}\right) + a_j^{3}\left(\frac{\partial X_j^{3}}{\partial P_i^{t}}\right)\right]\sin(\theta - \alpha_j) + \left[b_j^{3}\left(\frac{\partial P_j^{3}}{\partial P_i^{t}}\right) + b_j^{1}\left(\frac{\partial X_j^{1}}{\partial P_i^{t}}\right)\right]\cos(\theta - \alpha_j)$$

Substituting the latter two expressions into the integral above, replacing the trigonometric integrals by their equals in terms of the K's, and rearranging gives:

$$R^{-2}\int_{\alpha_j}^{\pi} X_{k\theta}^{1}(\partial X_{j\theta}^{1}/\partial P_i^{t})d\theta = b_k^{1}X_k^{1} \times (A_jK_{jk}^{4} + B_jK_{jk}^{2}) + a_k^{3}X_k^{3}(A_jK_{jk}^{1} + B_jK_{jk}^{2}) + a_k^{4}Y_k^{4}(A_jK_{jk}^{1} + B_jK_{jk}^{3}) + \sum a_k^{1}P_k^{1}(A_jK_{jk}^{1} + B_jK_{jk}^{3}) + a_k^{2}P_k^{2}(A_jK_{jk}^{1} + B_jK_{jk}^{3}) + b_k^{3}P_k^{3} \times (A_jK_{jk}^{4} + B_jK_{jk}^{2}) \qquad k \le j \quad (19)$$

where

$$A_j(P_i^{t}) = A_j = \sum a_j^{1}\left(\frac{\partial P_j^{1}}{\partial P_i^{t}}\right) + a_j^{2}\left(\frac{\partial P_j^{2}}{\partial P_i^{t}}\right) + a_j^{4}\left(\frac{\partial Y_j^{4}}{\partial P_i^{t}}\right) + a_j^{3}\left(\frac{\partial X_j^{3}}{\partial P_i^{t}}\right) \quad (20a)$$

$$B_j(P_i^t) = B_j = b_j^3\left(\frac{\partial P_j^3}{\partial P_i^t}\right) + b_j^1\left(\frac{\partial X_j^1}{\partial P_i^t}\right) \quad (20b)$$

The value of $\int_{\alpha_j}^{\pi} X_{j\theta}^1(\partial X_k\theta^1/\partial P_i^t)d\theta$, which gives rise to the L-integrals, may be obtained from Eq. (19) by interchanging j and k throughout (except the lower limit of the integral on the left-hand side) and replacing K-integrals by L-integrals. Since X_k^1, X_k^3, Y_k^4 only occur at station o, these may be omitted from the L terms:

$$R^{-2}\int_{\alpha_j}^{\pi} X_{j\theta}^1(\partial X_{k\theta}^1/\partial P_i^t)d\theta = \sum a_j^1 P_j^1 \times (A_k L_{kj}^1 + B_k L_{kj}^3) + a_j^2 P_j^2 (A_k L_{kj}^1 + B_k L_{kj}^3) + b_j^3 P_j^3 (A_k L_{kj}^4 + B_k L_{kj}^2) \qquad k < j \quad (21)$$

(*See Right Column*)

Although both engine and mount tube forces may occur at all stations, for simplicity in writing it has been assumed in the above expansion that just a single mount tube joins the ring at any one station. The modifications that occur when two or more mount tubes join the ring at one point are easily seen. The corresponding forces will have double subscripts to differentiate between them. The changes to be made in Eq. (22) consist of altering certain columns somewhat and adding more rows. The addition of more rows is indicated by the $\sum$-sign in Eq. (19) and in Eq. (21). The quantities inside the parentheses of Eq. (22) will be the same for each of the added rows. The column change is confined to the A_j constants where it is necessary to sum the first term of these over all the mount tubes at the point in question.

The three types of forces P_j^1, P_j^2, P_j^3 are independent of one another as are, of course, the redundants X_0^1, X_0^3, Y_0^4. This makes many of the partial derivatives, which measure the change in one load due to a unit change in another, identically zero. For example, if the redundant in question is one of the forces or moments at the cut, all A's and B's are zero except either (but not both) A_0 or B_0. Thus, for these redundants Eq. (22) reduces to just one column.

Once the various equilibrium equations have been solved in terms of the redundants, the values of the partial derivatives are known numerically. Since the equations are linear, the coefficient of any independent variable (redundant) is the partial derivative of the dependent variable with respect to that redundant.

With these facts in mind, the law of formation of Eq. (22) may be incorporated into a rule so that the use of the general expansion is unnecessary. This rule may be used for each redundant in turn.

Rule—Moments Normal to Plane of Ring

Step 1. The column of loads that appear outside the parentheses consists of all those that appear in Eq. (10). Therefore, list the forces and moments acting

By means of Eqs. (19) and (21), the general expansion for a ring of n stations may be now written:

$$\left(\frac{EI}{R^2}\right)\left(\frac{\partial U^1}{\partial P_i^t}\right) = \begin{array}{l} b_0X_0^1(\\ +a_0^3X_0^3(\\ +a_0^1Y_0^4(\\ +a_0^1P_0^1(\\ +a_0^3P_0^3(\\ +b_0^3P_0^3(\\ +a_1^1P_1^1(\\ +a_1^3P_1^3(\\ +b_1^3P_1^3(\\ \cdots\cdots\cdots \\ +a_n - 1^1P_n - 1^1(A_0L_{o(n-1)}^1 + B_0L_{o(n-1)}^3 + A_1L_{1(n-1)}^1 + B_1L_{1(n-1)}^3 + \cdots\cdots A_n - 1K_{(n-1)(n-1)}^1 + B_n - 1K_{(n-1)(n-1)}^3 \\ +a_n - 1^2P_n - 1^2(A_0L_{o(n-1)}^1 + B_0L_{o(n-1)}^3 + A_1L_{1(n-1)}^1 + B_1L_{1(n-1)}^3 + \cdots\cdots A_n - 1K_{(n-1)(n-1)}^1 + B_n - 1K_{(n-1)(n-1)}^3 \\ +b_n - 1^3P_n - 1^3(A_0L_{o(n-1)}^4 + B_0L_{o(n-1)}^2 + A_1L_{1(n-1)}^4 + B_1L_{1(n-1)}^2 + \cdots\cdots A_n - 1K_{(n-1)(n-1)}^4 + B_n - 1K_{(n-1)(n-1)}^2 \end{array} \quad (22)$$

$$\begin{array}{l} A_0K_{oo}^4 \quad + B_0K_{oo}^2 \quad + A_1K_{10}^4 \quad + B_1K_{10}^2 \quad + \cdots\cdots A_n - 1K_{(n-1)0}^4 \quad + B_n - 1K_{(n-1)0}^2 \\ A_0K_{oo}^1 \quad + B_0K_{oo}^3 \quad + A_1K_{10}^1 \quad + B_1K_{10}^3 \quad + \cdots\cdots A_n - 1K_{(n-1)0}^1 \quad + B_n - 1K_{(n-1)0}^3

on the half of the ring under consideration in a single column in order of their subscripts with those of the same subscript progressing in order of their superscripts. List the three redundants at the cut first. Do not list the loads 180° removed from the cut.

Step 2. The type of multiplier (a or b) for these loads is also determined from Eq. (10). It is seen that all loads of the type P^1, P^2, Y^4, X^3 have a-constants as multipliers and loads of the type P^3, X^1 have b-constants. Therefore, write the appropriate a or b and make the subscripts and superscripts identical with those of the loads they multiply.

Step 3. The A or B constants that are not zero are next written down inside the same parenthesis (these stay the same columnwise). This is done by using Eq. (20). The nonzero partial derivatives may be picked out by noting that, in general, each dependent force of a particular type is a linear function of all the independent forces of the same type. (The value of these derivatives are not needed here; all that is required is to note whether they are zero or not.) Having determined the subscripts of the A or B constants, list them in order of their subscripts from left to right, leaving space to insert the integrals.

Step 4. Multiply each A or B inside the first parenthesis by a K-integral and attach appropriate subscripts by observing that the first subscript on these integrals agrees with that of the A's or B's and that the second subscript is zero. Connect all terms by plus signs. This will complete the first parenthesis except for superscripts.

Step 5. Complete (except for superscripts) the remaining parentheses, noting that the first subscript on the integrals remains the same columnwise and that the second subscript, which remains the same by rows, agrees with the subscript of the unknown outside the corresponding parenthesis. If this happens to have a double subscript, use only the first number of this double subscript on the integral. In proceeding down a column, change from K-integrals to L-integrals at the point where the second subscript exceeds the first. The integrals then stay as L-integrals for the remainder of the column.

Step 6. The superscripts on all the integrals are determined by the type of multiplier (a or b) outside the parentheses and the type of multiplier (A or B) immediately preceding the integrals according to the following scheme:

Constant outside parenthesis	a	b	a	b
Constant multiplying integral	A	B	B	A
Superscript on integral	1	2	3	4

Therefore, attach all superscripts in this manner and connect all terms by plus signs. The result will be equal to EI/R^3 multiplied by the partial derivative of the energy due to bending normal to the plane of the ring with respect to the particular redundant used.

It is easy to see that Eq. (22) is identically zero for the redundants Y_0^5, Y_0^6, X_0^2.

By exactly the same process as that used above, Eq. (9) can be expanded for the case of moments in the plane of the ring. Instead of the A's and B's the following column numbers appear

$$C_i(P_i^t) = C_i = \sum c_i^1\left(\frac{\partial P_j^1}{\partial P_i^t}\right) + c_i^2\left(\frac{\partial P_j^2}{\partial P_i^t}\right) + c_i^6\left(\frac{\partial Y_j^6}{\partial P_i^t}\right) \quad (23a)$$

$$D_j(P_i^t) = D_j = \sum d_i^1\left(\frac{\partial P_j^1}{\partial P_i^t}\right) + d_i^3\left(\frac{\partial P_j^3}{\partial P_i^t}\right) + d_i^5\left(\frac{\partial Y_j^5}{\partial P_i^t}\right) \quad (23b)$$

$$F_j(P_i^t) = F_j = f_j^3(\partial P_j^3/\partial P_i^t) + f_j^2(\partial X_j^2/\partial P_i^t) \quad (23c)$$

See page 12, Eqs. (24) for the final result in terms of the K- and L-integrals.

A comparison of this equation with Eq. (22) will reveal the great similarity between the two equations and an explicit rule might be written for its formation. The important differences are that the column numbers C, D, F replace the A's and B's and the superscripts are attached to the integrals according to the plan below:

Constant outside parenthesis	c	d	f	c	d	f	f	c	d
Constant multiplying integral	C	C	C	D	D	D	F	F	F
Superscript on integral	1	5	6	7	8	9	10	11	12

Note also that the P^1 and P^3 forces must be listed twice for each subscript. The reason for this is obvious from an inspection of Eq. (12).

The remaining expansion of Eq. (9) is for the torsional moments in the ring ($s = 3$). For this case the column numbers are given by

$$B_j(P_i^t) = B_j = b_j^3(\partial P_j^3/\partial P_i^t) + b_j^1(\partial X_j^1/\partial P_i^t) \quad (25a)$$

$$H_j(P_i^t) = H_j = h_j^2(\partial P_j^2/\partial P_i^t) + h_j^3(\partial X_j^3/\partial P_i^t) \quad (25b)$$

$$Q_j(P_i^t) = Q_j = \Sigma q_j^1(\partial P_j^1/\partial P_i^t) + q_j^2(\partial P_j^2/\partial P_i^t) + q_j^4(\partial Y_j^4/\partial P_i^t) \quad (25c)$$

$$\left(\frac{EI}{R^3}\right)\left(\frac{\partial U^2}{\partial P_i^{\,t}}\right) = \qquad (c_2 = 1)$$

$$\begin{array}{llllllllll}
f_0{}^2X_0{}^2(& C_0K_{00}{}^6 & + D_0K_{00}{}^9 & + F_0K_{00}{}^{10} & + C_1K_{10}{}^6 & + D_1K_{10}{}^9 & + F_1K_{10}{}^{10} & + \ldots\ldots & C_{n-1}K_{(n-1)0}{}^6 & + D_{n-1}K_{(n-1)0}{}^9 & + F_{n-1}K_{(n-1)0}{}^{10}) \\
+d_0{}^5Y_0{}^5(& C_0K_{00}{}^5 & + D_0K_{00}{}^8 & + F_0K_{00}{}^{12} & + C_1K_{10}{}^5 & + D_1K_{10}{}^8 & + F_1K_{10}{}^{12} & + \ldots\ldots & C_{n-1}K_{(n-1)0}{}^5 & + D_{n-1}K_{(n-1)0}{}^8 & + F_{n-1}K_{(n-1)0}{}^{12}) \\
+c_0{}^6Y_0{}^6(& C_0K_{00}{}^1 & + D_0K_{00}{}^7 & + F_0K_{00}{}^{11} & + C_1K_{10}{}^1 & + D_1K_{10}{}^7 & + F_1K_{10}{}^{11} & + \ldots\ldots & C_{n-1}K_{(n-1)0}{}^1 & + D_{n-1}K_{(n-1)0}{}^7 & + F_{n-1}K_{(n-1)0}{}^{11}) \\
+c_0{}^1P_0{}^1(& C_0K_{00}{}^1 & + D_0K_{00}{}^7 & + F_0K_{00}{}^{11} & + C_1K_{10}{}^1 & + D_1K_{10}{}^7 & + F_1K_{10}{}^{11} & + \ldots\ldots & C_{n-1}K_{(n-1)0}{}^1 & + D_{n-1}K_{(n-1)0}{}^7 & + F_{n-1}K_{(n-1)0}{}^{11}) \\
+d_0{}^1P_0{}^1(& C_0K_{00}{}^5 & + D_0K_{00}{}^8 & + F_0K_{00}{}^{12} & + C_1K_{10}{}^5 & + D_1K_{10}{}^8 & + F_1K_{10}{}^{12} & + \ldots\ldots & C_{n-1}K_{(n-1)0}{}^5 & + D_{n-1}K_{(n-1)0}{}^8 & + F_{n-1}K_{(n-1)0}{}^{12}) \\
+c_0{}^2P_0{}^2(& C_0K_{00}{}^1 & + D_0K_{00}{}^7 & + F_0K_{00}{}^{11} & + C_1K_{10}{}^1 & + D_1K_{10}{}^7 & + F_1K_{10}{}^{11} & + \ldots\ldots & C_{n-1}K_{(n-1)0}{}^1 & + D_{n-1}K_{(n-1)0}{}^7 & + F_{n-1}K_{(n-1)0}{}^{11}) \\
+d_0{}^3P_0{}^3(& C_0K_{00}{}^5 & + D_0K_{00}{}^8 & + F_0K_{00}{}^{12} & + C_1K_{10}{}^5 & + D_1K_{10}{}^8 & + F_1K_{10}{}^{12} & + \ldots\ldots & C_{n-1}K_{(n-1)0}{}^5 & + D_{n-1}K_{(n-1)0}{}^8 & + F_{n-1}K_{(n-1)0}{}^{12}) \\
+f_0{}^3P_0{}^3(& C_0K_{00}{}^6 & + D_0K_{00}{}^9 & + F_0K_{00}{}^{10} & + C_1K_{10}{}^6 & + D_1K_{10}{}^9 & + F_1K_{10}{}^{10} & + \ldots\ldots & C_{n-1}K_{(n-1)0}{}^6 & + D_{n-1}K_{(n-1)0}{}^9 & + F_{n-1}K_{(n-1)0}{}^{10}) \\
+c_1{}^1P_1{}^1(& C_0L_{01}{}^1 & + D_0L_{01}{}^7 & + F_0L_{01}{}^{11} & + C_1K_{11}{}^1 & + D_1K_{11}{}^7 & + F_1K_{11}{}^{11} & + \ldots\ldots & C_{n-1}K_{(n-1)1}{}^1 & + D_{n-1}K_{(n-1)1}{}^7 & + F_{n-1}K_{(n-1)1}{}^{11}) \\
+d_1{}^1P_1{}^1(& C_0L_{01}{}^5 & + D_0L_{01}{}^8 & + F_0L_{01}{}^{12} & + C_1K_{11}{}^5 & + D_1K_{11}{}^8 & + F_1K_{11}{}^{12} & + \ldots\ldots & C_{n-1}K_{(n-1)1}{}^5 & + D_{n-1}K_{(n-1)1}{}^8 & + F_{n-1}K_{(n-1)1}{}^{12}) \\
+c_1{}^2P_1{}^2(& C_0L_{01}{}^1 & + D_0L_{01}{}^7 & + F_0L_{01}{}^{11} & + C_1K_{11}{}^1 & + D_1K_{11}{}^7 & + F_1K_{11}{}^{11} & + \ldots\ldots & C_{n-1}K_{(n-1)1}{}^1 & + D_{n-1}K_{(n-1)1}{}^7 & + F_{n-1}K_{(n-1)1}{}^{11}) \\
+d_1{}^3P_1{}^3(& C_0L_{01}{}^5 & + D_0L_{01}{}^8 & + F_0L_{01}{}^{12} & + C_1K_{11}{}^5 & + D_1K_{11}{}^8 & + F_1K_{11}{}^{12} & + \ldots\ldots & C_{n-1}K_{(n-1)1}{}^5 & + D_{n-1}K_{(n-1)1}{}^8 & + F_{n-1}K_{(n-1)1}{}^{12}) \\
+f_1{}^3P_1{}^3(& C_0L_{01}{}^6 & + D_0L_{01}{}^9 & + F_0L_{01}{}^{10} & + C_1K_{11}{}^6 & + D_1K_{11}{}^9 & + F_1K_{11}{}^{10} & + \ldots\ldots & C_{n-1}K_{(n-1)1}{}^6 & + D_{n-1}K_{(n-1)1}{}^9 & + F_{n-1}K_{(n-1)1}{}^{10}) \\
\vdots & \vdots & \vdots & \vdots & \vdots & \vdots & \vdots & & \vdots & \vdots & \vdots \\
+c_{n-1}{}^1P_{n-1}{}^1(C_0L_{0(n-1)}{}^1 + D_0L_{0(n-1)}{}^7 & + F_0L_{0(n-1)}{}^{11} & + C_1L_{1(n-1)}{}^1 & + D_1L_{1(n-1)}{}^7 & + F_1L_{1(n-1)}{}^{11} & + \ldots\ldots & C_{n-1}K_{(n-1)(n-1)}{}^1 & + D_{n-1}K_{(n-1)(n-1)}{}^7 & + F_{n-1}K_{(n-1)(n-1)}{}^{11}) \\
+d_{n-1}{}^1P_{n-1}{}^1(C_0L_{0(n-1)}{}^5 + D_0L_{0(n-1)}{}^8 & + F_0L_{0(n-1)}{}^{12} & + C_1L_{1(n-1)}{}^5 & + D_1L_{1(n-1)}{}^8 & + F_1L_{1(n-1)}{}^{12} & + \ldots\ldots & C_{n-1}K_{(n-1)(n-1)}{}^5 & + D_{n-1}K_{(n-1)(n-1)}{}^8 & + F_{n-1}K_{(n-1)(n-1)}{}^{12}) \\
+c_{n-1}{}^2P_{n-1}{}^2(C_0L_{0(n-1)}{}^1 + D_0L_{0(n-1)}{}^7 & + F_0L_{0(n-1)}{}^{11} & + C_1L_{1(n-1)}{}^1 & + D_1L_{1(n-1)}{}^7 & + F_1L_{1(n-1)}{}^{11} & + \ldots\ldots & C_{n-1}K_{(n-1)(n-1)}{}^1 & + D_{n-1}K_{(n-1)(n-1)}{}^7 & + F_{n-1}K_{(n-1)(n-1)}{}^{11}) \\
+d_{n-1}{}^3P_{n-1}{}^3(C_0L_{0(n-1)}{}^5 + D_0L_{0(n-1)}{}^8 & + F_0L_{0(n-1)}{}^{12} & + C_1L_{1(n-1)}{}^5 & + D_1L_{1(n-1)}{}^8 & + F_1L_{1(n-1)}{}^{12} & + \ldots\ldots & C_{n-1}K_{(n-1)(n-1)}{}^5 & + D_{n-1}K_{(n-1)(n-1)}{}^8 & + F_{n-1}K_{(n-1)(n-1)}{}^{12}) \\
+f_{n-1}{}^3P_{n-1}{}^3(C_0L_{0(n-1)}{}^6 + D_0L_{0(n-1)}{}^9 & + F_0L_{0(n-1)}{}^{10} & + C_1L_{1(n-1)}{}^6 & + D_1L_{1(n-1)}{}^9 & + F_1L_{1(n-1)}{}^{10} & + \ldots\ldots & C_{n-1}K_{(n-1)(n-1)}{}^6 & + D_{n-1}K_{(n-1)(n-1)}{}^9 & + F_{n-1}K_{(n-1)(n-1)}{}^{10})
\end{array} \qquad (24)$$

$$\left(\frac{GJ}{R^3}\right)\left(\frac{\partial U^2}{\partial P_i^{\,t}}\right) = \qquad \left(c_3 = \frac{EI}{GJ}\right)$$

$$\begin{array}{llllllllll}
b_0{}^1X_0{}^1(& B_0K_{00}{}^1 & + H_0K_{00}{}^3 & + Q_0K_{00}{}^7 & + B_1K_{10}{}^1 & + H_1K_{10}{}^3 & + Q_1K_{10}{}^7 & + \ldots\ldots & B_{n-1}K_{(n-1)0}{}^1 & + H_{n-1}K_{(n-1)0}{}^3 & + Q_{n-1}K_{(n-1)0}{}^7) \\
+h_0{}^3X_0{}^3(& B_0K_{00}{}^4 & + H_0K_{00}{}^2 & + Q_0K_{00}{}^{13} & + B_1K_{10}{}^4 & + H_1K_{10}{}^2 & + Q_1K_{10}{}^{13} & + \ldots\ldots & B_{n-1}K_{(n-1)0}{}^4 & + H_{n-1}K_{(n-1)0}{}^2 & + Q_{n-1}K_{(n-1)0}{}^{13}) \\
+q_0{}^4Y_0{}^4(& B_0K_{00}{}^5 & + H_0K_{00}{}^{14} & + Q_0K_{00}{}^8 & + B_1K_{10}{}^5 & + H_1K_{10}{}^{14} & + O_1K_{10}{}^8 & + \ldots\ldots & B_{n-1}K_{(n-1)0}{}^5 & + H_{n-1}K_{(n-1)0}{}^{14} & + Q_{n-1}{}^1K_{(n-1)0}{}^8) \\
+q_0{}^1P_0{}^1(& B_0K_{00}{}^5 & + H_0K_{00}{}^{14} & + Q_0K_{00}{}^8 & + B_1K_{10}{}^5 & + H_1K_{10}{}^{14} & + Q_1K_{10}{}^8 & + \ldots\ldots & B_{n-1}K_{(n-1)0}{}^5 & + H_{n-1}K_{(n-1)0}{}^{14} & + Q_{n-1}K_{(n-1)0}{}^8) \\
+h_0{}^2P_0{}^2(& B_0K_{00}{}^4 & + H_0K_{00}{}^2 & + Q_0K_{00}{}^{13} & + B_1K_{10}{}^4 & + H_1K_{10}{}^2 & + Q_1K_{10}{}^{13} & + \ldots\ldots & B_{n-1}K_{(n-1)0}{}^4 & + H_{n-1}K_{(n-1)0}{}^2 & + Q_{n-1}K_{(n-1)0}{}^{13}) \\
+q_0{}^2P_0{}^2(& B_0K_{00}{}^5 & + H_0K_{00}{}^{14} & + Q_0K_{00}{}^8 & + B_1K_{10}{}^5 & + H_1K_{10}{}^{14} & + Q_1K_{10}{}^8 & + \ldots\ldots & B_{n-1}K_{(n-1)0}{}^5 & + H_{n-1}K_{(n-1)0}{}^{14} & + Q_{n-1}K_{(n-1)0}{}^8) \\
+b_0{}^3P_0{}^3(& B_0K_{00}{}^1 & + H_0K_{00}{}^3 & + Q_0K_{00}{}^7 & + B_1K_{10}{}^1 & + H_1K_{10}{}^3 & + Q_1K_{10}{}^7 & + \ldots\ldots & B_{n-1}K_{(n-1)0}{}^1 & + H_{n-1}K_{(n-1)0}{}^3 & + Q_{n-1}K_{(n-1)0}{}^7) \\
+q_1{}^1P_1{}^1(& B_0L_{01}{}^5 & + H_0L_{01}{}^{14} & + Q_0L_{01}{}^8 & + B_1K_{11}{}^5 & + H_1K_{11}{}^{14} & + Q_1K_{11}{}^8 & + \ldots\ldots & B_{n-1}K_{(n-1)1}{}^5 & + H_{n-1}K_{(n-1)1}{}^{14} & + Q_{n-1}K_{(n-1)1}{}^8) \\
+h_1{}^2P_1{}^2(& B_0L_{01}{}^4 & + H_0L_{01}{}^2 & + Q_0L_{01}{}^{13} & + B_1K_{11}{}^4 & + H_1K_{11}{}^2 & + Q_1K_{11}{}^{13} & + \ldots\ldots & B_{n-1}K_{(n-1)1}{}^4 & + H_{n-1}K_{(n-1)1}{}^2 & + Q_{n-1}K_{(n-1)1}{}^{13}) \\
+q_1{}^2P_1{}^2(& B_0L_{01}{}^5 & + H_0L_{01}{}^{14} & + Q_0L_{01}{}^8 & + B_1K_{11}{}^5 & + H_1K_{11}{}^{14} & + Q_1K_{11}{}^8 & + \ldots\ldots & B_{n-1}K_{(n-1)1}{}^5 & + H_{n-1}K_{(n-1)1}{}^{14} & + Q_{n-1}K_{(n-1)1}{}^8) \\
+b_1{}^3P_1{}^3(& B_0L_{01}{}^1 & + H_0L_{01}{}^3 & + Q_0L_{01}{}^7 & + B_1K_{11}{}^1 & + H_1K_{11}{}^3 & + Q_1K_{11}{}^7 & + \ldots\ldots & B_{n-1}K_{(n-1)1}{}^1 & + H_{n-1}K_{(n-1)1}{}^3 & + Q_{n-1}K_{(n-1)1}{}^7) \\
\vdots & \vdots & \vdots & \vdots & \vdots & \vdots & \vdots & & \vdots & \vdots & \vdots \\
+q_{n-1}{}^1P_{n-1}{}^1(B_0L_{0(n-1)}{}^5 + H_0L_{0(n-1)}{}^{14} & + Q_0L_{0(n-1)}{}^8 & + B_1L_{1(n-1)}{}^5 & + H_1L_{1(n-1)}{}^{14} & + Q_1L_{1(n-1)}{}^8 & + \ldots\ldots & B_{n-1}K_{(n-1)(n-1)}{}^5 & + H_{n-1}K_{(n-1)(n-1)}{}^{14} & + Q_{n-1}K_{(n-1)(n-1)}{}^8) \\
+h_{n-1}{}^2P_{n-1}{}^2(B_0L_{0(n-1)}{}^4 + H_0L_{0(n-1)}{}^2 & + Q_0L_{0(n-1)}{}^{13} & + B_1L_{1(n-1)}{}^4 & + H_1L_{1(n-1)}{}^2 & + Q_1L_{1(n-1)}{}^{13} & + \ldots\ldots & B_{n-1}K_{(n-1)(n-1)}{}^4 & + H_{n-1}K_{(n-1)(n-1)}{}^2 & + Q_{n-1}K_{(n-1)(n-1)}{}^{13}) \\
+q_{n-1}{}^2P_{n-1}{}^2(B_0L_{0(n-1)}{}^5 + H_0L_{0(n-1)}{}^{14} & + Q_0L_{0(n-1)}{}^8 & + B_1L_{1(n-1)}{}^5 & + H_1L_{1(n-1)}{}^{14} & + Q_1L_{1(n-1)}{}^8 & + \ldots\ldots & B_{n-1}K_{(n-1)(n-1)}{}^5 & + H_{n-1}K_{(n-1)(n-1)}{}^{14} & + Q_{n-1}K_{(n-1)(n-1)}{}^8) \\
+b_{n-1}{}^3P_{n-1}{}^3(B_0L_{0(n-1)}{}^1 + H_0L_{0(n-1)}{}^3 & + Q_0L_{0(n-1)}{}^7 & + B_1L_{1(n-1)}{}^1 & + H_1L_{1(n-1)}{}^3 & + Q_1L_{1(n-1)}{}^7 & + \ldots\ldots & B_{n-1}K_{(n-1)(n-1)}{}^1 & + H_{n-1}K_{(n-1)(n-1)}{}^3 & + Q_{n-1}K_{(n-1)(n-1)}{}^7)
\end{array} \qquad (26)$$

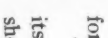

Fro
The
its
eve
alr
pu
mo
for
the
bi
nu
the
du
eli
so
of
is
ap
ha
us
su
ar
er
is
ri
D
co
te
re
ti
sp
ri
n

From an inspection of Eq. (14) for the torsional moment, it will be seen that the P^2 forces must be listed twice The superscripts on the integrals follow the scheme below:

Constant outside parenthesis	b	h	b	h	q	b	q	h	q
Constant multiplying integral	B	H	H	B	B	Q	Q	Q	H
Superscript on integral	1	2	3	4	5	7	8	13	14

The complete expansion is shown on page 12 in Eqs. (26).

The three equations (Eqs. (22), (24), and (26) may at first glance seem complicated. It has been found, however, that the equations for the ring can be written down almost automatically after a little practice. For this purpose the rules that were given explicitly for the moments normal to the plane of the ring and indicated for the other two cases are extremely convenient.

When all the elastic equations pertaining to the ring itself have been listed in literal terms, numerical values should be substituted so that the right-hand side of each equation becomes a linear function of the unknown forces and moments. The corresponding equations for the rubber and mount tubes must also be calculated numerically. The various components are then combined as indicated in Eq. (4). When this has been done, there will then be precisely as many equations as redundants. The dependent unknowns can then be eliminated by means of the equilibrium equations, the solution of which gives each dependent force in terms of the redundants. The resulting system of equations is solved simultaneously by the method of successive approximations or otherwise. All the redundants having been obtained, the equilibrium equations are used again to determine all the dependent forces. By substitution into the moment equations, the bending and torsional moments may be obtained. Almost the entire calculation can be set up in tabular form, and it is recommended that this be done.

Conclusion

The analysis given in this paper may be extended or specialized in a variety of ways. For example, if the ring is symmetrical and is loaded symmetrically (V, D, M_S), the equations are much simpler. In such a case the right- and left-side superscripts may be omitted and only half the ring considered with only three redundants acting at the cut.

It need scarcely be pointed out that the general equations are applicable with little modification to many ring problems that have no connection with engine mounts. In a considerable portion of such cases, the loading on the ring is known, and, if this loading is nondistributed, the problem is essentially a special case of the above more general solution. External moments applied to the ring can be provided for by considering that X_i^1, X_i^2, X_i^3 may act at stations other than the cut.

It seems evident that the same type of solution could be given for rings other than circular, but the integrals that would arise for such rings would in general be of a nonelementary character.

With regard to the numerical calculation, experience indicates that a minimum of five significant figures (not decimal points) should be retained throughout. The final simultaneous equations that contain only the redundant forces and moments will, by the Maxwell-Mohr Reciprocity Theorem, be axisymmetric. This affords a partial check on the off-diagonal terms. However, since errors in symmetry are not discovered until almost the last step and since many parts of the calculation have no reliable check, it is strongly recommended that all numerical work be done in duplicate. The only exception to this rule would be in the solution of the final equations; here each unknown should be checked in every equation, unless it has been obtained by the method of successive approximation, which is self-checking. If many rings are to be calculated, it may be advisable to compute tables of the integrals for every 5° or 10°. Intermediate points can be obtained by straight-line interpolation.

Acknowledgement

The author wishes to acknowledge the liberal assistance received from R. H. Tripp and K. W. Center of the Structures Department, Grumman Aircraft Engineering Corporation.

References

[1] Wright Aeronautical Corporation Report No. 353, *Predetermination and Control of Vibration in Aircraft Originating from the Engine*, pp. 18–23, 1937.

[2] Willis, J. G., *Stress Analysis of Engine Mounting Rings*, Journal of the Aeronautical Sciences, pp. 292–294, May, 1939.

Wing Flaps in Light Aircraft Design

MAURICE A. GARBELL*

Consolidated Vultee Aircraft Corporation

Introduction

THE USE OF WING FLAPS on light airplanes is often considered to be a complication of questionable value, because the attainment of high maximum lift coefficients results only in a nominal reduction of the stalling speed of such airplanes that ordinarily have a low wing loading.

This attitude has its origin in the design of heavy military aircraft where the principal function of wing flaps is to reduce the excessive stalling speed of highly loaded wings and where the flaps are not usually expected to contribute materially to the overall improvement of airplane performance.

On aircraft with high wing loading and low power loading the following factors are mainly instrumental in diminishing the value of wing flaps:

(1) Wing flaps improve the airplane performance at high lift coefficients only, where the flight and control characteristics of such aircraft, primarily designed for high-speed operation, are usually not considered satisfactory.

(2) The power/drag-area ratio is so high in this category of airplanes that aerodynamic improvements, such as those offered by wing flaps, cannot affect the most important performance items, except the stalling speed and the angle of glide, to any appreciable amount.

On aircraft with low wing loading and comparatively high power loading, such as the average light airplane, these factors are substantially modified:

(1) Flight and control characteristics of light aircraft are designed for low-speed operation, and full advantage can be taken of any improvement of performance at low flying speeds offered by wing flaps.

(2) The power/drag-area ratio is low, and aerodynamic improvements on the wing may affect the performance characteristics of the airplane considerably.

The purpose of this paper is to show some of the quantitative gains and design problems that may be expected from the incorporation of wing flaps on a typical four-seater light airplane of the immediate postwar period.

Symbols

C_D = drag coefficient referred to the wing area with flaps retracted

C_L = lift coefficient referred to the wing area with flaps retracted

C_l = rolling moment coefficient = L/qSb

C_n = yawing moment coefficient = N/qsB

g = acceleration of gravity (32.2 ft. per sec.^{2})

R = radius of curvature of a turn (ft.); in a climbing or descending turn, the radius of curvature of the osculating circle to the helix described by the velocity vector V.

S = wing area (sq.ft.)

t.hp.$_r$ = thrust horse power required

(t.hp.$_r$)$_R$ = thrust horse power required during a turn of radius R in level flight

V = true air speed (m.p.h.)

V_c = rate of climb (ft. per min.)

V_s = sinking speed (ft. per min.)

W = gross weight of the airplane (lbs.)

ψ = angle of sideslip

θ = angle of bank

φ = angle of climb

ρ = density of the air (slugs per cu.ft.)

μ = ground friction coefficient

Fundamental Aerodynamic Characteristics of a Typical Light Airplane

In order to obtain a quantitative basis for performance comparison, with and without flaps, a typical light airplane was chosen of a class that probably will have a great appeal to the nonprofessional or semi-professional flier of the immediate postwar era.

The following minimum design data serve to define this airplane within the needs of the present discussion:

Design gross weight	2,500 lbs.
Wing area	185 sq.ft.
Aspect ratio	7.5
Span	37.2 ft.
Power installed (Constant-speed propeller)	200 b.hp.
Wing loading	13.5 lbs. per sq.ft.
Power loading	12.5 lbs. per b.hp.

The lift-drag polar and the speed polar of the airplane are shown in Figs. 1 and 2.

The speed polar is the basis of the present performance comparison. The abscissas of the speed polar, $C_L^{-1/2}$, represent a forward speed, since

$$V_{m.p.h.} = (60/88)\sqrt{1/(\rho/2)}\sqrt{W/S}(C_L^{-1/2}) \quad (1)$$

The ordinates, $C_D/C_L^{3/2}$, can be interpreted either as the power required for a certain level flight condition, since

Presented at the National Light Aircraft Meeting, I.A.S., Detroit, April 27–28, 1944.

* Senior Aerodynamics Engineer.

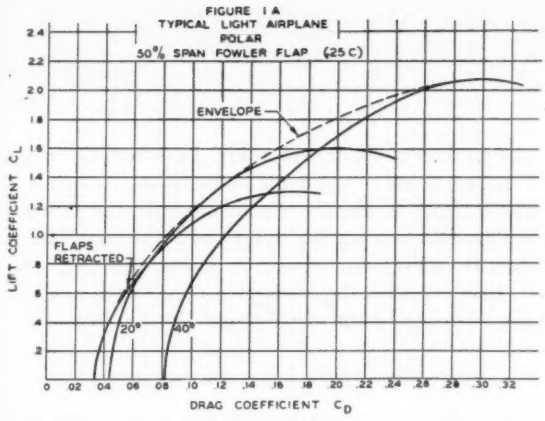

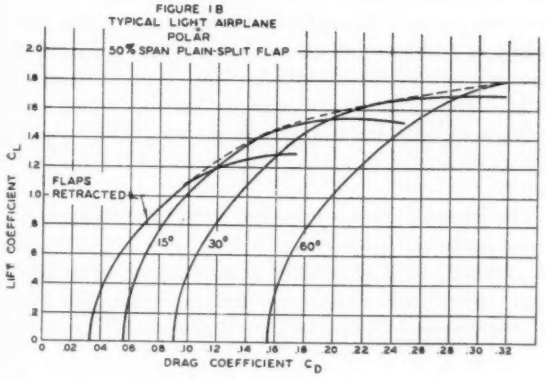

$$\text{t.hp.}_r = (1/550)\sqrt{1/(\rho/2)}\sqrt{W/S}W(C_D/C_L^{3/2}) \quad (2)$$

or as the sinking speed for the steady glide condition at the same air speed, since (assuming the angle of glide to be small)

$$V_s = 60\sqrt{1(\rho/2)}\sqrt{W/S}(C_D/C_L^{3/2}) \quad (3)$$

These relations are valid for nonaccelerated flight, both level and inclined (climb and descent); similar relations are also derived for steady turning flight.

A brief inspection of the speed polar shows that the point of minimum $C_D/C_L^{3/2}$ represents the air speed for minimum power required for level flight (or of minimum sinking speed in a glide) and that the point of tangency to the speed polar of a straight line through the origin 0 of the coordinates is the point of greatest L/D.

Figs. 1 and 2 show the effect of split flaps and of Fowler-type flaps on the lift-drag and speed polars of the given light airplane. An envelope is drawn tangent to all the polars obtained with the various flap deflections.

It is observed that the fundamental effect of the deflection of wing flaps is the extension and flattening of the low-speed end of the speed polar. This effect is most pronounced for the Fowler-type flap.

Climb Performance

Rate of Climb

Figs. 2a and 2b show a comparison of the speed polars of the airplane and the "power-available" speed polar. The rates of climb shown in Figs. 3a and 3b were obtained from the equation

$$V_c = 60\sqrt{1(\rho/2)}\sqrt{W/S}\,\Delta(C_D/C_L^{3/2}) \quad (4)$$

The improvement of the maximum rate of climb due to the optimum deflection of the Fowler-type flap is approximately 40 ft. per min. as compared to the unflapped airplane. (Figs. 3a, 3b, and 3c.) It is evident that the optimum rate of climb is obtained with the comparatively small flap deflection of 15° and is attained at a lower air speed than with flaps retracted (74 instead of 80 m.p.h.). It should be noted that the rate of climb decreases over that of the unflapped airplane with flaps deflected at air speeds in excess of the optimum speed for that flap deflection.

The use of flaps requires, therefore, a more accurate flying technique than is warranted with flaps retracted.

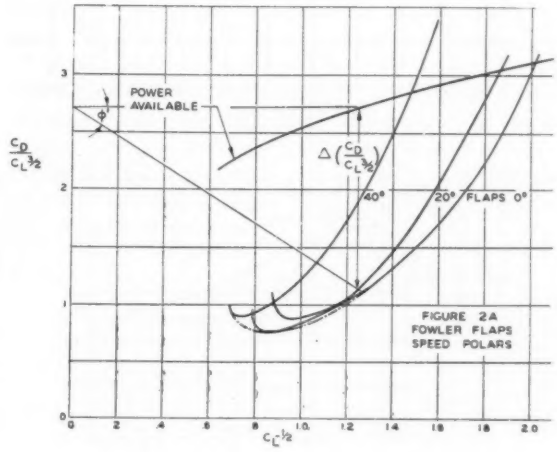

FIGURE 2A
FOWLER FLAPS
SPEED POLARS

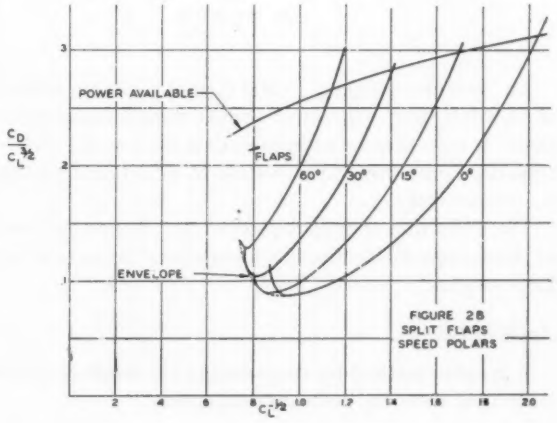

FIGURE 2B
SPLIT FLAPS
SPEED POLARS

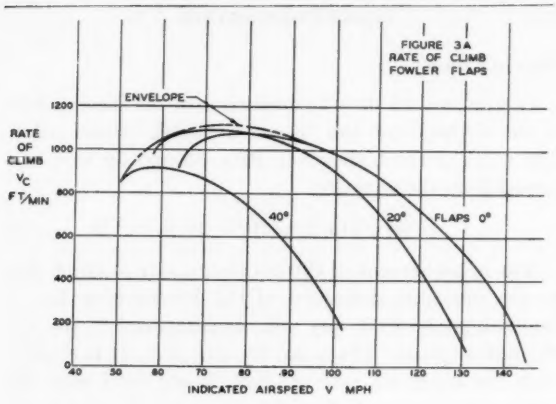

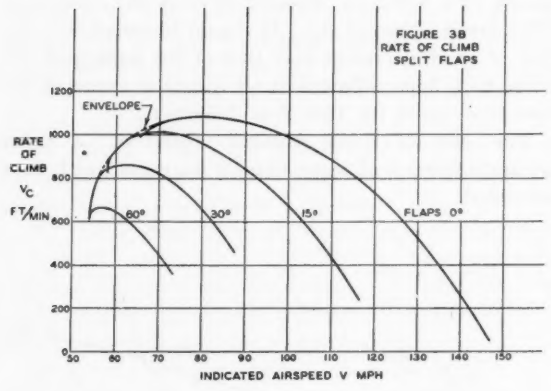

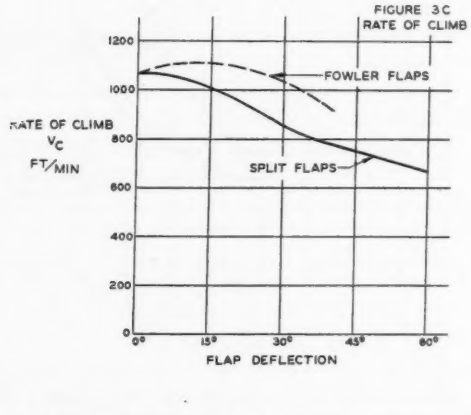

An absolute ceiling of 16,500 ft. and a service ceiling of 14,300 ft. were estimated[1] for the flaps-up configuration. It may then be estimated that the use of Fowler-type flaps may bring these values to 17,300 and 15,100 ft., respectively.

The deflection of split flaps does not change the rate of climb appreciably for small angles and reduces it for large angles.

Angle of Climb

A graphic method for determining the angle of climb is derived from the following expansion:

$$\sin\varphi = \frac{V_c}{V} = \frac{\sqrt{1/(\rho/2)}\sqrt{W/S}\,\Delta\,(C_D/C_L^{3/2})}{\sqrt{1\ (\rho/2)}\sqrt{W/S}C_L^{-1/2}} = \frac{\Delta(C_D/C_L^{3/2})}{C_L^{-1/2}} \qquad (5)$$

The method is illustrated in Fig. 2a, where the angle φ' is proportional to the angle of climb φ.

The increase of the angle of climb with the Fowler-type flap, and to a smaller degree with the split flap, is evident from Figs. 4a and 4b. It is also apparent, however, that excessive flap deflection reduces the angle of climb, especially if the airplane is flown too fast.

Take-Off Performance

Fig. 5 shows a comparison of the ground runs and take-offs over a 50-ft. obstacle with varying flap deflections for several values of the ground-friction coefficient μ. The usefulness of the wing flaps is found to increase with higher ground friction. This characteristic is of great importance in small airplanes which may, at times, be operated from sandy or soggy fields. Again, the Fowler-type flap is greatly superior to the split flap.

The curve of optimum ground runs, taken separately, has a particular importance for the possible operation of conventional light aircraft from the roofs of isolated, large factory and business buildings, where the take-off requirement is reduced to the mere lifting of the

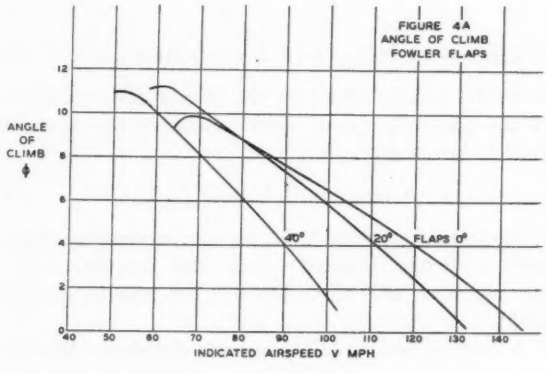

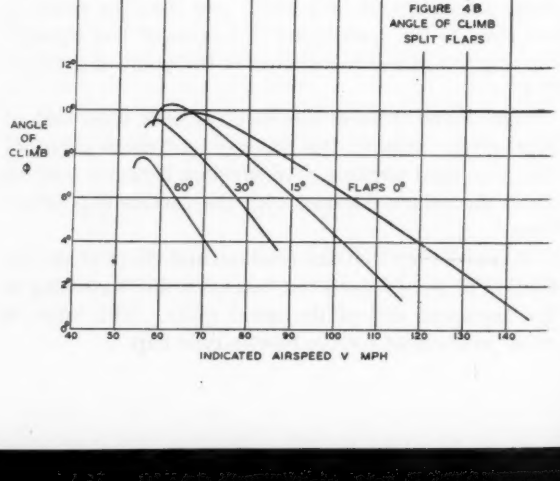

FIGURE 5
TAKE-OFF

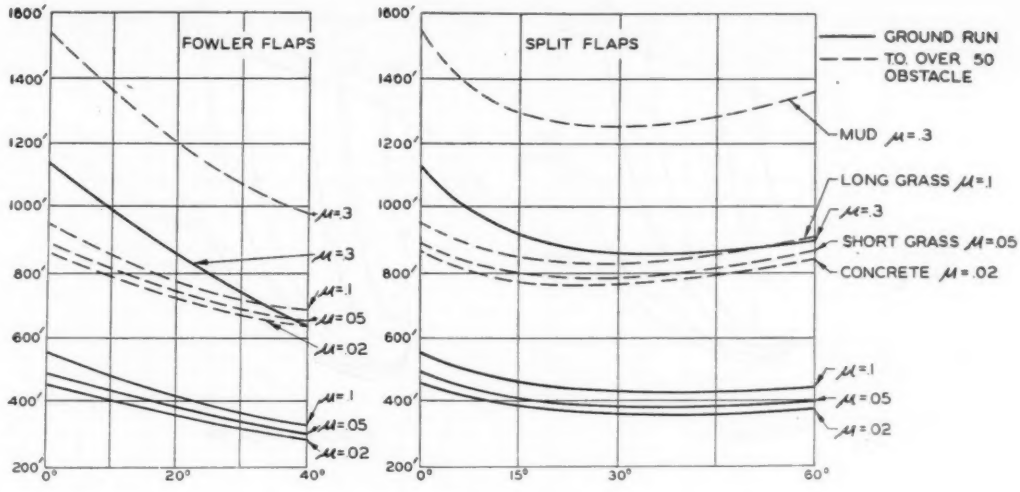

aircraft off the runway in the shortest possible distance.

Turning Performance

The power required for steady, level turning flight is:

$$(\text{t.hp.}_r)_R = \frac{1}{550}\sqrt{\frac{1}{\rho/2}}\sqrt{\frac{W}{S}}\,W\left(\frac{1}{\cos^{3/2}\theta}\right)\left(\frac{C_D}{C_L^{3/2}}\right) \quad (6)$$

where the angle of bank θ is defined by the following relation to the lift coefficient C_L and the radius of curvature R:

$$\tan\theta = \frac{V^2}{gR} = \left(\frac{1}{g}\right)\left(\frac{1}{\rho/2}\right)\left(\frac{W}{S}\right)\left(\frac{1}{C_L}\right)\left(\frac{1}{R}\right)\left(\frac{1}{\cos\theta}\right) \quad (7)$$

For a given turning radius R, therefore, the airplane (at a given altitude) flies at a certain angle of bank θ and absorbs the power $(\text{t.hp.}_r)_R$ depending upon the lift coefficient at which it is flown.

An analytic procedure to determine both the C_L (or air speed) and the angle of bank for minimum t.hp._r—that is, the most economical flying technique, for a given turning radius R—is quite complicated, and the following semigraphic procedure has been developed:

Eq. (6) can be rearranged to yield an effective value for $C_D/C_L^{3/2}$:

$$(C_D/C_L^{3/2})_e = (\text{t.hp.}_r)_R/\text{const.} = (C_D/C_L^{3/2})(1/\cos^{3/2}\theta) \quad (8)$$

and

$$\log\,(C_D/C_L^{3/2})_e = \log\,(C_D/C_L^{3/2}) - \log\,(\cos^{3/2}\theta) \quad (8a)$$

If the two terms on the right side of Eq. (8a) are plotted on a logarithmic scale, the vertical distances between the two curves show directly the values of $(C_D/C_L^{3/2})_e$—that is, the power required in nondimensional form as a function of $C_L^{-1/2}$ (Fig. 6).

Fig. 7 shows the curves of $(C_D/C_L^{3/2})_e$ for different radii of curvature, as compared to the power-available speed polar. For each radius of curvature a speed of maximum rate of climb can be found, as well as a speed of minimum power required (or minimum sinking speed); the limit radius for level flight at low level is a function of the maximum lift coefficient alone; at high altitude, the limit radius for level flight is determined from that equivalent speed-polar which is tangent to the power-available speed polar.

The numerical improvements shown in Fig. 7 indicate the superiority of the Fowler-type flap over the split flap.

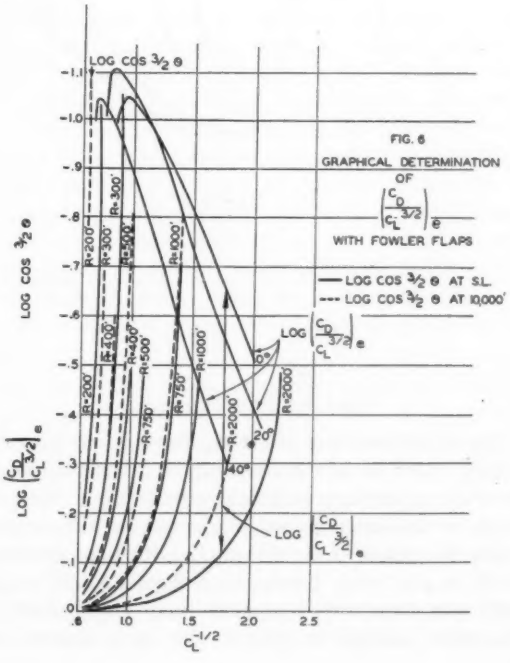

FIG. - 7A - TURNING PERFORMANCE AT SEA LEVEL

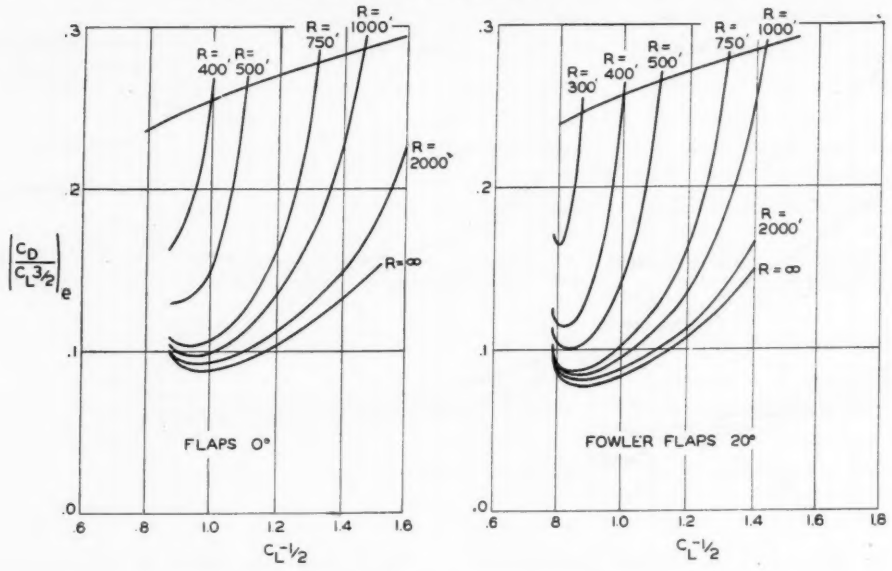

FIG. 7B - TURNING PERFORMANCE AT 10,000'

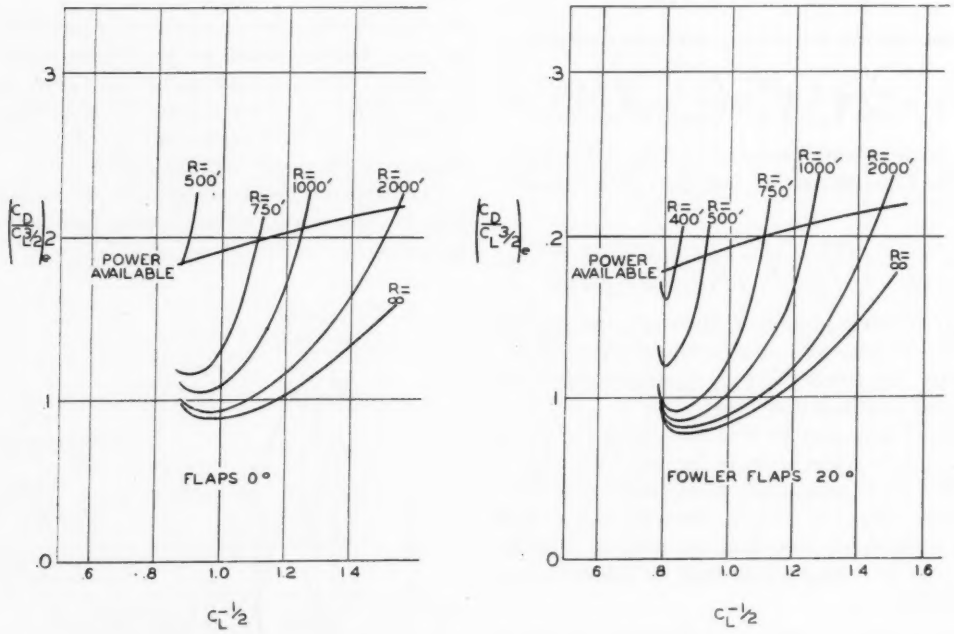

Landing Performance

The effectiveness of the wing flaps in reducing the stalling speed is not paramount in practical importance on an airplane with light wing loading. The decrease of the minimum stalling speed, on the airplane under discussion—from 64 m.p.h. with flaps retracted to 50 m.p.h. with Fowler-type flaps and 54 m.p.h. with split flaps fully extended—may not in itself be attractive enough to justify the complication and weight of a flap installation; nor does it offer sufficient information for the selection of the type of flap to be adopted.

The following consideration sheds some light on additional advantages offered by high-performance flaps during the landing.

The minimum sinking speed of the unflapped airplane at sea level is 560 ft. per min. With the optimum Fowler-flap setting of 20° this sinking speed is reduced

FIGURE 8
LANDING

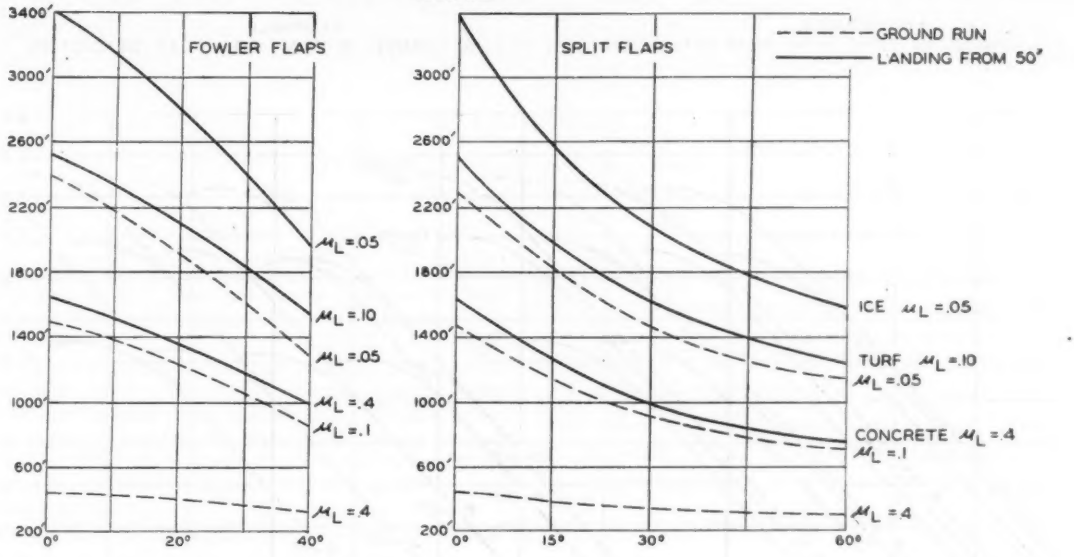

to 480 ft. per min. The air speed at which this minimum sinking speed is attained is simultaneously reduced from 73 to 62 m.p.h.

It may be noted that the maximum deflection of the Fowler-flap is not the optimum setting for the most gentle glide; it is also remarkable that the split flap reduces the air speed for minimum sinking speed but not the value of the minimum sinking speed itself.

The criterion of minimum sinking speed and of the air speed at which the minimum sinking speed is attained is significant for emergency landings in unfavorable conditions of visibility, at night and in foggy weather, when the airplane is to be flown to an unflared landing as gently as possible; the use of a nose-type tricycle landing gear is, of course, a necessary prerequisite for the full use of this flap characteristic.

It is, at times, contended in favor of the split flap that this device permits a steeper landing-approach glide and, hence, easier landings than the low-drag high-performance flap of the Fowler type. It is then said that the glide can be, at any time, "lengthened" by instantaneous retraction of the split flap. This method of flattening the glide, however, is considered unsatisfactory because the rapid retraction of the flap may reduce the maximum lift coefficient of the wing to a degree that is dangerous during a slow landing-approach glide. From many years of practical experience with similar devices on sailplanes and light powered aircraft, it has become apparent that the use of spoilers in conjunction with high-performance flaps is by far preferable. With the flaps set for minimum sinking speed and best rate of climb, the excessive length of the glide may then be reduced by the extension of the spoilers from the upper wing surface. When the need for flattening the glide arises, the spoilers are instantly retracted, and the high-lift and low-drag characteristics of the Fowler-type flap are at once available for a more efficient glide or, if necessary, for an optimum "wave-off" climb.

A comparison of the shortest landing distances is shown in Fig. 8. This is the only performance item in which the split flap attains results that are superior to those of the Fowler-type flap (without spoilers).

Stability and Control

The dynamic lateral stability is that stability characteristic of an airplane which is ordinarily changed most conspicuously by the deflection of wing flaps. The deflection of the flaps may produce changes in the two fundamental static stability derivatives affecting the dynamic stability—namely, the static directional stability derivative $dC_n/d\psi$ and the static directional rolling derivative $dC_l/d\psi$. The dihedral angle and the sweepback of the wing should be carefully chosen to obtain those values of the two aforementioned derivatives with flaps extended which will yield satisfactory dynamic lateral stability characteristics.

An important requirement for a flapped light airplane intended for the average private flier is that the trim C_L (or trim speed) for a given elevator angle is to be kept constant, regardless of flap deflection (Fig. 9). The size, aspect ratio, vertical and horizontal location, and angular setting of the horizontal tail are therefore not sufficiently determined by the desired amount of static longitudinal stability and longitudinal control but must be properly adjusted so that the change in down-wash caused by the flap deflection will produce

FIG. 9
PROPER & IMPROPER EMPENNAGE DESIGN

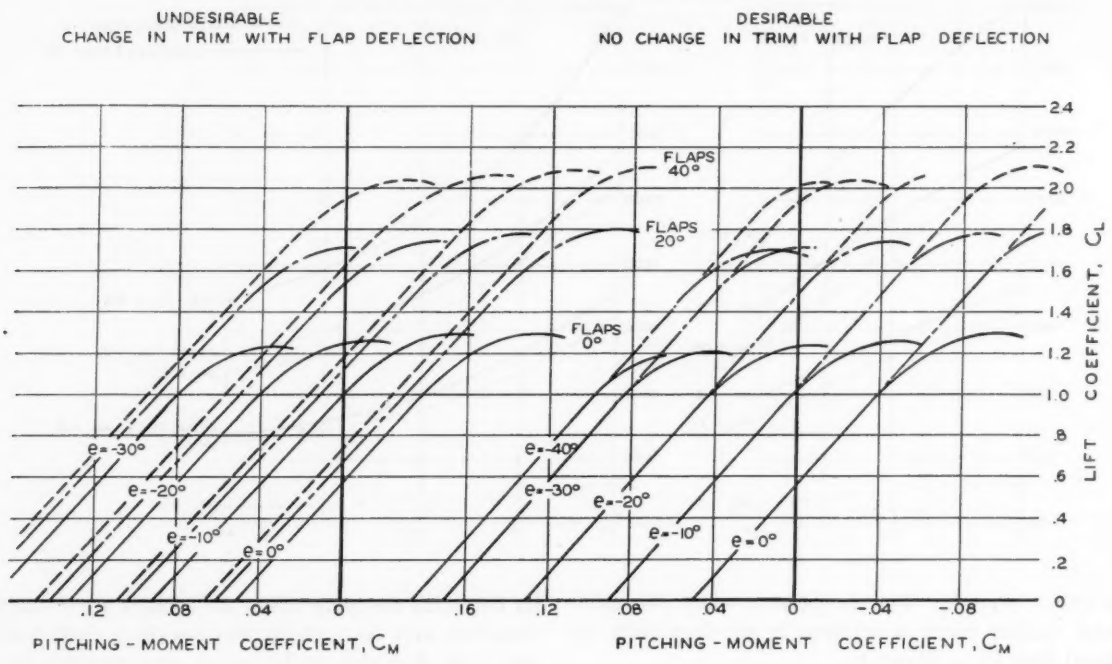

a balancing tail moment equal and opposite to the pitching moment due to the flaps. For this effect static wind-tunnel data alone are not fully sufficient. Flight tests are necessary to trace and eliminate any tendency toward even temporary changes of trim during sudden changes of power and other nonuniform flight conditions.

A nonprofessional pilot should not be expected to extend the flaps and to use simultaneously the elevator to retrim the airplane because of an unbalanced flap pitching moment; a constant trim C_L, with flaps retracted and extended and for any power setting, is greatly desirable to relieve the pilot of any additional control. Past experience in the automobilistic field has shown that the private buyer will not accept any device that even for a short time may change the manipulating characteristics of a vital control. In this respect it is believed that the designers will have to seek perfection far in excess of the comparatively lenient C.A.B. requirements.

The low flying speeds required for most efficient operation with high-performance flaps will necessitate the development of greatly efficient surface controls. Special attention must be paid to the aileron control; an aileron system may be fully satisfactory for normal flaps-up operation but may produce undesirable yawing-moment characteristics when used with flaps extended at low air speed. Proper attention should therefore be paid to the aerodynamic-kinematic requirements of low-speed operation.

Taxiing

The use of wing flaps on light airplanes increases the safety of ground operations in gusty weather. After a comparatively fast and steep glide with flaps extended and immediately upon contact with the ground, the pilot may retract the flap quickly (since the flap motions and control forces are small) and thus reduce the danger of "ballooning" in a subsequent gust substantially.

Conclusion

The installation of flaps on light aircraft is only justified if, in addition to lowering the stalling speed, they improve appreciably the take-off and landing performance and climb and turning characteristics of the aircraft over that without flaps. Only high-performance flaps are therefore justified, since other types of flaps, such as split flaps, may yield approximately the same stalling speed but do not adequately contribute to the improvement of the overall performance of the light airplane.

As a design problem, the flap must cease to be considered a mere accessory, but the entire wing and tail design must conform to the requirements of satisfactory stability and control with flaps retracted and extended.

Reference

[1] Oswald, B., *General Formulas and Charts for the Calculation of Airplane Performance*, N.A.C.A. T.R. No. 408, 1932.

A Note on Bending Beyond the Proportional Limit

M. YACHTER*

Brewster Aeronautical Corporation

ABSTRACT

Most theories of bending in the plastic range are based either upon the assumption of linear strain variation across the depth of the beam or by fitting some equation to the stress-strain curve.

In this paper the following problem is solved: Assuming the principle of minimum strain energy to be valid over the entire range of the stress-strain curve, find the exact stress distribution over the depth of a beam in pure bending (or combined bending and axial load, provided strain energy due to axial load and beam column effects are neglected) *compatible with equilibrium and minimum strain energy*.

Mathematically, this problem leads directly to a rather simple isoperimetric problem with variable limits in the calculus of variations. The solution leads to the construction of an auxiliary or generalized stress function, intimately connected with the actual stress through certain simple characteristics of the stress-strain curve (moduli ratios) and reducing to the actual stress for all values below the proportional limit. It is shown that the exact stress distribution, in the sense that it is compatible with equilibrium and minimum strain energy, is such that its associated generalized stress distribution is again *linear* across the depth of the cross section.

Once the associated generalized stress (as a curve vs. stress) has been determined from a given stress-strain curve, it is a comparatively easy matter to calculate maximum resisting moments for a given section on the basis of any limiting maximum fiber stress. Examples of such calculations for stainless steel and comparisons are given in the test.

SYMBOLS

S	=	stress, lbs. per sq.in.
$\epsilon = \epsilon(s)$	=	strain (as a function of stress), in. per in.
$\epsilon_m = \epsilon_m(s)$	=	modified strain (as a function of stress), in. per in.
E_0	=	straight-line modulus of elasticity, lbs. per sq.in.
$E_T = E_T(s)$	=	tangent modulus (as a function of stress) of modified stress-strain curve, lbs. per sq.in.
$E_s = E_s(s)$	=	secant modulus (as a function of stress) of modified stress-strain curve, lbs. per sq.in.
A, I, y	=	area, moment of inertia, and distance of fiber from c.g., respectively, corresponding to the original cross section of beam
$\bar{A}, \bar{I}, \bar{y}$	=	area, moment of inertia, and distance of fiber from c.g., respectively, as applied to the *reduced* cross section.
$\bar{r}$	=	distance from c.g. of original cross section to c.g. of reduced cross section, in.

Other symbols as well as those given above are defined as they occur in the text.

Dimensions are pounds and inches.

Received March 27, 1944.

* Stress Department. At present, Senior Research Engineer, Republic Aviation Corporation.

GENERAL RESULTS

SUPPOSE THAT THE CURVE marked "original" in Fig. 1 is a given stress-strain curve for a given material. At any point A on the original stress-strain curve, corresponding to a stress S and strain $\epsilon(s)$, let A_T be the area of the triangle $\overline{OAB}$ and A_c the corresponding area $\overline{OAB}$ under the original stress-strain curve. From the ratio $R = R(s) = A_c/A_T$. Evidently for stresses below the proportional limit $R = 1$, so that in general:

$$R(s) = (A_c/A_T) \geqq 1$$

Multiply the corresponding strain $\epsilon(s)$ by the above ratio and call this a modified strain $\epsilon_m = \epsilon_m(s) = R(s)\epsilon(s)$. A curve of S vs. $\epsilon_m(s)$ will be designated as a modified stress-strain curve. Since $R(s) \geqq 1$, we also have $\epsilon_m(s) \geqq \epsilon(s)$, so that the modified curve will appear as shown in Fig. 1.

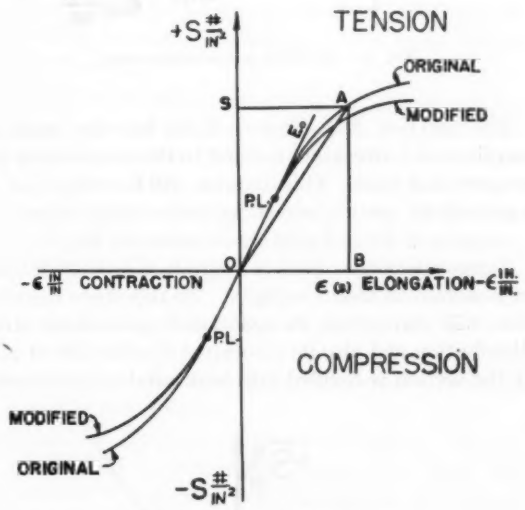

FIG. 1. Stress-strain curves.

Since the strain energy transferred to a fiber of unit area under a stress S is A_c, while $A_T = S\epsilon(s)/2$, we have:

Strain energy transferred to a fiber of unit area under

Stress $(S) = A_c = (A_c/A_T)\,A_T =$

$$R(s)(S\epsilon(s)/2 = S\epsilon_m(s)/2$$

That is: With respect to the modified stress-strain curve

the strain energy per unit area at stress S is given by $S\epsilon_m(s)/2$.

In Fig. 2, let $E_s = E_s(s) = \tan\beta$ and $E_T = E_T(s) = \tan\gamma$ be the secant modulus and tangent modulus, respectively, at point C of the modified stress-strain curve corresponding to the stress S and modified strain $\epsilon_m(s)$, while $E_0 = \tan\alpha$ is the original constant straight line modulus of the material below the proportional limit. Form the moduli ratios $E_0/E_s(s)$ and $E_0/E_T(s)$ and take the average:

$$\varphi(s) = {}^1/_2\{[E_0/E_s(s) + E_0/E_T(s)]\}$$

Obviously, $\varphi(s)$ is nondimensional and is equal to 1 below the proportional limit so that in general $\varphi(s) \geqq 1$.

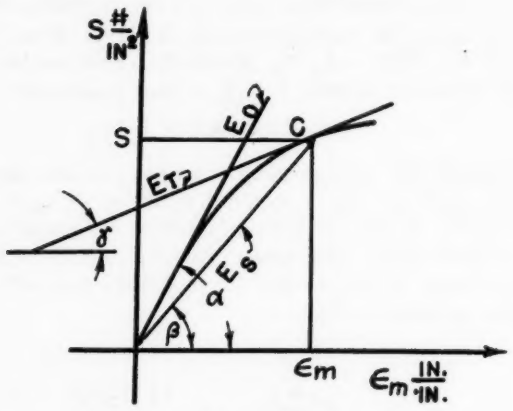

FIG. 2. Modified stress-strain curve.

The function $\bar{S} = \bar{S}(s) = S\varphi(s)$ has the same dimensions as a stress and is equal to the stress below the proportional limit. This function will be designated as a *generalized stress* as associated with a given stress.

A curve of $\bar{S}$ vs. S appears as shown on Fig. 3.

Suppose now that there is a certain stress distribution on a section as shown in Fig. 4. To this stress distribution will correspond its associated generalized stress distribution and also its associated distribution of $\varphi(s)$. If the section is divided into horizontal strips of small thickness Δy and the width of these strips is divided by their corresponding $\varphi(s)$, then all those strips whose corresponding stress is above the proportional limit will be *reduced* in width and the result will be a *reduced* cross section (shown by dotted lines in Fig. 4). This reduced section will have its own reduced area—$\bar{A}$, its reduced moment of Inertia—$\bar{I}$, and a new c.g. location. The distance of any fiber from this new c.g. will be designated by $\bar{y}$. In case the cross section is symmetrical about a horizontal axis and the stress-strain curves for tension and compression are identical, the c.g. does not move.

The complete solution of the problem, as proved in the theoretical part of this note, is given by the following theorem and its corollary.

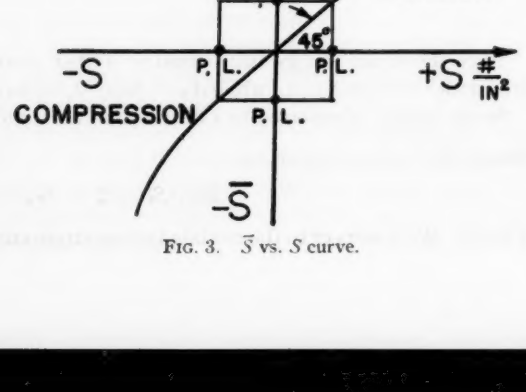

FIG. 3. $\bar{S}$ vs. S curve.

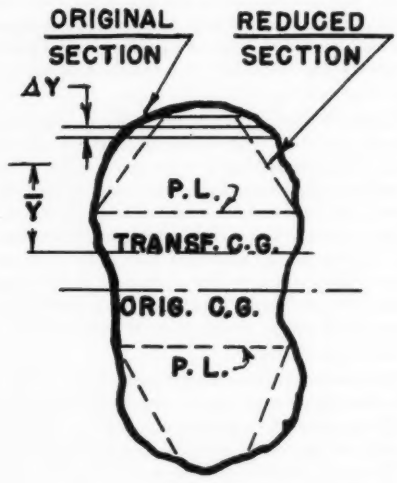

FIG. 4.

Theorem

The exact stress distribution S across the depth of the cross section, for pure bending, compatible with equilibrium and least work, is such that its associated generalized stress distribution

$$\bar{S} = \varphi(s)S = {}^1/_2[(E_0/E_s) + (E_0/E_T)]S$$

is *linear* across the depth of the actual cross section and, in the *reduced* section, is given by the generalized straight line formula:

$$\bar{S} = M\bar{y}/\bar{I}$$

Corollary

If in Fig. 3 the $\bar{S}$ scale is converted into a $\bar{y}$ scale with the c.g. of the reduced cross section at the origin and the maximum $\bar{y}$ corresponding to the maximum limiting fiber stress, then the actual stress distribution S across the depth is given by the curve $\bar{S}$ vs. S. For combined bending and axial loading, provided the beam-column effect is neglected and only bending energy is considered, it is proved later that:

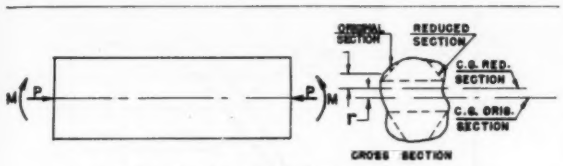

FIG. 5. Combined bending and axial load.

$$\bar{S}(s) = (P/A) + (\bar{M}\bar{y}/\bar{I})$$

where $\bar{M} = M - P\bar{r}$ and $\bar{r}$ is as shown in Fig. 5.

The procedure for the calculation of maximum resisting moments is as follows:

For a given material a curve of $\bar{S}$ vs. S for tension and compression is computed from the original stress-strain curve once and for all. Since in the process $\varphi(s)$ is also computed, it may also be drawn in as $\varphi(s)$ vs. S (see Fig. 6), although this is really not necessary.

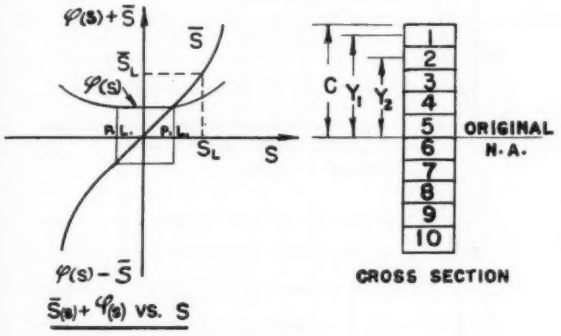

FIG. 6.

For a given cross section of the material, it is required to calculate the resisting bending moment so as not to exceed a certain maximum stress in the top (or bottom) fiber.

(A) First consider the simpler case in which the cross section is symmetrical about the original N.A. (normal axes) and the original stress-strain curves happen to be the same for tension and compression. In this case the c.g. of the section will remain in its original position. Let S_L be the desired limiting extreme fiber stress. Then, from Fig. 6, $\bar{S}_L$ will be its associated generalized stress. Since, by the theorem, $\bar{S}_L$ varies linearly across the depth of the section, the generalized stress at any other fiber is merely proportional to its distance from the c.g. (N.A.) and so is immediately determined. Hence, from Fig. 6 the corresponding actual stress at any fiber is also determined. Or, what amounts to the same thing, if the distance (C) (see Fig. 6) is laid off from the origin to $\bar{S}_L$ on the $\bar{S}$ ordinate, the curve $\bar{S}$ vs. S actually represents the stress distribution, where the stresses are read on the abscissa.

Now divide the cross section into a number of horizontal strips (comparative calculations show that ten strips are sufficient) calculate the areas of each strip and multiply by the stress corresponding to its midpoint. This gives the normal load Δp carried by each strip. Multiply these loads by their respective distances (of the midpoints) to the c.g. and sum. The result is the total resisting moment that the section can develop on the basis of a given maximum extreme fiber stress.

(B) In the general case, the cross section may not be symmetrical about the c.g. axis (i.e., the width may vary across the depth), the stress-strain curves may not be the same for tension and compression, and, finally, the section may even be composed of different materials. Hence, generally, the neutral axis (i.e., the c.g. axis of the reduced cross section) will shift. The location of the new neutral axis is determined by successive approximations as follows:

Assume a position of the N.A. to start with (say, at or near the original c.g. position). Divide the section into strips and calculate the strip loads (Δp) in the same manner as outlined in (A). If, by chance, the correct neutral axis location has been assumed then $\Sigma(\Delta p) = 0$; otherwise the next approximate N.A. location is $\bar{x} = \Sigma \Delta p / \Sigma \Delta p / \bar{y}$, where $\bar{x}$ is the distance from the assumed N.A. to the next approximate one and $\bar{y}$ is the distance from the assumed N.A. to any fiber (midpoint of strip). The N.A. moves toward the tension side if $\Sigma \Delta p$ is positive (tension) and toward the compression side if $\Sigma \Delta p$ is negative (compression), since $\Sigma \Delta p / \bar{y}$ is always positive. For proof of the above expression for $\bar{x}$ see "Proof of the Linearity of $\bar{S}$."

With regard to the location of the N.A., the following result will be proved in the section of this paper dealing with the theory.

If any N.A. location is assumed and the second approximation is toward the tension side, then the third approximation will be even further on the tension side, etc. The same holds, of course, in case the shifts are toward the compression side—that is, the N.A. locations are given by $\bar{x} = \Sigma \Delta p / (\Sigma \Delta p / \bar{y})$, each preceding result being used in the successive approximations, is, in general, a *monotonic convergent sequence* either *always* toward the tension side or *always* toward the compression side.

Because of the above result, another way of locating the N.A. axis is as follows:

Suppose the N.A. was assumed at Point A, Fig. 7, and the second approximation resulted in Point B. Now, instead of assuming Point B, suppose we assume Point C. In this case the third approximation may result either in Point F or in Point D. In the first case the N.A. must be above F, say at G, so that the choice of Point C instead of Point B was a step in the right direction.

In the second case, on the one hand, the N.A. must be below D and, on the other hand, it must be above B; hence it must be located somewhere between B and D, say at E. In either case, two trials will generally be sufficient to establish the N.A. with good accuracy. Finally, once the N.A. is located, the total resisting

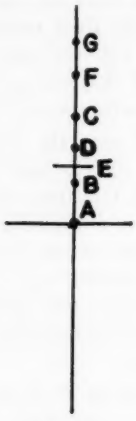

FIG. 7.

moment is calculated as outlined in (A) above for the symmetrical case.

For different tensile and compressive stress-strain curves the limiting extreme fiber stresses may also be different. Now for any maximum tensile fiber stress S_L its associated S_L is determined. For an assumed N.A. location, bearing in mind that S is linear, the maximum compressive S_L and, hence, the maximum compressive actual fiber stress is also determined. If this resulting stress is larger than the desired limiting compressive stress, then the latter will be the starting point in the calculations.

The problem treated so far deals with the determination of resisting moments of a section on the basis of desired limiting extreme fiber stresses. On the other hand, the reverse problem of finding the stress distribution due to a *given* moment cannot be treated in a direct manner. The only way in which it can be done is by trial and error—that is, a stress distribution is assumed and the resisting moment is calculated. If this is repeated, then the stress distribution for the given moment can be approximated by interpolation.

Numerical Results

The curves shown in Figs. 8, 9, and 10 are for corrosion resisting stainless steel; full hard, cold-rolled condition; and transverse direction. These curves have been calculated from the tangent moduli vs. stress curves for this material as given in Figs. 4–23 and 4–24 of reference 1.

Fig. (8) shows the original tensile and compressive strain curves and the *modified* compressive stress-strain curve. Fig. 9 shows $\bar{S}$ vs. S and $\varphi(s)$ vs. S for both tension and compression, while Fig. 10 is a combined or average tension-compression $\bar{S}$ vs. S curve.

The initial modulus of the material is 29×10^6 for both tension and compression. The proportional limit in tension is 54,000 lbs. per sq.in., while the tensile yield stress is 156,000 lbs. per sq.in. The proportional limit in compression is about 48,000 lbs. per sq.in. and the compressive yield stress is 180,000 lbs. per sq.in.

Resisting moments for a section of 1 by $1/4$ in., as shown in Fig. 11, have been computed on the basis of

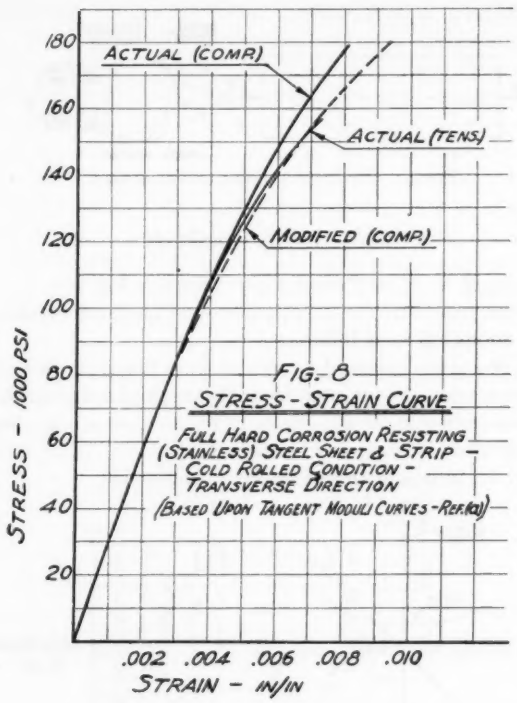

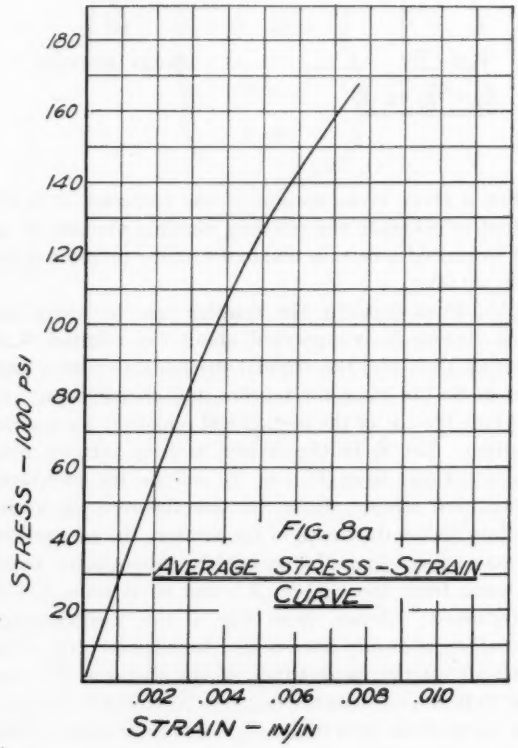

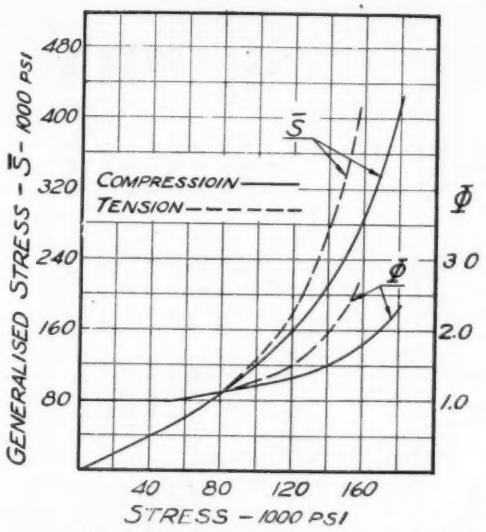

FIG. 9. Full-hard corrosion-resisting stainless-steel sheet and strip, cold-rolled condition, transverse direction.

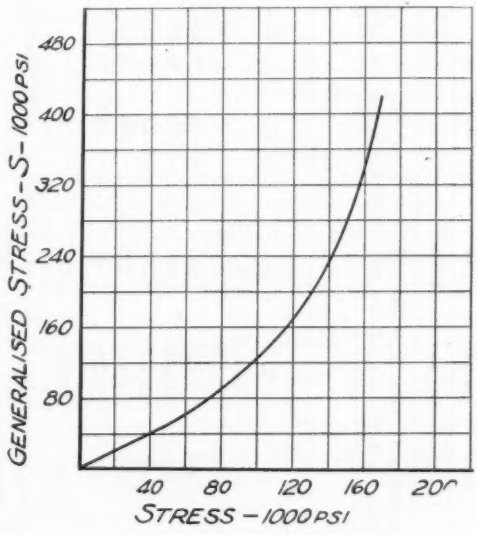

FIG. 10. Average $\bar{S}$ vs. S curve.

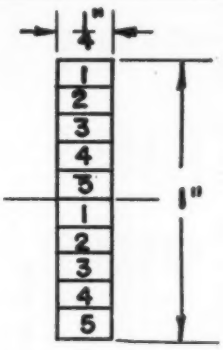

FIG. 11.

various limiting extreme fiber stresses and by the use of either the tension or compression stress-strain curve alone or both. Sample calculations are shown in Tables 1(a) and 1(b).

Table 2 shows results of other calculations of resisting moments on the basis of minimum strain energy, as well as on the basis of linear stress variation and linear strain variation.

From the results of Table 1(b) it will be seen that two trials are enough to determine the N.A. with good accuracy. But from the results it is also seen that, at least for a solid rectangular cross section, insofar as the resisting moment is concerned, the determination of the N.A. is really not important. For even though in the first trial (N.A. at c.g.) $\Sigma \Delta p$ involves a relative error of approximately 1,355/14,600 = 9.3 per cent, yet the error in the moment is only about (8,787 − 8,678/) 8,678 = 1.3 per cent. Further, if the average $\bar{S}$ vs. S curve (Fig. 10) is used, the error in total resisting moment is (8,842 − 8,678)/8,678 = 1.9 per cent. Thus, it is seen that within 1 to 2 per cent of error the average curve can be used to compute resisting moments and so the work is reduced to a minimum as in Table 1(a).

The ratios of moments on the basis of linear stress, linear strain and minimum energy (both curves used), are:

TABLE 1(a)

Symmetrical Case—Average $\bar{S}$ vs. S Curve (Fig. 10)

S_L = 168,000; $\bar{S}_L$ = 423,000 lbs. per sq.in.; ΔA of Strip = 0.1 (0.25) = 0.025
No Shift in N.A.

1 Strip	2 $\bar{y}$, in.	3 $\bar{S}$, lbs. per sq.in.	4 S, lbs. per sq.in.	5 Δp = (4) × 0.025	6 ΔM = (2) × (5)
1	0.45	380,000	163,500	4,090	1,840
2	0.35	296,000	151,500	3,782	1,322
3	0.25	211,700	133,000	3,321	830
4	0.15	127,000	100,200	2,504	376
5	0.05	42,300	42,300	1,058	53
Σ					4,421

M_{Total} = 2(4,421) = 8,842 in.lbs.

TABLE 1(b) Unsymmetrical Case—Both Tensile and Compressive $\bar{S}$ vs. S curves. S_L (Tension) = 156,000 lbs. per sq.in.; S_L (Comp.) = 180,000 lbs. per sq.in.

First Trial—N.A. at c.g.

	Tension							Compression						
1	2	3	4	5	6	7	8	9	10	11	12	13	14	15
Strip	$\bar{y}$	ΔA	$\bar{S}$	S	$\Delta p =$ (3) × (5)	$\Delta p/\bar{y} =$ (6)/(2)	ΔM	(2) × (6)$\bar{y}$	ΔA	$\bar{S}$	S	$\Delta p =$ (10) × (12)	$\Delta p/\bar{y} =$ (13)/(9)	$\Delta M =$ (13) × (9)
1	0.45	0.025	373,500	152,500	3,810	8,475	1,715	−0.05	0.025	− 41,500	− 41,500	− 1,040	20,800	52
2	0.35	0.025	291,000	142,000	3,550	10,150	1,241	−0.15	0.025	−124,500	−101,000	− 2,420	16,800	378
3	0.25	0.025	208,000	125,800	3,140	12,550	785	−0.25	0.025	−208,000	−138,000	− 3,450	13,800	862
4	0.15	0.025	124,500	97,000	2,420	16,100	363	−0.35	0.025	−291,000	−159,500	− 3,980	11,380	1,391
5	0.05	0.025	41,500	41,500	1,040	20,800	52	−0.45	0.025	−373,500	−173,000	− 4,325	9,610	1,948
Σ					13,960	68,075	4,156					−15,315	72,390	4,631

$\Sigma\Delta p = 13{,}960 - 15{,}315 = -1{,}355$; $\Sigma\Delta p/\bar{y} = 68{,}075 + 72{,}390 = 140{,}465$; $\bar{x} = -1{,}355/140{,}465 = -0.00966$; $M_{Total} = 4{,}156 + 4{,}631 = 8{,}787$ in.lbs.

Second Trial—N.A. at −0.025

	Tension							Compression						
1	2	3	4	5	6	7	8	9	10	11	12	13	14	15
Strip	$\bar{y}$	ΔA	S	S	$\Delta p =$ (3) × (5)	$\Delta p/\bar{y} =$ (6)/(2)	$\Delta M =$ (6) × (2)	$\bar{y}$	ΔA	$\bar{S}$	S	$\Delta p =$ (10 × (12)	$\Delta p/\bar{y} =$ (13)/(9)	$\Delta M =$ (13) × (9)
1	0.4625	0.0312	365,000	151,500	4,730	10,200	2,185	−0.025	0.025	− 39,500	− 39,500	− 986	19,730	49
2	0.35	0.025	276,500	139,500	3,485	9,970	1,220	−0.15	0.025	−118,500	− 97,500	− 2,435	16,210	365
3	0.25	0.025	197,500	122,800	3,065	12,260	766	−0.25	0.025	−197,500	−134,500	− 3,360	13,440	840
4	0.15	0.025	118,500	94,200	2,355	15,680	353	−0.35	0.025	−276,500	−156,200	− 3,905	11,130	1,367
5	0.05	0.025	39,500	39,500	986	19,730	49	−0.4375	0.01875	−346,000	−169,100	− 3,170	7,250	1,386
Σ					14,621	67,840	4,573					−13,856	67,760	4,007

$\Sigma\Delta p = 14{,}621 - 13{,}856 = +765$; $\Sigma\Delta p/\bar{y} = 67{,}840 + 67{,}750 = 135{,}600$; $\bar{x} = 795/135{,}600 = +0.00565$

Therefore, N.A. is between −0.00966 and −0.01935; $M_{Total} = 4{,}573 + 4{,}007 = 8{,}580$. N.A. average at −0.0145.

Third Trial—N.A. at −0.013

	Tension							Compression						
1	2	3	4	5	6	7	8	9	10	11	12	13	14	15
Strip	$\bar{y}$	ΔA	$\bar{S}$	S	$\Delta p =$ (3) × (5)	$\Delta p/\bar{y} =$ (6)/(2)	$\Delta M =$ (6) × (2)	$\bar{y}$	ΔA	$\bar{S}$	S	$\Delta p =$ (10) × (12)	$\Delta p/\bar{y} =$ (13)/(9)	$\Delta M =$ (13) × (9)
1	0.4565	0.02825	370,000	152,100	4,300	9,420	1,965	−0.05	0.025	− 40,500	− 40,500	− 1,011	20,220	51
2	0.35	0.025	283,500	140,800	3,520	10,040	1,230	−0.15	0.025	−121,200	− 99,000	− 2,475	16,500	371
3	0.25	0.025	202,200	124,100	3,102	12,410	775	−0.25	0.025	−202,200	−136,200	− 3,403	13,610	851
4	0.15	0.025	121,200	95,500	2,385	15,900	358	−0.35	0.025	−283,500	−157,900	− 3,940	11,230	1,378
5	0.05	0.025	40,500	40,500	1,011	20,220	51	−0.4435	0.02175	−359,000	−171,000	− 3,720	8,400	1,648
Σ					14,318	67,990	4,379					−14,549	69,960	4,299

$\Sigma\Delta p = 14{,}318 - 14{,}549 = -231$; $\Sigma\Delta p/\bar{y} = 67{,}990 + 69{,}960 = 137{,}950$; $x = -231/127{,}950 = -0.00168$; N.A. at −0.0147.

N.A. approx. at −0.0147+ = average of trials 2 and 3; $M_{Total} = 4{,}379 + 4{,}299 = 8{,}678$.

N.A. shift = approx. $1^1/_2$ per cent of depth of cross section.

TABLE 2

Resisting Moments—Comparative Results

Limiting Stresses → / Method ↓	S_L = 180,000, lbs. per sq.in.	S_L = 156,000	S_L = 156,000	S_L = 168,000	S_L = 156,000 (Tension) S_L = 176,000 (Compression)
Linear stress	7,500	6,500	6,500	7,000	6,500 (S_L = 156,000)
Linear strain	8,272 (compression curve)	6,912 (compression curve)	7,268 (tension curve)	7,725 (average curve)	7,340 (S_L = 164,000)
Minimum energy method	9,388 (compression curve only)	7,170 (compression curve only)	8,310 (tension curve only)	8,842 (average curve)	8,700 (both tension and compression curves)

NOTE: The above results, with the exception of the 8,842 figure, are based upon calculations not shown in this report.

minimum energy to linear stress = (133 per cent)
linear strain to linear stress = (113 per cent)
minimum energy to linear strain = (118 per cent)

Thus, the linear strain method yields results approximately midway between those given by the linear stress and minimum energy methods. If the average $\bar{S}$ vs. S curve is used and the limiting stress is taken as 168,000 for both linear stress and minimum energy, then the ratio of the resisting moments (minimum energy to linear stress), is 8,842/7,000 = 126 per cent.

It is easy to see that the above ratios will hold for all solid rectangular cross sections of the same material provided the same limiting stresses are kept. For an increase in either the width or the depth of the section will increase the resisting moments by the same factor irrespective of the methods used in computing the moments.

For other cross sections, such as I-beams, the corresponding ratios will be much smaller. For S_L above yield the ratios will be higher.

Fig. 12 reveals the behavior of bending in the plastic range. It is seen that the outside fibers are relieved by the inside fibers. This is even more sharply reflected in the notion of the reduced section which can be considered as one composed of layers of different materials. This is as it should be, for stressed elements with different moduli of elasticity *are* materially different.

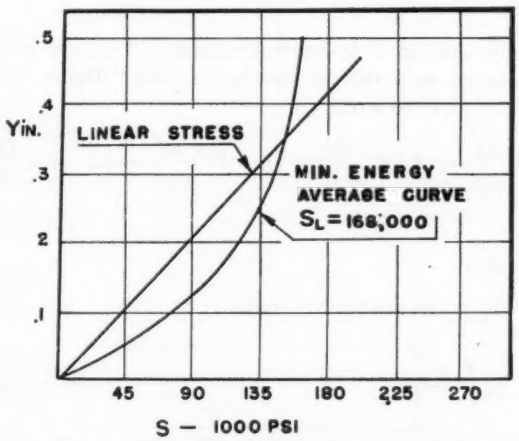

FIG. 12. Stress distribution—M_T = 8,842 in.lbs.

THEORY

Proof of the Linearity of $\bar{S}$

LET: $S = S(z)$ be the stress at a fiber at distance z from the reference axis (Fig. 13).

$\epsilon_m = \epsilon_m(s)$ = the modified strain corresponding to S as defined under "General Results."

$$dA = \omega(z)\, dz$$

(see Fig. 13). Then, for equilibrium, we have:

$$\oint S(z)\, dA = 0 \tag{1}$$

$$\oint S(z) z\, dA = M \tag{2}$$

where $\oint$ means integration throughout the section.

By the definition of ϵ_m, the strain energy transferred to the beam is:

$$W = {}^1/_2 \int_0^l \oint S(z)\epsilon_m(s)\, dA\, dx =$$

$$l/2 \oint S(z)\epsilon_m(s)\, dA \tag{3}$$

Without loss of generality we may write: $l/2 = 1$. Hence,

$$W = \oint S(z)\epsilon_m(s)\, dA \tag{4}$$

The problem is to determine a function $S(z)$ so as to make Eq. (4) a minimum without violating Eqs. (1) and (2), since equilibrium must always be satisfied.

This is a typical isoperimetric problem in the calculus of variations. Since there are no boundary conditions

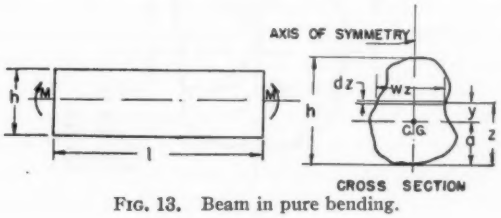

FIG. 13. Beam in pure bending.

N.A. approx. at −0.0147+ = average of trials 2 and 3; M_{Tavg} = 4,379 + 4,299 = 8,678.
N.A. shift = approx. 1½ per cent of depth of cross section.

for $S(z)$ at the limits (extreme fibers), the limits are variable. However, since in Eq. (4) the derivatives of $S(z)$ are not involved explicitly, the solution does not involve integration by parts as an intermediate step, so that the variable limits in this case do not require special consideration. Another result of the fact that the derivatives of $S(z)$ are not involved is that the solution, as shall presently be seen, leads in this case to a simple algebraic relation rather than to a differential equation.

Let $\eta(z) = \delta S(z)$ be an arbitrary small variation of $S(z)$. Then by the methods of the calculus of variations,[2] if λ_1 and λ_2 are undetermined multipliers, we have:

$$I(\alpha) = I[S(z) + \alpha\eta(z)] = \int_0^h \{[S(z) + \alpha\eta(z)]\epsilon_m(s + \alpha\eta) + \lambda_1[S(z) + \alpha\eta(z)]z + \lambda_2[S(z) + \alpha\eta(z)]\}\omega\, dz \quad (5)$$

so that:

$$0 = \frac{\delta I}{\delta\alpha} = \lim_{\alpha\to 0}\frac{I(\alpha) - I(0)}{\alpha} = \lim_{\alpha\to 0}\frac{1}{\alpha}\int_0^h \{[S(z) + \alpha\eta(z)][\epsilon_m(s) + \alpha\eta\epsilon_m'(s) + (\alpha\eta)^2\epsilon_m''(s) +] \ldots\ldots +$$
$$\lambda_1[S(z) + \alpha\eta(z)]z + \lambda_2[S(z) + \alpha\eta(z)] - [S(z)\epsilon_m(s) + \lambda_1 S(z)z + \lambda_2 S(z)]\}\omega\, dz \quad (6)$$

where $\epsilon_m'(s) = d\epsilon_m(s)/dS$; $\epsilon_m''(s) = d^2\epsilon_m(s)/dS^2$; etc.

In the limit, Eq. (6) reduces to:

$$\int_0^h \eta(z)[\epsilon_m(s) + S(z)\epsilon_m'(s) + \lambda_1 Z + \lambda_2]\omega(z)\, dz = 0 \quad (7)$$

Since $\eta(z)$ is arbitrary, while $\omega(z)$ is always positive, the integrand of Eq. (7) can always be made positive (or negative). Hence, Eq. (7) can be satisfied only if

$$\epsilon_m(s) + S(z)\epsilon_m'(s) + \lambda_1 z + \lambda_2 = 0 \quad (8)$$

Now, from the definitions of $E_s(s)$ and $E_T(s)$,

$$\epsilon_m'(s) = \frac{1}{E_T(s)}, \quad \frac{\epsilon_m(s)}{S} = \frac{1}{E_s(s)} \quad (9)$$

Hence, if

$$\varphi(s) = \tfrac{1}{2}\{[E_0/E_s(s)] + [E_0/E_T(s)]\} \quad (10)$$

then Eq. (8) reduces to:

$$\bar{S}(z) = \varphi(s)S(z) = -(E_0/2)(\lambda_1 z + \lambda_2) \quad (11)$$

Since λ_1 and λ_2, although as yet undetermined, are nevertheless constants, Eq. (11) states that *the generalized stress varies linearly across the depth of the cross section*, which was to be proved.

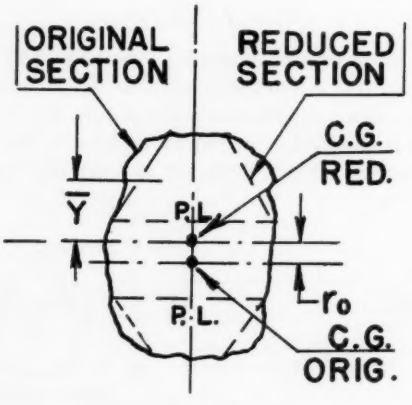

FIG. 14.

Proof of the Relationship

$$\bar{S} = M(\bar{y}/\bar{I})$$

From Eq. 11 we get:

$$S(z) = -\tfrac{1}{2}[E_0/\varphi(s)](\lambda_1 z + \lambda_2) \quad (12)$$

or writing

$$z = y + a \quad (13)$$

(see Fig. 13). Eq. (12) becomes:

$$S(y) = -\tfrac{1}{2}[E_0/\varphi(s)][\lambda_1(y + a) + \lambda_2] \quad (14)$$

Substituting Eq. (14) into Eq. (1),

$$\mathcal{F}\{[\lambda_1(y + a) + \lambda_2]/\varphi(s)\}dA = 0 \quad (15)$$

By the use of Eq. (15) and substitution of Eq. (14) into Eq. (2),

$$\mathcal{F}\frac{[\lambda_1(y + a) + \lambda_2]y}{\varphi(s)}\, dA = -\left(\frac{2}{E_0}\right)M \quad (16)$$

Since $\varphi(s) \geqq 1$ is nondimensional, $dA/\varphi(s)$ may be regarded as a *reduced* element of area. Hence, it is appropriate to write:

$$\mathcal{F}\frac{dA}{\varphi(s)} = \bar{A}; \ \mathcal{F}\frac{y\, dA}{\varphi(s)} = \bar{Q}_0; \ \mathcal{F}\frac{y^2\, dA}{\varphi(s)} = \bar{I}_0; \ \bar{r}_0 = \frac{\bar{Q}_0}{\bar{A}} \quad (17)$$

so that:

$\bar{A}$ = area of reduced section

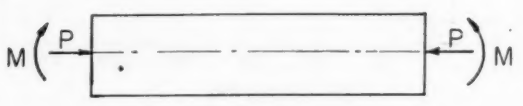

FIG. 15.

$\bar{Q}_0$ = static moment of reduced section about the *original* c.g. axis

$\bar{I}_0$ = moment of inertia of reduced section about the original c.g. axis

$\bar{r}_0$ = distance between c.g. of reduced section and original c.g.

For a symmetrical cross section and identical tensile and compressive stress-strain curves, the c.g. of the reduced section is identical with the original c.g., so that in this special case

$$\bar{Q}_0 = \bar{r}_0 = 0$$

In terms of the quantities defined above, we have from Eqs. (15) and (16):

$$\left.\begin{aligned} \lambda_1(a\bar{A} + \bar{Q}_0) + \lambda_2\bar{A} &= 0 \\ \lambda_1(a\bar{Q}_0 + \bar{I}_0) + \lambda_2\bar{Q}_0 &= -(2/E_0)M \end{aligned}\right\} \quad (18)$$

From Eq. (18):

$$\lambda_1 = -\left(\frac{2}{E_0}\right)M\left(\frac{1}{\bar{I}_0 - \bar{r}_0\bar{Q}_0}\right) = -\left(\frac{2M}{E_0}\right)\left(\frac{1}{\bar{I}_0 - \bar{A}\bar{r}_0^2}\right) = -\left(\frac{2}{E_0}\right)\left(\frac{M}{\bar{I}}\right) \quad (19)$$

where $\bar{I} = \bar{I}_0 - A\bar{r}_0^2$ is the moment of inertia of the *reduced* cross section about *its own* c.g. axis, and

$$\lambda_2 = (2/E_0)(M/\bar{I})(a + \bar{r}_0) \quad (20)$$

Substituting Eqs. (19) and (20) into Eq. (14),

$$S(y) = (1/\varphi(s))(M/\bar{I})(y - \bar{r}_0) \quad (21)$$

or $\bar{y}$ if $= y - \bar{r}_0$ is the distance from the c.g. of the *reduced section* to any fiber, Eq. (21) reduces to:

$$S(\bar{y}) = (1/\varphi(s))(M\bar{y}/\bar{I}) \quad (22)$$

So that, finally,

$$\bar{S}(\bar{y}) = S(\bar{y})\varphi(s) = M\bar{y}/\bar{I} \quad (23)$$

Combined Bending and Axial Load

The results to be derived are based upon the following two approximations:

(1) Energy due to axial load is neglected as compared to the bending strain energy.

(2) Beam-column effects are neglected. Without loss of generality, we may also work with a reference axis passing through the c.g. of the original section.

The theory is analogous to the pure bending case, so that in place of Eqs. (1), (2), and (14) we have:

$$\left.\begin{aligned} \oint S(y)\,dA &= P \\ \oint S(y)y\,dA &= M \end{aligned}\right\} \quad (24)$$

$$S(y) = -(E_0/2)[(\lambda_1 y + \lambda_2)/\varphi(s)] \quad (25)$$

Substitution of Eq. (25) into Eq. (24) results in:

$$\left.\begin{aligned} \lambda_1\bar{Q}_0 + \lambda_2\bar{A} &= -(2/E_0)P \\ \lambda_1\bar{I}_0 + \lambda_2\bar{Q}_0 &= -2(/E_0)M \end{aligned}\right\} \quad (26)$$

Solving Eq. (26) for λ_1 and λ_2 and simplifying results in:

$$\begin{aligned} \lambda_1 &= -(2/E_0)(\bar{M}/\bar{I}) \\ \lambda_2 &= (2/E_0)[(\bar{M}\bar{r}_0/\bar{I}) - (P/\bar{A})] \end{aligned} \quad (27)$$

where $\bar{M} = M - P\bar{r}_0$ is the moment about the c.g. axis of the *reduced* section. Substituting Eq. (27) into Eq. (25) and simplifying by the use of $\bar{y} = y - \bar{r}_0$,

$$S(\bar{y}) = [1/\varphi(s)][(P/\bar{A}) + (\bar{M}\bar{y}/\bar{I})] \quad (28)$$

or, finally,

$$\bar{S}(\bar{y}) = S(\bar{y})\varphi(s) = (P/\bar{A}) + (\bar{M}\bar{y}/\bar{I}) \quad (29)$$

To prove:

$$\bar{x} = \Sigma\Delta p/\Sigma(\Delta p/\bar{y})$$

Suppose that the c.g. of the reduced section is assumed to be at A (Fig. 16). Then

$$\bar{x} = \frac{\Sigma\bar{y}\Delta\bar{A}}{\Sigma\Delta\bar{A}} = \frac{\Sigma\bar{y}(\Delta A/\varphi(s))}{\Sigma(\Delta A/\varphi(s))} = \frac{\Sigma\bar{y}(S\Delta A/\bar{S})}{\Sigma(S\Delta A/\bar{S})}$$

since $\varphi(s) = \bar{S}/S$.

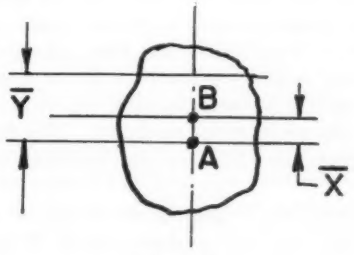

FIG. 16.

Now, since $\bar{S}$ is linear and must pass through the c.g. of the reduced section, we may write $\bar{S} = k\bar{y}$; also $S\Delta A = \Delta p$ (i.e., the strip loading). Substituting the above results into the expression for $\bar{x}$, we immediately get the result:

$$\bar{x} = \frac{\Sigma(\bar{y}\Delta p/k\bar{y})}{\Sigma(\Delta p/k\bar{y})} = \frac{\Sigma\Delta p}{\Sigma(\Delta p/\bar{y})} \quad (30)$$

To show the N.A. locations by the use of $\bar{x} = \Sigma\Delta p/\Sigma(\Delta p/\bar{y})$ in successive steps represent a monotonic sequence, consider Fig. 17. The line 13–16 is the $\bar{S}$ line and the curve 11–14 is the corresponding S curve on the basis of a limiting stress S_L given by 11–19: The $\bar{S}$ and S curves pass through an assumed N.A. location at point 1. The proportional limits are at points 6 and 9.

Suppose now that the curve 11–14 leads to the next N.A. location at point 2. Then the next $\bar{S}$ line, on the basis of the same limiting stress S_L is 13–18 and the corresponding S curve is 10–15, with the proportional limits at points 7 and 8. It is thus seen that on the tension side between points 2 and 19 the stresses, with the N.A. at point 2, will be less than those corresponding to the N.A. at point 1. Hence, the widths of the reduced section for the case of the N.A. at point 2 will

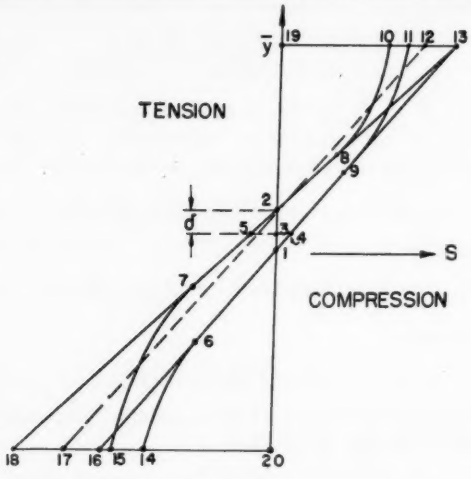

FIG. 17.

be *larger* than, or equal to, the corresponding widths of the reduced section for the N.A. location at point 1. By the same reasoning the widths of the reduced section on the compression side between points 3 and 20 (where 3–4 = 3–5) will be *less* than, or equal to, the corresponding widths for the N.A. location at point 1. As for the widths between 2 and 3 (δ), in general they fall within the linear range as shown. This being so, it follows that the next N.A. location must be above point 2.

Suppose that the δ range is not wholly in the linear range. Even then the tendency of the N.A. to shift upward can be counteracted only if the material concentrated in the range is relatively large as compared to the rest of the section. But in this case it follows from the formula for $\bar{x}$ that if point 1 is at the c.g. of the section then point 2 will move only a small distance, so that the δ strip will tend to be in the linear range. Although this point is not proved with complete mathematical rigor, it can be disregarded for all practical purposes.

Now, if we assumed that point 2 is below point 1, then, by analogous reasoning, it can be shown that the next N.A. location would move even further down.

Finally, it may happen that in the second approximation the stress 16–20 is above the compressive stress limit. Then the next S line would be, say, 12–17. However, it will be seen immediately that this does not change the results arrived at above.

Thus, the N.A. locations tend to move *always* in the same direction, up or down—that is, the N.A. locations by successive approximations form a monotonic sequence, which was to be proved.

Strictly speaking, the vanishing of the first variation of the strain energy integral leads to *either* a minimum or a maximum. Hence, even though it is clear from consideration of the limiting case when the stresses are in the linear range, that the first variation leads to a minimum, nevertheless from a somewhat more rigorous mathematical standpoint, it must be proved that the strain energy is actually a minimum by considering the second variation.

By the methods of the calculus of variations, we have, from Eq. (7),

$$I'(0) = \int_0^h \eta(z)\{\epsilon_m(s) + S(z)\epsilon_m'(s) + \lambda_1 z + \lambda_2\}\omega(z)\,dz \tag{31}$$

Hence,

$$\left.\begin{aligned} &I''(0) = \lim_{\beta\to 0}\frac{1}{\beta}\int_0^h [\eta(z)\{\epsilon_m(s+\beta\eta) + (S(z)+\beta\eta(z))\epsilon_m'(s+\beta\eta) + \lambda_1 z + \lambda_2\} - \\ &\eta(z)\{\epsilon_m(s) + S(z)\epsilon_m'(s) + \lambda_1 z + \lambda_2\}]\omega(z)\,dz = \lim_{\beta\to 0}\frac{1}{\alpha}\int_0^h \eta(z)\omega(z)\{\epsilon_m(s) + \beta\eta\epsilon_m'(s) + \ldots\ldots + S(z)\epsilon_m'(s) + \\ &S(z)\beta\eta\epsilon_m''(s) + \ldots\ldots + \beta\eta\epsilon_m'(s) + \ldots\ldots + \lambda_1 z + \lambda_2 - \epsilon_m(s) - S(z)\epsilon_m'(s) - \lambda_1 z - \lambda_2\}dz = \\ &\lim_{\beta\to 0}\frac{1}{\beta}\int^h \beta\eta^2(z)\omega(z)\{\epsilon_m'(s) + \ldots\ldots + S(z)\epsilon_m''(s) + \ldots\ldots + \epsilon_m'(s) + \ldots\ldots + \text{terms in powers of } \beta\}dz \\ &\longrightarrow \int_0^h \eta^2(z)\{S(z)\epsilon''(s) + 2\epsilon_m'(s)\}\omega(z)\,dz = \int_0^h \eta^2(z)\left\{S(z)\left(\frac{d}{dS}\right)\left[\frac{1}{E_T(s)}\right] + \left[\frac{2}{E_T(s)}\right]\right\}\omega(z)\,dz = \\ &\int_0^h \eta^2(z)\left(\left[\frac{2}{E_T(s)}\right] - \left\{\frac{S(z)}{[E_T(s)]^2}\right\}\left[\frac{dE_T(s)}{dS}\right]\right)\omega(z)\,dz = \int_0^h \frac{2\eta^2(z)}{E_T(s)}\left\{1 + \frac{1}{2}\left[\frac{S(z)}{E_T(s)}\right]\left[-\frac{dE_T(s)}{dS}\right]\right\}\omega(z)\,dz \end{aligned}\right\} \tag{32}$$

But $[S/E_T(s)]\,[-dE_T(s)/dS] > 0$ for all values of S. Hence, since all other quantities in the integrand of Eq. (32) are also positive, $I''(0) > 0$. Therefore the solution actually leads to a minimum.

CONCLUSION

It has been shown that on the basis of the extension of the principle of strain energy beyond the elastic

(*Continued on page 84*)

Mechanical Properties of Magnesium-Alloy Tubing

R. T. SCHWARTZ* AND G. M. MARTELL†
Air Technical Service Command

SUMMARY

This paper presents the mechanical properties of extruded round, seamless magnesium-alloy tubing, containing 6.55 per cent aluminum, 1.04 per cent zinc and 0.30 per cent manganese, which analysis is similar to that for Dowmetal J and AMC 57S. The tubing was characterized by a low ratio of proportional limit to ultimate strength in tension and a low proportional limit and yield strength in compression compared to those in tension. The tensile and compressive testing presented certain difficulties because of low shear resistance and sensitivity of the material to stress concentration. The marked difference between the stress-tangent modulus data for tension and compression and the correlation of the latter with column properties for knife-edge and flat end conditions are emphasized. Torsional properties were also determined.

Although the tests were made a few years ago, the data still are believed to reflect, in general, the characteristics of the wrought and extruded magnesium alloys of high tensile strength, and it is believed that the data are of value to illustrate certain characteristics typical of these alloys for aircraft structural applications, as well as to point out some of the difficulties of testing.

INTRODUCTION

THE INCREASING INTEREST and attention being paid to the use of magnesium alloys for structural components in aircraft demands a knowledge of their mechanical properties. Available data on the stress-strain characteristics and other mechanical properties of magnesium alloys are, in general, meager. Tensile, compressive, crushing, column and tension tests on commercial magnesium-alloy tubing were therefore undertaken.

MATERIAL

Round, seamless, magnesium-alloy tubings, of the nominal sizes given in Table 1 and varying in outside diameters from $^3/_4$ to $3^1/_2$ in. and in wall thickness from 0.042 to 0.400 in., were procured from the Aluminum Company of America. The tubing conformed to Army Air Forces Specification No. 11332, dated July 14, 1942, formerly Grade I, Specification No. 11318. This specification requires the following minimum tensile properties:

Tensile Strength, Lbs. per Sq.In.	Yield Strength at 0.002 In. per In. Offset, Lbs. per Sq.In.	Elongation in 2 In., Per Cent
36,000	17,000	7

Received June 22, 1944.

* Wright Field.

† Formerly with Army Air Forces Matériel Command, Wright Field.

The chemical analysis specified together with that determined on the tubing was:

Element:	Al	Mn	Zn	Ni	Cu	Fe	Si	Other Impurities	Mg
Specification:	5.8–7.2	0.15 min.	0.4–1.5	0.005 max.	0.05 max.	0.005 max.	0.30 max.	0.30 max.	Balance
Tubing:	6.55	0.30	1.04	<0.005	<0.05	<0.005	<0.30	<0.30	Balance

The tubing was produced by extrusion, using presses and conventional dies. During the extrusion operation, a mandrel fits into the center of the hollow cylindrical billet and travels forward into the plane of the die to form the inside diameter of the tubing. The thickness of the tubing walls was within specification limits.

PROCEDURE

Thirty-one different tubes were tested. These were cleaned thoroughly inside and out, weighed, the lengths measured, and the areas calculated from measurements of length, weight, and average density of 0.0652 lb. per cu.in. The latter value was determined by weighing

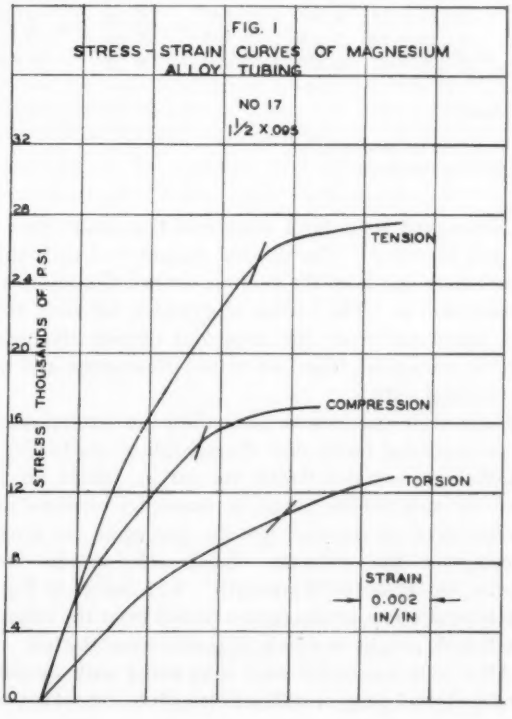

TABLE 1

Tensile Properties of Magnesium-Alloy Tubing

Spec. No.	Nominal Size, In.	Actual Size, In.	Modulus of Elasticity $\times 10^{-6}$, Lbs. per Sq.In.	Prop. Limit Tangent, Lbs. per Sq.In.	Prop. Limit 0.01% Offset, Lbs. per Sq.In.	Yield Strength 0.2% Offset, Lbs. per Sq.In.	Ultimate Strength, Lbs. per Sq.In.	Elongation in 2 In., Per Cent	Vickers Pyramidal No., 10 Kg
1	3/4 by 0.042	0.7795 by 0.0444	6.10	9,100	11,600	25,000	40,980	11.5	62.4
2	3/4 by 0.042	0.785 by 0.0422	6.20	9,000	13,750	29,300	42,020	14	64.5
3	3/4 by 0.042	0.775 by 0.0432	6.17	10,000	13,800	28,300	41,670	11	62.9
4	3/4 by 0.042	0.785 by 0.0423	6.17	9,500	12,550	26,600	42,640	16	61.6
5	3/4 by 0.042	0.785 by 0.0432	6.36	9,500	13,200	28,600	42,870	14	64.6
6	1 by 0.042	0.955 by 0.0420	6.05	11,200	15,000	28,200	43,060	12.5	63.9
7	1 by 0.065	1.055 by 0.0625	6.13	10,750	13,050	23,000	40,350	13	60.9
8	1 by 0.095	1.065 by 0.0913	6.21	8,600	12,330	24,700	40,540	12.5	59.7
9	1 1/2 by 0.042	1.495 by 0.0410	5.92	6,100	12,350	25,500	40,890	15	61.1
10	1 1/2 by 0.042	1.494 by 0.0393	6.27	7,900	10,750	20,400	41,220	13	56.3
11	1 1/2 by 0.042	1.494 by 0.0395	6.06	8,500	13,800	24,700	39,330	11	61.5
12	1 1/2 by 0.042	1.494 by 0.0379	5.90	8,500	10,850	21,600	40,100	12	61.8
13	1 1/2 by 0.065	1.500 by 0.0655	5.87	12,500	14,950	25,100	41,030	15	63.9
14	1 1/2 by 0.065	1.500 by 0.0655	6.17	10,900	13,950	25,000	40,960	12.5	61.1
14	1 1/2 by 0.065	1.500 by 0.0655	...	....	....	....	29,000	5.0*	61.1
15	1 1/2 by 0.095	1.516 by 0.0940	5.90	11,600	14,500	26,200	42,230	15	63.2
16	1 1/2 by 0.095	1.504 by 0.0945	5.95	11,500	14,250	26,400	42,910	15	62.8
17	1 1/2 by 0.095	1.505 by 0.0970	6.17	9,700	13,300	25,300	40,020	11	61.1
18	1 1/2 by 0.148	1.489 by 0.1490	6.20	10,800	18,600	34,800	42,820	8.5	79.6
19	1 1/2 by 0.148	1.492 by 0.1473	5.98	13,400	18,500	32,420	41,600	9	75.5
20	1 1/2 by 0.148	1.503 by 0.1461	5.97	11,000	13,100	23,700	41,750	14.5	60.3
30	1 1/2 by 0.148	1.504 by 0.1466	...	....	....	....	34,200	7.0*	67.7
30	1 1/2 by 0.148	1.504 by 0.1466	6.05	10,750	13,550	22,700	43,220	13.5	67.7
31	1 1/2 by 0.148	1.503 by 0.1461	6.03	10,800	13,450	22,600	38,830	10.5	66.0
21	2 1/2 by 0.095	2.523 by 0.0989	5.96	7,800	9,580	18,600	42,680	20.5	59.7
22	2 1/2 by 0.095	2.521 by 0.100	6.08	7,750	9,430	18,400	41,640	17.5	60.7
23	2 1/2 by 0.095	2.521 by 0.100	5.90	8,500	9,430	22,500	42,030	20.0	77.4
24	2 1/2 by 0.095	2.521 by 0.0995	6.05	11,300	13,400	22,600	36,920	9.5	64.1
25	2 1/2 by 0.32	2.511 by 0.3247	6.35	9,750	13,950	27,600	43,950	13.5	62.9
26	3 1/2 by 0.125	3.500 by 0.125	6.30	9,100	12,050	24,580	41,750	10.5	67.9
27	3 1/2 by 0.125	3.510 by 0.125	6.13	9,050	11,800	24,500	41,810	10.5	65.3
28	3 1/2 by 0.125	3.500 by 0.125	6.38	9,050	11,950	24,200	42,500	15.0	63.2
29	3 1/2 by 0.40	3.500 by 0.400	6.12	11,650	15,175	25,800	38,050	5.0†	70.6
Average			6.10	9,860	13,160	25,130	41,370	13.0	64.3

* Fracture at flaw in tube.

† Fracture at grips.

specimens cut from both thick and thin wall tubes in air and in water. The outside diameter of each tube was determined from the average of several micrometer measurements. The radius of gyration for each tube was calculated from the area and outside diameter. All test values are based on actual dimensions and not on nominal sizes.

Large-scale graphs were plotted for the determination of proportional limits and the moduli of elasticity, in which 1 in. equaled 0.0001 in. per in. strain on the abscissa, and 200 lbs. per sq.in. stress, for torsional and compressive curves, and 500 lbs. per sq.in. for tensile curves, on the ordinate. Small-scale graphs were plotted to obtain yield strength. The curves in Fig. 1 are typical stress-strain curves traced from the original small scale graphs in which all points were plotted.

All tensile specimens were snug-fitted with specially modified steel plugs of sufficient length to extend beyond the edge of the grips. Deformation for each tube was measured with two 1-in. Tuckerman optical strain gauges, diametrically opposed at the center of the tube. Sufficient length was allowed between grips to minimize any effects on the deformation readings.

Compressive data were obtained on specimens with a L/R, or slenderness ratio, of approximately 11,[1,2] with ends machined parallel to each other and perpendicular to the axis of the specimen and direction of loading. All specimens were mounted with the ends in Woods' metal contained in brass rings and the ends extended slightly through the Woods' metal. No correction was made for the mounted ends on the slenderness ratio. Tests on the 3/4- and 1-in. tubing were made in a special compression jig, Fig. 2, consisting of a hardened steel plunger contained in a cast-iron holder with a spherical seat used to eliminate any effect due to shifting of the testing machine heads. Specimens too large for the jig

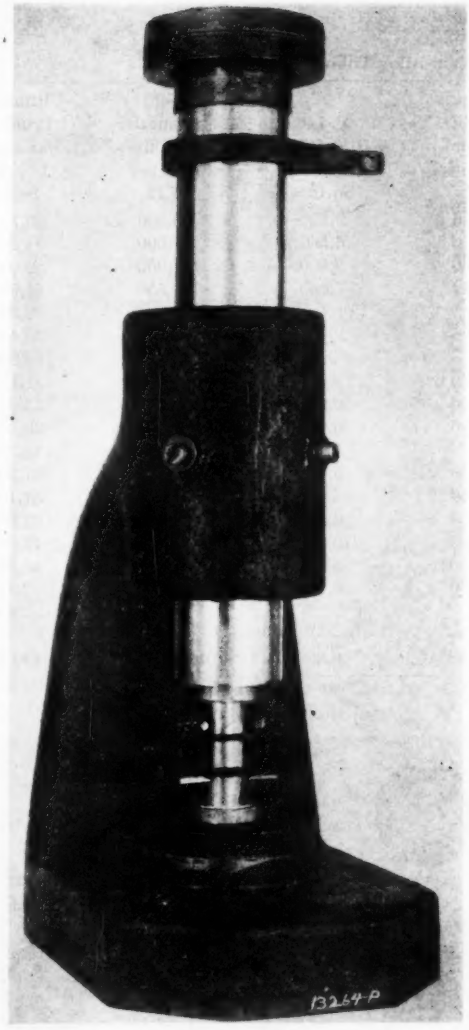

FIG. 2. Compression jig with specimen set-up.

were tested between a hardened steel plate and a spherical seat. Deformation was measured with two 1-in. Tuckerman optical strain gauges, diametrically opposed at the center of the tube. The crushing strength or compressive strength was the stress at the maximum load.

Flat end column specimens were tested between parallel, hardened steel plates attached to the heads of the testing machine. The specimens were carefully centered before testing. The knife-edge tests were made using knife-edge bearing plates attached to both heads of the testing machine. The plates were established in the same plane and in alignment and secured in place. The specimens were centered on the knife-edge plates by means of two sliding V-notch guide blocks. Some of the specimens that were slightly bowed were placed with the bowing parallel to the plane of the knife edges so that bending occurred at right angles to the bowing. The increase in length of the column specimens due to the depth of the knife-edge plates was allowed for in calculating the slenderness ratios.

All torsional specimens were snug-fitted with steel plugs, similar to those used in tension tests, of sufficient length to extend beyond the edge of the grips. A troptometer having a 12-in. radius was used on all specimens. Deformation was read in inches of arc with a scale graduated to 0.01 in. The L/D ratio of the tubes was approximately 15, which is specified for testing solid cylindrical specimens.[1] The gauge length used for the troptometer varied with the length of the tube.

Results and Discussion

Tension

Tensile properties and hardness of all tubings are given in Table 1. It will be noted that there was quite a range in tensile properties but that the lowest values were above the specification minimum requirements. A typical tensile stress-strain curve is shown in Fig. 1.

Table 4 gives a comparison of the ratios of the elastic properties to ultimate tensile strength for this tubing and for 24S-T aluminum alloy tubing.[3] The ratios of proportional limits to tensile strength are about half those of the aluminum alloy tubing.

The average modulus of elasticity in tension of 6.10 $\times$ 10^6 lbs. per sq.in. is lower than the value of 6.5 $\times$ 10^6 lbs. per sq.in. usually given for magnesium alloys. However, for accurate determination of modulus of elasticity, solid round bar specimens accurately machined are necessary.

Snug-fitting steel plugs, Fig. 3, conforming to Federal Specification QQ-M-151a, were used in several of the tubes in the initial tests, but difficulty was experienced, apparently because of the extreme notch sensitivity of the material and stress concentration. Failures occurred either at the radius near the end of

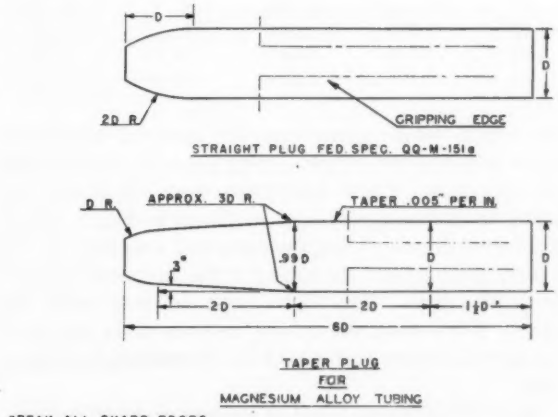

FIG. 3.

TABLE 2
Compressive Properties of Magnesium-Alloy Tubing

Specimen No.	Nominal Size, In.	Diameter Divided by Thickness, D/T	Modulus of Elasticity $\times 10^{-6}$, Lbs. per Sq.In.	Prop. Limit Tangent, Lbs. per Sq.In.	Prop. Limit 0.01% Offset, Lbs. per Sq.In.	Yield Strength 0.2% Offset, Lbs per Sq.In.	Ultimate or Crushing Strength, Lbs. per Sq.In.
2	3/4 by 0.042	18.6	6.44	2,200	9,120	20,400	50,700
3	3/4 by 0.042	18.0	6.64	4,000	6,560	17,000	51,310*
4	3/4 by 0.042	18.5	6.63	2,500	8,000	17,000	50,950*
5	3/4 by 0.042	18.2	6.44	4,040	7,080	17,550	51,970
6	1 by 0.042	22.7	...	....	....	....	42,230
7	1 by 0.065	16.9	...	....	....	....	55,170
8	1 by 0.095	11.7	...	....	....	....	56,600*
9	1 1/2 by 0.042	36.5	6.12	3,900	5,600	14,150	21,170
11	1 1/2 by 0.042	37.9	6.03	4,300	6,280	14,000	23,000
12	1 1/2 by 0.042	39.4	6.20	3,500	5,400	12,300	30,730
13	1 1/2 by 0.065	22.9	...	....	....	....	43,330
15	1 1/2 by 0.095	16.1	5.90	3,900	5,700	14,700	51,200
16	1 1/2 by 0.095	15.5	6.16	2,850	5,190	14,850	51,100
17	1 1/2 by 0.095	15.5	6.03	2,400	6,240	14,900	52,000
22	2 1/2 by 0.095	25.2	6.17	4,300	10,600	15,900	42,040
23	2 1/2 by 0.095	25.2	6.09	5,100	6,380	13,200	40,960
24	2 1/2 by 0.095	25.4	6.25	4,300	6,200	13,300	42,470
26	3 1/2 by 0.125	28.0	...	....	....	....	35,490
Average			6.24	3,640	6,800	15,330	44,020

* Buckled and sheared at one end.

TABLE 3
Compressive Properties of Magnesium-Alloy Tubing

Specimen No.	T/D	Crushing or Compressive Strength f_{cr} Lbs. per Sq.In.	$\frac{1}{\delta_s} = \frac{E}{S}\frac{T}{D}$	$\sigma_{crs} = f_{cr}/S$
2	0.0537	50,700	16.33	2.48
3	0.0557	51,310	20.20	3.02
4	0.0539	50,950	19.57	3.00
5	0.0550	51,970	19.92	2.96
9	0.0274	21,170	11.46	1.495
11	0.0264	23,000	11.43	1.642
12	0.0254	30,730	12.20	2.500
15	0.0620	51,200	24.83	3.48
16	0.0645	51,100	25.83	3.436
17	0.0645	52,000	26.70	3.490
22	0.0397	42,040	15.20	2.640
23	0.0397	40,960	17.75	3.105
24	0.0394	42,470	17.93	3.195

the plugs, where apparently the material would not draw or flow satisfactorily during the test, or at the end of the grips. These difficulties were eliminated by using special tapered plugs, as shown in Fig. 3, which permitted drawing along the taper and wrapping No. 60 emery cloth around the tubing at the surface in contact with the jaws. The cloth was wrapped with the emery side toward the tubing, and one sheet was used for approximately each 10,000 lbs. of estimated ultimate load.

Several specimens failed at stresses up to 40 per cent below average because of flaws in the tubes, which

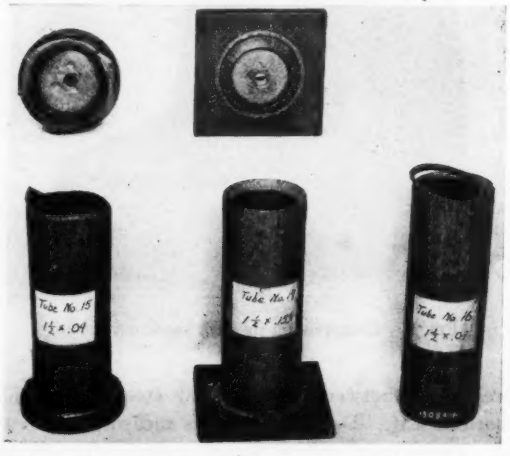

FIG. 4. Compressive specimens.

were probably due to inclusions in the metal. Duplicate tests were made on specimens from these tubes.

Compression

Compressive properties are given in Tables 2 and 3 and a typical stress-strain curve in Fig. 1.

In initial tests, the specimens were tested without any supporting medium for the ends, and difficulty was experienced because of the low shearing strength of the material. This was manifested by shear failure in the form of a ring at the end of each specimen as shown in tube No. 16, Fig. 4, which failed at 47,300 lbs. per sq.in. This difficulty was eliminated in specimens with D/T ratios over 10 by embedding each specimen approxi-

FIG. 5. Compressive specimens.

mately $^1/_4$ in. in Woods' metal, using oversize brass rings to restrain the alloy as shown in tube No. 15, Fig. 4, and tube No. 24, Fig. 5. The ends of the specimens protruded slightly beyond the Woods' metal. In the specimens with D/T ratios below 10, neither thicker plates, as shown in a specimen from tube No. 19, Fig. 4, which failed at 58,700 lbs. per sq.in., and one from tube No. 25, Fig. 5, which failed at 53,800 lbs. per sq.in., nor steel plates with a concentric groove, one-half the depth of the plate, as shown in another specimen from tube No. 25, Fig. 5, which failed at 50,400 lbs. per sq. in., gave satisfactory compressive failures. However, most of these specimens showed bulges near the ends, and shear failures may have occurred after the compression failure.

The rather wide variation in individual values of crushing strength or ultimate compressive stress of the $1^1/_2$ by 0.042 tubes with a D/T of 36 is not explained.

The variation of crushing strength with D/T ratio for an L/R ratio of 11 is shown in Fig. 6, plotted in the conventional way, and in Fig. 7 in terms of nondimensional variables δ_s and σ_{crs} where

$$\delta_s = (S/E)(D/T) \qquad (1)$$

and

$$\sigma_{crs} = f_{cr}/S \qquad (2)$$

where S = compressive yield strength, E = modulus of elasticity, and f_{cr} = compressive or crushing strength.

It is assumed that the crushing strength depends upon the mechanical properties of the material of each specimen, and it is expected that any empirical relation found between δ_s and σ_{crs} as the results of tests will show less scatter than a relation between D/T and f_{cr}.[4] The nondimensional curve is a hyperbola.

The proportional limits and yield strengths in compression averaged much lower than those in tension. The ratios are given in Table 4. It will be noted that the proportional limits are low and that the compressive yield strength is less than two-thirds of the tensile yield strength. There was no appreciable variation of proportional limit and yield strength with D/T ratio.

TABLE 4

Comparison of Average Tensile and Compressive Properties of 24S-T Aluminum-Alloy and Magnesium-Alloy Tubing. All Strength Values in Lbs. per Sq.In.

	Proportional Limit, Tangent	Proportional Limit, 0.01% Offset	Yield Strength, 0.2% Offset	Ultimate Strength
	Tensile Properties			
24S-T	33,500	44,000	53,000	69,700
Ratio to ultimate	0.48	0.63	0.76	1.00
Magnesium alloy	9,860	13,160	25,130	41,370
Ratio to ultimate	0.24	0.32	0.61	1.00
	Compressive Properties			
24S-T	29,600	34,800	46,780	....
Ratio to tensile property	0.88	0.79	0.88	....
Magnesium alloy	3,640	6,800	15,330	....
Ratio to tensile property	0.37	0.52	0.61	....

Column Properties

Column properties are given in Tables 5 and 6 and Fig. 8.

The elastic range of column failure for which Euler's equation applies begins at a slenderness ratio of 105 for

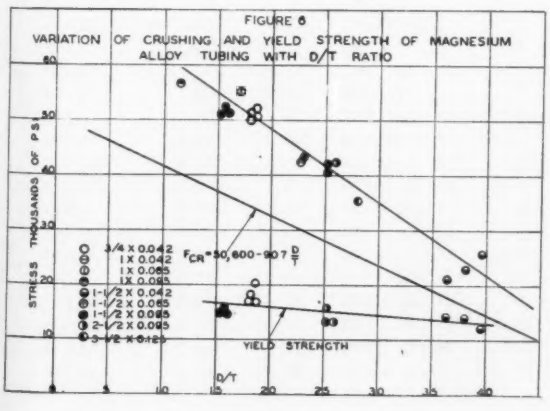

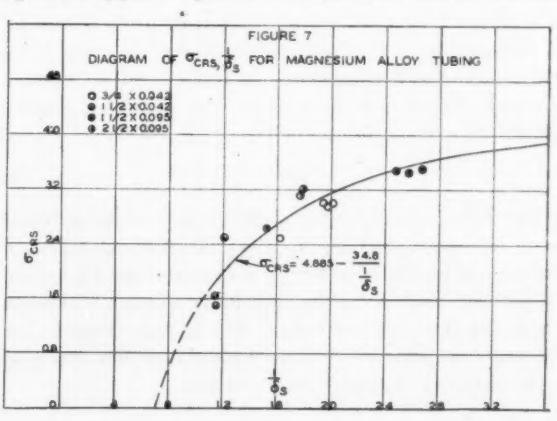

TABLE 5
Column Properties of Magnesium-Alloy Tubing
Knife-Edge Ends

Tube No.	Nominal Size, In.	D/T	L/R	Column Strength, Lbs. per Sq.In.
2	3/4 by 0.042	17.6	10.6	38,070
5	3/4 by 0.042	17.6	11.1	29,680
5	3/4 by 0.042	17.6	11.2	39,800
4	3/4 by 0.042	17.6	11.2	36,200
5	3/4 by 0.042	17.6	15.1	28,200
1	3/4 by 0.042	17.6	15.2	25,410
3	3/4 by 0.042	17.6	19.3	19,500
1	3/4 by 0.042	17.6	23.8	16,540
3	3/4 by 0.042	17.6	39.0	14,600
3	3/4 by 0.042	17.6	58.4	9,790
3	3/4 by 0.042	17.6	77.6	7,640
4	3/4 by 0.042	17.6	100.4	8,200
5	3/4 by 0.042	17.6	150	2,880
11	1 1/2 by 0.042	36.4	11.1	18,200
12	1 1/2 by 0.042	36.4	11.1	15,900
12	1 1/2 by 0.042	36.4	16.1	14,510
11	1 1/2 by 0.042	36.4	16.1	15,290
11	1 1/2 by 0.042	36.4	25.0	14,040
9	1 1/2 by 0.042	36.4	25.0	13,300
12	1 1/2 by 0.042	36.4	75.0	5,700
11	1 1/2 by 0.042	36.4	100.5	5,660
12	1 1/2 by 0.042	36.4	130.4	3,450
17	1 1/2 by 0.095	15.5	10.0	41,710
15	1 1/2 by 0.095	16.1	10.0	26,890
17	1 1/2 by 0.095	15.5	16.1	22,030
17	1 1/2 by 0.095	15.5	25.1	15,010
16	1 1/2 by 0.095	15.5	50.3	11,980
16	1 1/2 by 0.095	15.5	75.4	6,160
16	1 1/2 by 0.095	15.5	100.3	4,210
17	1 1/2 by 0.095	15.5	130.5	3,340
19	1 1/2 by 0.148	10.2	11.2	30,760
19	1 1/2 by 0.148	10.2	11.2	31,650
19	1 1/2 by 0.148	10.2	50.6	12,390
18	1 1/2 by 0.148	10.2	75.6	7,970
19	1 1/2 by 0.148	10.2	102.9	5,410
23	2 1/2 by 0.095	27.8	11.0	22,870
23	2 1/2 by 0.095	27.8	16.1	16,100
22	2 1/2 by 0.095	27.8	25.1	14,850
23	2 1/2 by 0.095	27.8	49.8	10,340

knife edges and 210 for flat ends, at a stress of about 5,000 lbs. per sq.in. Compressive stress-modulus curves for tube Nos. 11 and 15 were drawn, Fig. 9, from which the Engesser column curves were computed and plotted, Fig. 10, for comparison with the test data. A value of $K = 0.5$ for flat ends and $K = 1$ for knife edges was used in computing the Euler and the Engesser curves. Engesser's formula is the same as Euler's equation,

$$P/A = \pi^2 E/(KL/R)^2 \qquad (3)$$

where P = column load in pounds; A = cross-sectional area in square inches; L/R = slenderness ratio, in which L is length in inches, R is least radius of gyration in inches; and K is the end fixity constant, except that the tangent modulus, E^1, is substituted for Young's modulus, so that the formula applies above as well within the range of elastic failure.

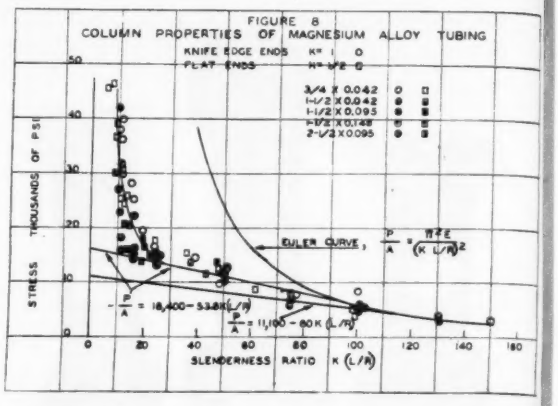

The Engesser curves were in good agreement with the test data, Fig. 10. It will also be noted that although Engesser curves were plotted for tube Nos. 11 and 15, test data from other tubes the same size were also used for comparative purposes. Since the tensile and compressive properties are comparable, the inclusion of the different tubings seems justifiable. The Engesser stress-modulus theory for column failure has also been found to apply to wrought aluminum alloy[5] and steel columns.[6] Tensile stress modulus curves for tube Nos. 11 and 15 were also drawn, Fig. 9, and these curves show the importance of using compressive data instead of tensile data when employing column formulas. The latter data would give a much higher stress modulus above about 4,000 lbs. per sq.in. than in compression at the same stress.

TABLE 6
Column Properties of Magnesium-Alloy Tubing
Flat End Conditions

Tube No.	Nominal Size, In.	D/T	L/R	Column Strength, Lbs. per Sq.In.
2	3/4 by 0.042	17.6	10.3	45,700
5	3/4 by 0.042	17.6	15.2	46,460
4	3/4 by 0.042	17.6	19.9	36,580
2	3/4 by 0.042	17.6	24.0	24,700
5	3/4 by 0.042	17.6	25.1	24,920
4	3/4 by 0.042	17.6	29.3	25,650
2	3/4 by 0.042	17.6	48.0	17,520
2	3/4 by 0.042	17.6	72.0	15,670
2	3/4 by 0.042	17.6	96	12,830
2	3/4 by 0.042	17.6	124	8,780
4	3/4 by 0.042	17.6	200	5,420
5	3/4 by 0.042	17.6	200	3,740
9	1 1/2 by 0.042	36.4	30.1	16,140
10	1 1/2 by 0.042	36.4	39.1	13,740
11	1 1/2 by 0.042	36.4	75.4	13,600
15	1 1/2 by 0.095	16.1	40.2	16,200
30	1 1/2 by 0.148	10.3	19.9	38,910
31	1 1/2 by 0.148	10.3	29.9	20,480
30	1 1/2 by 0.148	10.3	39.7	17,640
30	1 1/2 by 0.148	10.3	95.0	13,700
22	2 1/2 by 0.095	27.8	20.0	30,170
23	2 1/2 by 0.095	27.8	24.9	20,600
22	2 1/2 by 0.095	27.8	49.7	14,820
24	2 1/2 by 0.095	27.8	86.2	11,720

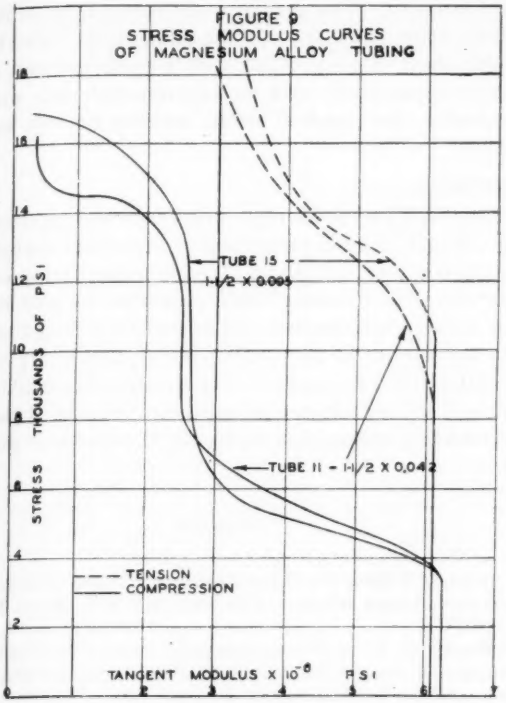

FIGURE 9

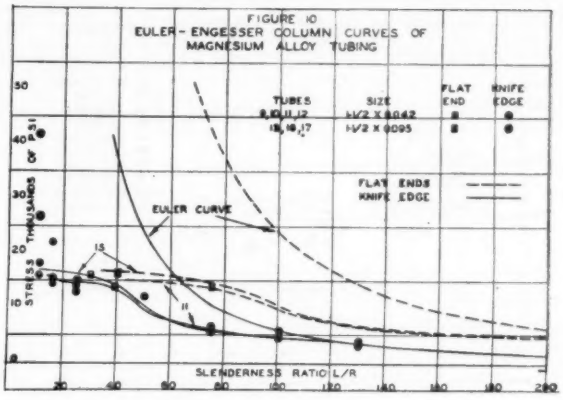

FIGURE 10

Torsional Properties

Torsional properties are given in Table 7 and Fig. 11, based on extreme fiber stress. The conventional equations for calculating stress and strain in torsion from the torque and troptometer readings were employed. These equations assume that the stress varies directly with the radial distance and linear stress-strain relationship. Values of ultimate torsional stress are plotted against D/T, ratio of outside diameter to

TABLE 7

Torsional Properties of Magnesium-Alloy Tubing

Spec. No.	Nominal Size, In.	Outside Diam. D, In.	Wall Thickness T, In.	Length Between Grips L, In.	D/T	T/D	L/D	Mod. of Rigidity G $\times 10^{-6}$ Lbs. per Sq.In.	Prop. Limit Tang., Lbs. per Sq.In.	Prop. Limit 0.01% Offset, Lbs. per Sq.In.	Yield Strength 0.2% Offset, Lbs. per Sq.In.	Ult. Strength, Lbs. per Sq.In.	Max. Torque, In.-Lbs.
1	3/4 by 0.042	0.7795	0.0444	12.3	17.6	0.0568	15.8	2.13	4,720	5,580	9,800	15,550	560
6-1	1 by 0.042	0.955	0.0420	16.16	22.7	0.044	16.9	2.38	5,600	6,580	9,300	15,480	815
6-2	1 by 0.042	0.955	0.0420	16.16	22.7	0.044	16.9	2.36	4,940	6,540	9,600	15,670	825
7-1	1 by 0.065	1.055	0.0625	16.15	16.9	0.0591	15.3	1.99	4,400	5,560	8,950	16,670	1,555
7-2	1 by 0.065	1.055	0.0625	16.10	16.9	0.0591	15.3	1.98	4,340	5,300	9,100	16,990	1,585
8-1	1 by 0.095	1.065	0.0913	20.0	11.7	0.0855	18.8	2.07	3,640	4,500	8,700	24,380	3,175
8-2	1 by 0.095	1.065	0.0913	20.1	11.7	0.0855	18.9	1.94	4,170	5,020	8,630	24,150	3,145
8-3	1 by 0.095	1.065	0.0913	16.0	11.7	0.0855	15.0	1.92	3,600	5,110	8,700	....	....
8-4	1 by 0.095	1.065	0.0913	16.0	11.7	0.0855	15.0	...	...	...	....	26,270	3,420
9	1 1/2 by 0.042	1.495	0.0410	22.5	36.4	0.0274	15.0	...	...	...	....	13,170	1,630
13-1	1 1/2 by 0.065	1.500	0.0655	22.3	22.9	0.0437	14.9	2.45	3,500	4,640	9,000	14,840	2,950
13-2	1 1/2 by 0.065	1.500	0.0655	22.54	22.9	0.0437	15.0	...	...	...	....	15,190	3,020
13-3	1 1/2 by 0.065	1.500	0.0655	22.5	22.9	0.0437	15.0	2.39	4,420	5,220	9,800	14,540	2,890
14	1 1/2 by 0.065	1.500	0.0655	22.6	22.9	0.0437	15.1	2.28	4,480	5,390	10,100	....	2,790*
15	1 1/2 by 0.095	1.516	0.0940	22.4	16.1	0.062	14.8	...	...	...	....	19,240	5,450
17-1	1 1/2 by 0.095	1.505	0.0970	22.6	15.5	0.0645	15.0	2.25	3,500	5,740	10,650	18,410	5,240
17-2	1 1/2 by 0.095	1.505	0.0970	22.5	15.5	0.0645	14.9	2.30	3,480	4,880†	....	....	....
20-1	1 1/2 by 0.148	1.503	0.1461	22.5	10.3	0.097	15.0	2.34	3,700	4,700	9,350	25,830	10,010
20-2	1 1/2 by 0.148	1.503	0.1461	22.5	10.3	0.097	15.0	2.34	3,500	5,240	10,500	26,320	10,200
31	1 1/2 by 0.148	1.503	0.1461	22.2	10.3	0.097	14.8	2.32	4,500	6,050	10,100	26,190	10,260
21	2 1/2 by 0.095	2.523	0.0989	37.5	25.5	0.0392	14.9	2.31	4,900	6,410	9,900	13,070	11,480
25	2 1/2 by 0.32	2.511	0.3247	33.6	7.7	0.13	13.4	2.23	4,200	6,400	8,500	25,800	55,900
	Average							2.22	4,200	5,490	9,450		

* Failure through gauge mark.

† Repeated loading test.

FIGURE 11
VARIATION OF TORSIONAL STRENGTH OF MAGNESIUM ALLOY TUBING WITH D/T RATIO

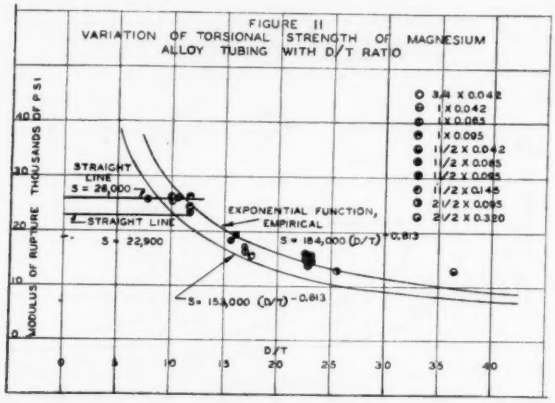

wall thickness, in Fig. 11. Any effects of L/D ratio, where L is the length between grips, were not investigated because of the lack of material, but it is not believed that there would be any appreciable effect within the range of D/T tested. The effect has been found to be appreciable, however, for thin-wall tubes of other materials.[7]

The torsional modulus of rupture in the range of failure by plastic shear averaged 63 per cent of the average tensile strength. For comparison, the shear strength in double shear of cylindrical pins machined from the 2.5 by 0.32 in. tubing was determined. These averaged 20,110 lbs. per sq.in. or about 45 per cent of the tensile strength. If a uniform distribution of stresses at the ultimate load in torsion is assumed instead of straight-line distribution, the ultimate strength in torsion of the 2.5 by 0.32 in. tube, Specimen No. 25, is then calculated to be 22,770 lbs. per sq.in. or about 52 per cent of the tensile strength.

There were no significant effects of variation of D/T ratio on the modulus of rigidity, proportional limits, and yield strength. The average yield strength in torsion was 9,450 lbs. per sq.in. All the tubing tested failed by plastic shear or by buckling with varying amounts of plastic deformation, and no experimental data were obtained in the region of elastic buckling for thin-wall tubing.

Equations

Equations for the average curves representing crushing strength, column properties, and torsional strength are given in Figs. 6, 7, 8, and 11, together with equations and curves representing these properties for material just meeting specification requirements for design use. The derivations of these minimum equations are not essential to this discussion. The equations for crushing strength and for torsional strength in the range of plastic buckling are applicable for D/T ratios less than 40.

References

[1] ANC-5, *Strength of Aircraft Elements*, 1942.

[2] Osgood, William R., *Column Strength of Tubes Elastically Restrained Against Rotation at the Ends*, N.A.C.A. Report No. 615, 1938.

[3] Warner, D. M., *24S Aluminum Alloy Tubing, Heat Treated, Tension and Compression*, A.A.F. Matériel Command Memorandum Report EXP-M-56–2551, 28 June, 1934.

[4] Osgood, William R., *The Crinkling Strength and the Bending Strength of Round Aircraft Tubing*, N.A.C.A. Report No. 632, 1938.

[5] Templin, R. L., Sturm, R. G., Hartmann, E. C., and Holt, M., *Column Strength of Various Aluminum Alloys*, Technical Paper No. 1, Aluminum Research Laboratories, The Aluminum Company of America, 1938.

[6] Basquin, O. H., *Tangent Modulus and the Strength of Steel Columns on Tests*, Technologic Paper of National Bureau of Standards, No. 263.

[7] Donnel, L. H., *Stability of Thin-Walled Tubes under Torsion* N.A.C.A. T.R. No. 479, 1933.

Motogliders—A Natural Link Between Gliders and Light Planes

WIESLAW Z. STEPNIEWSKI*

The de Havilland Aircraft of Canada Ltd.

SUMMARY

Several aspects of motoglider problems are considered. The official Federation Aéronautique Internationale (F.A.I.) definition of a motoglider is analyzed and compared with one based on the minimum sinking speed of a motoglider with its engine stopped. The influence on the speed polar diagram in power-off flight of such structural parameters as wing loading, aspect ratio, and minimum drag coefficient are considered. The possible limits for the performance of motogliders in powered flight are also examined. The power loading appears in these considerations as a new parameter in addition to the ones previously mentioned.

The following special problems are discussed: (1) means of reducing the drag of the propeller when the engine is stopped; (2) general design of the motogliders; and (3) the most suitable engines. Also presented are some aspects of general experience, accumulated during 3-year tests with motogliders in Poland. In conclusion, the paper states that, in the case of a nation-wide program (based on gliding) for attracting air-minded youth to an active part in aviation, motogliders might play their role as a natural link between gliders and light planes.

INTRODUCTION

GENERAL ECONOMIC CONDITIONS in the United States were better before the war, and will probably be better in the future, than in Europe. This fact, as well as the abundance of gasoline (in peacetime) at relatively low prices plus greater ground facilities, may lead the main current of the postwar development of the so-called "light aircraft" (in the airplane class) to the multiplace highly powered "family machines." The postwar tendencies in the American aircraft industry when compared with the probable European ways of construction may show, in the future, a close analogy to the situation in the prewar automobile industry, where differences between American and European techniques were so apparent.

Nevertheless, even under such conditions there will probably remain some place for other kinds of light planes, including motogliders. A general review of the problems represented by this last category may be of some interest to American aeronautical circles. This is especially true if, after the war, some kind of nation-wide aeronautical training scheme based on gliding is to be established. Then the motoglider, which to use nautical analogy may be compared to a sailing boat with an auxiliary engine, may become helpful in turning glider pilots into airplane pilots. Because of moto-gliders, this transition may become a gradual evolution. In addition, experience accumulated by the young people when gliding will create a deep understanding of the air. This understanding, so emphasized by all enthusiasts of gliding, will no doubt represent a sound basis for the aeronautical life of the future.

In addition to the above-mentioned aspects of training, motogliders may attract some adherents for their undoubted sport value. Finally, the usefulness of motogliders in meteorologic and aerologic research should not be overlooked. Some European scientists have considered motogliders especially suitable for aerologic research because of their low sinking speed and complete lack of vibration when descending with the engine off.

DEFINITION OF MOTOGLIDERS

According to the official F.A.I. division of all aircraft, motogliders or powered gliders belong in Class D and should adhere to the following requirements:

(1) Total weight: for the single-place machines $W \leq 350$ kg. (771.7 lbs.); for the multiplace machines, $W \leq 450$ kg. (992 lbs.).

(2) Cylinder displacement: for the single-place craft, volume $\leq$ 1,000 cu.cm. (61 cu.in.); for the multiplace craft having one engine, volume $\leq$ 1,300 cu.cm. (79.3 cu.in.); for those having more than one engine, volume $\leq$ 1,600 cu.cm. (97.6 cu.in.).

(3) The single-place, as well as multiplace, motogliders should have the span squared loading, $W/b^2 \leq$ 2.5 kg. per square meter (0.512 lb. per sq.ft.).

The above definition is based on certain characteristics that are easily obtainable. It represents definite advantages from the formal point of view but does not fully stress the most important characteristic of any motoglider—the ability to soar, with the engine stopped, in average aerologic conditions. The definition of motogliders based on this last characteristic introduces a certain difficulty of expressing in figures the rather indefinite term of "average aerologic conditions." In central Europe, as well as in the United States and in Canada, ascending currents of rate equal to, or higher than, 3.2 to 3.4 ft. per sec. (about 1 m. per sec.) are quite frequent over large areas on a normal sunny spring, summer, or early autumn day. Hence, the practical ability of any flying machine to soar with its engine stopped within an ascend-

Presented at the National Light Aircraft Meeting, I.A.S., Detroit, April 27–28, 1944.

* Design Engineer in charge of Structures Division.

ant current of 3.2 to 3.4 ft. per sec., may be considered the only necessary characteristic to classify this flying machine as a motoglider. In other words, the practical minimum sinking speed of a motoglider should not be higher than 3.3 ft. per sec., or some other arbitrary value, enclosed, of course, within logical limits representing the average aerologic conditions.

As can be seen from further considerations, it is possible to design a machine that fulfills the official requirements for motogliders but is unable to soar except in most favorable aerologic conditions. On the other hand, the motoglider definition, based on the minimum sinking speed, contains formal difficulties, which may cause considerable trouble, as based on values that are not necessarily 100 per cent incontestable. Unfortunately, there is no simple and sure method of measuring sinking speed in flight. Theoretical estimation of this value, based on wind-tunnel tests or analytical computation of the aerodynamic coefficients, is hampered by many uncertainties too well known to be mentioned here. All formal difficulties may become especially acute in the case of competitions, races, record flights, etc.

Nevertheless, for the purpose of this paper, any reference to the motoglider may be taken to designate a machine having, with its engine stopped, a minimum sinking speed at sea level not higher than 3.3 ft. per sec.

Notation

C_L	= coefficient of lift
C_D	= coefficient of drag
ΔC_D	= increase of drag
A	= aspect ratio
W	= weight (lbs.)
S	= wing area (sq.ft.)
P	= engine power (b.hp.)
V	= air speed (ft. per sec.)
V_z	= sinking speed (ft. per sec.)
V_C	= rate of climb (ft. per sec.)
V_{Cf}	= fictitious rate of climb (ft. per sec.), supposing that the whole effective power is used to overcome the effect of gravity
$V_{z_{opt.}}$	= sinking speed corresponding to best lift/drag ratio
D	= propeller diameter (ft.)
N	= propeller speed (r.p.m.)
n	= propeller speed (r.p.s.)
$J = V/nD$	= advance ratio or slip function
η	= propeller efficiency
T	= propeller thrust (lbs.)
μ	= ground friction coefficient
s	= take-off distance (ft.)
ρ	= air density (slugs)
g	= acceleration of gravity (32.17 ft. per sec.^{2})
T_c	= propeller thrust coefficient
Q_c	= propeller torque coefficient

Practical Minimum Sinking Speed

Minimum sinking speed is expressed by the well-known formula:

$$V_{z_{min.}} = \sqrt{\left(\frac{W}{S}\right)\left(\frac{2}{\rho}\right)\left[\frac{1}{(C_L^3/C_D^2)_{max.}}\right]} \qquad (1)$$

A glance at Eq. (1) will show that the lowest value of $V_{z_{min.}}$ will be obtained when $(C_L^3/C_D^2)_{max.}$ is as high as possible and when the wing loading W/S is as low as possible. But because of the fact that a low wing loading is usually associated with an increase in the overall dimensions and weight, as well as with reduction of flying speed, choice of this value for a glider is always a matter of compromise. The nature of this compromise is greatly influenced by other structural parameters, such as aspect ratio and minimum drag coefficient of the whole machine.* In the case of powered flight, the power loading should here be added as a new parameter.

In order to show in a simple analytical way the relations existing between performance and structural parameters, the polar diagram of the whole motoglider $[C_D = f(C_L)]$ will be replaced by the following parabolic equation (Fig. 1):

$$C_D = C_{D_{min.}} + (C_L^2/\pi A) \qquad (2)$$

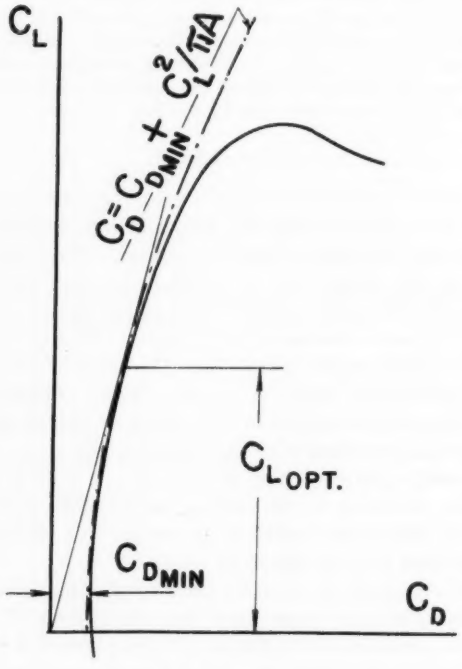

Fig. 1.

Then the theoretical minimum sinking speed can readily be expressed as a function of $C_{D_{min.}}$, A, and W/S.

Because of increasing discrepancies, for high angles of incidence, between the real $C_D = f(C_L)$ and that given

* For motogliders, $C_{D_{min.}}$ will refer to the drag with the engine stopped.

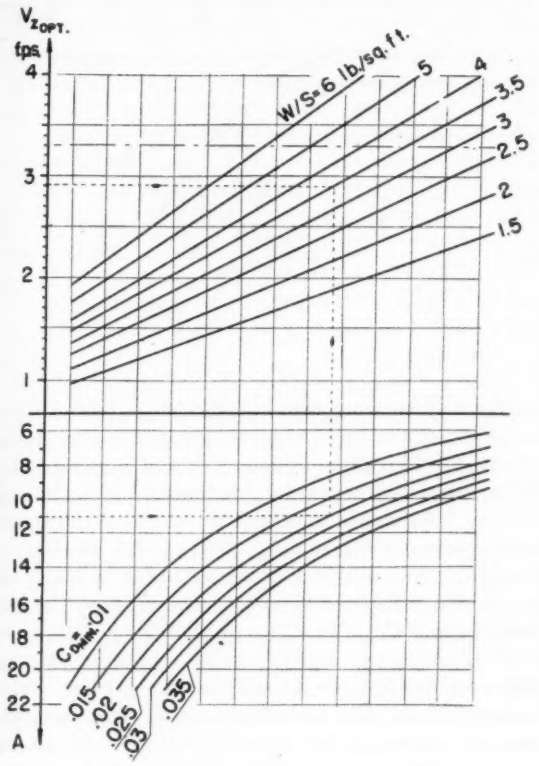

FIG. 2.

by Eq. (2), $V_{z_{min.}}$ found in this way is too low. A closer approximation of the real $V_{z_{min.}}$ will probably give the theoretical sinking speed based on Eq. (2) corresponding to the optimum lift/drag ratio: $(C_L/C_D)_{max.}$ This speed ($V_{z_{opt.}}$) may be expressed as:

$$V_{z_{opt.}} = 2\sqrt[4]{C_{D_{min.}}/A^3\pi^3}\,\sqrt{(W/S)(2/\rho)} \qquad (3)$$

and will be called in this paper *the practical minimum sinking speed.*

At sea level, Eq. (3) becomes:

$$V_{z_{opt.}} = 24.6\sqrt[4]{C_{D_{min.}}/A^3}\,\sqrt{W/S} \qquad (3a)$$

In order to show the importance of the span squared loading (W/b^2), which is mentioned in the official definition of powered gliders, Eq. (3a) may be rewritten as follows:

$$V_{z_{opt.}} = 24.6\sqrt[4]{C_{D_{min.}}/A}\,\sqrt{W/b^2} \qquad (4)$$

Eqs. (3) and (3a) show quite clearly that, as far as the practical minimum sinking speed is concerned, the most important factor is aspect ratio A, which is cubed under the fourth degree root, when $C_{D_{min.}}$ is to the power of one and wing loading W/S in these formulas is to the power of one-half.

When A, $C_{D_{min.}}$, and W/S are known, the values of $V_{z_{opt.}}$ given by Eq. (3a) can be easily found with the aid of Fig. 2 (see dotted lines and arrows). From given A, a horizontal is traced to the intersection with a curve representing $C_{D_{min.}}$. From this point, a vertical is drawn to the intersection with a straight line, corresponding to the given value of W/S. The ordinate of this last point is the required $V_{z_{opt.}}$. It is clear, that with the help of Fig. 2 one can easily check the combination of the parameters W/S, A, and $C_{D_{min.}}$ necessary to obtain $V_{opt.}$ not higher than 3.3 ft. per sec.

Eq. (4) is represented graphically by Fig. 3. In all respects Fig. 3 is analogous to Fig. 2. The only difference is in the fact that the W/S lines are replaced in Fig. 3 by lines representing W/b^2. The procedure for finding $V_{z_{opt.}}$ is exactly the same as on Fig. 2 (see dotted lines and arrows).

SPEED POLAR DIAGRAM

As is known from gliding practice, a low enough minimum sinking speed is the necessary condition for soaring and gaining altitude within ascendant currents, but this is not sufficient condition for performing a successful distance flight. In distance flights the glider must show an ability to pass through descending currents, or to fly against head winds, with the smallest possible loss of altitude. Thus, at highly increased

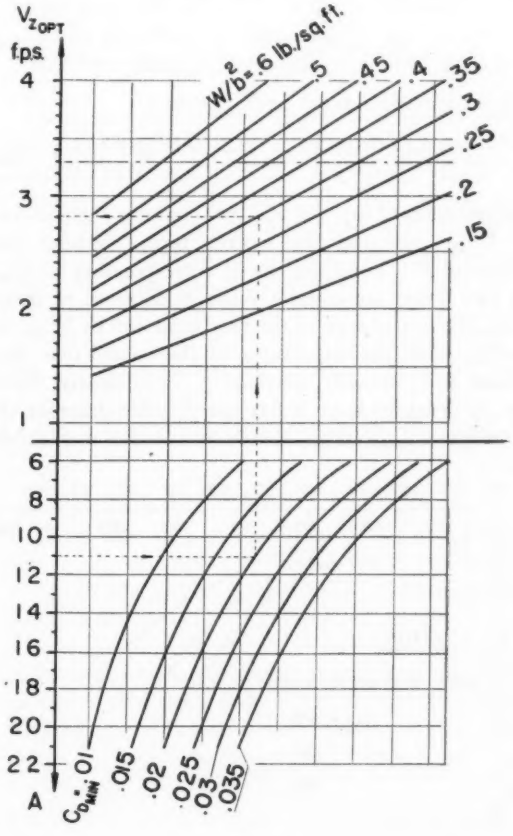

FIG. 3.

flying speeds needed for a quick escape from unfavorable areas, the sinking speed should remain as low as possible. For this reason, the general shape of the curve $V_z = f(V)$, called the speed polar diagram, is of prime importance for a performance glider. Obviously, the flatter the curve, the greater the ability to perform a successful distance flight.

In the case of motogliders one may consider that the presence of an auxiliary engine will provide sufficient means of escaping from unfavorable aerologic conditions. Undoubtedly such a reasoning is true to some extent. But distance flying is probably the most attractive feature of gliding in general; hence, the ability of a motoglider to perform, with its engine stopped, flights of this kind should be considered as the most desirable characteristic. Since the flat shape of the speed polar diagram is also favorably related to flying speeds reached in powered flight, then a little more attention will be paid to the analyses of parameters influencing its shape.

Sinking speed (for all practical purposes) can be expressed as:

$$V_z = V(C_D/C_L) \tag{5}$$

where V denotes flying speed. Substituting Eq. (2) for C_D, as well as considering that C_L may be expressed as $C_L = 2W/\rho SV^2$, Eq. (5) will become:

$$V_z = \frac{\rho C_{D_{min.}} V^3}{2W/S} + \frac{2W}{\pi\rho SA\,V} \tag{6}$$

or at sea level (V_z and V in ft. per sec.):

$$V_z = 0.00119\left(\frac{C_{D_{min.}}}{W/S}\right)V^3 + 267.8\left(\frac{W}{S}\right)\left(\frac{1}{A}\right)\left(\frac{1}{V}\right) \tag{6a}$$

The first term of Eqs. (6) and (6a) contains the parameter $C_{D_{min.}}$, whereas the second term contains the parameter A. For flying speed corresponding to $V_{z_{opt.}}$ the two terms are equal. With an increase in flying speed, the importance of the first term due to V^3 grows rapidly, while the importance of the second one, containing $1/V$, steadily decreases. This clearly shows that in order to have a flat speed polar diagram the expression $C_{D_{min.}}/(W/S)$ should be as small as possible.

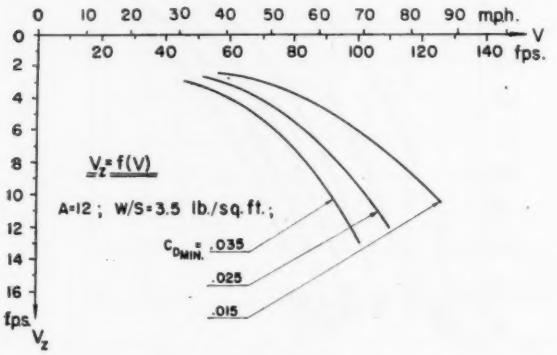

FIG. 4.

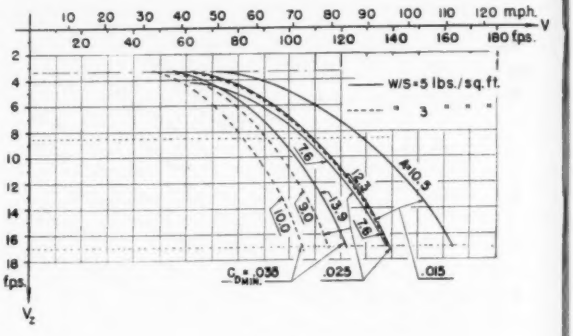

FIG. 5.

Or, for a given wing loading W/S, $C_{D_{min.}}$ will govern the shape of the speed polar diagram at higher flying velocities. This last statement is well illustrated by Fig. 4, where the speed polar diagrams of a glider having $W/S = 3.5$ lbs. per sq.ft. and $A = 12$ are shown for three different values of $C_{D_{min.}}$ (0.015, 0.025, and 0.035). From Fig. 4 it can readily be seen that at about 40 m.p.h. the difference between sinking speeds of the glider having $C_{D_{min.}} = 0.015$ and one having $C_{D_{min.}} = 0.035$ is only about 1.5 ft. per sec. At 60 m.p.h. this difference would grow to about 5 ft. per sec. This example shows best the importance of decreasing the drag of a motoglider when flying with its engine stopped. Since the resistance of the stopped propeller is one of the most important items, methods of reducing this drag will be considered later as a special problem.

It may be recalled here that for the higher wing loadings larger values of $C_{D_{min.}}$ have a smaller unfavorable effect on the shape of the speed polar diagram. In Fig. 5 one can see that for $W/S = 3$ lbs. per sq.ft. and $C_{D_{min.}} = 0.015$ the shape of $V_z = f(V)$ is identical with that for $W/S = 5$ lbs. per sq.ft. and $C_{D_{min.}} = 0.025$.* The aspect ratios ($A = 7.6$ for $W/S = 3$ and $A = 12.3$ for $W/S = 5$) giving the same values of $W/S/A$ in the second term of Eqs. (6) and (6a) helped to bring the speed polar diagrams to identity. But even for the same aspect ratios (i.e., $A = 7.6$ for $W/S = 5$ and $C_{D_{min.}} = 0.025$), the difference in the shape of speed polar diagrams at the higher flight velocities is negligible (Fig. 5).

LIMITS OF MOTOGLIDER PERFORMANCE

Free Flight

There may be many ways of approach to the discussion of such a combination of structural parameters W/S, A, and $C_{D_{min.}}$ as is necessary to create a real motoglider able to soar and perform distance flights. A rough estimate of the possible wing loadings, completed by an assumption of the minimum drag coefficients, seems to be the sound one. If the moto-

* In both cases the values of $C_{D_{min.}}/(W/S)$ are identical.

glider training has to follow, and to complete to some extent, the primary glider training, then the flying properties, as far as piloting is concerned, should not differ too much from those of the gliders. It means that the wing loading of the motogliders should not be considerably higher than normally used in glider construction. Following this line of reasoning, it seems that $W/S = 3$ lbs. per sq.ft. and $W/S = 5$ lbs. per sq.ft. may be chosen as sample values for the further considerations.

In all practical cases, the drag coefficient of a motoglider with its engine stopped will probably be included within the following limits: $C_{D_{min.}} = 0.015$ to 0.035. Hence, $C_{D_{min.}}$ 0.015, $C_{D_{min.}} = 0.025$, and $C_{D_{min.}} = 0.035$ may be proposed as three sample values for this parameter. With the use of Fig. 2 it is easy to find the aspect ratios assuring the practical minimum sinking speed $V_{z_{opt.}} = 3.3$ ft. per sec., when the wing loading and the minimum drag coefficient are equal to their sample values.

The aspect ratios found in this way are given in Table 1. In this table, there are also the span b and w/b^2, which would correspond to the respective values of W/S and A. In finding b, the total weight of the machine (when ready to fly) was assumed as $W = 770$ lbs. This weight seems to be reasonable for a single-place motoglider. Any total weight, considerably lower than 770 lbs., is scarcely probable, since the weight of the engine-propeller group alone plus the pilot's weight will make some 300 to 370 lbs., leaving for air-frame structure, gasoline, etc., 470 to 400 lbs. On the other hand, the total weight $W = 770$ lbs. (close to the weight specified in the official definition of motogliders) should not be exceeded by more than a small percentage for a properly designed machine of this kind.

TABLE 1

W/S, Lbs. per Sq.Ft.	$C_{D_{min.}}$	A	b,* Ft.	W/b^2,* Lbs. per Sq.Ft.	$(C_L/C_D)_{max.}$
5	0.015	10.5	40.0	0.481	23.3
	0.025	12.3	43.5	0.407	19.8
	0.035	13.9	46.3	0.359	17.6
3	0.015	7.6	44.1	0.395	19.8
	0.025	9.0	48.1	0.333	16.5
	0.035	10.0	50.7	0.300	14.8

* For $W = 770$ lbs.

The speed polar diagrams corresponding to the values of the design parameters listed in Table 1 are shown in Fig. 5. Those curves for $C_{D_{min.}} = 0.015$ should be considered the ideal performance of any motoglider having $W/S = 5$, or 3 lbs. per sq.ft., and showing the practical minimum sinking speed of about 3.3 ft. per sec. The speed polar diagrams corresponding to $C_{D_{min.}} = 0.025$ may be taken as an example of an average design, while those referring to $C_{D_{min.}} = 0.035$ will represent a machine that is not clean from an aerodynamic point of view when, in addition, little or nothing is done to reduce the drag of the stopped propeller.

The best gliding ratio $(C_L/C_D)_{max.}$, listed in the last column of Table 1, completes the picture of the possible performance of the sample motogliders in power-off flights.

Powered Flight

The picture of motoglider performance in power-off flight should be completed by a similar consideration of powered flight. Using the method described in reference 1, it is easy to find the following performance: (a) maximum horizontal speed at sea level, (b) maximum initial rate of climb, and (c) service ceiling. In order to do this it is necessary to draw the speed polar diagram of a machine and to know the fictitious rate of climb:

$$V_{cf} = 550\eta P/W$$

Some of the speed polar diagrams, shown on Fig. 5, in connection with the consideration of the free flight, may be used to predict the performance in the powered flight. Those curves corresponding to $C_{D_{min.}} = 0.015$ should be considered an ideal difficult to obtain in practice. Those for $C_{D_{min.}} = 0.025$ may represent the upper limit for a properly designed motoglider.

As to the fictitious rate of climb, the following considerations may be useful to evaluate its practical limits:

European practice has shown that engine power for single-place motogliders is included within 16 to 32 b.hp. This would give, for an average glider of this type weighing 770 lbs., the power loading within P/W = 48–24 lbs. per b.hp. These two limits can be taken as sample values for the considerations of the performance in powered flight. Assuming the propeller efficiency $\eta = 0.75$, the fictitious rate of climb will be as follows: about $V_{cf} = 8.5$ ft. per sec. for $W/P = 48$ lbs. per b.hp. and about $V_{cf} = 17.0$ ft. per sec. for $W/P = 24$ lbs. per b.hp.

For level flight, fictitious rate of climb is equal to the sinking speed:

$$V_{cf} = V_z$$

Thus, with help of Fig. 5, maximum flying speed at sea level can readily be found for W/S, W/P, and $C_{D_{min.}}$ chosen as the sample values. These speeds are listed in Table 2.

Maximum rate of climb at sea level is equal to the difference between the fictitious rate of climb (sea level) and the minimum sinking speed (3.3 ft. per sec.). This expressed in feet per minute will be as follows:

$$V_{c_0} = 60(V_{cf} - 3.3)$$

For $W/P = 48$ lbs. per b.hp., $V_{c_0} = 280$ ft. per min. The power loading $W/P = 24$ lbs. per b.hp. will raise this

TABLE 2

W/S, Lbs. per Sq.Ft.	W/P, Lbs. per B.Hp.	$C_{D_{min.}}$	$V_{max.}$ M.P.H.
5	48	0.015	82
		0.025	74
	24	0.015	112
		0.025	95
3	48	0.015	74
		0.025	61
	24	0.015	95
		0.025	79

NOTE: Aspect ratios—as shown on Fig. 5 and in Table 1.

figure considerably higher—to some 760 ft. per min. In the above calculations propeller efficiency was assumed to be $\eta = 0.70$.

The practical slope of climb, corresponding to the above rates of climb, will probably be close to 1:12 for the higher power loading, while for the lower one, it will be not too far from 1:5.

Service ceiling is found on Fig. 6 as an altitude at which the difference between the fictitious rate of climb and the sinking speed is equal to 100 ft. per min. The rate of decrease of power with altitude was accepted according to the curve given on page 244 of reference 2; the propeller efficiency was assumed to be $\eta = 0.7$. A glance at Fig. 6 will show that for $W/P = 48$ lbs. per b.hp. one may expect a service ceiling of about 8,000 ft.; for $W/P = 24$ lbs. per b.hp., it may reach as much as 20,000 ft.

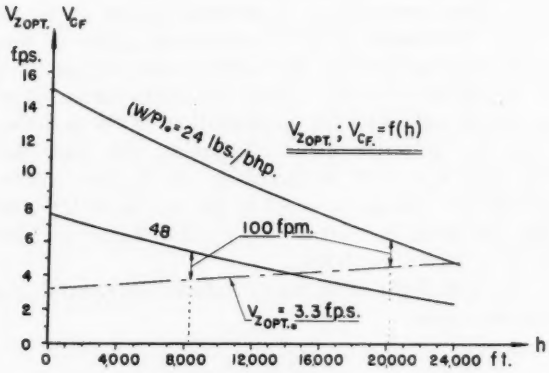

FIG. 6.

The take-off run on the ground is presented on Fig. 7 as a function of take-off speed. Several curves are drawn for different values of the ratio of static thrust T_0 to the total weight W. All these curves correspond to the following equation:

$$s = (1/2g)\{V_{t_0}^2/[(T_0/W) - \mu]\} \qquad (7)$$

Eq. (7) was chosen, keeping in mind that for the purpose of this paper simplicity and clearness of formulas may be more desired than a high accuracy. Ground friction coefficient in Eq. (7) was assumed to be $\mu = 0.08$.

Fig. 7 clearly shows two facts: (1) Even a slight increase of T_0/W over $T_0/W = 0.1$, which is assumed the lowest practical value, will cause a considerable gain in the take-off distance. (2) A low take-off speed is of prime importance for reducing the run on the ground.

A further examination of Fig. 7 will show that T_0/W within the limits 0.20 to 0.25, combined with a take-off speed of some 30 to 38 m.p.h., should assure the take-off run on the ground which can be favorably compared with the corresponding performance of any light plane.

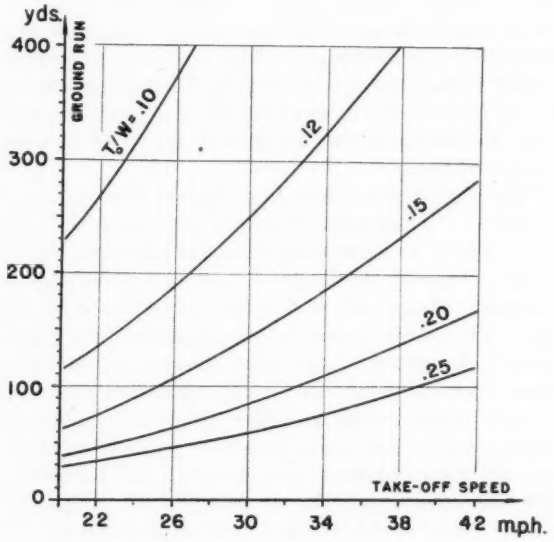

FIG. 7.

Table 3 may give some idea of what can be expected from a motoglider as far as the T_0/W ratio is concerned. In this table, for the engine power $P = 16$ b.hp., as well as for $P = 32$ b.hp. developed at different r.p.m., the propeller diameter D is shown for several design speeds (not far from the maximum speeds listed in Table 2).

TABLE 3

B.Hp.	Design Speed, M.P.H.	R.P.M.	D, Ft.	Design, V/nD	T_0, Lbs.	T_0/W
16	60	2,700	4.15	0.47	95	0.123
		2,200	4.60	0.52	105	0.136
	88	2,700	3.80	0.76	80	0.104
		2,200	4.20	0.84	95	0.123
32	.78	2,400	4.90	0.58	180	0.234
		2,000	5.35	0.64	195	0.253
	110	2,400	4.55	0.88	165	0.214
		2,000	5.00	0.96	180	0.234

NOTE: $W = 770$ lbs.

D was calculated to the following formula given in reference 2, page 249:

$$D = 300 \sqrt[4]{P/N^2V}$$

The static thrust T_0 was calculated by formula 15, reference 3:

$$T_0 = 550(aP/nD)$$

where a is $d\eta/d(V/nD)$ for the advance ratio $V/nD = 0$.

It is seen from the fifth column of Table 3 that values of the design advance ratio may roughly be divided into two groups: one close to $V/nD = 0.50$–0.55 and another close to $V/nD = 0.8$–0.85.

On Fig. 8 are presented two efficiency curves, $\eta = f(V/nD)$, which are drawn as an average of several two-blade propellers[4] and thus may be considered as typical efficiency curves that reach their $\eta_{max.}$ at $V/nD = 0.5$–0.55 and at $V/nD = 0.8$–0.85, respectively. The derivative $d\eta/d(V/nD)$ for $V/nD = 0$ yields the values of a necessary to calculate T_0. The values of T_0 are listed in the sixth column (Table 3) and those of T_0/W ($W = 770$ lbs.) in the last column.

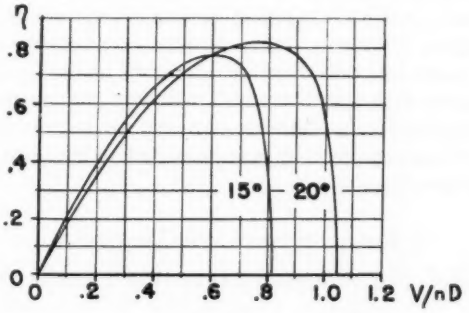

FIG. 8.

SPECIAL PROBLEMS OF MOTOGLIDERS

Drag of Engine-Propeller Groups

A reduction of the engine drag is as important in power-on as in power-off flight. But this problem can be linked to the larger one of reducing engine drag in general. Worth mentioning here is the pusher engine with horizontal cylinders, since this case is not often encountered in general considerations. The wind-tunnel tests conducted by the Institute for Gliding and Motogliding in Lwow, Poland, have shown that by cowling the cylinders their drag may be reduced to some 20 to 25 per cent of its initial value.

Among the other methods for reducing engine drag, there may be mentioned building the engine into the fuselage and driving the propeller by a special shaft, belt, or some other mechanical device. Structural complicity, however, may overbalance the aerodynamic gains.

As far as power-off flight is concerned, the best solution from the aerodynamic point of view would be a fully retractable engine-propeller group. Attempts toward this conception have been made by several motoglider designers. The disadvantage of such a device lies in a complexity perhaps even greater than in the case of the engine built into the fuselage.

As to the drag of the stopped propeller, the following example will show its importance: The drag coefficient of a stationary propeller is about $C_{D_p} = 1.05$.[4] Assuming an average value for the propeller diameter: $D = 4.7$ ft. and its solidity $\sigma = 0.09$, the increase of drag coefficient for a typical motoglider, having wing area of about 220 sq.ft., will be close to $\Delta C_D = 0.0075$ or more. This value of C_D, which in some cases may increase the minimum drag coefficient of the motoglider by as much as 40 to 45 per cent, shows the importance of this problem.

From the technical point of view it would be attractive to adopt fully feathered variable-pitch propellers for motogliders. The increase of drag due to the propeller in its feathered position would be negligible even for a highly "clean" motoglider. This solution, technically sound, will, however, be severely handicapped by the high price, a condition that may be relieved only by a wide development of light planes and motogliders.

A clutch installed between engine and propeller may be mentioned here as another means of reducing the propeller drag. With clutch disconnected, the propeller works "free-wheeling" and the torque coefficient can be assumed to be $Q_c = 0$.[6] Thrust (drag) of the propeller then will be:

$$T = T_c \rho V^2 D^2 \tag{8}$$

where T_c is the thrust coefficient corresponding to $Q_c = 0$.

Eq. (8) can be presented in the nondimensional form. Referring drag coefficient to the propeller disc area, Eq. (8) becomes:

$$C_{D_p} = 8T_c/\pi \tag{9}$$

For the propeller with low angle of blade setting (15°; design V/nD about 0.5), the average $T_c = 0.013$. For the higher blade setting (20°; design V/nD about 0.8), it will drop to some $T_c = 0.009$. For a motoglider having wing area $S = 220$ sq.ft. and a propeller measuring 4.7 ft. in diameter, the increase of the drag coefficient will be about $\Delta C_D = 0.001$ for the low-angle blade setting and about $\Delta C_D = 0.0007$ for the high one. From the aerodynamic point of view, both figures clearly show the high efficiency of this device. Additional weight (probably not too great) and the more complex construction may be mentioned as disadvantages of this solution. Nevertheless, it might be adopted with success, especially in the initial state of motoglider development. Compared with fully feathered propellers, this will prove less expensive and easier to make.

Starting the engine in flight is also one of the more important problems of motogliding. Among many possible solutions, one worth mentioning is that developed and successfully tested by the Institute for

Gliding and Motogliding. Valves operated by the pilot were installed in the cylinder heads, and their action was similar to that of the decompressor in a motor cycle. When the valves were opened, the torque exerted by the propeller was sufficient to turn the engine. After a few seconds of such a flight, the energy accumulated was sufficient to start the engine.

The "free-wheeling" propeller perhaps would not require any special decompressing device. The energy that it would represent at high r.p.m. should be sufficient to overcome compression in the cylinders.

General Design of Motogliders

It seems that motogliders in their general design should as much as possible resemble performance of training gliders. The two characteristic elements of glider construction which should be conserved in the motogliders are the pushed forward pilot's seat, assuring a good visibility, and the landing skid, which allows an exceptional freedom of landing even in rough terrains.

The main undercarriage necessary for take-off can be of the one-wheel or two-wheel type. That of the one-wheel type might be retractable or not, but it seems that the two-wheel type must be retractable, because of the necessity of drag reduction, as well as to provide for landing on a skid.

Fig. 9 shows schematically the general design of experimental motogliders designed and tested by the Institute for Gliding and Motogliding. The latest type (1939) had a two-wheel undercarriage, retractable into the fuselage.

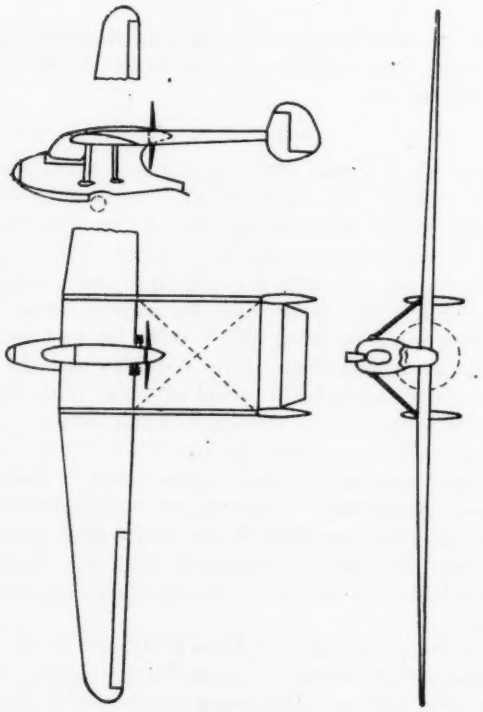

FIG. 9.

The Engine

A suitable engine is of prime importance for motogliding. Indeed, without solution of this problem, any development of motogliders can scarcely be imagined.

An examination of the possible limits for the motoglider performance seems to indicate that an engine developing a maximum power of about 25 to 30 b.hp. is suitable for the single-place machines. In order to keep a similar power loading, the two-place motogliders would require an engine of about 32 to 40 b.hp.

Prewar tendencies in the small engine construction show that engines with horizontal cylinders are definitely predominant in this category.

From experience, based on the tests made by the Institute for Gliding and Motogliding, as well as from opinions collected from several European designers of light planes and motogliders, it appears that with two-cylinder horizontal engines one must expect vibration troubles. These troubles, of course, are not impossible to overcome, but they are annoying to the designer. Engines with four horizontal cylinders give no trouble of this kind. In addition, they still are not expensive. For these reasons they may be considered as most suitable for motogliders.

Final Remarks and Conclusion

Since 1937 experiments have been made in Poland with the transition from gliders to motogliders of individual pilots, as well as of small groups. Experience has shown that even motogliders (single-place, of course) resembling a light plane rather than a glider (engine in front, fixed undercarriage, only flying properties close to the glider) did not present any particular difficulty to "pure" glider pilots. In the case of a motoglider similar to the one shown on Fig. 9, this transition was not much different from flying a new type of glider.*

The whole review of motoglider problems may be taken to indicate that these machines, if really able to soar, should be considered as belonging to the glider group. On the other hand, presence of the engine, as well as their possible performance in powered flight, introduces them to the group of light planes. This combined function of the motogliders seems to justify the opinion that they represent a natural link between gliders and light planes and that they might play some role in the whole development of national aviation. This is especially true in case of the establishment of a nation-wide program based on gliding and having as its

(*Continued on page 66*)

* In some cases the first flights were made in the gliding terrain by launching the motoglider like an ordinary glider—with a shock cord.

A Graphic Solution for Strains and Stresses from Strain Rosette Data

ROBERTO CONTINI*

Lockheed Aircraft Corporation

Introduction

It has been shown that the state of strain of a plane element through a point in a strained body is entirely determined by the measurement of three unit elongations on that plane element, provided all strains are small with respect to unity.[1]

In practice such measurements are taken on the surface of strained bodies by means of strain rosettes.

The most common types of rosettes are (a) the equiangular strain rosette, and (b) the 45° strain rosette with three or four gauges. A simple graphic construction, applicable to strain rosette data from either type of rosette mentioned, is presented in this paper. This construction gives a complete description of the state of strain at the point where strain measurements are taken, and it can be easily modified to describe the state of stress if the strained material is elastic and isotropic.

Certain properties characteristic of small deformations combined with the vectorial properties of sinusoidal currents have been utilized for the design of electrical strain computers.[2] To a large extent the construction presented in this paper performs graphically the same operations as the electrical computers perform electrically.

Notation and Conventions

The following notation and conventions are used in this paper:

- P = point of application of strain rosette on surface of strained body
- r_i = a direction through P on the plane tangent to the surface at P (i indicates any subscript used in the text)
- ϵ_i = unit elongation in direction r_i
- γ_{ij} = shearing strain = change in angle between two perpendicular directions r_i and r_j
- σ_i = normal stress on a plane perpendicular to r_i
- τ_{ij} = shear stress parallel to r_i (or r_j) acting on a plane perpendicular to r_j (or r_i)

Unit elongations are positive when changes in length are positive.

Shearing strains γ_{ij} are positive when changes in angle between r_i and r_j are negative.

Tensile normal stresses are positive and compressive normal stresses are negative.

Shear stresses τ_{ij} are positive when they produce negative changes in angle between r_i and r_j.

Angles are positive when measured counterclockwise.

Received June 13, 1944.

* Structures Research Engineer.

Description of Graphic Construction

The graphic construction is explained without proof under this heading. A detailed proof is given at the end of the paper.

Equiangular Strain Rosette

Let ϵ_1, ϵ_2, and ϵ_3 be three unit elongations measured along three directions r_1, r_2, and r_3 through a point P, as shown in Fig. 1.

Consider three unit vectors $\boldsymbol{i}$, $\boldsymbol{j}$, and $\boldsymbol{k}$, as shown in Fig. 2, and add the three vectors $\epsilon_1\boldsymbol{i}$, $\epsilon_2\boldsymbol{j}$, and $\epsilon_3\boldsymbol{k}$.

The resultant vector $\boldsymbol{r}$ has the following properties:

(1) Its magnitude is

$$r = 3(\epsilon_{max.} - \epsilon_{min.})/4 = 3\gamma_{max.}/4$$

where $\epsilon_{max.}$ and $\epsilon_{min.}$ are the algebraically larger and

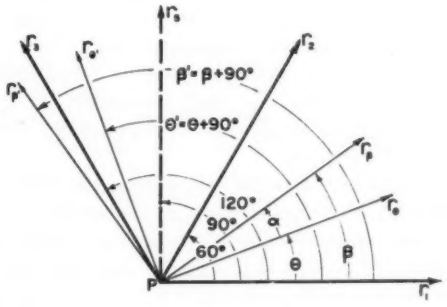

Fig. 1.

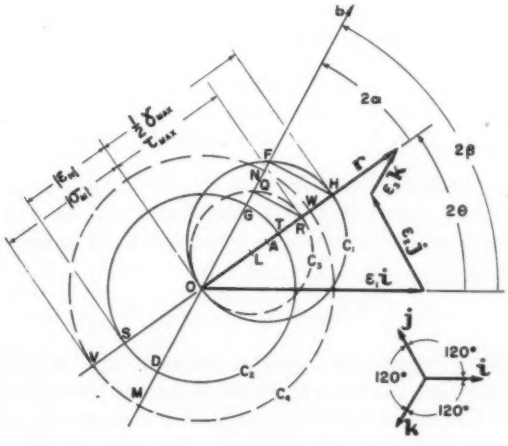

Fig. 2.

smaller principal strains, respectively, and $\gamma_{max.}$ is the maximum shearing strain.

(2) The angle 2θ (Fig. 2), i.e., the angle between $\boldsymbol{i}$ and $\boldsymbol{r}$ (measured from $\boldsymbol{i}$), is twice the angle between r_1 and the direction of the algebraically larger principal strain (measured from r_1).

In order to complete the construction take in Fig. 2 OA $= r/3 = \gamma_{max.}/4$ and with center in A, draw the circle C_1 of radius OA. Also, with center in O, draw the circle C_2 or radius $|\epsilon_m|$, where

$$\epsilon_m = (\epsilon_1 + \epsilon_2 + \epsilon_3)/3$$

The construction being thus completed, it is now possible to determine the unit elongation or the shearing strain in any direction.

If the unit elongation ϵ_β in the direction r_β at an angle β from r_1 (Fig. 1) is desired, draw in Fig. 2 an oriented line b through O inclined at an angle 2β from $\boldsymbol{i}$. The line b intersects C_2 in two points. Let the intersection on the positive side of b with respect to O be called the positive intersection, and the other the negative intersection.

The strain ϵ_β will be given by the magnitude of the vector whose origin is on the negative intersection of b with C_2 if $\epsilon_m > 0$ and on the positive intersection if $\epsilon_m < 0$, and whose end is on the intersection of b with C_1 other than O in all cases. The sign of ϵ_β is plus or minus according to whether the vector defined above has the same or opposite direction of b.

Thus in Fig. 2, ϵ_β is represented by DF, because ϵ_m is clearly larger than zero, and is positive. If ϵ_m were negative, then ϵ_β would be represented by GF and would still be positive.

The length of the vector FH, joining the intersection of b with C_1 with the intersection of $\boldsymbol{r}$ with C_1, is equal to one-half of the shearing strain $\gamma_{\beta\beta'}$ (where $\beta' = \beta + 90°$). The sign is positive or negative according to whether the angle from b to FH is plus or minus 90°. Thus from Fig. 2 $\gamma_{\beta\beta'}$ is negative.

In particular for $\beta = \theta$ and $\beta = \theta + 90°$, the principal strains SH and TH are obtained.

If the material is elastic and isotropic with

E = Young Modulus
μ = Poisson's Ratio
$G = E/2(1 + \mu)$ = Shear Modulus

and stresses are desired, take OL $= 2Gr/3 = \tau_{max.}/2$, and with center in L draw the circle C_3 of radius OL. Also, with center in O draw the circle C_4 of radius $|\sigma_m|$ where

$$\sigma_m = (E/1 - \mu)\epsilon_m$$

Stresses are now found in the same way as strains except that circles C_3 and C_4 must be used instead of C_1 and C_2 and that full lengths of shear stresses are represented instead of half of them. The rules for signs are also the same as for strains.

Thus in Fig. 2, since $\epsilon_m > 0$, σ_β is represented by MQ and is positive, while if ϵ_m were negative, σ_β would be represented by NQ and would be negative. The shear stress $\tau_{\beta\beta'}$ is represented by QR and is negative.

It can be seen from Fig. 2 that for the particular set of strains used, the strain circles C_1 and C_2 cut each other while the stress circles C_3 and C_4 do not.* By applying the rules explained above it can be found that the principal strains have opposite sign, while the principal stresses have the same sign.

In general, it can be stated that if the strain (or stress) circles cut each other, the principal strains (or stresses) have opposite sign. If they do not cut each other, the principal strains (or stresses) have the same sign. If the circles touch each other then one of the principal strains (or stresses) is zero.

45° Strain Rosettes

In the case of the three gauge 45° strain rosette, the three strains ϵ_1, ϵ_4, and ϵ_5 are measured along the three directions r_1, r_4, and r_5, shown in Fig. 4.

Consider the unit vectors $\boldsymbol{i}$ and $\boldsymbol{j}^*$ as shown in Fig. 5 and add the two vectors $(\epsilon_1 - \epsilon_5)\boldsymbol{i}$ and $(2\epsilon_4 - \epsilon_1 - \epsilon_5)\boldsymbol{j}^*$.

The resultant vector $\boldsymbol{r}^*$ has the property that its magnitude is

$$r^* = \epsilon_{max.} - \epsilon_{min.} = \gamma_{max.}$$

while the angle 2θ has the same significance as for the equiangular strain rosette.

The graphic construction is now identical to the one for the equiangular rosette except that the radius of C_1 is given by OA $= r^*/4 = \gamma_{max.}/4$, and the radius $|\epsilon_m|$ of C_2 is obtained by taking

$$\epsilon_m = (\epsilon_1 + \epsilon_5)/2$$

In the case of the four gauge 45° strain rosette, a fourth strain ϵ_6 is measured along the direction r_6 (Fig. 4) and $(\epsilon_4 - \epsilon_6)\boldsymbol{j}^*$ should be used in Fig. 5 instead of $(2\epsilon_4 - \epsilon_1 - \epsilon_5)\boldsymbol{j}^*$.

The quantities $(\epsilon_4 - \epsilon_6)$ and $(2\epsilon_4 - \epsilon_1 - \epsilon_5)$ should be equal because the sum of two perpendicular strains at a point is theoretically constant.† If, because of experimental errors, those two quantities are not equal, it is shown[2] that the effect of using $(\epsilon_4 - \epsilon_6)$ instead of $(2\epsilon_4 - \epsilon_1 - \epsilon_5)$ is equivalent to applying a correction of one-quarter of the difference $(\epsilon_1 + \epsilon_5) - (\epsilon_4 + \epsilon_6)$ to each of the strain readings.

Remarks on Graphic Construction

The amount of numerical computations necessary to complete the graphic constructions which have been described can be considerably reduced by means of a regular engineering scale.

For the equiangular rosette, for instance, if the length of $\boldsymbol{r}$ is read on the 20 scale, then the length OL corre-

* The stress circles were drawn by using $\mu = 0.3$ and disregarding the factor E.

† By virtue of this property the average of all of the four readings can be taken for ϵ_m.

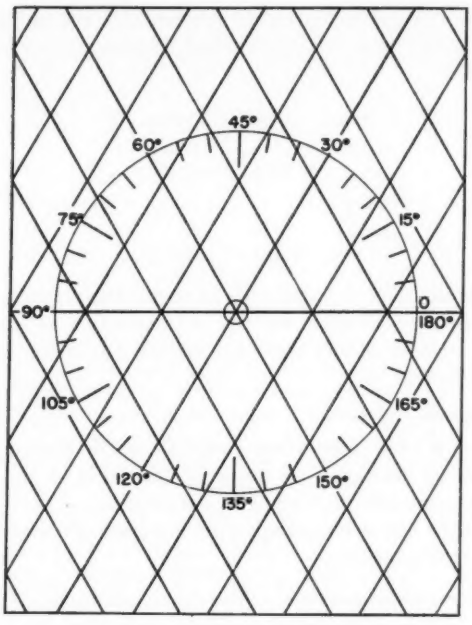

FIG. 3.

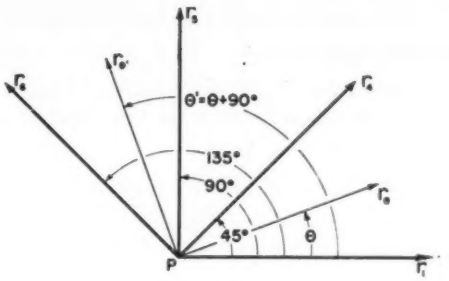

FIG. 4.

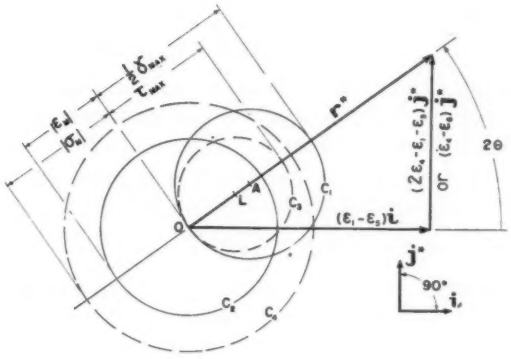

FIG. 5.

sponds to the same reading on the 60 scale. If, instead, ϵ_1, ϵ_2, and ϵ_3 are plotted with the 30 scale, the length of r read in the 40 scale gives the magnitude of the maximum shearing strain, and read in the 10 scale gives one-quarter of that magnitude. This latter reading can be used to plot OL with the 30 scale.

The use of prepared forms such as shown in Fig. 3 can also be helpful. If the construction is started at the center, the angle θ can be read directly on the graduated circle.

In the frequent case where the complete graphic representation of the state of strain or stress is not necessary, and instead, it is required to determine only principal strains and stresses and direction of principal stresses, it may be convenient to limit the graphic solutions described previous to the construction of the vector polygon, and derive all the required data numerically.

Table 1 shows how the necessary calculations can be arranged in simple form.

TABLE 1

	Equiangular Rosette	Three Gauge 45° Rosette	Four Gauge 45° Rosette
1	ϵ_1	ϵ_1	ϵ_1
2	ϵ_2	ϵ_4	ϵ_2
3	ϵ_3	ϵ_5	ϵ_5
4	① + ② + ③	① + ③	ϵ_6
5	④/3 = ϵ_m	④/2 = ϵ_m	① + ② + ③ + ④
6	r (graphically)	① − ③	⑤/4 = ϵ_m
7	2 ⑥/3 = $\gamma_{max.}/2$	2 × ②	① − ③
8	⑤ + ⑦ = $\epsilon_{max.}$	⑦ − ④	② − ④
9	⑤ − ⑦ = $\epsilon_{min.}$	r^* (graphically)	r^* (graphically)
10	⑤$E/(1-\mu)$ = σ_m	⑨/2 = $\gamma_{max.}/2$	⑨/2 = $\gamma_{max.}/2$
11	⑦$E/(1+\mu)$ = $\tau_{max.}$	⑤ + ⑩ = $\epsilon_{max.}$	⑥ + ⑩ = $\epsilon_{max.}$
12	⑩ + ⑪ = $\sigma_{max.}$	⑤ − ⑩ = $\epsilon_{min.}$	⑥ − ⑩ = $\epsilon_{min.}$
13	⑩ − ⑪ = $\sigma_{min.}$	⑤$E/(1-\mu)$ = σ_m	⑥$E/(1-\mu)$ = σ_m
14	θ (graphically)	⑩$E/(1+\mu)$ = $\tau_{max.}$	⑩$E/(1+\mu)$ = $\tau_{max.}$
15	.....	⑬ + ⑭ = $\sigma_{max.}$	⑬ + ⑭ = $\sigma_{max.}$
16	.....	⑬ − ⑭ = $\sigma_{min.}$	⑬ − ⑭ = $\sigma_{min.}$
17	.....	θ (graphically)	θ (graphically)

Analytic Proof of Graphic Solution

Equiangular Strain Rosette

Referring to Fig. 2, the magnitude of $\boldsymbol{r}$ is given by the sum of the components of the three vectors $\epsilon_1\boldsymbol{i}$, $\epsilon_2\boldsymbol{j}$, and $\epsilon_3\boldsymbol{k}$ along the line of $\boldsymbol{r}$, i.e.,

$$r = \epsilon_1 \cos 2\theta + \epsilon_2 \cos (2\theta - 120°) + \epsilon_3 \cos (2\theta - 240°) = \{\epsilon_1 - [(\epsilon_2 + \epsilon_3)/2]\} \cos 2\theta + (\sqrt{3}/2)(\epsilon_2 - \epsilon_3) \sin 2\theta \quad (1)$$

The sum of the components of the same three vectors along the direction perpendicular to $\boldsymbol{r}$ is zero, therefore

$$\epsilon_1 \cos (2\theta + 90°) + \epsilon_2 \cos (2\theta - 30°) + \epsilon_3 \cos (2\theta - 150°) = \{-\epsilon_1 + [(\epsilon_2 + \epsilon_3)/2]\} \sin 2\theta + (\sqrt{3}/2)(\epsilon_2 - \epsilon_3) \cos 2\theta = 0 \quad (2)$$

Consider a direction r_5 normal to r_1; then, using the known formulas for orthogonal transformation (reference 3, p. 43, Eqs. (11)):

$$\epsilon_2 = (\epsilon_1/4) + (3\epsilon_5/4) + (\sqrt{3}\gamma_{15}/4) \quad (3)$$

$$\epsilon_3 = (\epsilon_1/4) + (3\epsilon_5/4) - (\sqrt{3}\gamma_{15}/4) \quad (4)$$

Substituting Eqs. (3) and (4) into Eq. (1)

$$\begin{aligned} r &= \epsilon_1 \cos 2\theta - [(\epsilon_1/4) + (3\epsilon_5/4)] \cos 2\theta + 3\gamma_{15} \sin 2\theta/4 \\ &= {}^3/_4[(\epsilon_1 - \epsilon_5) \cos 2\theta + \gamma_{15} \sin 2\theta] \\ &= {}^3/_4[(\epsilon_1 \cos^2\theta + \epsilon_5 \sin^2\theta + \gamma_{15} \sin\theta \cos\theta) - (\epsilon_1 \sin^2\theta + \epsilon_5 \cos^2\theta - \gamma_{15} \sin\theta \cos\theta)] \\ &= 3(\epsilon_\theta - \epsilon_{\theta'})/4 \end{aligned} \quad (5)$$

where $\theta' = \theta + 90°$. Substituting Eqs. (3) and (4) into Eq. (2)

$${}^3/_4[(\epsilon_5 - \epsilon_1) \sin 2\theta + \gamma_{15} \cos 2\theta] = {}^3/_4[2(\epsilon_5 - \epsilon_1) \times \sin\theta \cos\theta + \gamma_{15}(\cos^2\theta - \sin^2\theta)] = 3\gamma_{\theta\theta'}/4 = 0 \quad (6)$$

Since $\gamma_{\theta\theta'} = 0$ the direction r_θ is a direction of principal strain (and also of principal stress). It can also be concluded that it is the direction of the algebraically larger principal strain (and stress), because from Eq. (5) since $r > 0$ it must be $\epsilon_\theta > \epsilon_{\theta'}$ or also $\epsilon_\theta = \epsilon_{max.}$, $\epsilon_{\theta'} = \epsilon_{min.}$, and $r = 3(\epsilon_{max.} - \epsilon_{min.})/4 = 3\gamma_{max.}/4$.

Strains and stresses in any direction r_β (Fig. 1) at an angle β from r_1 can be obtained in terms of the principal strains and stresses by means of the known formulas

$$\epsilon_\beta = \epsilon_m + (\gamma_{max.}/2) \cos 2\alpha$$

$$\gamma_{\beta\beta'} = -\gamma_{max.} \sin 2\alpha \quad (7)$$

$$\sigma_\beta = \sigma_m + \tau_{max.} \cos 2\alpha$$

$$\tau_{\beta\beta'} = -\tau_{max.} \sin 2\alpha \quad (8)$$

where $\epsilon_m = (\epsilon_{max.} + \epsilon_{min.})/2$, $\sigma_m = (\sigma_{max.} + \sigma_{min.})/2$, and $\alpha = \beta - \theta$ = angle from r_θ to r_β.

It is easily shown that

$$(\epsilon_1 + \epsilon_2 + \epsilon_3)/3 = \epsilon_m \quad (9)$$

By adding Eqs. (3) and (4) and adding ϵ_1 to both sides it can be written $\epsilon_1 + \epsilon_2 + \epsilon_3 = 3(\epsilon_1 + \epsilon_5)/2$. This proves Eq. (9) because the sum of two unit elongations in two directions perpendicular to each other is an invariant.

Since the normal stress perpendicular to the surface of the body is zero on the surface, Hooke's law can be written

$$\epsilon_{max.} = (\sigma_{max.} - \mu\sigma_{min.})/E$$

$$\epsilon_{min.} = (\sigma_{min.} - \mu\sigma_{max.})/E$$

$$\gamma_{max.} = [2(1 + \mu)/E]\, \tau_{max.}$$

hence

$$\epsilon_m = [(1 - \mu)/E]\sigma_m \quad (10)$$

With Eqs. (7), (8), and (10) in mind, the construction previously described for the determination of strains and stresses in any direction on the surface is easily understood.

45° Strain Rosettes

In the case of the three gauge 45° strain rosette, the following relations are obtained from Fig. 5 by projecting the two vectors $(\epsilon_1 - \epsilon_5)\boldsymbol{i}$ and $(2\epsilon_4 - \epsilon_1 - \epsilon_5)\boldsymbol{j}^*$ upon the line of $\boldsymbol{r}^*$ and upon the direction perpendicular to $\boldsymbol{r}^*$, respectively,

$$r^* = (\epsilon_1 - \epsilon_5) \cos 2\theta + (2\epsilon_4 - \epsilon_1 - \epsilon_5) \sin 2\theta \quad (11)$$

$$0 = -(\epsilon_1 - \epsilon_5) \sin 2\theta + (2\epsilon_4 - \epsilon_1 - \epsilon_5) \cos 2\theta \quad (12)$$

Since from the formulas for orthogonal transformation

$$\epsilon_4 = (\epsilon_1 + \epsilon_5 + \gamma_{15})/2 \quad (13)$$

the substitution of Eq. (13) into Eq. (11) gives

$$\begin{aligned} r^* &= (\epsilon_1 - \epsilon_5) \cos 2\theta + \gamma_{15} \sin 2\theta \\ &= (\epsilon_1 \cos^2\theta + \epsilon_5 \sin^2\theta + \gamma_{15} \sin\theta \cos\theta) - (\epsilon_1 \sin^2\theta + \epsilon_5 \cos^2\theta - \gamma_{15} \sin\theta \cos\theta) \\ &= \epsilon_\theta - \epsilon_{\theta'} \end{aligned}$$

and the substitution of Eq. (13) into Eq. (12) gives

$$(\epsilon_5 - \epsilon_1) \sin 2\theta + \gamma_{15} \cos 2\theta = 2(\epsilon_5 - \epsilon_1) \sin\theta \cos\theta + \gamma_{15} (\cos^2\theta - \sin^2\theta) = \gamma_{\theta\theta'} = 0$$

Hence, in the same way as for the equiangular rosette, it can be concluded that the angle θ defines the direction of the maximum strain, and that the magnitude of $\boldsymbol{r}^*$ is

$$r^* = \epsilon_{max.} - \epsilon_{min.} = \gamma_{max.}$$

For the four gauge 45° rosette the proof is exactly the same since the fourth reading can always be eliminated from the analytic standpoint.

References

[1] Mindlin, R. D., *The Equiangular Strain Rosette*, Civil Engineering, p. 546, August, 1938.

[2] Klemperer, W. B., *A Rosette Strain Computer*, N.A.C.A. T.N. No. 875.

[3] Love, A. E. H., *Treatise on the Mathematical Theory of Elasticity*, 4th Edition; The Macmillan Company, New York, 1927.

Note: The analytic proof concerning the vector summation for both equiangular and 45° rosettes is essentially the same as the one given in reference 2.

Investigation of the Wing-Wake Frequency with Application of the Strouhal Number

M. ZBIGNIEW KRZYWOBLOCKI*

Polytechnic Institute of Brooklyn

SUMMARY

The present paper consists of two parts. The aim of the first part is to record the results of calculation of the Strouhal Number in two-dimensional flow behind an infinite plate, an infinite circular cylinder, and an infinite airfoil. The results obtained are compared with those from previous tests, and sometimes a fair agreement is obtained. The most important conclusions are as follows:

(1) In general the Strouhal Number is not a constant.

(2) The Strouhal Number in the wake behind a body with sharp edges is approximately constant.

(3) The Strouhal Number in the wake behind a circular cylinder is constant only below the critical Reynolds Number. Above the critical Reynolds Number some assumptions permit one to conclude that as a first approximation the Strouhal Number is a linear function of the Reynolds Number.

(4) When the wake behind an airfoil consists of vortex rows, the value of the Strouhal Number behind the airfoil, referred to the projection of the airfoil on the direction perpendicular to the direction of the flow, may be assumed as a constant.

In the second part of this paper the results of some tests in a wind tunnel in two- and three-dimensional flow are presented. The following bodies were tested:

(a) Airfoil in two-dimensional flow.

(b) Airfoil of finite length.

(c) Airfoil with flap in two-dimensional flow.

(d) Airfoil with flap of finite length.

The purpose of the tests was to find and to compare the values of the Strouhal Number behind the above-mentioned bodies. The results of the tests proved that:

(a) When one refers the value of the Strouhal number of any airfoil in two-dimensional flow, with or without flaps, to the projection of the airfoil on the direction perpendicular to the direction of the airflow, the values of the Strouhal Number are within the limits of the values given by other investigators.

(b) The frequency in the wake behind the center span of a rectangular airfoil of finite length is not affected by the tip vortexes.

(c) The graph of frequency versus velocity appears to be a straight line but it is difficult to see whether it always passes through the origin of coordinates, although a slight tendency is visible. Blenk obtained straight lines passing through the origin, but his results do not agree with results obtained by Abdrashitov.

INTRODUCTION

THE PHENOMENON OF BUFFETING is an immediate problem and one cannot suppose that it is solved. The phenomenon of buffeting is closely connected with the problem of wing-wake frequency.

The aim of the first part of this paper is to present the results of calculation of the value of the Strouhal Number behind various bodies in two-dimensional flow. At first, brief reviews of buffeting and wake investigations are given. Later, all double vortex street characteristics and a comparison of those characteristics obtained by various investigations are presented.

In order not to complicate the calculation, the simplest possible ways will be used. The Strouhal Number behind the flat plate will be calculated and the results compared with those of the tests. Similar methods will be applied to a circular cylinder in two-dimensional flow in the range below the critical Reynolds Number. The picture is completely different when the Reynolds Number exceeds the critical value. Because in the present paper it is difficult to speak about the frequency of disturbances from the standpoint of the exact theory of turbulence, some simplifying assumptions will be made.

In the case of the infinite plain airfoil, the value of the Strouhal Number will be referred to the projection of the airfoil on the direction normal to the direction of the flow, according to the suggestion by Blenk. In order to calculate the form drag, the results of some investigators will be applied. In calculating the width of the wake behind an airfoil the results of tests performed by N.A.C.A. are used. The results of this calculation will be compared with the results of tests.

In the second part of this paper results of some tests in the wind tunnel are given. The tests deal with the value of the Strouhal Number behind several types of bodies.

SYMBOLS

h	=	distance between the rows of vortexes (breadth of street)
a	=	distance between successive vortexes in each row (spacing)
u	=	velocity of the total geometric pattern of the eddies relative to the undisturbed flow
Γ	=	intensity of a vortex
V	=	velocity of the flow
f	=	frequency
T	=	period
D_f	=	form drag per unit span
ρ	=	density
γ	=	kinematic coefficient of viscosity
d	=	diameter of the wire or breadth of the obstacle or lamina
S	=	fd/V = Strouhal Number
α	=	angle of incidence

Presented at the Aerodynamics Session, Twelfth Annual Meeting, I.A.S., New York, January 25–27, 1944.

* Instructor. Now at Brown University.

b = breadth
D = drag
C_D = drag coefficient
A = area
R = Reynolds Number
l = length of chord of an airfoil or breadth of a plate
K = constant
t = thickness of the plate or airfoil
C_{D_p} = coefficient of the profile drag
$t_{max.}$ = maximum thickness of airfoil
h_w = width of the wake behind the airfoil
p = distance of the trailing edge behind the vertex of parabolic wake distribution curve
δ = thickness ratio

Calculation of the Strouhal Number

A Brief Review of Buffeting

It is difficult to tell when the phenomenon of "buffeting" became, in reality, the cause of tail vibration, because reports had already been written in the year 1916 on the subject of tail vibration at certain critical speeds of flight. But this phenomenon received considerable attention after the well-known crash of the Junkers airplane G-AAZK at Meopham, Kent, England, on July 21, 1930. The accident was followed by many papers and tests in England, United States, and Germany. After extensive investigations conducted at the scene of the accident and in aerodynamic laboratories, the British came to the conclusion that the accident was caused by tail buffeting. The Germans, after no less extensive investigations, arrived at the conclusion that the accident could not have been due to buffeting. During the following years some investigators attempted to find the best solution of avoiding buffeting. From these tests the following conclusions can be drawn:

(a) The amplitude of tail vibration depends mostly on the position of the horizontal tail surfaces with respect to the wing in the vertical direction and little on the position in the horizontal direction.

(b) The rigidity of the rear part of the fuselage and that of the horizontal surfaces must be so great that the natural frequency of these parts does not coincide with the frequency of disturbances* behind the wing.

(c) The chief reason for tail vibration in a straight-line flight is caused by disturbances originating on the upper surface of the wing due to existing pressure gradient.

(d) The phenomenon of tail vibration in a sideslip is caused by disturbances having their origin at the wing and fuselage.

(e) Not only at large but at small angles of attack disturbances arise from the juncture of the wing and fuselage, which can cause tail vibration. The disturbances arise at both sides of the fuselage and usually in an unsymmetrical manner.

(f) The vibration may be avoided by location of the tail surfaces outside the region of disturbances.

(g) One of the best methods in practice was to fair properly the fuselage and wing with wing root fillets.

In the year 1933 the first American tests appeared on this subject. The best all-round results were obtained by the use of fillets and N.A.C.A. cowling. Some investigators came to the conclusion that sweeping the wing roots up slightly has a good effect. The next investigations brought the conclusion that properly designed wing root fillets may have a positive influence on the maximum speed of an airplane. In the years 1934–1939 there appeared a number of papers on this subject, including wind-tunnel tests, which sometimes dealt with tail buffeting, increase of speed, and some wake characteristics—i.e., the wake position, the location of the center of the wake, the wake width, the distribution of dynamic pressure across the wake, etc.

In the more recent papers the aerodynamic phenomenon of the wake is connected with the problem of vibrations of the tail surfaces.

Because of the part played by wing wake in the phenomenon of tail buffeting, some space will be devoted here to wake investigations.

A Brief Review of Wake Investigations

The investigations of wake characteristics have been carried out independently of the investigations of tail buffeting and were started much earlier than the investigations of tail buffeting. It is sufficient to mention that the problem in vortex motion was studied in the nineteenth century. In the twentieth century the periodicity of the vortex formation behind cylinders was studied by von Kármán, Rubach, Relf, Bernard, and many others. Von Kármán investigated the stability of the vortex system and gave relations between the vortex spacing, frequency, and drag. Levy, Hooker, and Rosenhead also made computation on the stability of the vortex system. The eddy frequency was studied by Relf, Simmons, and Lock. An excellent analysis of the vortex system is given by Lamb. A large number of tests were concerned with the determination of the Strouhal Number. Fage and Johansen investigated the value of the Strouhal Number behind flat plates and airfoils. Blenk studied the value behind cylinders, plates, and airfoils. Tyler studied this number behind obstacles of various sections. The summary of various investigations of this subject can be found in the works of Glauert, Dryden, Lamb, Goldstein, and others.

As was explained above, the wake characteristics play an important part in the phenomenon of tail buffeting. From the design point of view, it may be of interest to know the frequency with which the dis-

* Since most disturbances are due to vortex discharges, the words disturbance and vortex may be used indiscriminately.

turbances are formed behind the wing in order to avoid resonance with the rear part of the fuselage and tail surfaces.

The Kármán Trail

Frequency

The investigations carried through by von Kármán led to the result that a double vortex row of the stable type must fulfill the following conditions:

$$\sinh \pi h/a = 1 \tag{1}$$

or

$$h = 0.2806a \leqq 0.281a \tag{2}$$

The velocity of the total geometric pattern of the eddies and the intensity of a vortex are connected by means of formula:

$$\Gamma = 2\sqrt{2}au \tag{3}$$

The frequency and the period with which the vortexes are formed in each row are:

$$f = (V - u)/a = V[1 - (u/V)]/a \tag{4}$$

$$T = a/(V - u) \tag{5}$$

The Form Drag

The formation of the vortexes, combined with the general pressure distribution of the flow pattern, causes a form drag per unit of span:[1]

$$D_f = \rho\Gamma(V - 2u)(h/a) + \rho(\Gamma^2/2\pi a) \tag{6}$$

or

$$D_f = h\rho V^2[2.83\,(u/V) - 1.12\,(u/V)^2] \tag{7}$$

Frequency and the Strouhal Number

It should be noted that the formation of a double train of vortexes behind a body may be referred to the field of acoustical phenomena. Rayleigh observed[3] that the frequency of the note produced by air rushing past a cylindrical wire must satisfy the formula:

$$f = (V/d)f(\gamma/Vd) \tag{8}$$

Often, the frequency of vibration is referred to the velocity by means of the Strouhal Number given as:

$$S = fd/V \tag{9}$$

Rayleigh[3] constructed also an empirical formula as a representation of some observations of Strouhal for a circular wire:

$$fd/V = 0.195\,[1 - (20.1\gamma/Vd)] = 0.195\,[1 - (20.1/R)] \tag{10}$$

Many authors are of the opinion that from the practical standpoint the value of the Strouhal Number may be considered constant for the usual shapes.

Comparison of Kármán Trail Characteristics Obtained by Some Investigators

Breadth, Spacing, and Spacing Ratio. In Table 1 there are included values of spacing ratio behind various bodies found by some investigators.

Table 1

Body	Investigator	Spacing Ratio
Circular cylinder	von Kármán	0.281
	Tyler	0.308
	Gradual increase in spacing ratio downstream	
	Rosenhead and Schwabe	0.320
Elliptic Cylinder	Richards[3]	0.320
	The spacing ratio increases slowly farther down the wake	
Flat Plate	von Kármán and Rubach	0.300
	Fage and Johansen[3]	0.25 to 0.38
	Flat plate normal to the stream. The value 0.25 was obtained at a distance equal to 5 breadths of the plate, and 0.38 was obtained at a distance equal to ten breadths of the plate	
		Strouhal Number
Circular Cylinder	von Kármán	0.207 and 0.198
	For two different speeds	
	Blenk, Fuchs, and Liebers	0.207
Plate	Fage and Johansen	0.148
	Blenk, Fuchs, and Liebers	0.180
	Tyler	0.158
	von Kármán	0.144
Airfoil	Tyler	0.150
	Fage	0.150
	Blenk, Fuchs, and Liebers	0.210

Fage and Johansen investigated the wake behind a flat plate at incidences other than 90°, and Tyler investigated the wake behind plates and airfoils at various incidences. It was found that the ratio of the vortex spacing to the breadth facing the stream

$$a/(b \sin \alpha) \tag{11}$$

does not change much above 30° or 40° of incidence.

In the discussion given below an average value of the spacing ratio—constant for all bodies, independent of the shape—equal to 0.281 will be assumed.

Frequency and the Strouhal Number. Relf, Simmons, and Tyler investigated the frequency behind wires and circular cylinders. Tyler suggested the formula that agrees well with the formula given by Rayleigh.[3] Values of frequency behind a flat plate were investigated by Fage and Johansen; behind plates and airfoils at various angles of incidence, by Tyler and by Blenk, Fuchs, and Liebers.[4] Some results are given in Table 1.

In investigations of Blenk and Fage the value d in the Strouhal Number refers to the projection of the airfoil on the direction perpendicular to the direction of the flow. Nearly all investigators agree that if d is

the breadth of the obstacle across the stream, the Strouhal Number for plates and airfoils is nearly constant for angles of incidence greater than 24°–30°.

Many investigators referred the value of the Strouhal Number to the projection of the lamina on the direction perpendicular to the direction of the flow without taking into account the thickness of the lamina. In Blenk's investigations the thickness of the lamina is taken into account.

The Velocity of the Vortex Street. The vortex street passes down with the velocity $(V - u)$ relative to the body. In fact, there is no theory from which one can deduce values for u/V. Heisenberg,[3] on the basis of his theoretical considerations, came to the conclusion that for a flat plate this value may be accepted:

$$u/V = 0.2295 \tag{12}$$

According to Prandtl the assumptions underlying Heisenberg's considerations are not correct. Nevertheless, Goldstein[3] is of the opinion that this value may not be far from the truth in some cases, although the agreement is fortuitous, and that it may be accepted as a representative experimental value. Tyler in his tests found the limits of the value of u/V close to a cylinder equal to 0.358 and equal to 0.124 for measurements far behind the body.

Wakes Other Than Double Row of Vortexes

In wakes other than double row of vortexes, often no definite periods can be measured. The frequency of the most prominent disturbances, however, may be sometimes recorded. Consequently, one may refer the Strouhal Number to those wakes taking into account the mentioned frequency. Until now there is lack of formulas defining frequency of disturbances in any other type of wake than double row of vortexes.

Plate in Two-Dimensional Flow

Many investigators are of the opinion that in the case of bodies with sharp edges, the vortex system is geometrically similar over the whole range of Reynolds Number with the exception of small values. In the case of blunt and streamlined bodies, where the wake is produced by the separation of the boundary layer, it appears that the regular vortex rows disappear at the critical value of the Reynolds Number. In the range of higher Reynolds Numbers a turbulent wake with continuous vorticity distribution replaces the vortex system.

From Eqs. (2), (4), and (9) Strouhal Number is given by the relations:

$$S = \frac{fd}{V} = \frac{1 - (u/V)}{a/d} = \frac{0.281[1 - (u/V)]}{h/d} \tag{13}$$

Expressing the form drag per unit length in terms of the drag coefficient C_{Df} defined by D_f: $\rho V^2 d/2$ and substituting in Eq. (7) one has:

$$C_{Df}\rho V^2 d/2 = h\rho V^2[2.83(u/V) - 1.12(u/V)^2] \tag{14}$$

or

$$d/h = [1.59(u/V) - 0.63(u/V)^2]/0.281C_{Df} \tag{15}$$

Hence

$$S = \frac{1.59(u/V) - 2.22(u/V)^2 + 0.63(u/V)^3}{0.281C_{Df}} \tag{16}$$

In the following discussion the total drag coefficient C_D will be used instead of C_{Df} to compute approximate values of the Strouhal Number. For a plate in two-dimensional flow:

$$C_D = 2 \tag{17}$$

If one accepts Heisenberg's value $u/V = 0.2295$ one has from Eq. (16):

$$S = 0.128 \tag{18}$$

and from Eq. (15)

$$d/h = 0.591 \tag{19}$$

Assumption that S equals 0.15 from experimental data leads to:

$$u/V = 0.319 \tag{20}$$

and

$$d/h = 0.789 \tag{21}$$

Goldstein cites the value 0.648 for this ratio as given by Heisenberg (reference 3, page 564).

Some further remarks will be given concerning the rate of discharge of vorticity shed from the two sides of the plate. According to the Helmholtz-Kirchhoff-Rayleigh free streamline theory for flow past a flat plate, the rate of discharge of vorticity would be $V^2/2$.[3] Heisenberg put the average rate at which vorticity passes downstream in one row of the vortex street equal to the rate obtained from the Helmholtz-Kirchhoff-Rayleigh free streamline theory:

$$\Gamma(V - u)/a = V^2/2 \tag{22}$$

Applying Eq. (3) Heisenberg's value of u/V, Eq. (12), is obtained.

Goldstein gives the value of the rate of vorticity obtained from tests equal to $1.07\ V^2$ (reference 3, pages 555 and 563) but mentions in another place that, according to the investigation of Fage and Johansen, the rate of vorticity by the time the vortex street is formed is, in some cases, reduced almost to $V^2/2$.

Assuming, for comparative purposes, the value of u/V from Eq. (20) and substituting it into the term of the average rate at which vorticity passes downstream in one row of the vortex street leads to:

$$\Gamma(V - u)/a = 0.613V^2 \tag{23}$$

TABLE 2

C_D Ref. 6, Vol. IV, p. 142	R Ref. 6, Vol. IV, p. 142	S Eq. (16)	S Goldstein	S Blenk	S Eq. (10)	Notes
3.80	5	0.06745	..	..	....	R smaller than the
1.45	10^2	0.1766	0.12	0.16	0.156	critical Reynolds
1.00	$10^{2.3}$	0.2560	0.21	0.21	0.1948	number
0.30	10^3	0.853	Not given but seems to be high	..	0.1949	$R > R$ cr.

This appears to be in agreement with the above remark of Goldstein.

Circular Cylinder in Two-Dimensional Flow

As is known, the value of C_D for a circular cylinder is given by a curve with a sudden drop at the critical value of the Reynolds Number. One can conclude from Eq. (16) that the value of S is not constant through the entire region of the Reynolds Number. Using the data for the drag of an infinite cylinder from reference 6, Volume IV, page 142, and Heisenberg's value of u/V, the values shown in Table 2 from Eq. (16) are obtained.

The calculated values from Eq. (16) are compared with the test values given by Goldstein and Blenk. As may be seen from the table, the values of S from Eq. (16) are not much different from those obtained from tests in the subcritical range. The general shape of the function

$$S = 0.256/C_D = f(R) \tag{24}$$

obtained from Eq. (16) by using Heisenberg's values for u/V seems to be similar in the subcritical range of Reynolds Number to the curve obtained from tests and given by Goldstein[3] for a circular cylinder, although values obtained from Eq. (16) are on the average higher than those given by Goldstein. The values given by Blenk are sometimes higher than those of Goldstein. Eq. (10) shows fair agreement, but only in the region below the critical Reynolds Number.

In the range of the Reynolds Number higher than the critical, neither Eq. (16) nor Eq. (10) gives good values of S as compared with those given by Goldstein. According to Goldstein, in the range above the critical Reynolds Number the frequencies increase rapidly with R, which cannot be observed from Eq. (16) by using Heisenberg's value of u/V.

From the above, one may conclude that for plates Heisenberg's value of u/V gives the values of S in the whole range of Reynolds Number fairly close to values obtained from tests. For cylinders, Heisenberg's value of u/V gives the values of S fairly close to the values obtained from tests, but only in the subcritical range. Rayleigh's formula for the Strouhal Number may represent closely enough, from the practical standpoint, the true values of S, but only in the subcritical range. This conclusion is in accordance with that given by Tyler.[7]

One may approach this problem in still another way. The range of small values of the Reynolds Number will not be taken into consideration. For Reynolds Numbers below the critical, the geometric pattern of the wake behind a cylinder is similar to that behind a plate. The above given consideration and results for a plate are also valid in a first approximation for a circular cylinder. The difference is in the value of the ratio d/h. That is, many pictures and investigations of the Kármán trail behind a circular cylinder justify the assumption that as a first approximation at a distance behind the cylinder one may assume:

$$d/h = 0.85 \text{ to } 1.04 \tag{25}$$

As is known the width of the Kármán trail increases downstream. All measurements taken far enough from the body give also higher values of h. Tyler obtained the values shown in Table 3 for h in wind tunnel for various circular cylinders.

TABLE 3

Diameter in Cm.	Speed of Air	Distance Behind Cylinder in Cm.	S	d/h
3.580	202.7 cm./sec.	11.50	0.177	0.944
2.500	222.0 cm./sec.	10.00	0.169	0.835
1.400	114.3 cm./sec.	10.00	0.184	0.824
0.320	295.0 cm./sec.	1.00	0.197	0.930
0.285	292.0 cm./sec.	1.30	0.197	0.803
0.420	288.0 cm./sec.	2.00	0.197	1.013
0.585	293.0 cm./sec.	2.50	0.195	1.054

From Eqs. (2), (4), and (9):

$$S = 0.281[1 - (u/V)](d/h) \tag{26}$$

Application of the value of d/h from Eq. (25) and of the value of u/V from Eq. (20) derived from the experimental value of S for plates leads to

$$S \sim 0.163 \text{ to } 0.199 \tag{27}$$

These values are within the limits of values given by von Kármán, Blenk, and others.

The picture is completely different when the Reynolds Number exceeds the critical value. Goldstein is of the opinion that in the range beyond the critical

Reynolds Number $R > 10^5$ no definite periods can be measured behind a cylinder. The frequencies of the most prominent disturbances, however, could be recorded, and there is no doubt that they increase rapidly with R. For the range below the critical Reynolds Number the flow in the wake is periodic; above the critical 1 Reynolds Number the flow is aperiodic. One must also assume that at the critical Reynolds Number there occur some basic changes in the wake. To obtain a better review of this phenomenon one probably has to look for a solution in the theory of turbulence.

If one assumes that the eddy frequency in turbulent flow behind a body is related to the mean velocity of flow and the viscosity of the fluid by the formula*

$$f = (1/K)(V^2/\gamma) \tag{28}$$

where K is a constant depending on the shape of the body, one obtains the relation:

$$S = (1/K)R \tag{29}$$

To find the constant K for a cylinder, the value of the Strouhal Number for a Reynolds Number of 500,000 is taken as 0.2375 from Goldstein's diagram (reference 3, Volume II, page 419, Fig. 149). This gives:

$$K = 2.11 \times 10^6 \tag{30}$$

Fig. 1 shows a comparison of the present results with those of Goldstein. The agreement is fair.

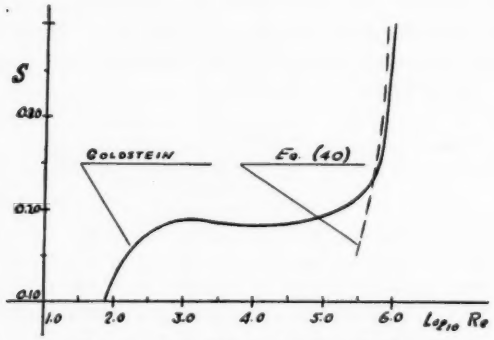

FIG. 1. S vs. R for a circular cylinder.

AIRFOIL IN TWO-DIMENSIONAL FLOW

As was explained before, some investigators tested airfoils at large angles of incidence in order to find the Strouhal Number. The conclusion was drawn that for angles of incidence between 20° and 90° the Strouhal Number is constant and equal to 0.15. But the same value was found for a plate, and, strictly speaking, an airfoil at these angles of incidence acts like a plate.

But from the practical standpoint the most important range of angles of incidence is that below and at the stalling point. For airfoils in water for 0° angle of attack at the speed of about 17.5 cm. per sec., Tyler obtained values of the Strouhal Number equal to 1.13 and 0.915. These values are high and they decreased with the decrease of angle of attack. At about 20° angle of attack the Strouhal Number reached the value of 0.15 and was constant for larger angles.

In the above-mentioned tests Tyler referred the value of S to the length of the chord. Later calculations performed by Tyler referred to the projection of the airfoil on the direction perpendicular to the direction of the flow, and as a result a fairly constant value of the Strouhal Number through the entire range of the angle of attack was obtained.

Blenk[4] investigated airfoils in the water tunnel and came to the conclusion that the Strouhal Number for airfoils is equal to 0.21 and is independent of the angle of attack.

Let it be assumed that there exists behind an airfoil a region of vortex rows through the full range of angle of attack from 0° to 90°. The above assumption permits one to speak about the dimensions a and h in the full range of angle of attack. When applying the vortex street characteristics measured during tests behind an airfoil, it is doubtful whether the form drag in Eqs. (6) and (7) can be identified with the total drag. In case of flat plate and cylinder the friction drag is small enough to be neglected. But in the case of elongated bodies the skin friction plays an important part and cannot be neglected. In the discussion below the approximate drag coefficient as the profile drag coefficient will be taken.

Since C_{D_p} is referred to the chord l, Eq. (15) becomes:

$$l/h = [1.59(u/V) - 0.63(u/V)^2]/0.281C_{D_p} \tag{31}$$

The method of calculation of the Strouhal number is based on the following assumptions:

(a) The shape of the wake behind airfoil will be taken from experimental data.

(b) The distance between rows of vortexes will be assumed equal to the width of the wake.

(c) The breadth of the lamina will be taken as the projection of the airfoil on the direction perpendicular to the direction of the stream according to Blenk's suggestion.

(d) C_{D_p} will be some function of the angle of attack.

These assumptions will permit one to calculate the ratio u/V and the Strouhal Number. Each of these points will be discussed.

Some investigators are of the opinion that the origin of the wake should be shifted to the point of $0.15l$ from the trailing edge because of the already finite boundary layer width at the wing trailing edge.[10] The width of the wake may be given as:[10]

$$h_w = 2l(0.68\, C_{D_p}{}^{1/2})(X + 0.15)^{1/2} \tag{32}$$

* That is purely a guess. The author was guided by the results obtained by Schlichting[5] during his investigation on flow along a flat plate. For indifferent (or neutral) oscillation Schlichting obtained the following expressions for the period of the disturbing flow: $T_1 = 10.1 \times 10^4\ (\gamma/V^2)$ and $T_2 = 14.8 \times 10^4\ (\gamma/V^2)$.

TABLE 4

The Calculated Wake Characteristics for an Airfoil of 15 Per Cent Thickness Ratio

$\alpha°$	α, rad.	C_{D_p}, Eq. (44)	h/l, Eq. (32)	$K = d/h$, Eq. (45)	Average Value, K	u/V, Eq. (31)	S, Eq. (13)	$f(l/V)$, Eq. (49)
14.325°	0.250	0.030	0.452	0.870		0.006	0.243	0.618
20°	0.349	0.180	1.105	0.437		0.014	0.122	0.251
45°	0.785	0.830	2.372	0.343	0.391	0.062	0.091	0.111
90°	1.570	2.000	3.694	0.278		0.116	0.069	0.067
$\alpha°$	α, rad.	C_{D_p}, Eq. (44)	h/l, Eq. (47)	$K = d/h$	Average Value, K	u/V, Eq. (31)	S, Eq. (13)	$f(l/V)$, Eq. (49)
14.325°	0.250	0.030	0.605			0.008	0.181	0.461
20°	0.349	0.180	0.743			0.044	0.175	0.361
45°	0.785	0.830	1.251	0.65	0.65	0.124	0.160	0.197
90°	1.570	2.000	1.539			0.255	0.136	0.136

where X is measured from the trailing edge of the airfoil and is expressed as a fraction of the chord:

$$X = \frac{\text{distance behind trailing edge}}{\text{wing chord}} \tag{33}$$

Let it be assumed that the measurements are taken at a constant average distance behind the airfoil equal to three and one-half times the length of the chord. In that case:

$$h_w = (2l)(0.68C_{D_p}{}^{1/2})3.65^{1/2} \tag{34}$$

Assuming that the wake is caused by a lamina, located in the place of the airfoil leads to the value of the distance between the rows of vortexes:

$$h = h_w \tag{35}$$

The ratio d/h for the present calculations will differ from value of this ratio behind flat plate and cylinder because the shape of the wake in case of airfoil differs from the shape of wake behind a flat plate. In some cases for small angles of attack and for angles of attack above stalling, it is possible to apply the value of d/h behind a flat plate to an airfoil, as a short calculation may prove.

Let Heisenberg's value of

$$d/h = 0.648 \tag{36}$$

be used. This gives, with Eq. (32),

$$d = 0.648(2l)(0.68C_{D_p}{}^{1/2})3.65^{1/2} \tag{37}$$

Assuming zero angle of attack and the value

$$C_{D_p} = 0.01 \tag{38}$$

for purposes of illustration leads to

$$d = 0.168l \tag{39}$$

Hence,

$$l/h = 3.86 \tag{40}$$

This corresponds to the maximum thickness of an airfoil of 16.8 per cent thickness ratio, which may correspond approximately to the chosen value of C_{D_p}.

From Eqs. (31) and (40) the ratio of velocities can be calculated:

$$u/V = 0.0068 \tag{41}$$

The value of the Strouhal can be calculated from Eq. (13), giving

$$S = 0.181 \tag{42}$$

The significance of this result should not be overestimated, since the result depends almost entirely on the assumed value of d/h.

The quantity u/V is small when C_{D_p} is small. The values of C_{D_p} will be chosen for purposes of illustration as $C_{D_p} = 0.01$ for zero angle of attack and as $C_{D_p} = 0.03$ for angle of stalling equal to $^1/_4$ rad. or 14.325°. Between 0° and 14.325° the value of C_{D_p} is a quadratic function of the angle of attack of the shape:

$$C_{D_p} = 0.01 + 0.32\alpha^2 \tag{43}$$

For airfoils above the stalling point, tests generally show that the drag coefficient is a linear function of the angle of attack.[11] For this reason the following relationship is applied:

$$C_{D_p} = 1.492\alpha - 0.341 \tag{44}$$

It gives the value of C_{D_p} equal to 0.03 for the angle of attack of $^1/_4$ rad. and the value of 2.0—i.e., the same as for a plate in two-dimensional flow for the angle of attack of 90°.

The procedure of calculations is as follows:

(a) Substitution of Eq. (43) or (44) into Eq. (32) gives the ratio h/l.

(b) Application of Eq. (32) permits to calculate the ratio:

$$K = \frac{d}{h} = \frac{l \sin \alpha + t_{max.} \cos \alpha}{(2l)\ 0.68\ (1.492\alpha - 0.341)^{1/2}3.65^{1/2}} \tag{45}$$

where d represents the projection of the airfoil on the direction perpendicular to the direction of the flow.

(c) Substitution of the ratio h/l into Eq. (31) permits the calculation of u/V.

(d) Eq. (13) gives S.

(e) For angles of attack above stalling instead of the value d/h from Eq. (45), the value d/h behind flat plate may be used. Strictly speaking, Eq. (32) should not be applied at great angles of attack. The values of the ratio u/V and S are too small at great angles of attack when Eq. (32) is used (see Table 4).

(f) When applying the Heisenberg's value for d/h, equal approximately to 0.65, the value of h/l will be calculated from the equation:

$$d = 0.65h = l \sin \alpha + t_{max.} \cos \alpha \qquad (46)$$

For 15 per cent thickness ratio:

$$h/l = (\sin \alpha + 0.15 \cos \alpha)/0.65 \qquad (47)$$

(g) Frequency may be calculated from the formula:

$$f = (V - u)/a = (V/l)(l/h)[1 - (u/V)]0.281 \qquad (48)$$

The value

$$f(l/V) = (l/h)[1 - (u/V)]0.281 \qquad (49)$$

will be tabulated. As is seen, frequency is a linear function of velocity at a constant angle of incidence, and, in general, its value decreases with increase of angle of attack when the velocity is constant.

The value u/V has to be calculated as explained in point (c). Heisenberg's value u/V does not supply a good result. Substitution of this value into the above explained method gives values of S equal to 3.85 for 0°, 5.85 for 5°, 3.34 for 14.325°, 0.458 for 25°, 0.197 for 60°, and 0.127 for 90°.

For purposes of illustration the given method was at first applied to the range of angles of attack above stalling. The chosen thickness ratio was equal to 15 per cent. The results of calculation for two cases—i.e., for d/h from Eq. (45) and for d/h equal to 0.65—are given in Table 4.

Below stalling there exists behind an airfoil a wake different from double vortex street. The prominent disturbances in this wake were measured, as mentioned above, and the Strouhal Number was calculated for certain velocities. But one can introduce the idea of "equivalent vortex street with respect to the frequency." This fictitious double vortex street should have the frequency and, consequently, the value of the Strouhal Number equal to the frequency of prominent disturbances and to the Strouhal Number in the real wake at least in the tested range of velocities and Reynolds Number if the dimensions of the fictitious vortex street are properly choosen. The calculation performed according to the schedule given above for thickness ratio equal to 15 per cent, with application of Eqs. (43) and (45) showed that the values of S and $f(l/V)$ are equal to 0.161 and 1.073 for 0°, to 0.206 and 1.024 for 3°, to 0.241 and 0.841 for 8°, and to 0.243 and 0.618 for 14.325°, relatively.

For illustration purposes the above explained method was applied also to an airfoil with split flap. The values of S were in the limits between 0.104 and 0.169.

Wind-Tunnel Tests

General Description

Some tests were performed in the wind tunnel of the Polytechnic Institute of Brooklyn. The wind tunnel of the closed-return type and of 42-in. square throat possesses a turbulence of 0.6 per cent. The aim of these tests was to measure the Strouhal Number behind the following bodies: (a) plain airfoil of infinite and finite length and (b) airfoil with flap of infinite and of finite length.

Because of a decision to check the influence of the wake on a solid body, located behind the airfoil, a special device for measuring the frequency had to be applied.

For this purpose a flat steel plate of dimensions 3.5 by 3 in. was used, loosely supported by four wires. To measure the frequency of the plate three methods were tried: (a) stroboscope, (b) mechanical recorder, and (c) electric induction.

As the best results were obtained by the third method,* it was used. Below the plate was attached a magnet on which a coil was wound. The oscillation of the plate induced changes of voltage which, through an amplifier, were transferred to an oscillograph. Pictures taken by a photographic apparatus permitted the calculation of frequency from the number of waves. For each point at least two pictures were taken. Figs. 2 and 3 show the apparatus and Fig. 4 shows a typical example of the frequency curves.

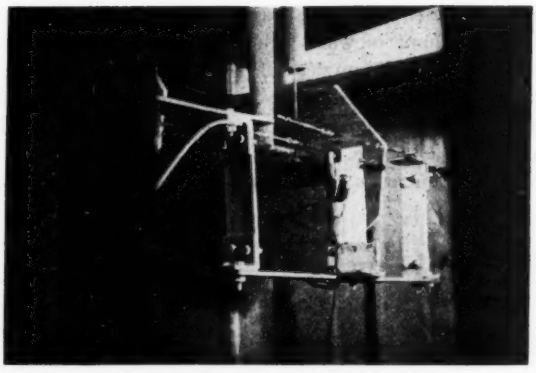

Fig. 2. Mounting of the plate.

* The idea was suggested by John Margosian, B.E.E., Research Associate, Department of Aeronautical Engineering, Polytechnic Institute of Brooklyn.

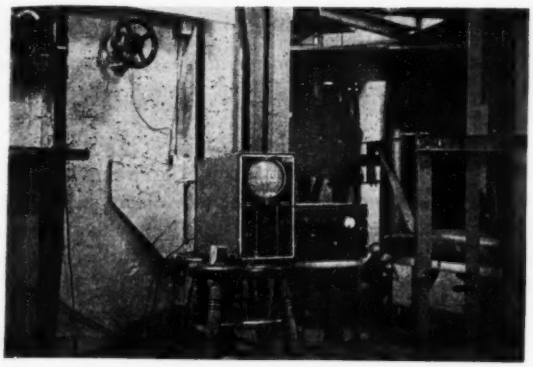

FIG. 3. Component apparatus.

FIG. 4. Oscillograms.

PLAIN AIRFOIL AND AIRFOIL WITH FLAP OF INFINITE LENGTH

The airfoil used had the following characteristics: airfoil, Clark Y; span, 24 in.; chord, 8 in.; A.R., 3; shape, rectangular; thickness ratio, 11.3 per cent; maximum thickness, 0.9 in.; flap—type of flap, split flap; length, full span; width, $0.2c = 1.6$ in. The maximum deflection of the flap with respect to the airfoil chord is 45°.

When the airfoil with flap was tested, the full deflection of the flap was applied. The center of the plate was located approximately 5 in. behind the trailing edge of the airfoil. The vertical position of the plate with respect to the plain airfoil was chosen at the level of the upper edge of the airfoil. The results of tests by Duncan and Abdrashitov[13] showed that the plane of the upper edge of the airfoil gives the maximum amplitude. The optimum vertical location of the plate with respect to the airfoil with flap was found by use of a silk thread.

The conditions of the two-dimensional flow were obtained by attaching flat plates at both ends of the airfoils. For the plain airfoil the value of d was calculated from the formula

$$d = l \sin \alpha + t_{max.} \cos \alpha \qquad (50)$$

and for the airfoil with flap the value of d was calculated from the formula:

$$d_{fl} = d_{plain} + C_{fl} \sin [45° + \alpha°] =$$
$$l \sin \alpha + t_{max.} \cos \alpha + C_{fl} \sin [45° + \alpha°] \qquad (51)$$

where C_{fl} = chord of the flap.

The results of the tests carried out by the author are given in Table 5 and in Figs. 5 and 6.

For plain airfoil below 10° angle of attack it was impossible to obtain good pictures of the frequency,

TABLE 5

The Values of the Strouhal Number in Two-Dimensional Flow

	Full Flap Deflected, Two-Dimensional Flow				Plain Airfoil, Two-Dimensional Flow			
Angle of attack	V, ft. per sec.	d, in.	f(1/sec.)	S	V, ft. per sec.	d, in.	f(1/sec.)	S
25°	56.2	5.70	20	0.169	55.7	4.20	23	0.145
	102.2		40	0.185	104.8		45	0.150
	132.0		54	0.194	124.0		?	?
	141.8		58	0.195	144.3		65	0.157
20°	44.6	5.03	20	0.188	48.0	3.58	24	0.149
	101.8		42	0.173	98.0		50	0.152
	130.4		52	0.168	124.2		62	0.149
	141.5		66	0.196	141.7		70	0.148
15°	44.6	4.32	24	0.193	57.8	2.94	38	0.161
	104.0		45	0.156	98.0		60	0.150
	126.0		55	0.157	126.5		80	0.155
	140.8		70	0.179	143.0		90	0.154
10°	48.6	3.57	25	0.153	51.8	2.28	43	0.158
	100.4		48	0.143	99.1		80	0.153
	129.5		64	0.147	126.0		100	0.150
	143.3		72	0.150	141.2		120	0.161
5°	48.0	2.81	32	0.187	53.5	1.59	64	0.159
	98.0		60	0.144	...		...	...
	127.0		70	0.130	120.0		105?	0.116?
	142.2		80	0.159	144.1		115?	0.106?
0°	49.9	2.02	45	0.153	...	0.90	...	...
	99.2		90	0.152	74.2		110?	0.111?
	126.5		110	0.146	117.4		135?	0.087?
	144.2		132	0.154	146.2		?	?
−5°	...	..	...	...	53.5	1.59	70	0.174

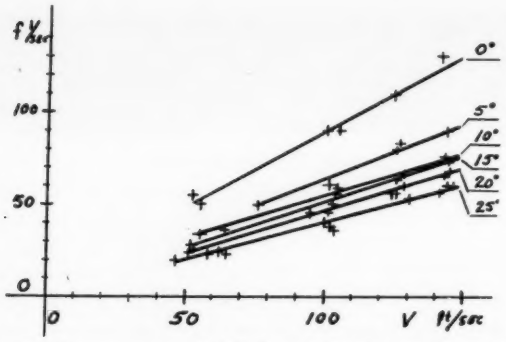

FIG. 5. Frequency vs. V, full flap deflected, two-dimensional flow.

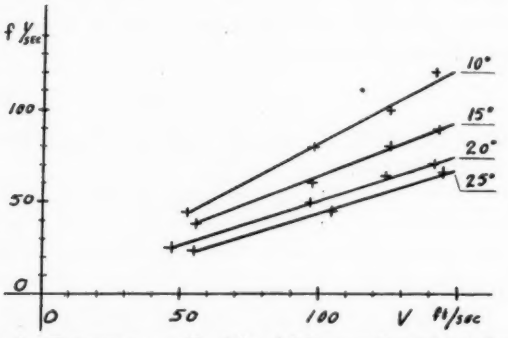

FIG. 6. Frequency vs. V, plain airfoil, two-dimensional flow.

and as a result values included in the table are not certain. At high frequencies some discrepancies were obtained, possibly because of the fact that inertia forces are playing an important part at those frequencies.

Blenk, in his investigation of the frequency behind a cylinder in the wind tunnel and behind airfoil in the water tunnel, obtained a linear function of the frequency with respect to the velocity, and those straight lines passed always through the origin of the system of coordinates. Abdrashitov, in his investigations, also obtained straight lines as the curves of frequency against velocity, but those straight lines did not pass through the origin of coordinates. Abdrashitov expressed the opinion that at small velocities the law of variation of frequency with velocity will be different from that at a greater velocity. As may be seen from the diagrams, some of the straight lines, which are the averages of the points, tend slightly to pass through the origin of coordinates (Figs. 5, 6, 7, 8).

PLAIN AIRFOIL AND AIRFOIL WITH FLAP OF FINITE LENGTH

The aim of this part of tests was to find the values of the Strouhal Number in the plane of symmetry behind an airfoil of finite length. The same airfoil was used as in the first part of the tests. The results are given in Table 6 and in Figs. 7 and 8.

GENERAL CONCLUSIONS AND REMARKS

From the above given considerations the following conclusions can be drawn, referring to the two-dimensional flow:

(1) In general, the Strouhal Number is not constant.

(2) The Strouhal Number in the wake behind a body with sharp edges—i.e., a plate—is approximately constant and independent of the Reynolds Number. The calculation performed showed a fair agreement with various tests.

(3) The Strouhal Number in the wake behind a circular cylinder is constant only in the range below the critical Reynolds Number. The calculation performed for this range of the Reynolds Number is in fair accordance with tests performed by various investigators. Regarding the range above the critical Reynolds Number, some assumptions made permit one to conclude that, as a first, rough approximation, the Strouhal Number in this range is a linear function of the Reynolds Number.

(4) When there is a wake behind an airfoil consisting of vortexes, various methods applied in calculating the value of the Strouhal Number appear to justify the conclusion that the Strouhal Number is a constant value, provided the Strouhal Number is referred to the projection of the airfoil on the direction perpendicular to the direction of the flow, according to the suggestion made by Blenk and others. However,

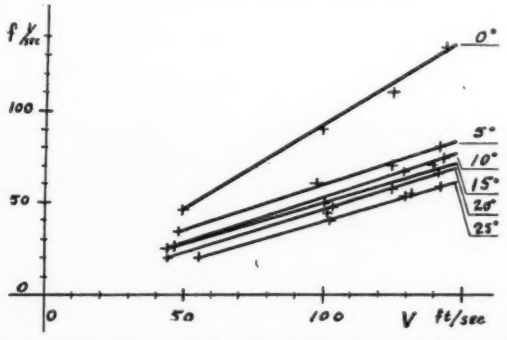

FIG. 7. Frequency vs. V, full flap deflected, three-dimensional flow.

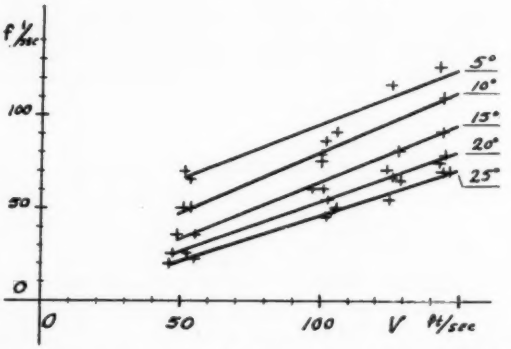

FIG. 8. Frequency vs. V, plain airfoil, three-dimensional flow.

TABLE 6

The Value of the Strouhal Number in Three-Dimensional Flow

Full Flap Deflected, Three-Dimensional Flow					Plain Airfoil, Three-Dimensional Flow			
Angle of attack	V, ft. per sec.	d, in.	f(1/sec.)	S	V, ft. per sec.	d, in.	f(1/sec.)	S
25°	47.4	5.70	20	0.201	47.4	4.20	20	0.148
	59.3		23	0.184	54.6		21	0.135
	65.0		23	0.168	102.2		45	0.154
	100.2		40	0.189	104.1		50	0.168
	102.2		38	0.176	126.0		53	0.147
	103.1		37	0.171	129.3		65	0.176
	130.0		52	0.190	143.5		70	0.171
	141.6		54	0.182	145.8		70	0.168
	144.0		60	0.198	...		...	...
	146.0		60	0.195	...		...	...
20°	51.0	5.03	24	0.197	48.5	3.58	23	0.142
	52.8		25	0.199	51.2		23	0.134
	61.8		24	0.164	103.2		52	0.150
	95.2		45	0.199	104.1		46	0.132
	127.6		55	0.181	124.0		70	0.168
	129.0		60	0.195	128.0		65	0.152
	143.0		65	0.199	143.5		72	0.150
	143.4		68	0.191	145.0		77	0.158
15°	51.7	4.32	26	0.182	49.2	2.94	34	0.169
	61.3		?	?	56.8		34	0.147
	101.7		45	0.160	97.2		60	0.151
	102.2		50	0.176	100.1		60	0.147
	126.8		56	0.159	128.2		80	0.153
	129.0		60	0.167	128.5		80	0.152
	142.8		74	0.186	143.9		90	0.154
	143.4		72	0.181	144.0		90	0.151
10°	57.7	3.57	32	0.166	50.3	2.28	50	0.189
	63.3		34	0.160	51.2		50	0.185
	102.7		50	0.144	100.1		78	0.148
	103.0		54	0.156	100.2		75	0.142
	127.6		62	0.145	144.0		110	0.145
	129.1		64	0.148	...		...	...
	144.8		72	0.148	...		...	...
5°	78.0	2.81	50	0.150	51.0	1.59	70	0.182
	102.2		59	0.133	52.8		66	0.166
	104.2		60	0.138	102.0		85?	0.110
	127.8		80	0.147	105.8		90?	0.113
	128.0		82	0.150	126.2		115?	0.121
	144.2		90	0.146	142.0		125?	0.117
0°	51.7	2.02	52	0.169	51.7	0.90	90	0.131
	53.5		50	0.158	52.8		100	0.142
	101.6		90	0.144	86.1		145?	0.126?
	105.6		90	0.150	102.2		115?	0.084?
	125.2		110	0.148	...		...	...
	142.0		130	0.154	..		...	...
−5°	...		...	...	50.3	1.59	80	0.210
	...		...	...	102.2		95?	0.123?

discrepancies exist between the calculation and the tests because of lack of a method of calculating the wake characteristics in a purely theoretical way.

(5) When, for angles below stalling instead of a wake different from double vortex street, one assumes a fictitious double vortex street equivalent to the real wake with respect to the frequency, the calculation performed for the chosen dimensions of the equivalent vortex street showed that the values of the Strouhal Number are within the limits given by other investigators, at least in the range of tested velocities.

(6) The characteristic values of the wake behind various bodies—such as width, breadth, and ratio u/V—depend on the shape of the body, and until now it is not possible to apply a general rule.

(7) With regard to the value of the ratio u/V, it appears that the value given by Heisenberg or any value close to that may give fairly good results for flat plates and cylinders. For airfoils, the present assumptions showed that this ratio depends on the angle of attack. Whether these assumptions are right or not is an open question.

From the tests performed one may conclude:

(1) When one refers the value of the Strouhal Number of any airfoil in two-dimensional flow with or without flap to the projection of the airfoil on the direction perpendicular to the direction of the airflow, the values of the Strouhal Number are within the limits given by other investigators.

(2) The above conclusion appears to prove that the suggestion of Blenk is entirely justified.

(3) The value of the Strouhal Number behind airfoils may be assumed to be a constant value in the tested range of R.

(4) The frequency in the wake behind the center part of a rectangular airfoil of finite length is not affected by the tip vortexes.

(5) The function of frequency versus velocity appears to be a straight line, but it is difficult to see whether it always passes through the origin of coordinates, although a slight tendency is visible. Blenk obtained straight lines passing through the origin, but his results do not agree with those obtained by Abdrashitov.

A few remarks will be given concerning the method used in measuring the frequency. The chief advantages of this method are that it is simple and easy to control. But in the course of the tests two disadvantages were quite evident: first, at high frequencies some discrepancies were obtained, probably due to the fact that inertia forces are playing, at those frequencies, an important part; second, the reading of pictures presented some difficulties, with reference to fractions* of waves, because the waves were often of irregular shapes.†

* The exposure time of the camera was set at $^1/_{10}$ sec., consequently one cycle on the picture represented 10 cycles per sec.

† The author is indebted to Mr. John Margosian for his invaluable help in the solution of the electrical part of the tests.

References

[1] Glauert, H., *The Elements of Airfoil and Airscrew Theory*, Cambridge University Press, Cambridge, England, 1930.

[2] Lamb, Horace, *Hydrodynamics*, 6th Edition; Cambridge University Press, Cambridge, England, 1932.

[3] Goldstein, S. (Editor), *Modern Developments in Fluid Dynamics*, Vols. I and II; Clarendon Press, Oxford, England, 1938.

[4] Blenk, H., Fuchs, D., and Liebers, F., *Über Messungen von Wirbelfrequenzen*, Luftfahrtforschung, Bd. 12, No. 1, p. 38, March 28, 1935.

[5] Prandtl, L., and Tietjens, O. G., *Applied Hydro and Aeromechanics;* McGraw-Hill Book Company, Inc., New York and London, 1934.

[6] Durand, W. F., *Aerodynamic Theory;* Julius Springer, Berlin, Germany, 1935.

[7] Tyler, E., *Vortex Formation Behind Obstacles of Various Sections*, Philosophical Magazine, Series 7, Vol. 11, No. 72, pp. 849–890, April, 1931.

[8] Schlichting, H., *Amplitudenverteilung und Energiebilanz der kleinen Störungen bei der Plattenströmung*, Nachrichten, Gesellschaft der wissenscheflen zu Göttingen, M.P.K. Band I, p. 47, 1935.

[9] Betz, A., *A Method for the Direct Determination of Wing Section-Drag*, N.A.C.A. T.M. No. 337, 1925.

[10] Silverstein, Abe, Katzoff, S., and Bullivant, W. Kenneth, *Downwash and Wake Behind Plain and Flapped Airfoils*, N.A.C.A. T.R. No. 651, 1939.

[11] Jacobs, Eastman N., and Abbott, Ira H., *Airfoil Section Data Obtained in the NACA Variable Density Tunnel as Affected by Support Interference and Other Corrections*, N.A.C.A. T.R. No. 669, 1939.

[12] Weinziger, Carl J., and Harris, Thomas A., *Wind Tunnel Investigation of NACA 23012, 23021 and 23030 Airfoil with Various Sizes of Split Flap*, N.A.C.A. T.R. No. 668, 1939.

[13] Abdrashitov, G., *Tail Buffeting*, Central Aero-Hydrodynamical Institute, Moscow, Report No. 395, 1939. Translation: N.A.C.A. T.M. No. 1041, February, 1943.

Analytic Investigation of Problems Concerning the Flow of Cooling Air in Light Airplane Engine Installations*

JOHN R. WESKE†

Case School of Applied Science

Introduction

An attempt is made to define certain characteristics of the engine cooling systems in terms that may be related readily to the performance of the airplane as a whole. Particular consideration is given to submerged installations and to the problem of blower-induced circulation of the cooling air. The scope of the investigation is confined to the establishment of theoretical relations, from which a number of conclusions are derived pertaining to the design of cooling systems. For best performance it is found desirable that the cooling air blower be placed close to the air outlet.

Previous published investigations of flow systems related to the cooling system of light airplane engines, which include theoretical analysis, are those by Rokus and Troller[1] dealing with ventilating systems of airships and several papers dealing with the characteristics of condenser cooling water systems on ships by Schmidt,[2, 3] Weske,[4, 5] and Hewins and Reilly.[6]

Typical System

For purposes of investigation of the flow of cooling air in light airplane engine installations, a typical ducted engine cooling system shown schematically in Fig. 1 is considered. The cooling system consists of the following basic elements:

Flow resistance, r.
Heater, h.
Fan, b.
An air inlet, i.
An air outlet, o.

An element a representing the effect of propeller or boundary layer wake upon the cooling airflow upstream of the inlet. The engine e and the propeller p are shown merely to indicate the flow of mechanical energy.

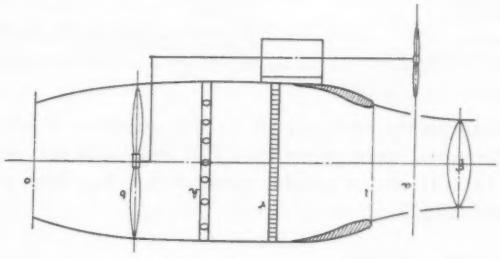

Fig. 1.

In applying the following analysis to a particular installation, it may be necessary to eliminate one or more of these basic elements. In view of the operating conditions of light planes, it is permissible to neglect compressibility of the air, with the exception of the increase of specific volume produced in the heater. The actual installation is reduced to its correspondent ideal system by neglecting hydraulic losses, except insofar as they are accounted for explicitly.

Theoretical Considerations

For the purpose of securing a reference quantity for the analysis, consider an installation requiring a quantity $M = Q\rho$ of cooling air where Q volume is the rate of flow and ρ is the mass density, both at undisturbed flow conditions. This quantity of air passes through an area F located in undisturbed flow and moving relative to the air at the flying speed of the airplane, V.

The rate of momentum of the air far upstream of the intake is

$$D = Q\rho V = F\rho V^2 = 2Fq$$

where $q = \rho(V^2/2)$ velocity pressure of undisturbed flow. The corresponding rate of energy is $E = DV = F\rho V^3$. The area F may be referred to as "momentum area," in analogy to momentum thickness. It was chosen as a reference quantity in preference to the equivalent parasite area f, which is exactly twice as large, $f = 2F$, for reasons that will appear later.

The effect of the various basic elements of the cooling installation upon its performance has been defined

Presented at the National Light Aircraft Meeting, I.A.S., Detroit, April 27–28, 1944.

* In reviewing the manuscript of the present paper, Dr. Th. Troller, Director, Daniel Guggenheim Airship Institute, drew attention to the fact that the axial-flow blower, which operates in a casing and therefore is inherently less afflicted by induced drag than the propeller, has potentially, and in some instances actually higher, efficiency than the latter. For the case $\eta_b/\eta_p > 1$, Dr. Troller pointed out that the blower-induced system has absolute superiority over the self-induced system with regard to efficiency.

† Professor of Aerodynamics.

TABLE 1

ITEMS OF ENERGY BALANCE AND EFFICIENCIES

	GAIN OR LOSS	POWER LOSS OR GAIN RATIO	EFFICIENCY	REMARKS
WAKE EFFECT	$Q_0(\gamma_i - \gamma)V$	$e_a = 1 - \frac{\gamma_i}{\gamma}$		
INLET	$(1-\eta_i)Q_0V_i^2$	$e_i = (1-\eta_i)\left(\frac{V_i}{V}\right)^2$	$\eta_i = \frac{Q(H_0+q)}{\frac{1}{2}V^2}$; $\eta_i^* = 1$	ASTERISK: DISREGARDING HYDRAULIC LOSSES, EXCEPTING THOSE EXPRESSIBLE INTERNALLY
RESISTANCE	$Q\Delta H_r$	$e_r = \frac{\Delta H_r}{2q}$		$\eta = \left(\frac{V_2}{V}\right)^2$
HEATER	HEAT: $\frac{Q\rho g}{J}C_p(T''-T')$; WORK: $Q\rho g R(T''-T')$	$e_h = \frac{\rho g}{2q}R(T''-T')$		
BLOWER	$Q\Delta H_b$	$e_b = \frac{\Delta H_b}{2q}$		
OUTLET	$(1-\eta_0)Q(H_0+q)$	$e_o = (1-\eta_0)\frac{V_1^2+\left(\frac{\Delta H_b}{q}\right)}{q}$	$\eta_0 = \frac{-2V}{Q(H_0+q)}$	
OVERALL, SELF-INDUCED			$\eta = \frac{Q\Delta H_r}{(D+D_0)V}$; $\eta = \frac{1}{K+\frac{1}{\eta_0}}$	
OVERALL BLOWER INDUCED			$\eta' = \frac{Q\Delta H_r}{(D+D_0)V + \frac{\eta_b}{\eta_0}Q\Delta H_b}$; $\eta' = \frac{1}{(K-\kappa)\frac{\eta_b}{\eta_0} + \kappa\frac{\eta_b}{\eta_p}}$	η_p = PROPULSIVE EFFICIENCY; η_b = BLOWER EFFICIENCY; $\kappa = \frac{\Delta H_b}{\Delta H_r}$

quantitatively and related to the quantity F whose value was chosen as unity. The equations are given in Table 1 and a graphic presentation has been prepared (Fig. 2).

Quantities Derived

The quantities derived for the most part are self-explanatory. The following comments are offered:

(a) Wake Effect: The wake effect takes into account the action of the propeller wake upon the air entering the intake or of the boundary layer wake. It may be represented adequately by an increase, $V_i > V$, or a decrease $V_i < V$ of the velocity of approach, V, respectively.

(b) Flow Resistance: On its passage through the fin area the cooling air suffers a loss of pressure and an increase of its temperature. The former is accounted for by a drop of total pressure ΔH_r.

(c) Heater Effect: The quantity of heat transferred for a temperature rise of $T'' - T'$ degrees is

$$Q\rho g C_p(T'' - T')$$

The corresponding displacement work is

$$Q\rho g J(C_p - C_v)(T'' - T') = Q\rho g R(T'' - T')$$

(d) The effect of the blower is taken into account by an increase of total pressure ΔH_b.

(e) For the purpose of this investigation the losses of the inlet, being primarily of a hydraulic nature, are disregarded. The losses of the outlet, however, are accounted for by way of an efficiency to be defined in the next paragraph.

Nondimensional power gain or loss ratios are established by relating the various rates of energy tabulated in Column 2 of Table 1 to the power corresponding to the rate of momentum of the cooling air at undisturbed flow conditions. These power gain or loss ratios may also be interpreted to represent ratios of momentum areas, the reference area being the momentum area of undisturbed flow, F. This manner of presentation has the advantage that the various efficiencies appear in the graphic presentation, Fig. 2, and their value may be read directly on the scale of ordinates.

Efficiencies

In defining efficiencies it is to be noted that the energy corresponding to the momentum drag at inlet is divided into two parts—namely, the energy relative to the airplane and, second, that part of the energy which the cooling air has relative to undisturbed flow by virtue of the fact that during its passage through the cooling air system it becomes a part of the airplane. This latter quantity Qq consequently appears in the efficiencies, Column 4 of Table 1.

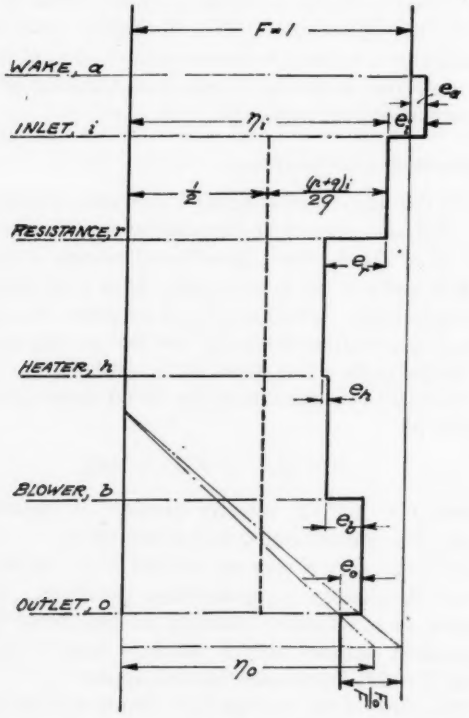

FIG. 2.

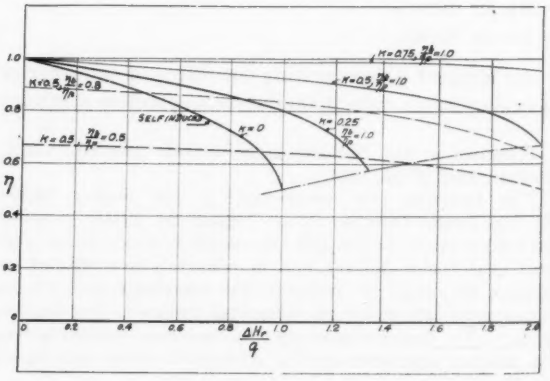

FIG. 3.

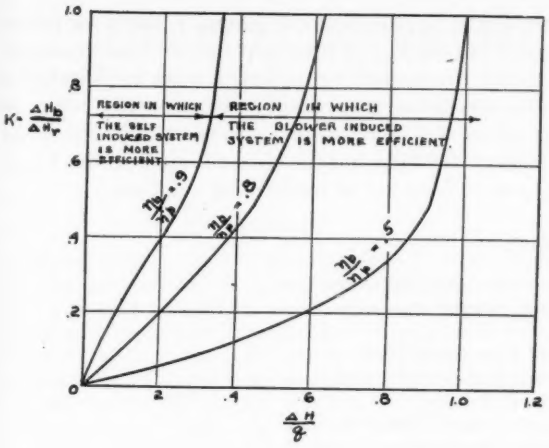

FIG. 4

Comparison of Self-Induced and Blower-Induced Systems

In carrying through the comparison the following simplifications have been made:

The wake effect at inlet has been neglected, likewise the heating effect. The efficiency of the inlet has been assumed to be unity. Hydraulic losses of the outlet are disregarded. Curves are drawn in Fig. 3 for the overall efficiency of a self-induced system against nondimensional pressures drop in the flow resistance as abscissa. Corresponding curves are plotted for the blower-induced system.

The latter curves have been plotted for various ratios of blower output to loss in the resistance $K = -\Delta H_b/\Delta H_r$ and also for various values of blower efficiency to propulsive efficiency.

This graph leads to the interesting result that for certain ranges of operation the efficiency of the blower-induced system is superior to that of the self-induced system. Fig. 4 may be used to determine which of the two systems is more efficient for a particular set of values $\Delta H_r/q$, η_b/η_p, and $K = \Delta H_b/\Delta H_r$. Points to the right of the curve representing a given value η_b/η_p indicate superior efficiency for the blower-induced system, while points to the left of the curve indicate superiority of the self-induced system.

It may be concluded from the foregoing that choice of a low baffle pressure drop decreases the drag of a self-induced cooling system, whereas in a blower-induced system even high baffle pressure drops do not result in an appreciable increase of drag. In the latter case, however, it is essential that the blower characteristics be well matched to the characteristics of the cooling system, in particular to the baffle area in order to attain maximum efficiency.

The investigation also brings out the fact that the airplane propeller, which in a self-induced system is the source of supply of the energy for the circulation of the cooling air, is a highly efficient device. It follows that if a blower-induced cooling system is to be employed instead of a self-induced system, requiring an additional item of engine equipment—namely, the blower—this blower of necessity must be designed for highest attainable efficiency.

BLOWER DESIGN

The requirements in regard to the design of the blower are similar to the specifications for limit load units in turbine design. The principal requirements as applied to the blower are enumerated.

(a) Optimum strength-weight ratio compatible with safety.

(b) Minimum weight-power ratio. The weight power ratio of the blower may be taken into account by a correction to the efficiency of the blower as follows:

$$\eta_b' = \eta_b \Big/ \left[1 + (\omega_b - \omega_p)\frac{V}{L/D}\,\frac{\eta_b}{\eta_p}\right]$$

where η_b' = corrected efficiency of the blower, and η_b = measured efficiency of the blower. In this equation the weight of the blower per horsepower is related to the weight of the propeller per horsepower ω_p by means of the L/D ratio of the airplane.

(c) Minimum space-power ratio. This refers to the additional space in the engine compartment required by the blower.

(d) Optimum noise level.

(e) Optimum Mach Number. This requirement constitutes an upper limit of the tip speed of the blower. Considerations of the effect of Mach Number, however, are not likely to affect the blower design, since the tip speed probably is limited by noise level.

(f) Optimum Reynolds Number. It is known that the efficiency of axial flow blowers decreases greatly as the Reynolds Number, based upon the chord of the blades, is less than 150,000.

The relatively high efficiency of the propeller as an indirect source of energy for cooling air circulation may be attributed to the fact that the air, while flowing past the propeller blades, is accelerated. This is known to result in efficient interaction of the blades and the air stream. It is of interest to note that the operation of blower devices such as the Sirocco type of blower, which has been used for this purpose, and ejectors using the energy of exhaust, which have been proposed, is also based upon acceleration of the air during energy transfer. This would lead to the suggestion that in order to secure maximum efficiency axial flow blowers, if applied in engine cooling systems, should be designed to operate on the impulse principle by which energy is transferred to the air largely in the form of kinetic energy. This is the case in a particular design of axial flow blower—namely, the Schicht type.[7] A blower of this type preferably should be placed at a point in the system where acceleration of the air is beneficial—at the air outlet.

On theoretical grounds it may also be postulated that in order to secure minimum weight-power ratio the blower be located in the part of the cooling system where the highest velocity occurs. It may be seen from Fig. 2 that in blower-induced systems the highest uniform velocity occurs in the vicinity of the air outlet. While the recommendation of placing the blower near the outlet appears to have general validity for power-plant installations of light airplanes for which compressibility effects may be neglected, some modification of this conclusion may possibly be necessary when accounting for temperature effects in high-speed airplanes. If a Schicht-type blower is applied, this blower would of necessity be followed by a diffuser.

References

[1] Rokus, F., and Troller, Th., *Tests on Ventilating Openings for Aircraft*, Journal of the Aeronautical Sciences, Vol. 3, pp. 203–208, April, 1936.

[2] Schmidt, H. F., *Theoretical and Experimental Study of Condenser Scoops*, Journal of the American Society of Naval Engineers, Vol. 42, No. 2, pp. 1–38, February, 1930.

[3] Schmidt, H. F., *Investigation of the Action of Condenser Scoops Based upon Model Tests*, Discussion, Journal of the American Society of Naval Engineers, Vol. 51, No. 3, pp. 460–480, August, 1939.

[4] Weske, J. R., *Investigation of the Action of Condenser Scoops Based upon Model Tests*, Journal of the American Society of Naval Engineers, Vol. 51, No. 2, pp. 191–213, May, 1939.

[5] Weske, J. R., *Discussion of Paper by A. Métral*, Proceedings of 5th International Congress of Applied Mechanics, Cambridge, 1939, pp. 461–465.

[6] Hewins, S. F., and Reilly, J. R., *Condenser Scoop Design;* Annual Meeting Paper, Society of Naval Architects and Marine Engineers, 1940.

[7] Soerensen, E., *Constant Pressure Fans*, N.A.C.A. T.M. No. 927, January, 1940.

(*Continued from page 46*)

aim the attracting of air-minded youth to an active part in aviation.

References

[1] Stepniewski, W., *The Prediction of Performance*, Aircraft Engineering, Vol. 12, Nos. 141 and 142, pp. 329–331, 338, 361–365, November and December, 1940.

[2] Durand, W. F., *Aerodynamic Theory*, Reprinted Edition, Vol. V; California Institute of Technology, 1943.

[3] Stepniewski, W. Z., *Take-off Distance of Glider Train*, Journal of the Aeronautical Sciences, Vol. 11, No. 1, pp. 55–62, January, 1944.

[4] Hartman, E. P., and Biermann, D., *The Aerodynamic Characteristics of Full-Scale Propellers Having 2, 3, and 4 Blades*, N.A.C.A. T.R. No. 640, 1938.

[5] Perring, W. G. A., and Callen, C., *The Influence of a Stopped Airscrew on the Lift and Drag of an Airfoil*, British Air Ministry, R. & M. No. 1347, 1930.

[6] Hartman, E. P., and Biermann, D., *The Negative Thrust and Torque of Several Full-Scale Propellers*, N.A.C.A. T.R. No. 641, 1938.

Bearing Strength in Airplane Design

ALBERT EPSTEIN*

Republic Aviation Corporation

ABSTRACT

Allowable bearing stress is a value based on an arbitrary amount of deformation of a body subjected to a bearing pressure. There is no fixed value for a particular material, the value depending upon the degree of restraint of surrounding fibers to the flow of the material under the direct bearing pressure. The allowable stress for aluminum alloys is generally associated with the elongation of a hole in a plate subjected to uniform bearing pressure from a pin. The stress thus obtained is considerably less than the stress that may be used as the allowable bearing pressure on a rivet or on the wall of a tube in a socket joint.

The bearing stress criteria for aluminum alloys, if applied to heat-treated steel, would permit allowable stresses as much as 50 per cent greater than those used at present for steel.

In bolted joints consideration should be given to the permanent elongation that may occur in the bolt hole after the joint is subjected to limit load. Appreciable set may reduce the service life of the joint, especially when the joint is subjected to shock or vibration.

The allowable strength values for some single-rivet joints may be almost as high as the acting failing strength. In several applications, described in this paper, it is desirable to use some factor or margin of safety with these values becaues of discrepancies between computed and actual rivet loads.

The load-deflection characteristics of riveted joints are important in themselves, and they, rather than the allowable strength, may be the controlling factor in some phases of the design. The greater the deflection, the poorer will be the torsional rigidity of a wing. High joint deflection may reduce to an appreciable degree the effectiveness of wing skin in carrying tension loads.

INTRODUCTION

THE SUBJECT OF BEARING STRENGTH in airplane structural design is one of considerable importance. Yet the behavior of a material subjected to a bearing load and the basic principles underlying the strength values that have been, or are now, in general use are not commonly known. In any riveted, bolted, or socket joint, the allowable bearing strength is a requisite item for design as is the shear strength of the bolt or the tensile strength of the sheet. The bearing strength values given in Government publications[1–4] have been used as required, but often without appreciation of the significance of the values.

For a period of several years, the bearing strength for any particular material was a fixed value regardless of application, and the relatively common misconception existed that bearing strength is a fundamental property of a material as is tension or shear.

Actually, bearing strength is based on arbitrary rules and has no absolute value for a specific material.

It is the purpose of this paper to explain the significance of bearing strength in its various ramifications. The material used has been drawn largely from investigations made by the author in his association, for many years, with the Matériel Command† of the Army Air Forces and, more recently, with Republic Aviation Corporation.

This paper is concerned only with isotropic materials, and deals specifically with aluminum alloys and steel.

FUNDAMENTALS

Definition

Bearing stress, strictly defined, is a purely hypothetical term, since there is no such thing as a bearing stress in the same sense that there may be a tensile stress in a member. Bearing produces a localized stress condition that involves a complex stress pattern that varies widely with the bearing application involved. The term "bearing stress" denotes the value obtained by dividing the force acting between two surfaces by the component of the area of contact normal to the force.

A localized stress condition may not be directly associated with failure. Thus the problem becomes: What does this stress condition, or bearing stress, signify, and how does it apply in design? Some parameter other than failure must be established to express the significance of bearing stress insofar as strength is concerned. Bearing involves elastic deformation or plastic flow of material; hence, a logical step becomes the establishment of some degree of deformation as the limiting value to be tolerated and terming the corresponding bearing stress the allowable stress.

Taking the elementary bearing application shown in Fig. 1(a) as an example, the localized pressure on the rectangular block produces a localized strain that is relatively high at the area of contact and rapidly reduces at points away from the immediate vicinity of application of the force. This condition is well illustrated by photoelastic photographs.[5, 6] The value of the deformation is a function not only of the compressive strain at the immediate area of contact but also of the strain pattern in the general vicinity. The predominant factor, at least for high loads, is the localized strain. There is elastic deformation, followed by plastic flow as the cylinder penetrates the surface of the rectangular block (the block being of a softer

Received March 3, 1944.

* Assistant Chief Research Engineer.

† Now Air Technical Service Command.

material than the cylinder). The allowable bearing stress may then be specified as the stress corresponding to some specific value of deformation.

Bearing Load vs. Deflection Variations

Unfortunately, there is no absolute amount of deformation corresponding to a specific bearing pressure. The basic factor controlling differences in amount of deformation appears to be the restraint offered by adjacent fibers to the flow of material at the area of bearing pressure. Fig. 1 illustrates the divergence of stress-deflection characteristics that may occur. The cylinder was of hardened steel and had a diameter of 0.421 in.; the rectangular block was 24S-T aluminum alloy with the dimensions 0.521 by 1.5 by 3.0 in. In curve 1(a), the bearing was against the 1.5- by 3.0-in. face; in curve 1(b), the bearing was against the 0.521- by 3.0-in. face. The reason for the greater deformation in the second case is the lower restraint of the fibers adjacent to the loaded area, resulting from the proximity of these fibers to the edge of the block. At a bearing stress of 180,000 lbs. per sq.in., the block had bulged in thickness in the plane of the bearing surface from 0.521 to 0.603 in. In test 1(a), at the same stress, there was a negligible change in the external dimensions of the block. In view of the disparity, an allowable bearing stress for these applications must either be a variable or be selected arbitrarily on a conservative basis.

Basis of Allowable Bearing Stresses

Since the major applications of bearing are in bolted and riveted joints, the common representation of bearing (the one used for many years as the sole basis of allowable bearing stress) is that of a pin acting on a hole in a plate. The deflection due to a specific bearing pressure between the pin and plate is taken as the relative movement between the pin and the plate when a load is applied as shown in Fig. 2.

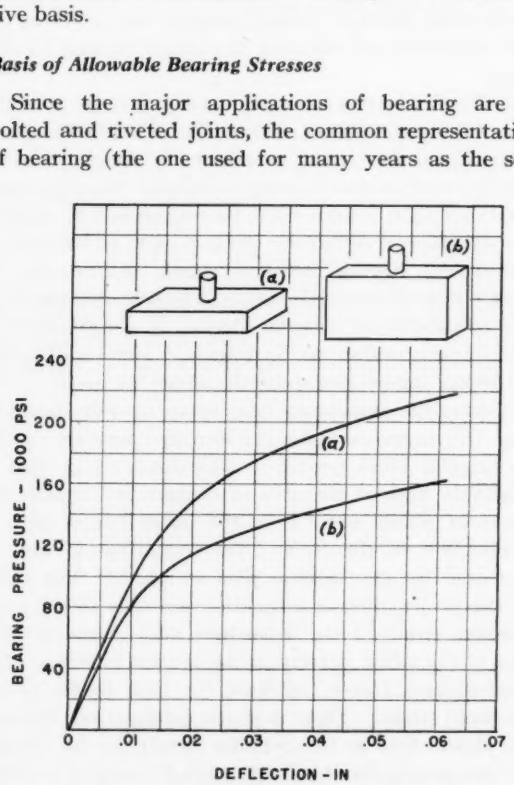

FIG. 1. Bearing stress-deflection curves for steel block bearing on flat surface of 24S-T aluminum-alloy block.

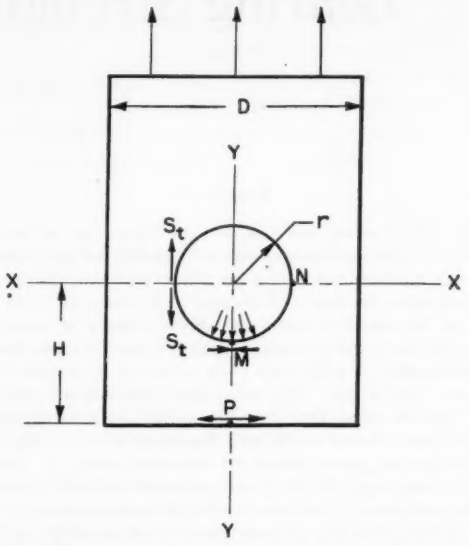

FIG. 2. Plate subjected to bearing load through pin in hole.

Strains in Elastic Range

The strain condition is considerably more complex than in the cases already considered. The bearing pressure is nonuniform, having its maximum intensity at point *M* (Fig. 2) and decreasing to zero at point *N*. Another factor here is that there are tension strains tangent to the hole diameter due to tension stresses that reach a maximum at point *N*. Assuming an infinitely rigid pin (all deformation taking place in the sheet), the hole elongation due to some average bearing pressure, taken with respect to the *X*-*X* axis (the reference line generally used), is the summation in the *Y*-*Y* direction of the strains due to the varying compression forces in the immediate area of contact between pin and plate, the strains due to tension forces tangent to the hole, and the strains due to the various other principal stresses involved in transmitting the pin load from the direct area of contact to tensile load through axis *X*-*X*.

Frocht and Hill[7] have investigated the problem of stress concentrations around a hole loaded by a pin. They used photoelasticity and made strain gauge measurements on a large aluminum-alloy plate. A few of their results, listed in Table 1, indicate the variety of strain conditions that may exist depending upon the ratio of hole diameter to plate width, or to edge distance, and the type of fit.

It is interesting to note the relatively minor degree of variation of the maximum tensile stress tangent to

TABLE 1

1	2	3	4	5	6
Joint	$\frac{H^*}{2r}$	$\frac{D^*}{2r}$	Type of fit†	Concentration factor K‡	$\frac{\text{Maximum tensile stress}^{**}}{\text{Average bearing stress}}$
1	1.35	1.33	0.0005 press fit	2.0	6††
2	2.38	2.38	0.0005 press fit	2.7	1.9
3	1.35	2.38	0.0005 press fit	3.0	2.2
4	1.35	2.38	0.0185 clearance	3.4	2.5
5	3.95	6.65	0.0005 press fit	6.3	1.1
6	2.33	6.65	0.0005 press fit	7.2	1.3

* The dimensions are as noted in Fig. 3.

† The fit pertains to an 8-in. diameter pin in a 1-in. thick plate.

‡ The concentration factor K is the ratio between the maximum tensile stress at the edge of the hole to the average tensile stress $K = S_t/[P/(D - 2r)t]$

** The last column is simply $S_t/(P/2rt)$.

†† This value is not comparable to those below since the specimen has much less tension area than bearing area.

the hole, even for large differences in the ratio of plate width to hole diameter (column 3 vs. column 6). Thus, comparing joints 2 and 6, the ratio of tensile stress to bearing stress varies only from 1.9 to 1.3, while the plate width is almost tripled. Since the tensile strains represent only part of the total joint deformation, it is natural to conclude that the hole elongation for a unit bearing pressure is relatively independent of the ratio of plate width to hole diameter (assuming the joint is not critical in tension). The data of Brown's investigation[8] on bearing strength of aluminum alloys indicates no significant change in stress-deflection characteristics when the ratio of plate width to hole diameter varies from 10.6 to 5.3. Since dimensionally similar plates with holes will obviously have the same bearing stress-strain characteristics, with the strain measured in terms of hole diameter, a bearing value can thus be set for a particular material for the condition of uniform bearing across the thickness of a hole, provided that there is a reasonable distance from the hole to the sheet edge normal to the load and that the sheet does not buckle at low stresses.

As the hole approaches the edge of the sheet, shearing forces and the consequent shearing deformation become increasingly significant. The segment of material between the edge of the hole and the edge of the sheet tends to act as a beam, the compression stress tangent to the hole at point M, Fig. 2, and the tension stress at point P, increasing as the edge distance decreases.[9] Thus, less pin load is required per unit deformation.

Strains in the Plastic Range

As noted in Table 1, the first material set may tend to result from tension rather than from compression, even when the average tensile stress is only about 20 per cent of the average bearing stress. As soon as the proportional limit is exceeded, the tensile stress concentration factor naturally is reduced. Unless the sheet is critical in tension, deformation due to localized compressive stresses represents the major part of the total deformation at appreciable values of hole elongation.

Referring to Fig. 2 again, it should be noted that, if the direction of forces is reversed, the tensile stress tangent to the hole is virtually eliminated. The hole elongation per unit load should, therefore, be less in this case than in the case previously discussed. This strain condition is a common one in design, a particular example being the bearing of the pin on a wing hinge fitting with the fitting under a compression load.

Behavior of Material Under Bearing Load

With the ratios of bolt diameter to sheet thickness normally used in aircraft construction, a high bearing stress results in a thickening of that portion of the sheet subjected to this stress (the outside fibers bulging outward, in view of the lack of restraint to such flow). If the bearing stress were based on the actual thickness instead of the original thickness, an appreciably lower value would be obtained. When the distance of the bearing hole to the edge of the sheet is a minimum of a few diameters, the original thickness may more than double. In such cases the ultimate strength is obtained when the bulged metal under the bearing pin chips off. Complete failure finally results from tension or shear but resistance of the sheet to plastic flow under bearing pressure is the factor that establishes the maximum load that the joint can carry. The use of the original bearing area in computations yields a hypothetical bearing pressure in contrast to the true computed bearing pressure obtained throughout the loading in the case of Fig. 1.

With high ratios of pin diameter to sheet thickness, the sheet may buckle under the pin pressure rather than thicken, as already described. An extreme case is illustrated in Fig. 3(a). An 0.020-in. thick Alclad 24S-T aluminum-alloy sheet was loaded by a $^3/_8$-in. pin, with the outside sheets of the joint $^1/_8$-in. 24S-T. The maximum bearing stress developed was only 43,300 lbs. per sq.in. The rigidity of the outside sheets, or plates, in such tests is an important factor in controlling the

FIG. 3. Failures resulting from bearing pressure on thin sheet. (a) $^{3}/_{8}$-in. pin and 0.020-in. sheet; maximum stress = 62,500 lbs. per sq.in. (b) $^{3}/_{16}$-in. pin and 0.014-in. sheet, with $^{1}/_{2}$-in. steel cover plates; maximum stress = 116,000 lbs. per sq.in.

value of the bearing pressure that can be attained, in view of the restraint they offer to the buckling of the test sheet. The test sheet in Fig. 3(b) is 0.014-in. Alclad 24S-T, the pin used was $^{3}/_{16}$ in. in diameter, and the outside plates were $^{1}/_{2}$-in. thick steel. The maximum bearing stress developed in this case was 116,000 lbs. per sq.in. The metal in front of the pin alternately thickened and chipped off until the hole came sufficiently close to the edge so that the shearing strength of the material ahead of it equaled the applied load.

Reference 10 gives further details on the behavior of sheet subjected to bearing pressure.

PLATE BEARING—ALUMINUM ALLOY

Standard of 4 Per Cent Hole Elongation

The original concept of bearing strength in metal aircraft construction was involved with plate bearing. The author has no record of the source of the original allowables for bearing of aluminum alloys, but the figure of 75,000 lbs. per. sq.in. for 17S-T is probably the value originally used for the material.[11] Brown, in his investigation of bearing strength in 1933,[8] established the use of a hole elongation equal to 4 per cent of the hole diameter as the criterion for ultimate bearing strength. Brown recognized that any criterion for determining the allowable bearing stress was arbitrary and, therefore, based his deformation value on considerations of service experience. It was reasoned that, since 75,000 lbs. per sq.in. bearing stress had proved satisfactory in service for 17S-T aluminum alloy, the hole elongation corresponding to this stress would be a reasonable criterion for other aluminum alloys. Curves of bearing stress versus hole deformation for a number of specimens indicated approximately 75,000 lbs. per sq.in. at a deformation of 4 per cent of the pin diameter; therefore, this value was selected as the criterion.

Brown also ran tests on 24S-T and 24S-RT in which he established a bearing strength value of 90,000 lbs. per sq.in. for these materials on the basis of a 4 per cent hole elongation. Another item investigated was the effect of edge distance on bearing strength. The tests on edge distance were carried to a minimum H/d distance of 2, where H is the distance from the centerline of the hole to the edge of the sheet and d is the hole diameter Brown concluded that there was no change in bearing strength for H/d values of 2 or greater, the bearing value being that corresponding to a 4 per cent hole elongation.

Shear-Out Formula

The bearing strengths determined by Brown were generally considered as absolute values for aluminum alloys, regardless of the application involved. When a bolt or rivet was close to the edge of the sheet, an allowable load was determined from a "shear-out" formula. If this load was less than that corresponding to the allowable bearing stress, it was then used for the design.

The shear-out formula was $P_s = 2(H\text{-}r)tf_s$,[1] where P_s is the shear-out strength, H is the distance from the center of the hole to the edge of the sheet, r is the hole radius, t is the thickness of the sheet, and f_s is the allowable shearing strength. The theory behind the formula was that a bolt close to the sheet edge would tend to shear out a slug along two lines, the length of each shear line being conservatively taken as the distance from the edge of the hole to the edge of the sheet. Although the formula was intended specifically for use in the analysis of lugs, it has been applied to all cases where shear-out strength is a factor. For 24S-T aluminum-alloy sheet with a bearing strength of 90,000 lbs. per sq.in. and a shear strength of 37,000 lbs. per sq.in., the shear-out strength becomes equal to the bearing strength at a $H/2r$ ratio of 1.71, which meant that the bearing strength of 90,000 lbs. per sq.in. could be used to that particular ratio.

Standard of 2 Per Cent Set

The aluminum-alloy bearing strength values based upon a hole elongation of 4 per cent were superseded by the current strength values given in reference 4. Values are now listed for $1.5d$ and $2d$ edge distances and for yield and ultimate strength, in contrast to the corresponding single value previously used. The yield strength is based on a hole permanent set of 2 per cent of the diameter; the ultimate strength, on actual failing strength, as compared to the former 4 per cent hole elongation. The term "bearing failure" is now used to describe any failure other than rivet of bolt shear and sheet tension normal to the load.

Fig. 4 shows typical curves of bearing stress versus elongation of hole in per cent of diameter for 24S-RT, 24S-T, and 17S-T, based on average material properties. It will be noted that the 4 per cent hole elongation points fall below the 2 per cent set points on all the curves. Thus, for these particular specimens, the ultimate bearing strength under the former criteria would be less than the yield bearing values under the current criteria. It might be noted that the set cri-

terion shows up more of a difference between 24S-RT and 24S-T than does the total elongation criterion. It should also be noted that, although there is no significant difference between the stresses corresponding to a 4 per cent hole elongation for edge distance of two and six times the hole diameter, a disparity exists for higher values of hole elongation.

Current bearing strength values for aluminum alloys are appreciably higher than previous values. For 24S-T aluminum alloy, the ultimate allowable stresses for 1.5*d* and 2*d* edge distances are 120,000 and 99,000 lbs. per sq.in., respectively, as compared to the superseded value of 90,000 lbs. per sq.in.

The shear-out formula, already given, was revised in reference 4 to permit the use of a greater effective shear area. The additional area equals 0.234*dt* when the edge normal to the direction of the load is straight. The computed shear-out strength for 24S-T sheet for the 1.5*d* edge condition corresponds to a bearing strength of 89,300 lbs. per sq.in. (using the reference 4 allowable shear strength value of 40,000 lbs. per sq.in.). A discrepancy of almost 10,000 lbs. per sq.in. thus exists between the two methods. Since the 99,000 lbs. per sq.in. is based on actual tests, the shear-out formula should apparently be revised. Tests involving edge distances less than 1.5*d* may be used as a basis for such revision to cover the case of fittings having small edge distances. The edge distance to be used for stress analysis should, of course, be the minimum value considering shop tolerance.

Maximum Bearing Stress That May Be Developed

A series of lap joints of 1-in. wide strips of Alclad 24S-T sheet with a single $^3/_{16}$-in. bolt, $1^1/_4$ in. from the edge, were tested to determine the maximum stresses that could be developed. The stresses, based on original sheet thickness, ranged from 148,000 to 174,000 lbs. per sq.in. for sheet gauges from 0.032 to 0.081 in., with no specific variation with sheet gauge. Failure took place by the sheet tearing across the width, a result of stress concentration at the hole. The sheet thickened at the area of bearing contact by approximately 50 per cent. It thus appears that the maximum true bearing stress is 115,000 lbs. per sq.in. for the joints tested.

A 2-in. wide lap joint with a $^3/_{16}$-in. bolt developed 200,000 lbs. per sq.in. in bearing (based on original thickness) before the sheet tore. In a double shear joint, a stress of 240,000 lbs. per sq.in. was realized. However, the stress based on the thickened area was only 110,000 lbs. per sq.in.

The above data are, naturally, of academic consideration only.

Discussion of Section

A discussion of this section relative to its significance in airplane design will be limited to bolted joints, since the subject of riveted joints is treated later in this paper.

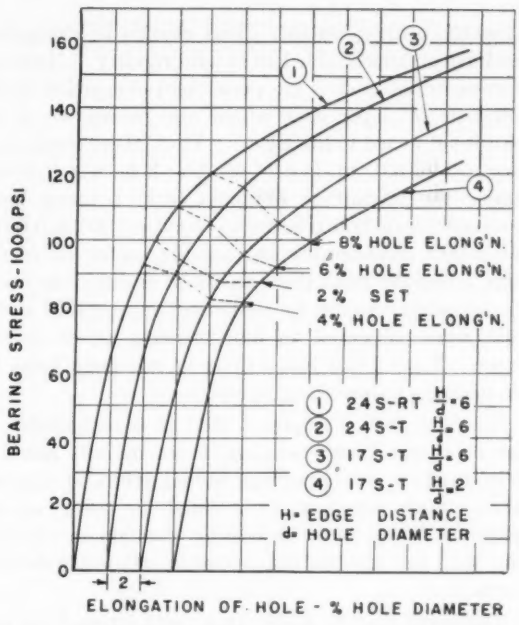

FIG. 4. Bearing stress-deflection curves for 24S-T aluminum alloys, with pin bearing on hole in sheet.

The hole elongation or set determined in plate bearing tests will be developed in bolted joints (designed as described below) only when the load per bolt is uniform and when there is no significant friction among the plates of the joint to resist part of the load. When different size bolts are used in a joint, the load will be proportioned according to the relative load-deformation rates of each bolt in combination with the plate on which it bears. Thus, at limit load the deformation of the plate bearing against the smallest bolts may be appreciably more than the allowable value (bolts may be loaded exclusively in shear) when the total joint strength is obtained by summing up the strength of each element of the joint. In many double-shear bolted joints and in all lap joints, the clamping action of the bolt head and the nut, due to the installation tension in the bolt, will tend to reduce the deflection rate from the value obtained in a bearing test.

However, it is impractical to consider deviations in setting up a standard, and a value of allowable bearing stress based on a nominal amount of hole deformation appears to be a reasonable procedure in setting up such a standard. The actual amount of deformation to use is a matter of opinion, but one of the basic considerations is the amount of joint deflection or set that is to be tolerated.

From Fig. 4 it will be noted that the hole elongation at limit load for 24S-T is increased from 1.8 to 3 per cent when the allowable limit bearing stress is increased from 60,000 to 80,000 lbs. per sq.in. (former to present

allowable bearing stress). This change in elongation results in an appreciable loss in joint rigidity. However of more importance is the permanent elongation of the bolt hole of 2 per cent which may result when the joint is subjected to limit load. Thus, there would be a clearance of 0.01 in. in a $^1/_2$-in. bolt hole, which would nullify the advantage obtained from reaming holes (common $^1/_2$-in. hole tolerance, 0.500 (−0.000 + 0.001)) and might considerably shorten the useful life of the joint, especially when there are shock or vibratory loads. The clearance would be increased appreciably if the joint were subjected to limit bearing stress several times. A joint that had a drive fit was made loose by ten loadings to limit bearing stress.

It is the author's opinion that it is undesirable to permit a significant permanent set in bolt holes at limit load in the important bolted joints of the airplane. Such set may be avoided by using an appropriate fitting factor or margin of safety in conjunction with the 120,000 lbs. per sq.in. allowable bearing stress.

The point may be raised that yield stresses are permitted at limit load and that permanent set results from these stresses. However, practically, the yield stress is seldom closely approached in a basic sheet or extrusion, since the maximum ultimate compression stress used is generally the yield stress and the average tensile yield strength of 24S-T is approximately 50,000 lbs. per sq.in. as compared to an ultimate design value that is seldom in excess of 60,000 lbs. per sq.in. The difference between yield and ultimate is less in the case of the artificially aged alloys.

There are no requirements for using reduced bearing strength for the connecting elements of rigid joints, although these joints may be subjected to shock or vibratory loads.[3] However, the use of some reduced strength is considered desirable where such loads are frequent and appreciable. Joints used for engine cowling may be subjected to severe vibratory loads in conjunction with a rather high static load. In these cases, the use of the bearing factor of 1.5 given in reference 2 for such applications may even be on the low side.

Plate Bearing—Steel

Test Procedure

Since the allowable bearing strength values for heat-treated steel were established prior to the adoption of a 4 per cent hole elongation as a standard, an investigation[12] was initiated to determine what strengths would be obtained if that standard were followed. The setup used for this investigation was similar to that for aluminum-alloy sheet bearing tests. The jig plates (Fig. 5) were normalized X-4130 steel $^3/_4$ in. thick. The bearing pin was $^1/_2$ in. in diameter and was heat-treated to 280,000 lbs. per sq.in. tensile strength

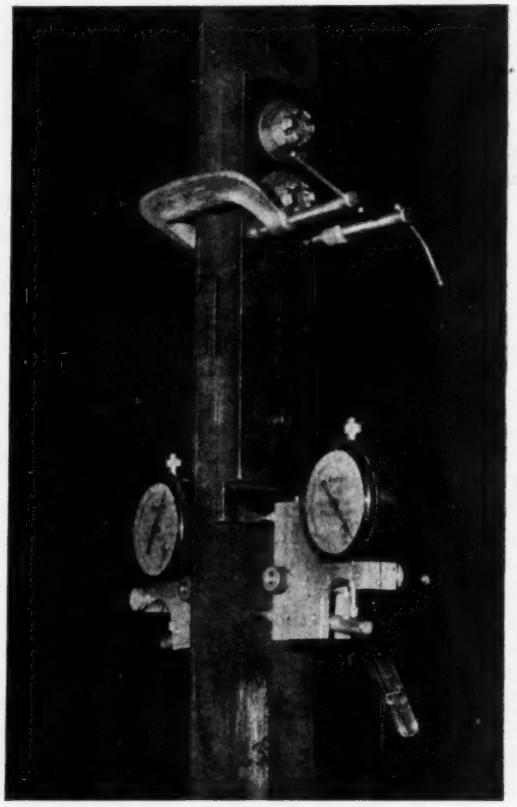

Fig. 5. Typical setup for plate bearing strength test.

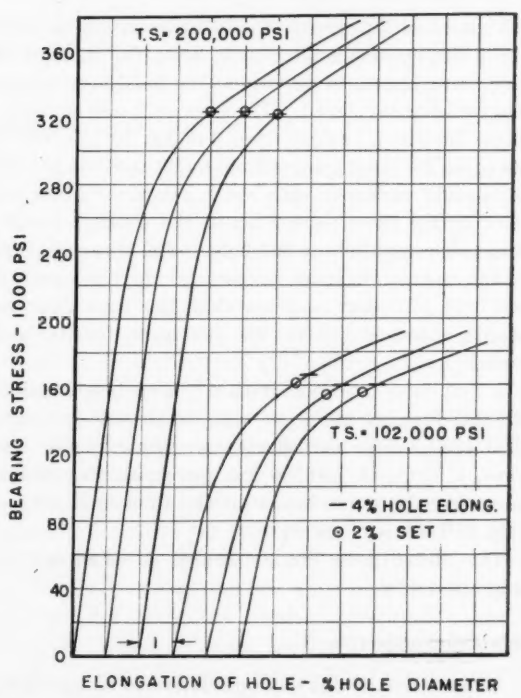

Fig. 6. Bearing stress-deflection curves—X-4130 steel.

to minimize pin deformation as a factor in the joint deflection. The test specimen was X-4130 steel $^1/_8$ in. thick and 3 in. wide, with the center of the bearing pin hole located 2 in. from the plate edge.

The specimens were made in four tensile strength groups as follows: (a) normalized, (b) 125,000–140,000, (c) 150,000–170,000, and (d) 180,000–200,000.

In each group four tensile coupons were taken, and the average of their strength values were used for the correlation with bearing strength.

For determining the bearing hole elongation, a value of sheet deflection over the length between the lower arm of the dial gauge frame and the center of the bearing pin (Fig. 5) was computed by the formula PL/AE, and this value was subtracted from the hole elongation plus sheet deflection from an average of the two dial gauge readings. No correction was made for the bearing deflection of the pin relative to the jig plates.

Results

Fig. 6 shows the bearing stress versus hole elongation results obtained for the normalized steel (102,000 lbs. per sq.in.) and the highest strength sheet used (200,000 lbs. per sq.in.). Fig. 7 shows the plot of bearing strength versus tensile strength, with the bearing strength based on a 4 per cent hole elongation. Allowable values from reference 3 are included for comparison.

With the present bearing strength criterion of a 2 per cent set at limit load and failing strength at ultimate load, the values given in Fig. 7 could be appreciably increased, provided that close edge distance or tensile strength is not the controlling factor. According to the deflection curves of Fig. 6, the 2 per cent set points correspond approximately to the 4 per cent total elongation points, and thus the allowable ultimate values would be 50 per cent higher than those listed in Column 3 of Table 2, considering the set criteria.

Miller's investigation[13] shows what maximum stress for various edge distances may be expected for 150,000 lbs. per sq.in. tensile strength sheet. For an edge distance factor of 1.5, the bearing pressure at failure is given as 220,000 lbs. per sq.in., while for a factor of 2.0, it is 290,000 lbs. per sq.in. The failing strength values would thus apparently be lower than those based on set criteria.

Table 2 lists the existing allowable bearing strength values, those based on a hole elongation of 4 per cent (with edge distance not critical), and the values for 150,000 lbs. per sq.in. tensile strength steel based on the present bearing strength criteria.

The yield bearing strength values based upon 2 per cent set are, apparently, not critical for heat-treated steel, and the question of permanently elongated holes at limit load does not exist.

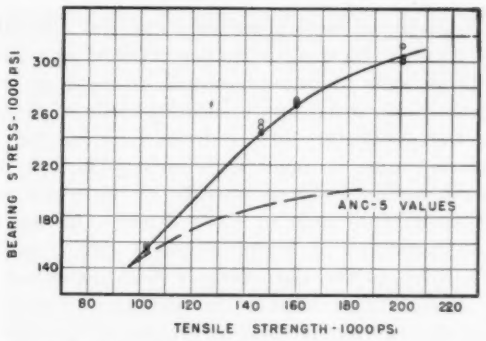

FIG. 7. Bearing strength (based on 4 per cent hole elongation) versus tensile strength—X-4130 steel.

TABLE 2

Bearing Strength Values for Heat-Treated Steel Using Different Standards

1	2	3	4	5
Tensile strength, lbs. per sq.in.	ANC-5 bearing values, lbs. per sq.in.	4% hole elongation bearing values, lbs. per sq.in.	Failing strength values, ——lbs. per sq.in.—— Edge	Distance
125,000	175,000	200,000	$2d$	$1.5d$
150,000	190,000	250,000	290,000	220,000
180,000	200,000	285,000		
200,000		300,000		

The values given in columns 4 and 5 conflict with those based on the shear-out formula, although not to an appreciable degree. The bearing pressures for the $1.5d$ and $2d$ edge distance conditions, assuming a straight edge normal to the direction of load, are 210,000 and 300,000 lbs. per sq.in., respectively, as compared to the 220,000 and 290,000 values given in the table. Thus, the shear-out formula gives approximately zero margins for these two edge distances. With an edge distance equal to the hole diameter, the margin is 15 per cent.

It appears that the shear-out formula is more applicable to steel than to 24S-T and could take care of the allowable bearing strength values for heat-treated steel, with the maximum strength limited to a $2d$ edge condition and with a fitting factor or appropriate margin of safety used where there is a question of the accuracy of the design load or assumed load distribution among the elements of a bolted joint or where other considerations, such as shock or vibration, are involved.

RIVET BEARING

General Description

The bearing condition considered here is that of a plate bearing on a rivet made of a lower tensile strength material than that of the plate. If there were an ab-

solute bearing strength value for a material, the value would logically be expected to depend only upon some parameter, such as ultimate tensile strength or yield strength. However, since bearing values depend upon the application involved, an experimental investigation must be made with each application and allowable strength criteria must be set up which may differ from those used in other cases. The bearing pressure produced by a rivet causes a cutting action, as compared to the thickening or buckling action of plate under edge pressure. The resistance to material flow under bearing pressure is greater in the case of the rivet than in the case of the plate, and, thus, less deformation may be expected under corresponding conditions. The plate fibers can bulge outwardly, whereas the rivet fibers under pressure are restrained by adjacent fibers.

Experimental Investigations

The problem of rivet bearing strength assumed importance with the general adoption of A17S-T aluminum-alloy rivets several years ago, the A17S-T material being rated at a tensile strength of 38,000 lbs. per sq.in. in contrast to the 62,000 value for 24S-T. A bearing strength of 60,000 lbs. per sq.in., based on a 4 per cent rivet-diameter joint elongation, was established by Warner[14] in 1935, with $^1/_8$- and $^5/_{32}$-in. diameter undriven A17S-T rivets acting on 24S-T sheet 0.051 in. thick. The 4 per cent elongation represented the combined deformation of rivet and sheet. (At the time, there was no differentiation between the bearing strengths of 17S-T rivets and sheet.)

With tests of riveted joints (using A17S-T rivets) showing failing strengths greatly in excess of allowables based on a 60,000 lbs. per sq.in. bearing value, the author initiated an investigation[15] in 1937 to determine if higher allowables could be used.

The tests were made in a three-plate double shear jig of the type commonly used for shear tests on aluminum-alloy rivets. The setup was similar to that in Fig. 5. The center bearing plate was made from steel heat-treated to 200,000 lbs. per sq.in. tensile strength to eliminate plate deformation. These plates were varied in thickness, and $^1/_8$- and $^1/_4$-in. undriven rivets of A17S-T and 17S-T aluminum alloy were used as the specimens. Deformations were measured with a Ewing extensometer attached to the two center plates. Fig. 8 shows some of the bearing stress deflection results obtained for the rivets. Corresponding rivet shear stresses are also noted.

The bearing strength of the rivet based on a 4 per cent deformation increases with a decrease in sheet thickness. The problem is not one of pure bearing but one of combined bearing and shear. Naturally, if a low ratio of rivet diameter to sheet thickness is used, the shear deformation will be more significant than the bearing deformation and the bearing stress corresponding to 4 per cent total deformation will be low. Thus,

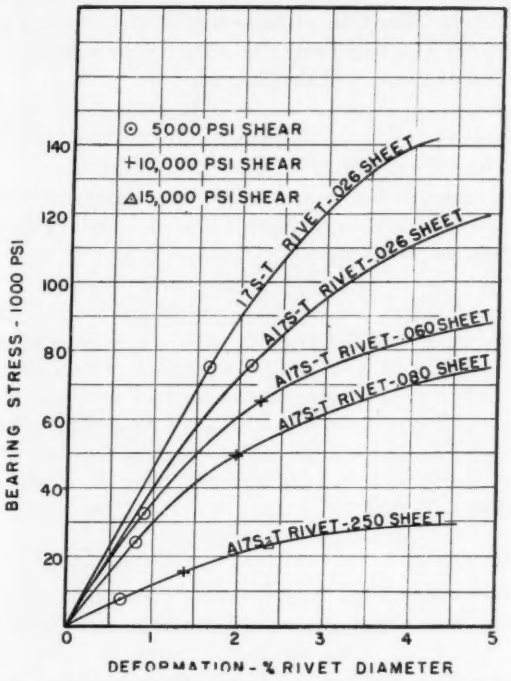

FIG. 8. Bearing stress-deflection curves for $^1/_4$-in. A17S-T and 17S-T undriven rivets.

the bearing stress for $^1/_4$-in. A17S-T rivets at a deformation of 4 per cent was found to vary from 70,000 to 110,000 lbs. per sq.in. for 0.080- to 0.026-in. sheet, respectively.

Criteria for Establishing Bearing Strength

It was planned originally to base the bearing strength of the rivet upon the stress corresponding to a deformation (4 per cent) which agreed with the standard value being used for plate bearing strength, by the fallacy of such a procedure, shown by the discussion immediately above, soon became apparent.

A check was then made of the deformation of rivets in which shear was the predominant stress. It was reasoned that the deformation of such rivets, when they were subjected to loads corresponding to two-thirds of the ultimate shearing strength (limit load), might indicate a deformation to use when bearing is critical. At a shear stress of 16,700 lbs. per. sq.in. (two-thirds of ultimate value of 25,000), a $^1/_4$-in. rivet bearing against a $^1/_4$-in. plate deformed 3.2 per cent of its diameter, and a $^1/_8$-in. rivet tested with a $^1/_8$-in. plate deformed 2.5 per cent. Since such deformations corresponded to limit load design (ignoring shank expansion due to upsetting and the restraining effect of the heads) when shear is critical, it appeared inconsistent to restrict maximum bearing stresses for rivets to strain values much less than these. A comparison was made of these shear deformations and of the bearing deformations of the $^1/_4$-in. rivets when subjected

to 60,000 lbs. per sq.in. bearing on the 0.026- up to the 0.080-in. sheet. The latter deformations were found to vary from 1.6 per cent of the diameter for the 0.026-in. sheet to 2.8 per cent for the 0.080-in. sheet. It seemed logical and conservative, therefore, to allow 60,000 lbs. per sq.in. bearing stress for limit load and 90,000 lbs. per sq.in. for ultimate load, the same as for 24S-T plate. Since 90,000 lbs. per sq.in. was the maximum allowable bearing stress for aluminum alloys at that time, there was no need to establish a higher bearing value for 17S-T rivets, even though the deformation of a $^1/_4$-in. rivet in 0.060 plate at 60,000 lbs. per sq.in. bearing stress was only 1.6 per cent—well within the proportional limit. Ninety thousand pounds per square inch thus became the ultimate bearing strength value for A17S-T and 17S-T rivets in reference 1.

The maximum bearing stress developed in this investigation was 186,000 lbs. per sq.in. The test specimen was a $^1/_4$-in. 17S-T rivet bearing on 0.026-in. sheet. This stress value is considerably in excess of the true bearing stress of approximately 115,000 lbs. per sq.in. sustained by 24S-T sheet in a plate bearing test.

Rivet Deformations

A noteworthy characteristic of these tests was the manner in which shearing and bearing loads affect a rivet. Examination of failed rivets and of rivets removed from the testing machine at bearing stresses from 50,000 lbs. per sq.in. to near failure indicates that the steel plate causes a flow of the rivet material, leaving a groove with smooth sides, until the applied load reaches the double shear strength of the uncut rivet portion, at which time failure occurs. The resulting sheared surface, in contrast to that left by the bearing groove, is rough and irregular. One of the $^1/_4$-in. rivets tested with 0.026 plate was removed just before failure, after having experienced a bearing pressure of 150,000 lbs. per sq.in. Approximately three-fifths of the rivet had been smoothly cut through. This rivet (shown in Fig. 9) failed under a load of 955 lbs. compared with the double shear value of 2,640 lbs. Another rivet failed at a shearing stress of 22,400 lbs. per sq.in. with the bearing stress 109,000 lbs. per sq.in. In a third case, the failing shear stress was 27,000 lbs. per sq.in., but the bearing stress was only 42,000 lbs. per sq.in. When bearing is critical, only the material adjacent to the plate is affected, whereas in shear the entire rivet section forward of the plate is deformed.

When the sheet allowable bearing strengths were increased for reference 4, the values for rivets were also raised, a value three and one-third times the shear strength being used. The amount of rivet permanent set at limit load for the current rivet bearing values is still negligible compared to the 2 per cent set used for sheet bearing.

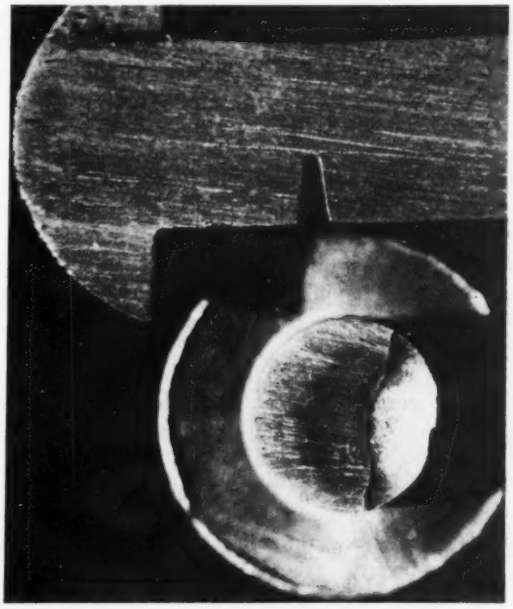

FIG. 9. Sections through $^1/_4$-in. undriven A17S-T rivets just prior to and after failure. Bearing stress = 150,000 lbs. per sq.in.; shear stress = 9,800 lbs. per sq.in.

Bearing of Steel Bolts

The value of bearing strength to use for steel bolts of 125,000 lbs. per sq.in. tensile strength acting in steel fittings of 180,000 lbs. per sq.in. tensile strength is a problem similar to that of the soft aluminum-alloy rivet bearing on a sheet of harder material. The author does not know of any investigation made to determine allowable values for the bolts, but it appears from the rivet investigation that it is safe to use the bearing strength value of the fitting material for the bolts.

PIN-SOCKET JOINTS

Definition

The problem of pin-socket joints is somewhat of a departure from the usual applications of bearing strength. A pin-socket joint consists of a tube or rod telescoping in another tube or socket, through which a bending moment is transmitted. Such joints are common in landing gear structures.

Stress Analysis Methods

Socket joints are generally analyzed as simple structural elements with bearing, socket-wall tear-out, and bending stresses determined according to arbitrary simplified distributions of stress and with allowable strengths taken as the commonly accepted values for the material.[3, 4] Such a procedure is highly conservative, since the computed stresses may be much higher than those actually induced. Also, the re-

sistance to bearing deformation is greater than that of a plate in a bolted joint, and therefore the use of higher allowable stresses would be justified. The simple stress formulas are convenient to use in the absence of a rational procedure for accurately analyzing socket joints, but with them must be associated fictitious values of allowable stress, these values being determined by substituting test results in the formulas. However, these fictitious values are not constant; they are functions of such elements as the degree of embedment of the pin in the socket, the fit of the pin, the distance between socket faces, and the ratio of beam to socket diameter. It would be advisable, therefore, to use a test specimen dimensionally similar to the structure being considered. The tests herewith reported indicate hypothetical stress values that may be attained with some types of joints.

The usual method of stress analysis arbitrarily assumes that the bending moment of the pin is transmitted to the socket through a triangular distribution of bearing pressure (shown in Fig. 10(b)), the maximum bearing pressure in such a case being determined by the formula

$$f_{br} = 6M/dC^2$$

(the symbols are defined in the figure). Values of bearing stresses given in this section are based on this formula. Actually, at higher loads the distribution tends to depart from a linear condition, and, furthermore, an appreciable part of the moment is resisted by frictional resistance of the pin in the socket.

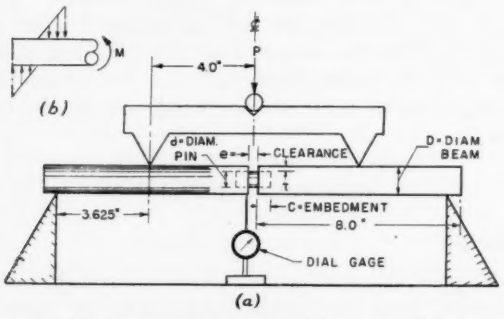

FIG. 10. (a) Setup for pin-socket joint test. (b) Assumed resisting forces on pin.

Test Procedure and Results

The test specimen[16] consisted of two X-4130 steel rods with holes drilled to accommodate the pin. The basic variable was the degree of embedment or the ratio of the length of pin inserted in the socket to the diameter of the pin. The fit of the pin in the sockets was snug, the clearance approximating 0.001 in. The rods and pins were heat-treated to a nominal value of 160,000 lbs. per sq.in. Deflection readings were taken at the face of one of the sockets to determine the moment at which elastic behavior ceased. Fig. 10(a) shows the setup used. The loading for each of the specimens was carried to the point where the load dropped off because of pin bending, pin slippage, or socket-wall tearing. Fig. 11 shows load-deflection curves for two of the specimens and includes descriptions of them. In the first of these, the proportional limit corresponds to a bearing stress of 217,000 lbs. per sq.in. In the second, which pertains to an appreciably larger degree of embedment, the bearing stress is 230,000 lbs. per sq.in. The maximum bearing stresses were 522,000 and 417,000 lbs. per sq.in., respectively, with the pin slipping out of the socket in the first case and with the wall of the socket rupturing in the second case. The pin of the second specimen, with a tensile strength of 155,000 lbs. per sq.in., was subjected to a hypothetical bending stress of 525,000 lbs. per sq.in. (using the formula $f_t = My/I$). This high computed stress is possible because of the shortness of the beam.

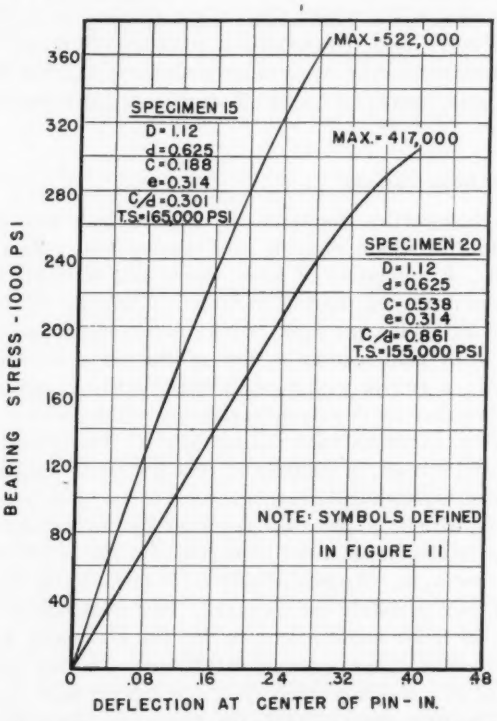

FIG. 11. Bearing stress-deflection curves for pin-socket joints.

These bearing values are based upon the original degree of embedment. As the pin gradually slipped from the socket, the embedment decreased and the stress correspondingly increased. In the test of Specimen 15 the pin was scratched at the entrance plane of the socket to determine the final degree of embedment corresponding to maximum load. The bearing stress computed in this case was 755,000 lbs. per sq.in. Fig. 12 shows the bearing deformation of a pin that had been subjected to a bearing stress of 436,000 lbs. per sq.in. (based on original embedment). It is note-

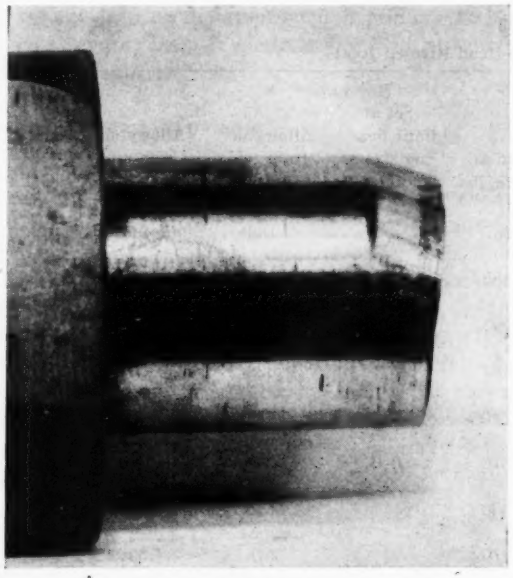

FIG. 12. Bearing deformation of pin edge after being subjected to computed bearing stress of 436,000 lbs. per sq.in. in socket test.

worthy that in that part of the joint of Specimen 15 in which the original pin embedment was maintained (in all the tests, the pin maintained its original embedment in one of the sockets, slipping only from the other), and in which the hypothetical stress of 522,000 lbs. per sq.in. might have some significance, there was no perceptible deformation of either the pin or sockets. Since the bearing stress is determined from an assumed stress distribution, the true maximum bearing stress developed could not be determined.

Using the formula $6M/C^2(2l)$ for socket wall stress, a value of 530,000 lbs. per sq.in. was obtained for Specimen 20. With the actual degree of embedment at maximum load, a computed stress of 950,000 lbs. per sq.in. was obtained for Specimen 15.

Conclusion

It would appear from this investigation that an ultimate bearing stress equal to twice the tensile strength of the material is a safe value to use in this type of joint when the joint is analyzed under the assumptions of load distribution made herein. This statement (which presupposes that the socket wall will not rupture) is based on the use of an ultimate stress 50 per cent higher than the proportional limit as determined in the socket test. The proportional limit of Specimen 15 (Fig. 11) is 217,000 lbs. per sq.in., whereas the tensile strength is 155,000 lbs. per sq.in.

PROTRUDING-HEAD RIVETED JOINTS

Foreword

The subject of riveted joints, both the protruding-head type and the flush type, is covered from the general standpoint of strength rather than from a bearing consideration specifically, since there often is not a clearly defined distinction between bearing, rivet shear, and other factors that affect the ultimate strength of a joint.

Only lap joints are discussed, in view of the relative infrequency with which double shear riveted joints are used.

Distinctive Characteristics

Basically, a protruding-head riveted lap joint (Fig. 13(a)) acts according to the principles discussed for plate bearing. There is bearing of the rivet shank against the plate (with the corresponding tendency of the plate to deform the rivet in bearing) and there is shear stress on the shank, which has a maximum value through the plane between the two sheets. However, there are other important factors that represent a departure from the basic conditions that apply to a double-shear type of bolted joint and which are stimulated in a plate bearing test. First there is an expansion of the shank, caused by the riveting process, which increases the effective shear area and, to a smaller extent, the bearing area. Second, the driving process alters the shear strength of the rivet material. A third effect is that of the clamping action of the rivet ends, which helps to resist part of the load. (This effect may also exist in a bolted joint, as already noted.) Finally, the eccentric loading causes a nonuniform bearing of the rivet on the sheet.

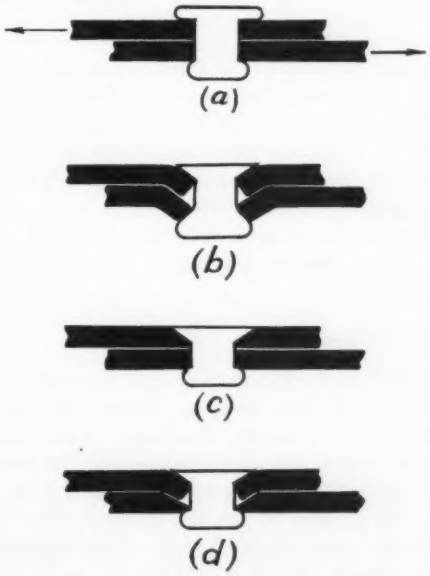

FIG. 13. Four types of riveted joints.

Rivet Expansion

The expansion of the shank is a function of the hole size, since the shank will normally expand until the

TABLE 3
Characteristics of Protruding-Head Riveted Joints

1	2	3	4	5	6	7	8	9	10
Spec. No.	Rivet dia., in.	Sheet thick., in.	Load at 4% set, lbs.	1.5 × col. 4, lbs.	Load at failure, lbs.	Set at limit bearing stress, % of col. 2	Allowable from ref. 3, lbs.	Allowable from ref. 4, lbs.	Col. 6 / Col. 9
1	3/32	0.032 0.091 0.032	250	375	267	...	186	217	1.23
2	1/8	0.032 0.040	400	600	485	0.2	328	389	1.24
3	1/8	0.040 0.040	475	713	505	0.8	331	389	1.30
4	1/8	0.091 0.032	370	555	422	...	328	389	1.08
5	5/32	0.032 0.040	640	960	720	0.0	449	509	1.41
6	5/32	0.040 0.051	615	924	670	0.0	518	596	1.13
7	5/32	0.156 0.064	530	795	620	...	518	596	1.04
8	5/32	0.064 0.051	595	894	670	...	518	596	1.12
9	3/16	0.051 0.064	1,000	1,500	1,180	0.1	784	974	1.21
10	3/16	0.064 0.091	1,100	1,650	1,190	2.2	828	974	1.22
11	3/16	0.250 0.091	890	1,335	1,045	...	828	974	1.07
12	1/4	0.091 0.081	...	...	1,920	...	1,472	1,764	1.09
13	1/4	0.250	1,610	2,415	1,810	...	1,472	1,764	1.02

NOTES: (1) Sheet material up through 0.091 inch gauge is Alclad 24S-T. (2) 3/32, 1/8, and 5/32 in. rivets are A17S-T; 3/16 rivets, 17S-T. (3) Values for equal gauge joints are averages of two or three specimens; other values are averages of five specimens. (4) Limit bearing stress is 76,000 lbs. per sq.in. for gauges 0.051 and less; 78,000 lbs. per sq.in. for heavier gauges.

sheet hole is completely filled. The degree of expansion will tend to be less for the larger rivets, since the clearance between the hole and the rivet does not increase in a linear proportion to the rivet diameter. Thus, a No. 30 drill (0.1285) may be used for a 1/8-in. rivet and a No. 11 (0.191) for a 3/16-in. rivet. The drill tolerance, as for example +0.004 − 0.000 for a 3/16-in. rivet, may considerably affect these basic conditions.

Material Property Change

Material property change due to upsetting is a function of the rivet temper—*W* (as quenched) or *T* condition—just prior to upsetting. There is an appreciable drop in the shearing strength (in pounds per square inch) of 17S-T wire when it is upset in the *W* condition and allowed to age, the strength being based on actual rather than nominal area. Brueggeman[17] shows a drop from 37,500 to 34,000 lbs. per sq.in. when the wire is upset 8 per cent. If the wire is driven in the *T* condition, a small increase in strength will result. Thus, A17S-T rivets that are driven in the aged condition are not appreciably inferior to 17S-T rivets driven in the *W* condition.

Clamping Action

The effect of rivet head clamping action for a flush joint would be difficult to determine. An attempt was made by the writer to obtain a general value of clamping action for a joint of 0.040-in. sheet with a 5/32-in. flat-head rivet. Slotted holes were cut in the sheet, and washers were placed against the rivet heads. The maximum load obtained was 25 lbs.

Rivet Canting

The eccentric loading causes rivet rotation (canting) in the joint, which in turn induces a tensile load on the rivet. If failure does not eventually result from rivet shear or tearing of the sheet (for high ratios of rivet diameter to sheet thickness), the rivet may fail in tension with the manufactured head coming off, or the driven head may pull out of the sheet. Thus, the tensile strength of the rivet head may be a factor in the strength of a lap joint. Appreciable bearing deformation is not likely to occur in lap joints, since a small degree of deformation will allow the rivet to cant and induce the aforementioned tensile load. Thus, an appreciable thickening of the sheet under bearing pressure is rare in these joints. However,

resistance to bearing deformation is a primary factor in joint strength, since it controls the load at which canting takes place.

Criteria for Allowable Strength

Until reference 4 was issued, the values used for uniform bolt bearing on plates and the basic shear values of the rivet material were used for protruding-head riveted joints, with no consideration for the shank expansion and the change in material strength due to upsetting (except for the increase of A17S-T design shear strength from 25,000 to 27,000 lbs. per sq.in. a few years ago[2]). For the current allowables, higher basic shear values are used in conjunction with areas based upon upset rivet diameter instead of nominal diameter. For the large size 24S-T rivets, the increase in strength over previous values is as much as 25 per cent.

Experimental Results

Table 3 gives representative strength characteristics of protruding(flat)-head riveted lap joints having one rivet each. The specimen width was $^{15}/_{16}$ in. and the edge distance was approximately 1 in. These specimens were made at different times in the Republic Aviation company shop as part of a general rivet investigation. No measurements were made of the size of hole drilled and no attempt was made to obtain consistent degrees of upsetting.

The limit load bearing strength for a protruding-head riveted joint is based on a 2 per cent set in plate bearing tests. Therefore, it might be expected that the set at limit bearing stress for a joint of two equal-gauge sheets would be at least 4 per cent, with the added rivet deformation. Column 7 of Table 3 is included to show the actual set realized at this stress. The discrepancy between the values of this column and 4 per cent is mainly due to the difference between the sheet material properties, and those upon which the allowable bearing strength is based, and the large edge distance of the specimens (the 2 per cent set stress is based on a 2*d* edge distance, and generally the amount of set for the same load reduces as the edge distance increases). The effect of clamping action probably accounts for the remainder.

A comparison between columns 5 and 6 indicates that, if the flush-riveted-joint allowable strength criteria (described later) were applied to protruding-head riveted joints, the yield load would not even come close to being critical. However, the difference in values in the two columns would be reduced to some extent if a 2*d* edge distance had been used for the specimens.

There is an appreciable scatter in the ratios of failing strength to allowable strength, but the trend is toward a lowering of the ratio with an increase in the combined thickness of the joint sheets. The reason for this is, probably, the increased eccentricity. In this respect, notice the 2 per cent margin shown in column 10.

Materials Factor of Safety

The exact value of materials factor of safety to consider is open to question. In joints where the load per rivet is accurately known, a value of a few per cent may be satisfactory. However, there are often appreciable variations between assumed distributions among rivets and actual distributions. For example, shear lag may cause a considerable difference in the rivet loading across a skin splice as compared to the common assumption of uniform load. Also, departures of the neutral axis of a spar cap from a straight line may have a pronounced effect on the loading of rivets attaching the cap to the web. Another case is the transferring of load from a fitting to another structural element through a line of rivets in the direction of the load. The relative deflection of the sheet, as compared to the joint deformation, controls the degree of uniformity of the loads among the rivets. Thus, in a long joint, large sheet deflections will cause the end rivets to be more highly loaded than the center rivets. The following test data indicate the unconservatism in assuming a uniform load distribution.

Lap Joint 1

Sheet—0.064 in. thick, $2^1/_2$ in. wide; Alclad 24S-T.
Rivets—$^5/_{32}$-in. A17S-T; Spacing—2 in.
Average load per rivet, based on two specimens each.
3 rivet splice—705 lbs.
8 rivet splice—687 lbs.
13 rivet splice—622 lbs.

Lap Joint 2

Sheet—$^3/_{16}$ in. thick, $2^7/_8$ in. wide; 24S-T.
Rivets—$^1/_4$-in. 17S-T; Spacing—2 in.
Average load per rivet, based on two specimens each.
3 rivet splice—1980 lbs.
8 rivet splice—2030 lbs.
13 rivet splice—1760 lbs.

No specific materials factor of safety can be recommended for any particular application, but some factor would appear advisable where there may be a question of the accuracy of the computed loads on the individual rivets of multi-rivet joint. There is further discussion of this subject later in this paper.

Rivet Bearing Strength in Joints

In the section of this paper on rivet bearing, it was noted that under high bearing pressure a steel plate will cut into the rivet, thereby reducing the effective shear area. When the bearing stress was 42,000 lbs. per sq.in., an undriven A17S-T rivet failed in shear at a stress of 27,000 lbs. per sq.in, whereas with a bearing stress of 108,000 lbs. per sq.in. the rivet sheared at a stress of 22,400 lbs. per sq.in. (based on nominal area). Therefore, with an allowable ultimate bearing pressure

of 100,000 lbs. per sq.in. for A17S-T rivets,[4] it would appear unconservative to use the full expanded area of the rivet in obtaining an allowable load. Tests were run to ascertain whether lap riveted joints showed the same trend of reduced strength. Joints were made with Alclad 24S-T 2-in. wide sheet and $^5/_{32}$-in. A17S-T rivets. Each joint was in triplicate and had three rivets, spaced 1 in. apart, in line with the load. The values obtained for failing loads per rivet, and the corresponding shear and bearing stresses (based on nominal upset shank diameter of 0.159 in.) are given in Table 4.

TABLE 4
Effect of Bearing Stress Value on Ultimate Shear Strength

Sheet thickness, in.	Load per rivet, lbs.	Shear stress, lbs. per sq.in.	Bearing stress, lbs. per sq.in.	Allowable load, lbs.
0.064	687	34,500	67,400	596
0.051	698	35,000	86,000	596
0.040	726	36,400	114,000	596
0.032	726	36,400	143,000	509
0.025	506	25,400	127,000*	...

* Sheet tore.

It appears from these tests that the reduced shear values obtained with the use of steel bearing plates have little significance in lap joints of Alclad 24S-T sheet. The probable reasons are that the thickening of the sheet under bearing pressure results in a bearing stress lower than the computed value and that the high degree of canting (in the case of the thinner sheets) results in a greater effective shear plane through the shank.

In a double shear joint, lower values of shear may be obtained. In a joint of 0.032-in. Alclad 24S-T sheet and a $^5/_{32}$-in. A17S-T rivet, the double shear load at failure was only 850 lbs., as compared to the allowable shear value of 596 × 2 = 1,192 lbs. With the higher yield strength aluminum alloys, this effect may be more pronounced because of the smaller degree of thickening of the sheet under the rivet pressure.

FLUSH-RIVET JOINTS

General Description

Flush-riveted joints represent much more of a departure from the basic bearing conditions than do protruding-head riveted joints. In the dimpled joint, Fig. 13(b), the overlap of the two sheets contributes appreciably to the strength of the joint, and a value of bearing strength based on sheet thickness has little significance, since the rivet does not bear against the sheet edge. The rivet of a lap joint rotates under load, and failure generally takes place by cracking of the dimple on the side of the formed head, by cracking of the manufactured head of the rivet, or by tearing of the sheet (starting from the dimple) on the side of the manufactured head. It should be apparent that the failing strength of the joint will increase with the amount of overlap of the two sheets. Thus, a dimpled joint using a 78°-head rivet will tend to be stronger than a joint using a 115°-head rivet. It should also be apparent that bearing, in its fundamental sense, plays little part in the strength of the joint.

A machine countersunk joint, Fig. 13(c), has the rivet head and part of the shank bearing against the sheet in which the countersink exists, thus apparently providing a large bearing area. However, under the eccentric load that a lap joint sustains, the rivet tends to bear only against the sheet area nearest the shear plane. If the countersink extends through the sheet, there may be bearing only against the sharp edge of the sheet (at the shear plane) which will readily collapse, permitting greatly increased joint deformation and further rotation of the rivet. If failure does not ultimately occur by rivet shear, the sheet will generally tear from the countersunk hole. The undesirability of the usual type of machine countersunk joints for thin sheets arises from the poor deflection characteristics caused by the "feather" edge at the inner face of the countersink. The bearing strength (or resistance of the sheet to deformation caused by a bearing force) has direct significance in this type of joint in contrast to its small importance in the case of a dimpled joint.

The flush joint in which one sheet is dimpled and the other is countersunk, Fig. 13(d), tends to duplicate the behavior of the dimpled joint. The overlap of the dimple into the second sheet is effective in resisting part of the shear, and, although there is direct bearing action on the countersunk sheet, that sheet is normally heavier than the dimpled sheet and is, therefore, not critical.

Allowable Strength Criteria

With regard to allowable strengths for flush-riveted joints, the 4 per cent hole elongation criterion for bearing upon nominal rivet diameters was in effect until reference 3 was issued. There was no discrimination as to the flush-riveting process used. The author had pointed out in 1939[10] that comprehensive tests of riveted lap joints appeared to be a more rational procedure of determining the bearing strengths of these joints than did plate bearing tests. The following year he reviewed the results of the available riveted joint tests and found a fairly constant margin of 35 per cent between failing and allowable loads[1] for A17S-T protruding-head riveted joints.[18] There did not appear to be any logical way of evaluating that margin, but an appreciable value seemed desirable because of the uncertainty of individual rivet loads (discussed in the previous section), of the difference between average and minimum properties, and of the possibility of

loose or ineffective rivets (often a result of oversize drilling used to make parts of an assembly match).

The failing stresses for the flush-riveted joints were found to vary over a wide range as compared to existing allowables.[2] Same dimpled joints attained hypothetical bearing stresses (based upon sheet thickness) of more than twice the allowable and hypothetical shear stresses (based upon the nominal area of the rivet shank) of almost three times the allowable, whereas the failing strengths of some of the machine countersunk joints were even less than the allowables. Not only the rivet head angle but the dimpling technique appeared to be a parameter for joint strength.

Another point noted was that for d/t ratios greater than 5.5 the use of fixed bearing strength values for protruding-head riveted joints appeared unwarranted, since buckling of the sheet against the rivet started to become critical at about this value. This 5.5 limit was set for the protruding-head rivet allowable load tables of reference 3, which reference also established the allowables for flush joints on a rational basis. These latter allowables are based on a joint set of 4 per cent of the nominal rivet diameter for yield load and on the actual failing strength for ultimate load, a materials factor of safety of 1.15 being used in conjunction with these strengths.

However, no values are given for the frequently used flush joint where one sheet is dimpled into the countersunk hole of the second sheet.

Fig. 14 illustrates the marked difference that may exist between machine-countersunk and dimpled joints, both from the standpoints of failing load and rigidity. The same allowable strengths were used for these joints prior to the issuance of reference 3. This figure also shows elongation characteristics of four joints having 0.051-in. sheet as one part of the joint and 0.051- to 0.250-in. sheet as the other part. The failing loads are all about the same; however, when the second, heavier, sheet is machine-countersunk, the joints have more rigidity at lower loads but greater permanent set at high loads.

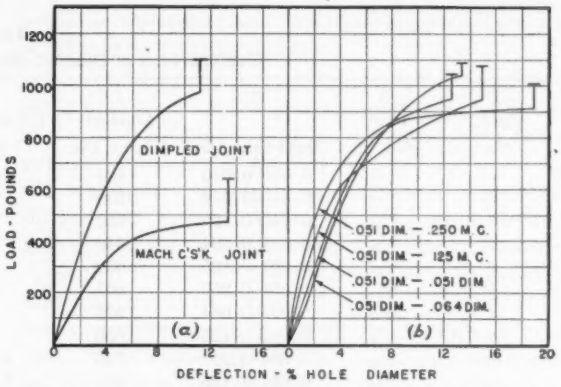

FIG. 14. Comparative load-deflection curves. (a) Dimpled and machine countersunk riveted joints—$^{5}/_{32}$ 17S-T 115°—head rivets, 0.051 Alclad 24S-T sheet. (b) Varying thickness of one sheet in riveted joints using $^{5}/_{32}$ A17S-T rivets.

Tabulated Values of Strength

Tables 5, 6, and 7 give representative strength characteristics of dimpled, dimpled-machine-countersunk, and machine-countersunk single rivet joints, respectively, as made by Republic Aviation Corporation. The specimens were $^{15}/_{16}$ in. wide, and the rivet edge distance was approximately 1 in. The joints were prepared in the shop and not under laboratory conditions. Comparing Columns 5 and 6 of Table 5, it will be noted that one and one-half times the load at 4 per cent set is in every case considerably higher than the load at failure. It thus appears that the failure load controls the allowable strength of these 115° dimpled riveted joints. The margins given in Column 9 are all above the minimum of 15 per cent, thus indicating that the allowables for dimpled joints can take care of considerably greater discrepancies between computed and actual loads per rivet than

TABLE 5
Characteristics of Dimpled Riveted Joints

1	2	3	4	5	6	7	8	9
Spec. No.	Rivet dia., in.	Sheet thick., in.	Load at 4% set, lbs.	1.5 × col. 4, lbs.	Load at failure, lbs.	Col. 6 / 1.15	Allowable load from ref. 3, lbs.	Col. 6 / Col. 8
1	$^{1}/_{8}$	0.025	338	507	455	396	315	1.45
2	$^{1}/_{8}$	0.032	371	557	441	384	380	1.16
3	$^{1}/_{8}$	0.040	390	585	510	443	420	1.21
4	$^{5}/_{32}$	0.040	613	920	732	636	560	1.31
5	$^{5}/_{32}$	0.051	603	905	770	670	640	1.20
6	$^{5}/_{32}$	0.032	565	848	633	550	500	1.27
7	$^{5}/_{32}$	0.064	695	1,040	855	745	675	1.27
8	$^{3}/_{16}$	0.051	900	1,350	1,070	930	890	1.20
9	$^{3}/_{16}$	0.064	1,000	1,500	1,209	1,050	1,040	1.16

NOTES: (1) Sheet is Alclad 24S-T in equal gauges for each joint. (2) $^{1}/_{8}$- and $^{5}/_{32}$-in. rivets are A17S-T; $^{3}/_{16}$ rivets are 17S-T. Rivet head angle is 115°. (3) Values for joints 2, 4, 5, 6 are averages of at least five specimens. Values for other joints are averages of two specimens.

TABLE 6

Characteristics of Dimpled-Machine-Countersunk Riveted Joints

1 Spec. No	2 Rivet dia., in.	3 Sheet thick., in.	4 Load at 4% set, lbs.	5 1.5 × col. 4, lbs.	6 Load at failure, lbs.	7 Col. 6 / 1.15	8 Allowable from ref. 3	9 Col. 6 / Col. 8
1	5/32	0.040–0.040	400	600	675	586	560	1.07*
2	5/32	0.040–0.064	630	945	792	689	560	1.41
3	5/32	0.040–0.125	650	975	810	704	560	1.44
4	5/32	0.051–0.064	640	960	812	705	640	1.27
5	5/32	0.051–0.125	630	945	925	804	640	1.45
6	5/32	0.051–0.250	665	997	875	760	640	1.37
7	5/32	0.064–0.064	575	862	750	650	675	1.11
8	5/32	0.064–0.125	650	975	920	842	675	1.36
9	5/32	0.064–0.250	715	1,070	920	842	675	1.36
10	3/16	0.051–0.125	910	1,365	1,215	1,055	890	1.37
11	3/16	0.051–0.250	870	1,300	1,140	992	890	1.28
12	3/16	0.064–0.064	780	1,170	1,100	957	1,040	1.06
13	3/16	0.064–0.125	1,000	1,500	1,350	1,175	1,040	1.30
14	3/16	0.064–0.250	900	1,350	1,350	1,175	1,040	1.30

* Column 5 value used.

NOTES: (1) All sheet 0.064 and lighter is Alclad 24S-T. (2) 5/32 rivets are A17S-T; 3/16 rivets are 17S-T with head angle of 115°. (3) First sheet listed for joint is dimpled; second sheet is countersunk. (4) Allowables given are for dimpled joints of the lighter gauge of Column 3. (5) Values given are averages of two or three specimens.

TABLE 7

Characteristics of Machine-Countersunk Riveted Joints

1 Spec. No.	2 Rivet dia., in.	3 Sheet thick., in.	4 Load at 4% set, lbs.	5 1.5 × col. 4, lbs.	6 Load at failure, lbs.	7 Col. 5 / 1.15	8 Col. 6 / 1.15	9 Allowable from ref. 3	10 Col. 5 or 6 / Col. 9
1	1/8	0.051–0.051	279	418	420	365	365	261	1.60
2	5/32	0.032–0.032	169	254	390	221	339	230	1.11
3	5/32	0.051–0.051	350	525	480	456	417	367	1.31
4	5/32	0.051–0.125	370	555	590	482	512	367	1.61
5	5/32	0.064–0.064	481	722	597	628	519	460	1.30
6	5/32	0.081–0.081	531	797	617	693	537	518	1.19
7	3/16	0.051–0.051	420	630	640	548	556	452	1.39
8	3/16	0.051–0.125	465	697	720	607	626	452	1.55

NOTES: (1) All sheet 0.081 and lighter is Alclad 24S-T. (2) 1/8 and 5/32 rivets are A17S-T; 3/16 rivets are 17S-T, with head angle of 115°. (3) First sheet listed for joint is countersunk. (4) The lower values of Columns 5 and 6 are used to obtain the margins in Column 10. (5) Values given are averages of two or three specimens.

can the protruding-head rivet joint allowables. Omitting Specimen 1, the scatter of the Column 9 values is not appreciable. This fact might be suspected, since the allowables[3] are based on tests of riveted joints.

From Table 6 the following significant points are indicated:

(a) The strength of a joint having one sheet dimpled and a heavier sheet machine-countersunk is at least as great as that of a dimpled joint having sheets of the the same gauge as the dimpled sheet of the first joint. Thus, the values in reference 3 for dimpled joints should be applicable to the dimpled-machine-countersunk joints of unequal gauge. If the gauges are equal, the strength values are not appreciably less than reference 3 values.

(b) With the exception of Specimen 1, the strength at yield load is at least two-thirds the failing strength, which means that the latter controls the value of the allowable strength the same as it does in the case of joints in which both sheets are dimpled.

(c) From the standpoints of failing strength and of strength based on a 4 per cent set, joints of dimpled sheets are superior to joints of identical gauges with one sheet dimpled and the other machine-countersunk.

The two significant points of Table 7 are the increase in the allowable and in the ratio of yield to ultimate load, with the diminution in the ratio of countersink depth to sheet thickness. These follow naturally from the behavior of a lap machine-countersunk joint under load, as already described. In joint 2, where the countersink extends into the second sheet (head depth for 5/32-in. rivet is 0.045), the failing strength and yield load are particularly low.

According to the results for Specimens 4 and 8, machine-countersunk joint allowable strengths for equal gauge combinations appear applicable to unequal gauge combinations.

In considering the above comments, it must be remembered that the number of specimens tested is hardly sufficient to determine reasonably accurate

averages, that the technique of dimpling is an important parameter insofar as joint strength is concerned, that the flushness of the head of a machine-countersunk joint is also an important parameter, and that expanded rivet shank dimeters may vary considerably with consequent effect on strength.

Riveted Joints—Summary

Joint Deflection

As may be concluded from the two previous sections, the establishment of rational criteria for riveted joint bearing strengths which would be universally applicable does not appear possible. There are three parameters that may be used: overall deflection, set, and failing strength. Fixed joint deflection bears no relation to the yield parameter used for basic stresses, such as tension, but it has some significance in that it limits the loss in rigidity which a joint causes in a structure. The loss in rigidity caused by machine-countersunk joints joining a section of wing skin to front and rear spar caps may be equivalent to a large percentage of the loss caused by dropping to the next lower skin gauge.

Joint deflection characteristics may play an important part in wing skin chordwise splices. If the joint is relatively flexible, the effectiveness of the skin in carrying tension loads may be appreciably reduced. If the joint rigidity were zero, to take an extreme case, all the skin tension load would be transferred at the joint to continuous spars and stringers. More rivets than are required from a strength consideration alone may thus be desirable.

The amount of total elongation that should be allowed is a function of the loss in rigidity that will be accepted, and no reasonable criterion can be set. When skin gauges are selected on the basis of flutter considerations, it is believed highly desirable to consider joint rigidity, even though the allowable strength of the joint is an independent item.

Joint Permanent Set

Set, as a parameter, is related to yield and controls the maximum permissible permanent distortion in the joint at limit load. However, the value of set to use for design is a matter of opinion. In the case of dimpled, protruding-head, and most dimpled-machine-countersunk joints, the failing strength appears to be lower than allowable loads, based on the 4 per cent permanent set rule, and, therefore, the set value, unless it is reduced, would appear to be only an academic consideration for these joints.

The set criteria, however, will often establish the allowable loads for machine-countersunk joints. The considerably lower failing strength of a thin-sheet-gauge machine-countersunk joint, as compared to a dimpled joint, should discourage its use in highly loaded sections; the lower value corresponding to a 4 per cent set should be a further deterrent.

The objection to a significant value of permanent set at limit load, already given for bolted joints, applies also to riveted joints. The shortcoming of the failing strength criterion is that it does not recognize this set, which may be highly undesirable in a machine-countersunk joint. The use of a materials factor of 1.15 appreciably reduces below 4 per cent the amount of set that may be obtained at limit load, an advantage that may not exist for bolted joints. A check of the load-deflection curves of the various machine-countersunk joints made at Republic Aviation Corporation, on the basis of the allowable loads of reference 3, reveals an insignificant amount of set for limit load. However, this is not a general rule and the likely amount of set for important joints should still be checked.

Comparison of Criteria

The criteria in effect for flush joints appear more satisfactory than those for protruding-head joints. A definite minimum materials factor of safety is established for the first case; whereas, in the second, the factor will vary considerably and may approach zero. Also, the bearing strength values for the protruding head joints appear to have little relationship to the actual joints. However, regardless of the criteria used, if the significance of the allowable strengths is appreciated, appropriate margins may be provided in accordance with the type of joint under consideration.

Although there is no provision for reducing bearing strengths of riveted joints, it should be cautioned that reduced values will be found desirable in locations subjected to severe vibratory loads. This factor has already been discussed for the case of bolted joints.

Conclusion

This paper was prepared to describe the physical significance of bearing pressure rather than to set design values.

Specific values must, obviously, be established for stress analysis purposes. However, it is hoped that the material of this paper will permit more judicious use of these values.

References

[1] Army-Navy-Civil Committee on Aircraft Design Criteria, ANC-5, *Strength of Aircraft Elements*, pp. 4-4, 4-6–4-10, 4-25, 5-4–5-13, 5-19. U.S. Government Printing Office, Washington, D.C., 1938.

[2] ANC-5, *Strength of Aircraft Elements*, pp. 4-5, 4-7, 4-10–4-12, 4-38, 5-4–5-14, 5-20, October, 1940.

[3] ANC-5, *Strength of Aircraft Elements*, pp. 4-4, 4-5, 4-8, 4-10–4-16, 4-43, 5-4–5-17, 5-26–5-29, December, 1942.

[4] ANC Bulletin, *Strength of Aircraft Elements*, pp. 4-4, 4-5, 4-12–4-15, 5-4–5-18B, 5-27, 6-6–6-10, Amendment 1 (to December, 1942, Edition), October, 1943.

[5] Frocht, M. M., *Photoelasticity*, p. 320; John Wiley & Sons, New York, 1941.

[6] Coker, E. G., and Filon, L. N. G., *A Treatise on Photoelasticity*, p. 356; Cambridge University Press, London, 1931.

[7] Frocht, M. M., and Hill, H. N., *Stress Concentrations Around a Circular Hole in a Plate Loaded Through a Pin in the Hole*, Journal of Applied Mechanics, pp. A-5–A-9, March, 1940.

[8] Brown, C. G., and Carpenter, S. R., *Tests on Aluminum Alloy Sheet to Determine Allowable Bearing Values;* Army Air Forces Information Circular No. 691, U.S. Government Printing Office, Washington, D.C., July, 1934.

[9] Timoshenko, S., *Theory of Elasticity*, p. 120; McGraw-Hill Book Company, New York, 1934.

[10] Epstein, A., *Investigation of Bearing Strength of Aluminum Alloy Sheet;* Army Air Forces Matériel Command Memorandum Report Serial No. STR-51-174, March, 1939.

[11] Niles, A. S., *Airplane Design*, p. 127; A.A.F. Matériel Command publication, 1926 (available supply has long been exhausted).

[12] Wilkie, J., and Goertzel, G., *Bearing Test—X4130 Steel;* Republic Aviation Corporation Engineering Research Test Report No. 230.

[13] Miller, R. A., *The Bearing Strength of Steel and Aluminum Alloy Sheet in Riveted or Bolted Joints*, Journal of the Aeronautical Sciences, pp. 22–24, November, 1937.

[14] Warner, D. M., *Investigation of A17S-T Rivets;* A.A.F. Matériel Command Memorandum Report Serial No. M56-2747, January, 1935.

[15] Fuller, F. B., *Bearing Tests on Heat-Treated Aluminum Alloy Rivets;* A.A.F. Matériel Command Memorandum Report Serial No. M56-3085, July, 1937.

[16] Yasines, S. F., *Investigation of Strength of Pin-Socket Joints;* Republic Aviation Corporation Engineering Research Report No. 238.

[17] Brueggeman, W. C., *Mechanical Properties of Aluminum Alloy Rivets*, N.A.C.A. T.N. No. 585, November, 1936.

[18] Epstein, A., *Strength of Riveted Joints;* A.A.F. Matériel Command Memorandum Report Serial No. Exp. M-51/M601, February, 1940.

(*Continued from page 30*)

range, the problem of pure bending in the plastic range can be solved rigorously by the introduction of a generalized stress and a reduced or transformed cross section in terms of which the problem reduces to the linear type.

At present, no test results are available to the author so that no comparison between theory and experiment could be made. The theoretical calculations seem to give reasonable results. Should this theory be verified by experimental results, it would mean that the hypothesis of least work in the plastic range is justified, a result that would be far reaching. Finally, the theory should prove to be of interest if for no other reason than the mathematical elegance of the results and their physical interpretation.

Acknowledgment

Acknowledgment is made to Mr. Abner Rasumoff of the Stress Department for his assistance in the numerical work.

References

[1] *ANC-5*, Revised Edition, December, 1942.

[2] Wilson, E. B., *Advanced Calculus;* Ginn & Company, Boston, 1912.

Lag Determination of Altimeter Systems

RICHARD M. HEAD*

Lockheed Aircraft Corporation

Introduction

A knowledge of the true altitude of an airplane in flight is essential before the true speed can be determined; hence, in any maneuver in which the rate of change of pressure is appreciable, the lag of the altimeter must be known in order to correct the indicated reading of the altimeter.

The altimeter system is composed of two separate coupled systems, acoustical and mechanical. The acoustical system is made up of tubing, additional volumes, and, occasionally, restrictions to damp out vibrations. Because of the presence of these elements, any pressure change out at the static holes will be delayed in reaching the altimeter. The altimeter itself comprises the mechanical system. Because of the inertia of the moving parts, viscous and Coulomb damping, a further delay results. The combined lag of these two systems becomes appreciable for high rates of change of pressure, such as experienced in a dive, and, hence, must be corrected for in order to obtain the true altitude.

The existing methods for correcting for this lag involve only the acoustical system, that of the instrument being considered negligible. This assumption undoubtedly holds for small rates of change of pressure; however, for high rates, this quantity can no longer be neglected. It is the purpose of this paper to consider the total lag of altimeter systems and to present curves that will permit a direct and simple determination of the correction term.

Notation

m = mass coefficient (lbs. per ft. per sec.^{2})
c = damping coefficient (lbs. per ft. per sec.)
k = spring coefficient (lbs. per ft.)
F = maximum Coulomb friction force (lbs.) (occurring while there is motion)
ζ = damping ratio, or the ratio of the actual damping coefficient to the critical damping coefficient
τ = characteristic time, or the time to drop from the initial point to $1/e$ times that value when a step function is applied (sec.)
α = peak number
P_{cm} = F/k (ft. of altitude)
t = time (sec.)
p = pressure altitude as indicated on the altimeter (ft.)
$p_1(t)$ = indicated pressure altitude at the back of the altimeter or the altimeter reading if there were no lag in instrument itself (ft.)
$p_2(t)$ = pressure altitude at the static head or the true altitude (ft.)
ω_n = $\sqrt{k/m}$ = undamped natural circular frequency (rad. per sec.)
ω = $\sqrt{1-\zeta^2}\omega_n$ = natural circular frequency (rad. per sec.)
δ = $2\pi\zeta/\sqrt{1-\zeta^2} \cong 2\pi\zeta$ (for ζ small) = logarithmic decrement
D = Coulomb friction term or the constant difference between the double amplitude curve for pure viscous damping and that of the experimental curve when plotted semilogarithmically (ft.)
K = $e^{-\zeta\omega_n\pi/\omega}$
b = $e^{-\pi/\omega\tau}$

Statement of the Problem

Photographic data on the altimeter are obtained in flight, and the problem is to obtain the actual pressure altitude from the indicated at any instant. In order to realize a solution, certain characteristics of the particular system in question must be determined. As will be brought out in subsequent sections, these characteristics consist of the characteristic time of the system—or the time required for the instrument to drop from its initially applied pressure to $1/e$ times that value when a step function is applied out at the static holes; the ratio of the actual damping coefficient to the critical damping coefficient, ζ, for the instrument alone; the natural frequency of the system when a step function is applied, ω_n; and the Coulomb friction term, P_{cm}, of the particular altimeter involved. All four of these characteristics are necessary for an accurate determination of the lag in the altimeter during a particular maneuver; however, the last three are practically negligible for small rates of change of pressure but become more appreciable as the rate of change becomes greater.

Methods for determining these quantities and for developing curves that will give the lag directly are presented and may be applied to any altimeter system.

Step Function Response of an Altimeter

A step function is the easiest type of function to analyze as well as to perform experimentally; consequently, it is the response of the altimeter to this kind of forcing function that will first be considered. The following analysis is similar to that of Kennedy.[1]

Presented at the Summer Annual Meeting, I.A.S., Los Angeles, July 27–28, 1944.

* Research Engineer, Flight Test Group.

The equation of motion of an altimeter when a step function is applied to it is

$$mp + c\dot{p} + kp = \pm F$$

where p equals the reading of the altimeter in feet and F equals Coulomb friction force; or

$$\ddot{p} + (c/m)\dot{p} + (k/m)p = \pm (k/m)(F/k)$$

Since F/k equals distance the constant Coulomb friction force could stretch the spring of stiffness k equals P_{cm},

$$\zeta = \frac{c}{2\sqrt{km}};\ \omega_n = \sqrt{\frac{k}{m}};\ \omega = \sqrt{1-\zeta^2}\,\omega_n$$

then

$$\ddot{p} + 2\zeta\omega_n\dot{p} + \omega_n{}^2 p = \pm\omega_n{}^2 P_{cm} \qquad (1)$$

The complementary equation is

$$\ddot{p} + 2\zeta\omega_n p + \omega_n{}^2 p = 0$$

having the general solution

$$p = C_1 e^{\lambda_1 t} + C_2 e^{\lambda_2 t}$$

where

$$\lambda_1 = -\zeta\omega_n + \sqrt{\zeta^2\omega_n{}^2 - \omega_n{}^2} = -\zeta\omega_n + i\omega$$
$$\lambda_2 = -\zeta\omega_n - \sqrt{\zeta^2\omega_n{}^2 - \omega_n{}^2} = -\zeta\omega_n - i\omega$$
$$p = C_1 e^{(-\zeta\omega_n + i\omega)t} + C_2 e^{(-\zeta\omega_n - i\omega)t}$$

or

$$p = Ae^{-\zeta\omega_n t}\cos(\omega t - \varphi)$$

For the particular solution, assume an equation of the form

$$p = \alpha$$
$$\dot{p} = 0$$
$$\ddot{p} = 0$$

therefore, $\alpha = \pm P_{cm}$ is the particular solution, and the complete solution is

$$p = Ae^{-\zeta\omega_n t}\cos(\omega t - \varphi) \pm P_{cm} \qquad (2)$$

Solving for the peak values of this damped oscillatory motion by means of difference equations:

$$p_0 = A\cos(-\varphi) + P_{cm}\ (\text{at } t = 0, p = p_0)$$
$$p_1 = -AK\cos(-\varphi) + P_{cm}$$
$$= -BK - P_{cm} \quad \text{for } K = e^{-\zeta\omega_n\pi/\omega}$$
$$p_2 = BK^2 - P_{cm}$$
$$\vdots$$
$$p_{\alpha+1} = -K[P_\alpha - (-1)^\alpha P_{cm}] + (-1)^\alpha P_{cm}$$
$$p_{\alpha+1} + Kp_\alpha = (-1)^\alpha(K+1)P_{cm}$$

where α = peak number. Solving the complementary equation

$$p_{\alpha+1} + Kp_\alpha = 0$$

we have

$$p_\alpha = A'(-K)^\alpha$$

For the particular solution, assume $p_\alpha = -(-1)^\alpha D$; then

$$(-1)^\alpha(1-K)D = (-1)^\alpha(1+K)P_{cm}$$
$$D = [(1+K)/(1-K)]P_{cm}$$

therefore

$$p_\alpha = A'(-K)^\alpha - (-1)^\alpha D$$

at $\alpha = 0$, $p = p_0$; therefore, $p_0 = A' - D$, $A' = p_0 + D$, and

$$p_\alpha = (p_0 + D)(-K)^\alpha - (-1)^\alpha D \qquad (3)$$

The experimental step function response of an altimeter alone is shown in Fig. 1. When the double am-

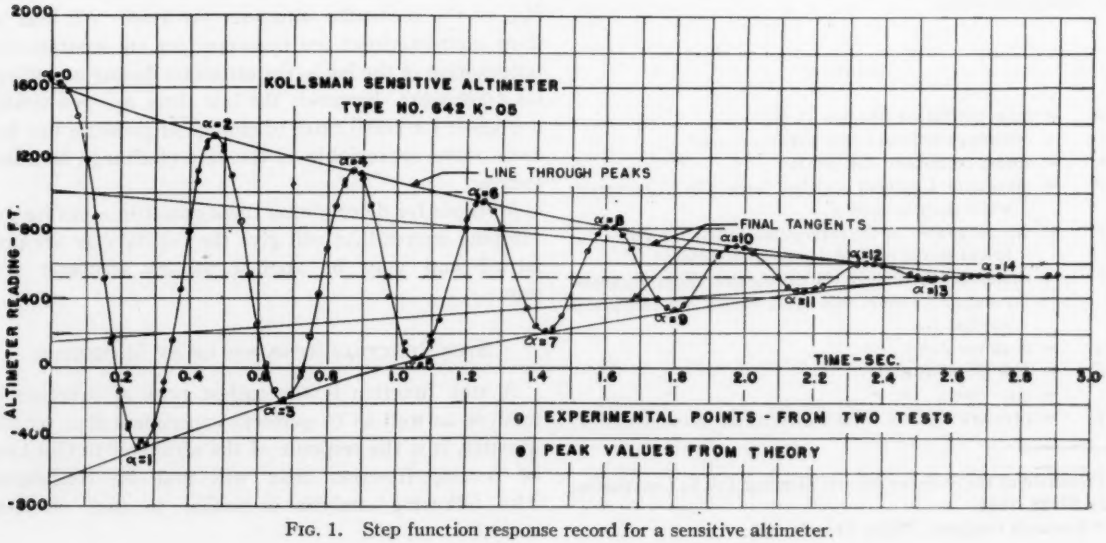

FIG. 1. Step function response record for a sensitive altimeter.

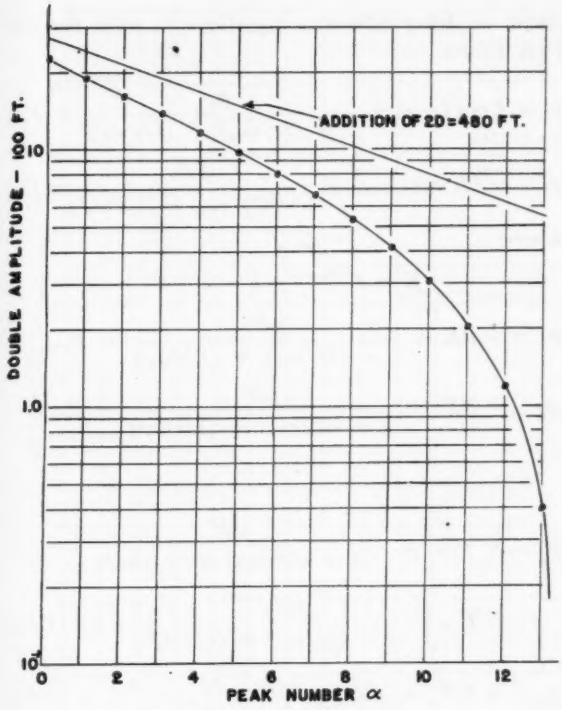

FIG. 2. Semilog plot of Fig. 1.

plitude is plotted against the peak number on semilogarithmic paper (Fig. 2), it is found that both viscous damping and Coulomb friction are present. Coulomb friction is constant and independent of velocity while there is motion, the double amplitude decreasing constantly at the rate of $8P_{cm}$ per cycle. However, if the double amplitude is plotted against the peak number, it curves downward, approaching a vertical asymptote at the peak number where the double amplitude is zero. In pure viscous damping proportional to velocity, the double amplitude versus α is a pure exponential curve giving a straight line on semilog paper; hence, it can be separated from Coulomb friction in the present analysis by finding the amount $2D$, by trial and error, which must be added to the curve to obtain a straight line. From Fig. 2, it is seen that $2D = 480$ ft. Using this curve in conjunction with Fig. 3, the damping ratio, ζ, is found to be 0.0395. Using $\zeta = 0.0395$ and $\alpha = 1$ in the latter curve gives $e^{-\delta/2} = 0.881$, where δ = logarithmic decrement.

$$P_{cm} = [(1 - e^{-\delta/2})/(1 + e^{-\delta/2})]D$$

then $P_{cm} = [(1 - 0.881)/1.881](240) = 15.18$ ft.

Because of the fact that the Coulomb friction becomes predominant as the velocity approaches zero, the slope of the line through the peaks approaches the value it would have if only Coulomb friction were present. Therefore, by drawing the final tangents in Fig. 1 and finding that the double amplitude decreases from 863 ft. to zero in 14 semicycles or at the rate of

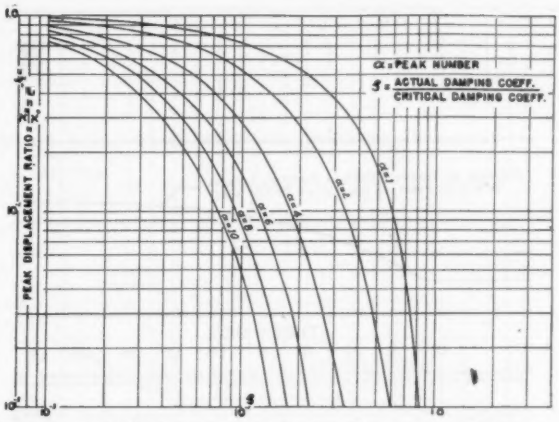

FIG. 3. Peak displacement ratios of oscillatory transients as a function of damping ratio.[1]

$863(2/14) = 123.3$ ft. per cycle, P_{cm}, is found to be $123.3/8 = 15.40$ ft., since the double amplitude for pure Coulomb friction decreases constantly at the rate of $8P_{cm}$ per cycle. The difference between these two values is slightly greater than 1 per cent, but the uncertainty in the drawing of the final tangents precludes any greater accuracy.

Using the values for ζ and P_{cm} determined in Eq. (3), the different peak values are directly obtainable, and the correlation between these theoretical values and the experimental ones is shown on Fig. 1. These values are close enough to justify extending the theoretic analysis to the complete altimeter system.

Two electrical pressure indicating units, consisting of a metallic bellows linked to a thin Dural beam on which are cemented electrical strain gages (Fig. 4), are installed in the system of a test airplane with a nose pitot—one replacing the altimeter and the other connected to the static head. The natural frequency of these units is 100 cycles per sec. From the oscillograph record of these units when a step function is applied at the static holes, it is seen that the pressure at the altimeter follows closely an exponential, while the

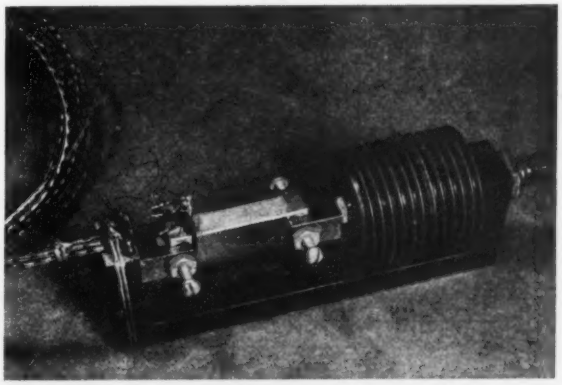

FIG. 4. Oscillograph pressure recording unit.

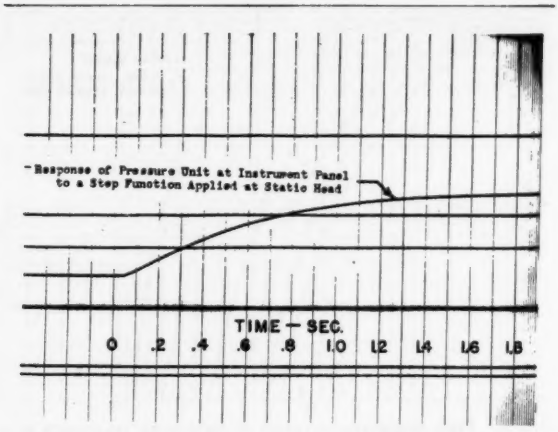

FIG. 5. Oscillograph record of response of oscillograph pressure unit installed at altimeter to step function applied at static head.

pressure at the static head is actually a step function (Figs. 5 and 6).

Hence, proceeding to the theoretic analysis with an exponential forcing function applied to the altimeter alone, the equation of motion is

$$\ddot{p} + 2\zeta\omega_n\dot{p} + \omega_n^2 p = \pm\omega_n^2 P_{cm} + \omega_n^2 p_0 e^{-t/\tau} \quad (4)$$

The complementary and first particular solutions are identical to the case of an applied step function. The second solution may be obtained as follows:

Assume an equation for p of the form $p = a + be^{-t/\tau}$

$$\dot{p} = -(b/\tau)e^{-t/\tau}$$
$$\ddot{p} = (b/\tau^2)e^{-t/\tau}$$

$$\left(\frac{b}{\tau^2}\right)e^{-t/\tau} - \left(\frac{b}{\tau}\right)e^{-t/\tau}2\zeta\omega_n + \omega_n^2(a + be^{-t/\tau}) = \omega_n^2 p_0 e^{-t/\tau}$$

Therefore $a = 0$ and

$$b = p_0/[1 - (2\zeta/\tau\omega_n) + (1/\tau^2\omega_n^2)]$$

Therefore, the complete solution of the equation of motion of an altimeter with an exponential forcing function applied is

$$p = Ae^{-\zeta\omega_n t}\cos(\omega t - \varphi) + \frac{p_0 e^{-t/\tau}}{1 - (2\zeta/\tau\omega_n) + (1/\tau^2\omega_n^2)} \pm P_{cm} \quad (5)$$

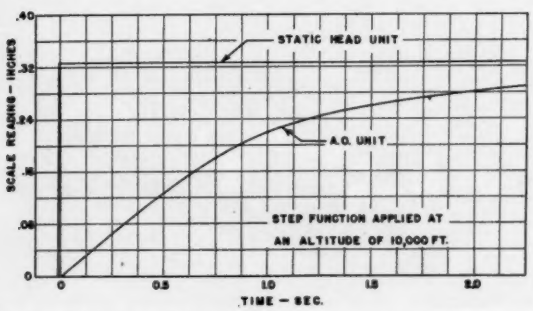

FIG. 6. Response of two oscillograph pressure units to step function applied at static head.

Again applying difference equations to solve for the peak values:

$$p_0 = A\cos(-\varphi) + \frac{p_0}{1 - (2\zeta/\tau\omega_n) + (1/\tau^2\omega_n^2)} + P_{cm}$$

$$p_1 = -AK\cos(-\varphi) + \frac{p_0 b}{1 - (2\zeta/\tau\omega_n) + (1/\tau^2\omega_n^2)} + P_{cm}$$

where

$$K = e^{-\zeta\omega_n\pi/\omega}; \quad b = e^{-\pi/\omega\tau}$$

$$p_1 = -BK + \frac{p_0 b}{1 - (2\zeta/\tau\omega_n) + (1/\tau^2\omega_n^2)} - P_{cm}$$

$$p_2 = BK^2 + \frac{p_0 b^2}{1 - (2\zeta/\tau\omega_n) + (1/\tau^2\omega_n^2)} - P_{cm}$$

$$p_{\alpha+1} = -K\left[p_\alpha - \frac{p_0 b^\alpha}{1 - (2\zeta/\tau\omega_n) + (1/\tau^2\omega_n^2)} - (-1)^\alpha P_{cm}\right] + \frac{p_0 b^{\alpha+1}}{1 - (2\zeta/\tau\omega_n) + (1/\tau^2\omega_n^2)} + (-1)^\alpha P_{cm}$$

$$p_{\alpha+1} + Kp_\alpha = \frac{p_0}{1 - (2\zeta/\tau\omega_n) + (1/\tau^2\omega_n^2)}(K + b)b^\alpha + (1 + K)(-1)^\alpha P_{cm}$$

Solving the complementary equation:

$$p_{\alpha+1} + Kp_\alpha = 0$$

gives

$$p_\alpha = A'(-K)^\alpha$$

For the first particular solution assume

$$p_\alpha = -(-1)^\alpha D$$
$$(-1)^\alpha(1 - K)D = (-1)^\alpha(1 + K)P_{cm}$$
$$D = [(1 + K)/(1 - K)]P_{cm}$$

For the second particular solution assume

$$p_\alpha = B'b^\alpha$$

$$B'(b + K)b^\alpha = \frac{p_0}{1 - (2\zeta/\tau\omega_n) + (1/\tau^2\omega_n^2)}(K + b)b^\alpha$$

Therefore

$$B' = p_0/[1 - (2\zeta/\tau\omega_n) + (1/\tau^2\omega_n^2)]$$

then

$$p_\alpha = A'(-K)^\alpha + \frac{p_0 b^\alpha}{1 - (2\zeta/\tau\omega_n) + (1/\tau^2\omega_n^2)} - (-1)^\alpha D$$

Therefore

$$p_0 = A' + \frac{p_0}{1 - (2\zeta/\tau\omega_n) + (1/\tau^2\omega_n^2)} - D$$

(at $\alpha = 0$, $p = p_0$)

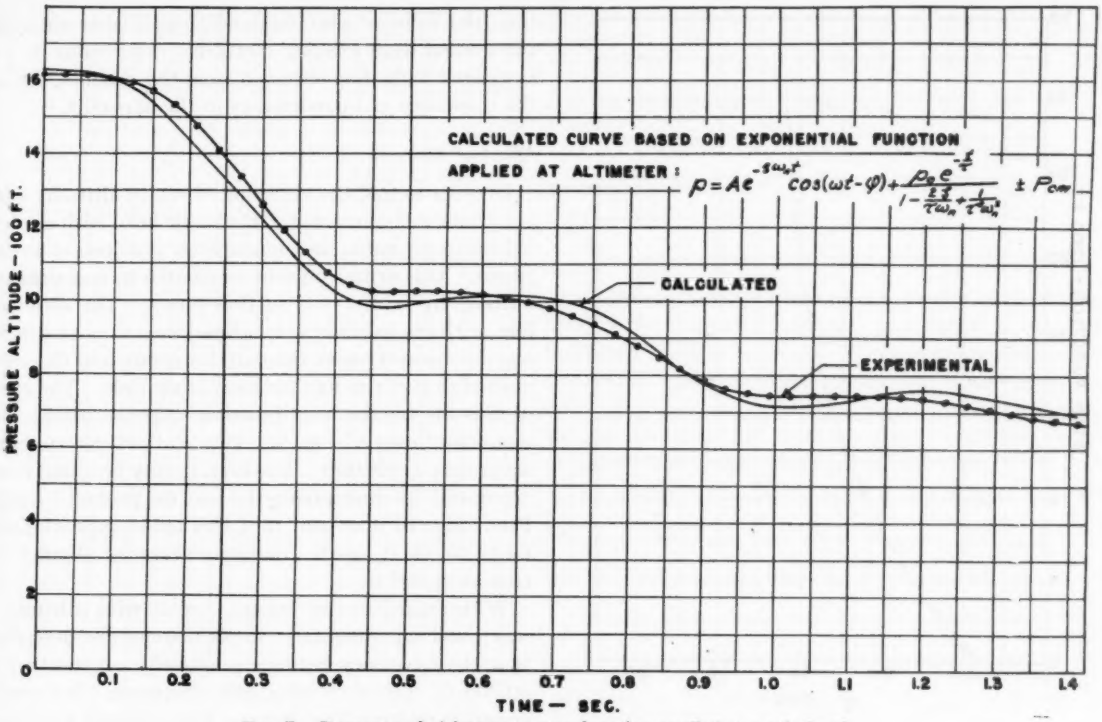

FIG. 7. Response of altimeter to step function applied at static head.

$$A' = p_0\left(1 - \frac{1}{1 - (2\zeta/\tau\omega_n) + (1/\tau^2\omega_n^2)}\right) + D$$

and

$$p_\alpha = p_0\left(1 - \frac{1}{1 - (2\zeta/\tau\omega_n) + (1/\tau^2\omega_n^2)}\right)(-K)^\alpha + \frac{p_0 b^\alpha}{1 - (2\zeta/\tau\omega_n) + (1/\tau^2\omega_n^2)} + (-1)^\alpha D(K^\alpha - 1) \quad (6)$$

This equation may be used to obtain the peak values. However, it is more desirable in this case to see how closely the solution follows the experimental data through its complete transient state; hence, in comparing the two in the following sections, the complete curve as obtained from Eq. (5) will be used instead of Eq. (6).

Experimental Response

The experimental response of a sensitive altimeter in the automatic observer panel of the test airplane when a step function is applied at the pitot static head is shown in Fig. 7. From the previously obtained data on the altimeter alone, together with the values of the characteristic time, τ, and natural frequency, ω_n, obtained from Fig. 7, Eq. (5) can be solved completely for the same value of the step function if the boundary conditions are applied. This calculated response curve is also shown in Fig. 7, the discrepancy between the two being due to the fact that a constant mean frequency was used in the calculated curve; whereas, experimentally, it is not a constant. This experimental variation in frequency also affects the amplitude of the oscillations, as can easily be seen from an examination of Eq. (5). However, even with the amplitude and frequency differing from this cause, the maximum deviation is only about 40 in 1,000 or about 4 per cent, but it may be considerably diminished by expressing the natural frequency as a function of the time (obtainable from the experimental curve) in Eq. (5).

Because of the fact that all maneuvers in which altimeter lag becomes noticeable cover quite a range of altitudes, the effect of altitude on the various quantities in Eq. (5) must be considered. Since the characteristics of the altimeter are constants, independent of altitude, the only quantities that need be considered are τ and ω_n.

τ, the characteristic time, is defined as being the time required for the altimeter to drop from its initial value to $1/e$ times that value. However, since the resistance of the tubing through which the air is flowing varies with the rate of flow, τ will vary with the step function applied, since it is equal to RC, the product of the resistance and the capacitance of the system. This is further borne out by Fig. 8, where τ is determined experimentally for different values of step function. The rate of change of pressure when a step function is applied is much greater than occurs during even the fastest dives; hence, if a curve of τ versus step function is plotted as in Fig. 8 and extrapolated to zero step func-

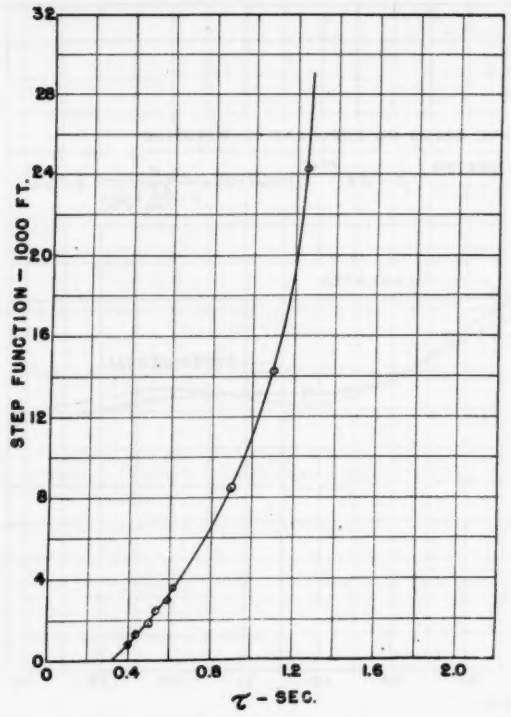

FIG. 8. Effect of magnitude of step function on characteristic time.

tion, the value of τ so obtained gives a truer value for the system than existing methods. This value of τ is compared with that obtained from the product, RC, of the resistance and capacitance in the appendix.

Effect of Altitude

In order to find the variation of τ with altitude, a 50-gal. drum was connected to the static head with a solenoid-operated valve and manometer connection in between. This drum could be evacuated to any pressure altitude by means of a suction pump. The altimeter line, with the solenoid valve closed, was then evacuated a given amount above the barrel pressure and the valve opened to give the step function at altitude. The effect of altitude on the step function response of the altimeter is shown in Fig. 9. This method determines τ accurately at altitude; however, it may be found fairly accurately by multiplying the τ at the ground by p/p_0. From Fig. 10 it is seen that this holds approximately up to 25,000 ft., with a maximum error of about 5 per cent at 12,000 ft.

With regard to the variation of ω_n with altitude, it was found experimentally, in the manner just described, that the frequency remains practically constant up to 20,000 ft. and then gradually decreases. No simple equation relating this decrease with altitude was found because of the many variables involved, with the result that until an equation is developed it will be necessary to determine this variation of frequency experimentally in a manner similar to that described. However, unless

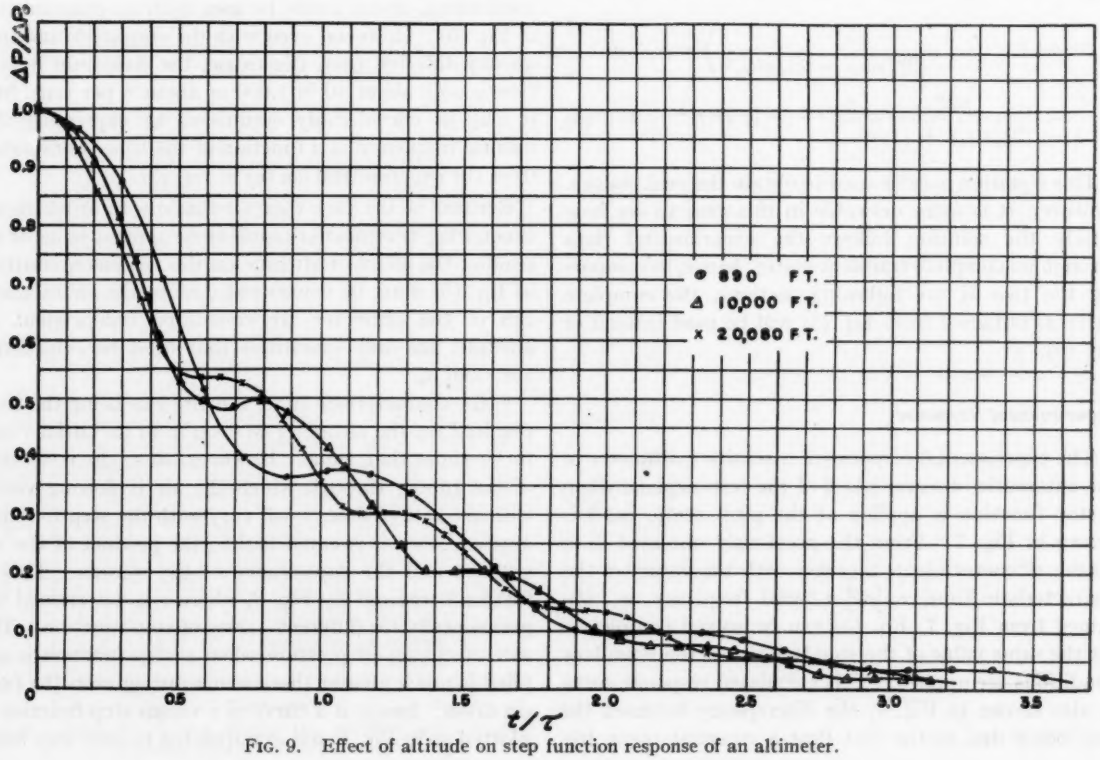

FIG. 9. Effect of altitude on step function response of an altimeter.

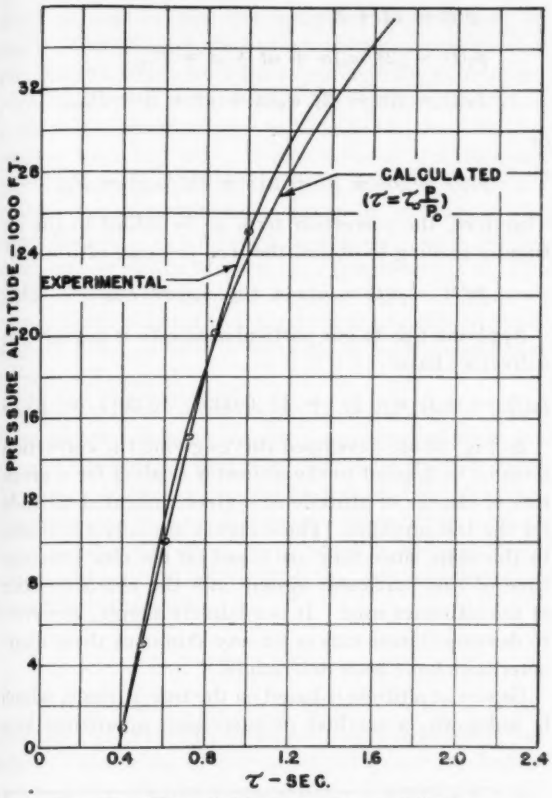

FIG. 10. Effect of altitude on characteristic time.

extreme accuracy is desired, it is sufficient to use the value of ω_n determined at field altitude throughout the altitude range considered.

GENERALIZED SOLUTION APPLIED TO AN AIRPLANE IN FLIGHT

In Eq. (5) $p(t)$ represents the indicated altitude when a step function is applied at the static head. The problem of an airplane in flight, undergoing rapid changes in pressure, is to determine the pressure at the static head corresponding to the altimeter reading at the same instant. Since a step function applied at the head results in an exponential forcing function being applied to the instrument itself, this problem may be solved in two steps: by finding the pressure as a function of time at the back of the instrument from the altimeter reading and, from these values, finding the pressure as a function of time at the static head as follows:

For the pressure at the back of the instrument from altimeter reading:

$$\ddot{p} + 2\zeta\omega_n\dot{p} + \omega_n^2 p = \pm\omega_n^2 P_{cm} + \omega_n^2 p_1(t)$$

where

p = altimeter reading
$p_1(t)$ = pressure at back of altimeter, or indicated pressure if there were no lag in the altimeter itself

Then

$$p_1(t) = (1/\omega_n^2)\ddot{p} + (2\zeta/\omega_n)\dot{p} + p \mp P_{cm} \qquad (7)$$

For the pressure at the static head, from $p_1(t)$

$$p_1(t) + (1/\tau)\dot{P}_1(t) = (1/\tau)p_2(t)$$

where $p_2(t)$ equals actual pressure at the static head; then

$$p_2(t) = \tau p_1(t) + p_1(t) \qquad (8)$$

Thus, this analysis precludes a knowledge of the equation of the indicated pressure as a function of time throughout a dive or climb. Applying this method to a particular case in which a cosine curve closely approximates the dive curve, with a maximum deviation of 1.6 per cent (Fig. 11), we have $p(t) = 8{,}250 \cos \Omega t$ = equation of indicated pressure altitude curve.

The solution for a cosine curve in the general form is:

$$p(t) = A \cos \Omega t$$

$$p_1(t) = -(1/\omega_n^2)A\Omega^2 \cos \Omega t - (2\zeta/\omega_n)A\Omega \sin \Omega t + A \cos \Omega t \mp P_{cm}$$

$$p_2(t) = (\tau/\omega_n^2)A\Omega^3 \sin \Omega t - (2\zeta\tau/\omega_n)A\Omega^2 \cos \Omega t - \tau A\Omega \sin \Omega t - (1/\omega_n^2)A\Omega^2 \cos \Omega t - (2\zeta/\omega_n)A\Omega \sin \Omega t + A \cos \Omega t \mp P_{cm}$$

or

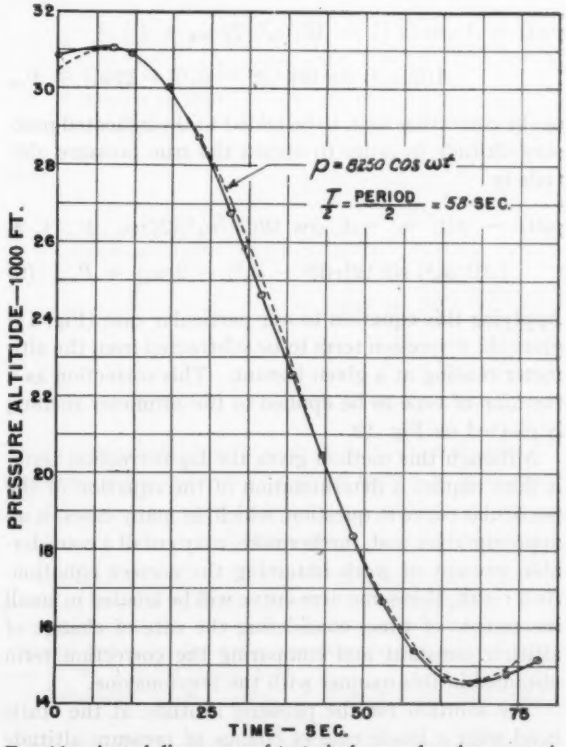

FIG. 11. Actual dive curve of test airplane and cosine approximation.

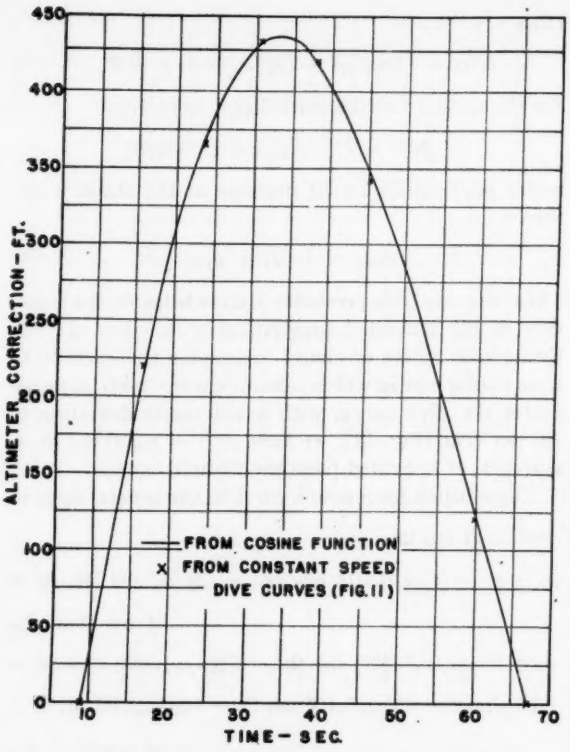

FIG. 12. Correction to be subtracted from altimeter reading to obtain true altitude for particular dive (Fig. 11).

$$p_2(t) = A \cos \Omega t \,[1 - (\Omega^2/\omega_n^2)(2\zeta\tau\omega_n + 1)] + A(\Omega/\omega_n^2) \sin \Omega t[\tau(\Omega^2 - \omega_n^2) - 2\zeta\omega_n] \mp P_{cm}$$

or the correction term to be added to the indicated pressure altitude in order to obtain the true pressure altitude is

$$p_2(t) - p(t) = -A \cos \Omega t(\Omega^2/\omega_n^2)(2\zeta\tau\omega_n + 1) + (A\Omega/\omega_n^2) \sin \Omega t[\tau(\Omega^2 - \omega_n^2) - 2\zeta\omega_n] \mp P_{cm} \quad (9)$$

Applying this equation to our particular case (Fig. 11) gives the correction term to be subtracted from the altimeter reading at a given instant. This correction as a function of time to be applied to the altimeter reading is plotted on Fig. 12.

Although this method gives the lag correction term, it does require a determination of the equation of the particular curve in question, which, in many cases, is an approximation and, furthermore, may entail a considerable amount of work obtaining the correct equation. As a result, this same dive curve will be treated in small increments of time, considering the rate of change of altitude constant and comparing the correction term obtained in this manner with the previous one.

The solution for the pressure altitude at the static head with a linear rate of change of pressure altitude at the altimeter is, in the general case:

$$p(t) = \alpha t + \beta$$

$$p_1(t) = (2\zeta/\omega_n)\alpha + \alpha t + \beta \mp P_{cm}$$

$$p_2(t) = \alpha\tau + (2\zeta/\omega_n)\alpha + \alpha t + \beta \mp P_{cm}$$

or

$$p_2(t) = (\alpha t + \beta) + \alpha[\tau + (2\zeta/\omega_n)] \mp P_{cm}$$

Therefore, the correction term to be added to the altimeter reading to obtain the true pressure altitude is:

$$p_2(t) - p(t) = \alpha[\tau + (2\zeta/\omega_n)] \mp P_{cm} \quad (10)$$

Applying this to our particular case (α is negative in a dive) we have:

$$p_2(t) - p(t) = \alpha \{\tau + [2\,(0.0395)/13.20]\} \mp 15.18$$

In Fig. 13 are developed curves giving the correction term to be applied to the altimeter reading for a given rate of change of altitude at a given indicated altitude for the test airplane. These curves are only applicable to this ship, since they are based on the characteristic time of this particular system and the characteristics of the altimeter used. It is relatively simple, however, to develop similar curves for any ship once these characteristics have been determined.

Since τ at altitude is based on the true altitude, which is unknown, a method of successive approximations

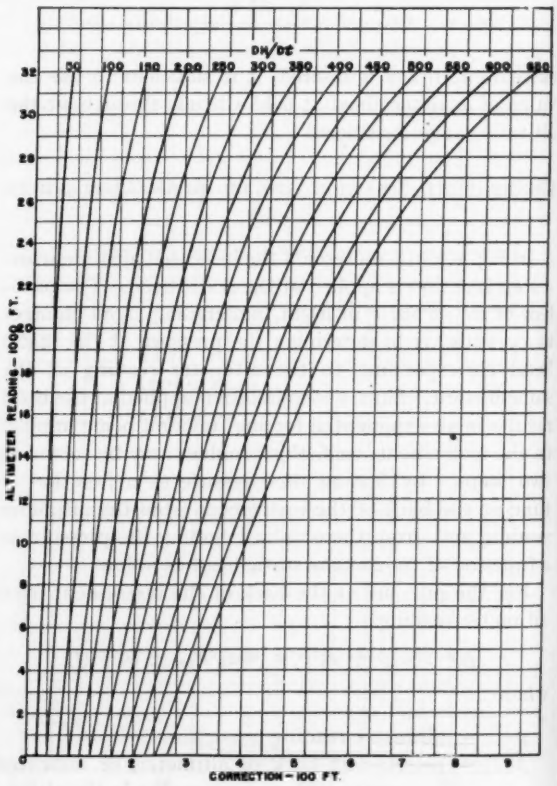

FIG. 13. Correction to be subtracted from altimeter to obtain true altitude for constant-speed dives.

must be used so that the indicated altitude may be used. This is accomplished by taking the value of τ for a given altitude from the experimentally determined curve and, with rate-of-climb as a parameter, determining the correction term to be added to the indicated reading from Eq. (10). A new value of τ is obtained corresponding to this new altitude and the process repeated, two approximations generally sufficing. The correction term as a function of altitude is then plotted with rate of climb or dive as a parameter (Fig. 13). If the airplane is in a climb where α is positive, the correction term is added to the indicated pressure altitude, while if it is in a dive, α being negative, the correction term is subtracted.

Applying these curves to Fig. 11, the correction terms for different points on the curve are obtained from the slope of the curve at that point, and the correction curve for the complete dive is also plotted on Fig. 12. This curve shows that the maximum deviation of this method from the other is about 4 ft., which is more accurate than necessary but shows that this simpler method is perfectly satisfactory.

Conclusions

The treatment of the lag in altimeter systems is not new but has been ably dealt with by Wiedemann[3] and others. However, in practically all cases, the instrument lag is considered negligible. Furthermore, the variation of the characteristic time of the system with the magnitude of the applied step function is apparently not considered. This paper incorporates the instrument lag with that due to the line, since, with the increasingly faster rates of climb and diving speeds of present-day airplanes, this quantity can no longer be neglected. In addition, an attempt is made to arrive at a truer value of τ than that obtained by existing methods.

From the equations presented, a family of curves similar to that of Fig. 13 may be developed for any altimeter system, once the constants of the system have been determined by the simple experimental method outlined. Such a family of curves will enable the easy and accurate determination of the lag at any instant in a climb or dive for the given airplane.

A knowledge of the true altitude will result in a more accurate knowledge of true speed, Mach Number, etc., with the resulting increased accuracy in flight-test data.

Appendix

The value of the characteristic time of the system may be determined by a method other than that described in the main body of the paper—that is, by finding the resistance and capacitance of the system, τ being the product of RC.[2, 3]

The resistance of the altimeter system of the test airplane was determined experimentally in the following manner: An oxygen bottle equipped with a flow regulator valve was connected to a fitting that enclosed the static head. To this fitting was also attached a pressure line leading from one side of a water U-tube. An altimeter case—no parts inside—with a metal face was connected in place of the sensitive altimeter in the automatic observer's compartment. Two air hoses led from this metal face: one to the other side of the U-tube for measuring the pressure differential between the static head and the altimeter, and the other to a 1,000-cu.cm. flask filled with water and inverted in a pail of water. This latter arrangement was used to determine the rate of flow for a given pressure drop. The curve of ΔP versus q (volume rate of flow) was plotted, and the slope for zero pressure drop was taken as the value of R_0. This value was found to be 3.384×10^2Gm./cm.^{4}/sec. when R_0 was multiplied by the ratio of the viscosity of air to that of oxygen. The capacitance was determined from the relation $C = \dfrac{V}{\rho(a')^2}$, where V = volume of the system, ρ = density of air under the atmospheric conditions occurring at the time, and a' = velocity of sound in the tubing of the system. The volume was found by a simple pressure differential process to be 1,235 cu.cm. The value of a' was determined from the equation[4]

$$a' = a\left[1 - \frac{\gamma'}{r\sqrt{2n}} + \left(\frac{\gamma'}{r\sqrt{2n}}\right)^2 - \left(\frac{\gamma'}{r\sqrt{2n}}\right)^3 + \dots\right]$$

where

a = velocity of sound in air
$\gamma' = \sqrt{\mu/\rho_0} + 0.338\sqrt{\nu}$
r = radius of tube
n = frequency

thus

$$C = \frac{1235}{(12.26 \times 10^{-4})(284.05 \times 10^2)^2} =$$

$$1.248 \times 10^{-3}\ \frac{\text{cm.}^4\ \text{sec.}^2}{\text{Gm.}}$$

or

$$\tau = R_0 C = (3.384 \times 10^2)(1.248 \times 10^{-3}) = 0.422 \text{ sec.}$$

This corresponds closely enough to the previously determined value ($\tau_0 = 0.41$ sec.) to form a good check.

References

[1] Kennedy, Charles, *Measuring the Coulomb and Viscous Components of Friction*, Instruments, Vol. 15, October, 1942.

[2] DeJuhasz, K. J., *Graphical Analysis of Delay of Response in Airspeed Indicators*, Journal of the Aeronautical Sciences, (Volume 10, No. 3, p. 91) March, 1943.

[3] Wiedemann, Hans, *Inertia of Dynamic Pressure Arrays*, N.A.C.A. T.M. 998, December, 1941.

[4] Crandall, I. B., *Theory of Vibrating Systems and Sounds*, D. Van Nostrand Co., Inc., New York, 1926.

The Influence of Structural Deformation on Airplane Characteristics

ALEXANDER H. FLAX*

Curtiss-Wright Corporation

Introduction

THE EFFECTS OF ELASTIC DEFORMATION of wings and tail on the air loads imposed upon them has been studied in the past by a number of investigators.[1–4] These previous investigations have been mainly concerned with the occurrence of instability conditions, such as divergence, or loss of control, such as aileron reversal. Much of the previous work has been done on the basis of simplified equivalent two-dimensional wings or on the basis of the semirigid wing, commonly used in British reports on flutter and aero-elastic effects. Also, the effects of induced down-wash have usually been treated in a rough manner or neglected.

It is proposed here to include the effects of induced down-wash and to consider the wing as a three-dimensional structure. The analysis made will treat not only the criteria for divergent instability and other critical conditions but also the aerodynamic characteristics, including spanwise lift distribution, for speeds below divergence.

The subject can best be introduced by consideration of a simplified model, as shown in Fig. 1. This consists of a wing of infinite span deriving its torsional stiffness from two springs of such configuration that the elastic center lies a distance *ec* behind the aerodynamic center.

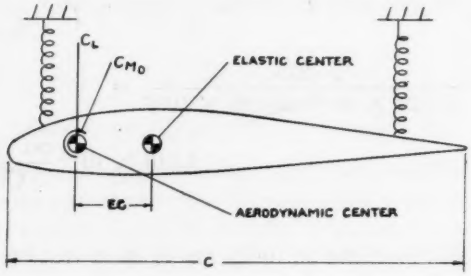

FIG. 1.

Definitions

c = chord

a_0 = $(\partial C_L/\partial\alpha)_\infty$ slope of the lift curve for aspect ratio = ∞

θ_0 = initial angle of attack

θ_1 = angle of attack increment due to twist

q = dynamic pressure $\rho V^2/2$

K = spring stiffness in torsion ft.lbs. per rad. per unit length

Then, writing the equation for equilibrium of the wing,

$$[C_{M_0} + a_0 e(\theta_0 + \theta_1)]qc^2 - K\theta_1 = 0$$

This may be solved for θ_1 to give

$$\theta_1 = (C_M + a_0\theta_0 e)qc^2/(K - a_0 eqc^2) \qquad (1)$$

Divergence occurs when θ_1 approaches ∞ as the denominator of this expression approaches zero. This leads to the q for divergence

$$q_{cr} = K/a_0 ec^2 \qquad (2)$$

Dividing Eq. (1) by K in numerator and denominator

$$\theta_1 = (c_M + a_0 e\theta_0)qc^2/K[1 - (q/q_{cr})] \qquad (3)$$

The expression for the torsional deflection of the wing in the case where the structural twist introduces no additional load (static test condition) is

$$\theta_1' = (C_M + a_0 e\theta_0)qc^2/K \qquad (4)$$

Thus the formula for θ_1 becomes

$$\theta_1 = \theta_1'/[1 - (q/q_{cr})] \qquad (5)$$

Thus, deflection of the wing under air loads for a given attitude of the wing is seen to increase rapidly as q_{cr} is approached. In fact, for $q = q_{cr}/2$ the deflection under air load will be twice what it is under static load corresponding to the given initial flight conditions, the load being increased accordingly. It should be noted that Eq. (5) corresponds in form to Southwell's equation for the deflection of a column as the buckling load is approached.

Pugsley has found empirically that the simple relationship (Eq. (5)) seems to apply to complicated actual wing structures. Casting Eq. 5 in a slightly different form,

$$1/q - 1/q_{cr} = \frac{1}{\theta}\left[\frac{(C_M + a_0 e\theta_0)c^2}{K}\right] \qquad (5a)$$

This expression indicates that a plot of $1/q$ versus $1/\theta$ should be a straight line. A plot of $1/q$ versus $1/\theta$ was made for a typical wing subjected to a given aileron deflection at various speeds, and this plot is shown in Fig. 2. The calculated points shown were obtained by successive approximation involving repeated cycles of twist and spanwise load computation for each value of

Presented at the Aerodynamics Session, Twelfth Annual Meeting, I.A.S., New York, January 25–27, 1944.

* Now Chief of Aerodynamics and Stress Analysis, P-V Engineering Forum, Inc.

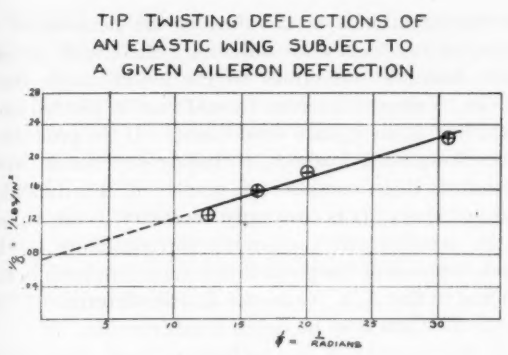

FIG. 2.

q. It is seen that the points fall reasonably near a straight line. This relationship may be quite valuable in studying aero-elastic problems.

An examination of Eq. (2) shows that q_{cr} is independent of the initial loading and initial angle of attack. On the other hand, the equation also shows that marked increases in aerodynamic loads may occur considerably below the divergence q. This increase must be taken into account in computing the aerodynamic loads for design. It is an important fact that, if this is properly done and finite deflections are obtained, it is automatically checked that the divergence speed lies above the design q investigated. This indicates that determination of q_{cr} is a secondary problem.

FINITE WING

Next the problem of twist and spanwise distribution for a wing of finite span and varying properties will be considered. Considering the torsional equilibrium of an element of wing of length dx, the fundamental differential equation for the problem is obtained as:

$$d/dx[GJ(d\theta/dx)] + q(C_{M_0} + C_L e)c^2 = 0 \qquad (6)$$

where GJ is the torsional stiffness and C_{M_0}, C_L, e, and θ vary along the span. This equation may be written for convenience

$$d/dx[GJ(d\theta/dx)] + M_a(x, \theta) = 0$$

where M_a represents the applied aerodynamic moments including effects of down-wash. This means that M_a at any station is a function not only of the angle of twist at that station but also of the angle of twist at every other station. Since a direct solution of this equation is difficult, a physical approach to the problem is desirable. The principle of virtual work may be utilized. The total internal energy may first be set down, as well as the work done by the external forces:

$$W_i = \int_0^l \frac{GJ}{2}\left(\frac{d\theta}{dx}\right)^2 dx; \quad W_e = \int_0^l \int_0^\theta M_a d\bar{\theta}\, dx \qquad (8)$$

The principle of virtual work states that if the wing be given a virtual displacement such that the new angle O' is given by $\theta' = \theta + \epsilon\eta(x)$, where η is an arbitrary deflection function satisfying the boundary conditions and ϵ is an infinitesimal quantity approaching zero. Then the variation of the energy difference $\delta(W_i - W_e)$ to the first order of magnitude will vanish. Thus, the virtual work equation becomes:

$$\delta\left[\int_0^l \frac{GJ}{2}\left(\frac{d\theta}{dx}\right)^2 dx - \int_0^l \int_0^\theta M_a d\bar{\theta}\, dx\right] = 0 \qquad (9)$$

By Euler's equation of the Calculus of Variations,[13] it may easily be verified that the value of θ, which minimizes Eq. (9), is that function which exactly satisfies the differential Eq. (7).

Employing the Rayleigh-Ritz method for solution of such problems, θ may be expressed as a sequence of form:

$$\theta = \sum_{n=1}^{j} a_n f_n \qquad (10)$$

where the a's are arbitrary constants and the f's are arbitrary functions that satisfy the boundary conditions of the problem; j is merely the number of terms, $a_n f_n$, employed. Eq. (9) may then be replaced by the condition:

$$\sum_{n=1}^{j} \frac{\partial}{\partial a_n}\left[\int_0^l \left(\frac{GJ}{2}\right)\left(\frac{d\theta}{dx}\right)^2 dx - \int_0^l \int_0^\theta M_a d\bar{\theta}\, dx\right]\delta a_n = 0 \qquad (11)$$

Thus, j simultaneous linear equations may be obtained for solution of the j unknowns $a_1, a_2, a_3, a_4 \ldots\ldots a$

Eq. (11) may be differentiated to give

$$\sum_{n=1}^{j}\left\{\int_0^l GJ\left(\frac{d\theta}{dx}\right)\left[\frac{\partial}{\partial a_n}\left(\frac{d\theta}{dx}\right)\right] dx - \int_0^l M_a\left(\frac{\partial\theta}{\partial a_n}\right)dx\right\}\times \delta a_n = 0 \qquad (12)$$

It is to be noted that in the partial differentiation M_a is regarded as a constant over the range of virtual displacement. Using the ith equation and substituting Eq. (10) for θ,

$$\int_0^l GJ f_i' \sum_{n=1} a_n f_n' dx - \int_0^l M_a f_i dx = 0 \qquad (13)$$

Substituting for M_a from Eq. (6),

$$\int_0^l GJ \sum_{n=1}^{j} a_n f_n' f_i' dx - q\int_0^l (C_{M_0} + C_L e)c^2 f_i dx = 0 \qquad (14)$$

Now C_L may be regarded as being composed of an initial value C_{L_0}, because of the initial attitude of the wing, and a series of incremental lift distributions depending on the elastic twist. Then

$$C_L(x, \theta) = C_{L_0} + \sum_{n=1}^{j} a_n C_{L_n}(x) \qquad (15)$$

where each C_{L_n} gives the lift distribution for the wing twisted through the angle $\theta = (1)f_n(x)$ spanwise. There will be as many C_{L_n}'s as there are f_n's in Eq. (10) or, in other words, j. The C_{L_0} and C_{L_n}'s are computed

The Influence of Structural Deformation on Airplane Characteristics

ALEXANDER H. FLAX*
Curtiss-Wright Corporation

Introduction

The effects of elastic deformation of wings and tail on the air loads imposed upon them has been studied in the past by a number of investigators.[1–4] These previous investigations have been mainly concerned with the occurrence of instability conditions, such as divergence, or loss of control, such as aileron reversal. Much of the previous work has been done on the basis of simplified equivalent two-dimensional wings or on the basis of the semirigid wing, commonly used in British reports on flutter and aero-elastic effects. Also, the effects of induced down-wash have usually been treated in a rough manner or neglected.

It is proposed here to include the effects of induced down-wash and to consider the wing as a three-dimensional structure. The analysis made will treat not only the criteria for divergent instability and other critical conditions but also the aerodynamic characteristics, including spanwise lift distribution, for speeds below divergence.

The subject can best be introduced by consideration of a simplified model, as shown in Fig. 1. This consists of a wing of infinite span deriving its torsional stiffness from two springs of such configuration that the elastic center lies a distance *ec* behind the aerodynamic center.

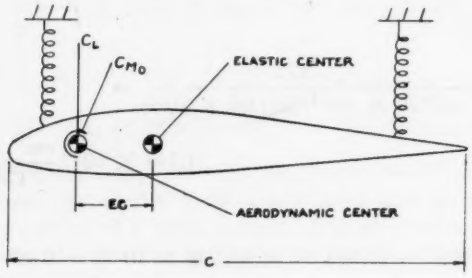

Fig. 1.

Definitions

c = chord
a_0 = $(\partial C_L/\partial\alpha)_\infty$ slope of the lift curve for aspect ratio = ∞
θ_0 = initial angle of attack
θ_1 = angle of attack increment due to twist
q = dynamic pressure $\rho V^2/2$
K = spring stiffness in torsion ft.lbs. per rad. per unit length

Then, writing the equation for equilibrium of the wing,

$$[C_{M_0} + a_0 e(\theta_0 + \theta_1)]qc^2 - K\theta_1 = 0$$

This may be solved for θ_1 to give

$$\theta_1 = (C_M + a_0\theta_0 e)qc^2/(K - a_0 eqc^2) \quad (1)$$

Divergence occurs when θ_1 approaches ∞ as the denominator of this expression approaches zero. This leads to the q for divergence

$$q_{cr} = K/a_0 ec^2 \quad (2)$$

Dividing Eq. (1) by K in numerator and denominator

$$\theta_1 = (c_M + a_0 e\theta_0)qc^2/K[1 - (q/q_{cr})] \quad (3)$$

The expression for the torsional deflection of the wing in the case where the structural twist introduces no additional load (static test condition) is

$$\theta_1' = (C_M + a_0 e\theta_0)qc^2/K \quad (4)$$

Thus the formula for θ_1 becomes

$$\theta_1 = \theta_1'/[1 - (q/q_{cr})] \quad (5)$$

Thus, deflection of the wing under air loads for a given attitude of the wing is seen to increase rapidly as q_{cr} is approached. In fact, for $q = q_{cr}/2$ the deflection under air load will be twice what it is under static load corresponding to the given initial flight conditions, the load being increased accordingly. It should be noted that Eq. (5) corresponds in form to Southwell's equation for the deflection of a column as the buckling load is approached.

Pugsley has found empirically that the simple relationship (Eq. (5)) seems to apply to complicated actual wing structures. Casting Eq. 5 in a slightly different form,

$$1/q - 1/q_{cr} = \frac{1}{\theta}\left[\frac{(C_M + a_0 e\theta_0)c^2}{K}\right] \quad (5a)$$

This expression indicates that a plot of $1/q$ versus $1/\theta$ should be a straight line. A plot of $1/q$ versus $1/\theta$ was made for a typical wing subjected to a given aileron deflection at various speeds, and this plot is shown in Fig. 2. The calculated points shown were obtained by successive approximation involving repeated cycles of twist and spanwise load computation for each value of

Presented at the Aerodynamics Session, Twelfth Annual Meeting, I.A.S., New York, January 25–27, 1944.

* Now Chief of Aerodynamics and Stress Analysis, P-V Engineering Forum, Inc.

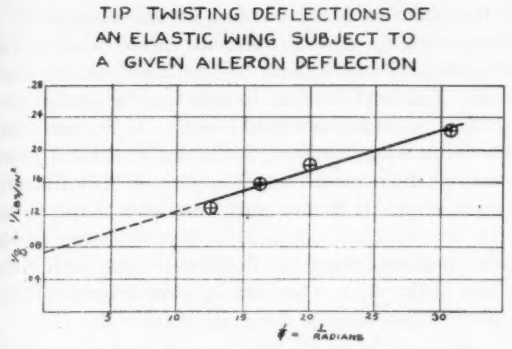

FIG. 2.

q. It is seen that the points fall reasonably near a straight line. This relationship may be quite valuable in studying aero-elastic problems.

An examination of Eq. (2) shows that q_{cr} is independent of the initial loading and initial angle of attack. On the other hand, the equation also shows that marked increases in aerodynamic loads may occur considerably below the divergence q. This increase must be taken into account in computing the aerodynamic loads for design. It is an important fact that, if this is properly done and finite deflections are obtained, it is automatically checked that the divergence speed lies above the design q investigated. This indicates that determination of q_{cr} is a secondary problem.

FINITE WING

Next the problem of twist and spanwise distribution for a wing of finite span and varying properties will be considered. Considering the torsional equilibrium of an element of wing of length dx, the fundamental differential equation for the problem is obtained as:

$$d/dx[GJ(d\theta/dx)] + q(C_{M_0} + C_L e)c^2 = 0 \quad (6)$$

where GJ is the torsional stiffness and C_{M_0}, C_L, e, and θ vary along the span. This equation may be written for convenience

$$d/dx[GJ(d\theta/dx)] + M_a(x, \theta) = 0$$

where M_a represents the applied aerodynamic moments including effects of down-wash. This means that M_a at any station is a function not only of the angle of twist at that station but also of the angle of twist at every other station. Since a direct solution of this equation is difficult, a physical approach to the problem is desirable. The principle of virtual work may be utilized. The total internal energy may first be set down, as well as the work done by the external forces:

$$W_i = \int_0^l \frac{GJ}{2}\left(\frac{d\theta}{dx}\right)^2 dx; \quad W_e = \int_0^l \int_0^\theta M_a d\bar{\theta}\, dx \quad (8)$$

The principle of virtual work states that if the wing be given a virtual displacement such that the new angle O' is given by $\theta' = \theta + \epsilon\eta(x)$, where η is an arbitrary deflection function satisfying the boundary conditions and ϵ is an infinitesimal quantity approaching zero. Then the variation of the energy difference $\delta(W_i - W_e)$ to the first order of magnitude will vanish. Thus, the virtual work equation becomes:

$$\delta\left[\int_0^l \frac{GJ}{2}\left(\frac{d\theta}{dx}\right)^2 dx - \int_0^l \int_0^\theta M_a d\theta\, dx\right] = 0 \quad (9)$$

By Euler's equation of the Calculus of Variations,[18] it may easily be verified that the value of θ, which minimizes Eq. (9), is that function which exactly satisfies the differential Eq. (7).

Employing the Rayleigh-Ritz method for solution of such problems, θ may be expressed as a sequence of form:

$$\theta = \sum_{n=}^{j} a_n f_n \quad (10)$$

where the a's are arbitrary constants and the f's are arbitrary functions that satisfy the boundary conditions of the problem; j is merely the number of terms, $a_n f_n$, employed. Eq. (9) may then be replaced by the condition:

$$\sum_{n=1}^{j} \frac{\partial}{\partial a_n}\left[\int_0^l \left(\frac{GJ}{2}\right)\left(\frac{d\theta}{dx}\right)^2 dx - \int_0^l \int_0^\theta M_a d\theta\, dx\right]\delta a_n = 0 \quad (11)$$

Thus, j simultaneous linear equations may be obtained for solution of the j unknowns $a_1, a_2, a_3, a_4 \ldots\ldots a$

Eq. (11) may be differentiated to give

$$\sum_{n=1}^{j}\left\{\int_0^l GJ\left(\frac{d\theta}{dx}\right)\left[\frac{\partial}{\partial a_n}\left(\frac{d\theta}{dx}\right)\right] dx - \int_0^l M_a\left(\frac{\partial\theta}{\partial a_n}\right)dx\right\}\times \delta a_n = 0 \quad (12)$$

It is to be noted that in the partial differentiation M_a is regarded as a constant over the range of virtual displacement. Using the ith equation and substituting Eq. (10) for θ,

$$\int_0^l GJ f_i' \sum_{n=1} a_n f_n' dx - \int_0^l M_a f_i dx = 0 \quad (13)$$

Substituting for M_a from Eq. (6),

$$\int_0^l GJ \sum_{n=1}^{j} a_n f_n' f_i' dx - q\int_0^l (C_{M_0} + C_L e)c^2 f_i dx = 0 \quad (14)$$

Now C_L may be regarded as being composed of an initial value C_{L_0}, because of the initial attitude of the wing, and a series of incremental lift distributions depending on the elastic twist. Then

$$C_L(x, \theta) = C_{L_0} + \sum_{n=1}^{j} a_n C_{L_n}(x) \quad (15)$$

where each C_{L_n} gives the lift distribution for the wing twisted through the angle $\theta = (1)f_n(x)$ spanwise. There will be as many C_{L_n}'s as there are f_n's in Eq. (10) or, in other words, j. The C_{L_0} and C_{L_n}'s are computed

taking into account induced down-wash, either by the method of ANC-1[8] or by the simpler approximation of 0 (Schrenk[9]). Substituting Eq. (15) into Eq. (14),

$$\int_0^l GJ \sum_{n=1}^{j} a_n f_n'' f_i' dx - q \int_0^l \left(C_{M_0} + C_{L_0} e + e \sum_{n=1}^{j} a_n C_{L_n} \right) \times f_i c^2 dx = 0 \quad (16)$$

Regrouping terms,

$$\sum_{n=1}^{j} a_n \left(\int_0^l GJ f_n' f_i' dx - q \int_0^l e C_{L_n} f_i c^2 dx \right) = q \int_0^l (C_{M_0} + C_{L_0} e) f_i c^2 dx \quad (17)$$

If we let i take on values from 0 to j, we obtain j simultaneous equations of this type which will enable us to solve for the j unknowns (a_1, a_2, a_3, ... a_j). These equations will be of the form:

$$\left.\begin{aligned} C_{11}a_1 + C_{12}a_2 + C_{13}a_3 + \ldots\ldots + C_{1j}a_j &= B_1 \\ C_{21}a_1 + C_{22}a_2 + C_{23}a_3 + \ldots\ldots + C_{2j}a_j &= B_2 \\ \ldots\ldots\ldots\

noted that q_{cr} represents the characteristic value of the differential Eq. (6). In this respect q_{cr} bears a position in the aero-elastic problem corresponding to the positions of critical load and critical frequency in the buckling and vibration problems, respectively. In these problems it has been found that use of rather arbitrary deflection forms in conjunction with the energy method usually leads to a satisfactory determination of the critical value.

If in the series (10) for θ only one term is used corresponding to linear twist, then

$$\theta = a_1 f_1 = \theta_t(x/l) \tag{23}$$

where θ_t is the twist at the wing tip and l is the wing semispan. The vanishing of C_{11}, as defined by Eq. (19), is the condition for divergence. Then

$$C_{11} = \int_0^l GJ\left(\frac{1}{l}\right)^2 dx - q\int eC_{L_1}\left(\frac{x}{l}\right)C^2 dx = 0 \tag{24}$$

or

$$q_{cr} = (1/l)(\textstyle\int_0^l GJdx / \int_0^l C_{L_1} exc^2 dx) \tag{25}$$

It is assumed that $C_{L_1} = (\partial C_L/\partial\alpha)_A\theta$ where $(\partial C_L/\partial\alpha)_A$ is the value of $\partial C_L/\partial\alpha$ for the wing of finite aspect ratio, thus roughly taking account of induced down-wash. To evaluate the integral in the denominator, it may be noted that for linearly tapered wings

$$C = C_R[1 - (1 - \lambda)(x/l)] \tag{26}$$

where $\lambda = c_T/c_R$, c_T is the chord at the tip, and C_R is the root chord. Further $\bar{C}$, the mean chord of the wing is given by

$$\bar{c} = (c_R + c_T)/2$$
$$\bar{c}^2 = c_R^2[(1 + \lambda)/4]^2$$

The integral may then be evaluated as

$$\textstyle\int_0^l C_{L_1} exc^2 dx = c^2(\partial C_L/\partial\alpha)_A el^2 \dfrac{2(1 + 3\lambda + 6\lambda^2)}{15(1 + \lambda)^2} \tag{27}$$

The divergence formula is now written:

$$q_{cr} = \textstyle\int_0^l GJdx/(\partial C_L/\partial\alpha)_A \bar{c}^2 l^2 eK \tag{28}$$

where

$$\kappa = 2(1 + 3\lambda + 6\lambda^2)/15(1 + \lambda)^2$$

A curve of κ versus taper ratio λ is in Fig. 3.

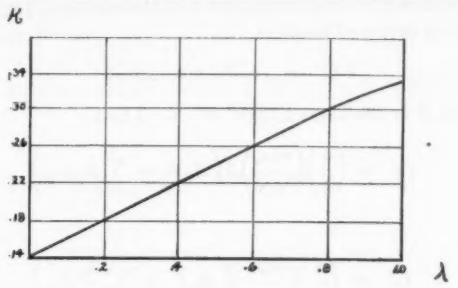

FIG. 3.

ROLLING MOMENTS OF A FLEXIBLE WING

It is well known that the maneuverability of the airplane in roll may be seriously diminished by the structural deformation accompanying the operation of the aileron. This is due to the fact that deflection of the ailerons produces not only the desired rolling moment but also a pitching moment which twists the wing. This antisymmetrical wing twist causes a rolling moment that opposes the rolling moment of the ailerons. This effect becomes worse as the speed increases, until at the aileron reversal speed all lateral control is lost.

The problem may be treated by determining the spanwise load distribution in a manner similar to that already used to determine symmetrical distributions. The value of C_L may be given as

$$C_L = \frac{m_s c_s}{c}\sum_{n=1}^{\infty} A_m \sin m\theta \tag{29}$$

where the $m = dC_L/d\alpha$ and the subscript s denotes values at the plane of symmetry. Only antisymmetrical distributions of C_L need be considered, so that the equation for C_L at any point on the span may be written:

$$C_L = C_{L_\delta}\,\delta + \textstyle\sum C_{L_n} a_n \tag{30}$$

where C_{L_δ} is the distribution due to unit δ, and a_n is defined by saying that the antisymmetrical twist is given by

$$\theta = \sum_{n=1}^{j} a_n f_n(x)$$

Here again, as before, the f_n's are a set of arbitrary deflection functions satisfying boundary conditions. The values of a_n are given by

$$a_n = \Delta_n/\Delta$$

as in the symmetrical case, with the exception that instead of Eq. (20),

$$B_i = g\int_0^l C_{L_\delta}\delta e f_i c^2 dx + q\delta\int_0^l \frac{\partial C_M}{\partial\delta} f_i c^2 dx \tag{31}$$

The value of C_{L_n} is

$$C_{L_n} = \frac{m_s c_s}{c}\sum_{m=1}^{\infty} A_{nm} \sin m\theta \tag{32}$$

so that the total value of C_L (for antisymmetrical distributions) is

$$C_L = C_{L_\delta}\delta + \frac{m_s c_s}{c}\sum_{n=1}^{j}\sum_{m=1}^{\infty} a_n A_{mn} \sin m\theta$$

The rolling moment coefficient is given by reference 8 as

$$C_l' = \text{rolling moment}/qsb$$

where S is the wing area and b is the span. The value of C_l' in terms of loads is

$$C_l' = (\pi/4)(m_s c_s/4S)A_2 \tag{33}$$

where A is the aspect ratio, b^2/S. Then

$$C_l' = \left(\frac{\pi}{4}\right)\left(\frac{m_s c_s}{4S}\right)A\left(A_{2_\delta}\delta + \sum_{n=1}^{j} a_n A_{2_n}\right)$$

or

$$C_l' = \left(\frac{\pi}{4}\right)\left(\frac{m_s c_s}{4S}\right)\left(A_{2_\delta}\delta + \sum_{n=1}^{j}\frac{\Delta_n}{\Delta}A_{2_n}\right) \tag{34}$$

Reversal of aileron effect occurs when the rolling moment coefficient vanishes. This occurs when

$$\Delta C_{l_\delta}' + \sum_{n=1}^{j}\Delta_n A_{2_n} = 0 \tag{35}$$

Simplified Formula for Reversal Speed

To obtain a rapid estimate of the reversal speed, only one term of Eq. (10) is used, so that

$$\theta = a_1 f_1 \tag{36}$$

Then

$$a_1\left(\int_0^l GJ(f_1')^2 - q\int_0^l eC_{L_n}f_1c^2dx\right) = q\left(\int_0^l eC_{L_\delta}\delta f_1c^2dx + \int_0^l \frac{\partial C_M}{\partial\delta}\delta f_1c^2dx\right)$$

or

$$a_1 = \frac{q\int_0^l [eC_{L_\delta} + (\partial C_M/\partial\delta)]\delta f_1c^2dx}{\int_0^l GJ(f_1')^2dx - q\int_0^l eC_{L_n}f_1c^2dx} \tag{37}$$

From Eq. (34), the condition for aileron reversal is

$$A_{2_\delta}\delta + A_{21}\frac{q\delta\int_0^l [eC_{L_\delta} + (\partial C_M/\partial\delta)]f_1c^2dx}{\int_0^l GJ(f_1')^2dx - q\int_0^l eC_{L_n}f_1c^2dx} = 0 \tag{38}$$

Noting that

$$\int GJ(f_1')^2dx/\int eC_{L_n}f_1c^2dx = q_{cr}$$

the equation for reversal, q, q_r becomes

$$q_r = \frac{(A_{2_\delta}/A_{21})q_{cr}}{\dfrac{A_{2_\delta}}{A_{21}} - \dfrac{[eC_{L_\delta} + (\partial C_M/\partial\delta)]\int_0^l f_1c^2dx}{e\int_0^l C_{L_n}f_1c^2dx}} \tag{39}$$

Assuming linear deformation and neglecting induced down-wash,

$$\frac{\mu C_{L_\delta}}{(\partial C_L/\partial\alpha)} = \frac{A_{2_\delta}}{A_{21}} = \frac{\int_{(1-\gamma)l}^{l} C_{L_\delta}\,xcdx}{\int^l (\partial C_L/\partial\alpha)(x^2/l)cdx}$$

where the aileron span is γl. For a linearly tapered wing, this integral may be evaluated using Eq. (26)

$$\mu = \frac{[1-(1-\gamma)^2/2] - [(1-\lambda)/3][1-(1-\gamma)^3]}{[4-3(1-\lambda)]/12} \tag{40}$$

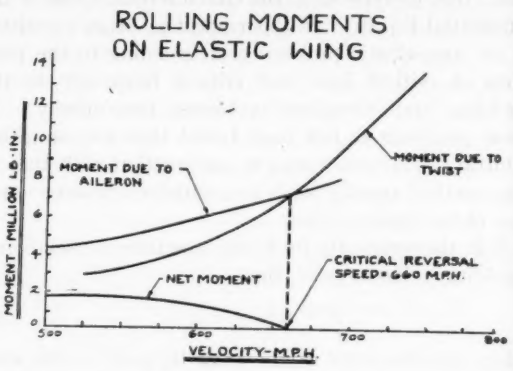

Fig. 4.

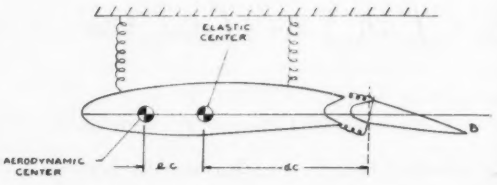

Fig. 5.

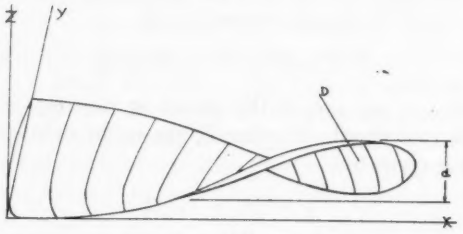

Fig. 6.

A curve of μ is provided in Fig. 7 for various values of γ and λ. Also, there is the parameter ζ described by

$$\zeta = \int_{(1-\gamma)l}^{l}(x/l)c^2dx/\int_0^l (x/l)^2c^2dx = 30\left\{\frac{1-(1-\gamma)^2}{2} - \frac{2}{3}(1-\lambda)[1-(1-\gamma)^3] + \frac{(1-\lambda)^2}{4}[1-(1-\gamma)^4]\right\}\Big/(1+3\lambda+6\lambda^2) \tag{41}$$

A curve of ζ versus γ and λ is provided in Fig. 8. Eq. (39) then becomes

$$q_r = \frac{\mu q_{cr}}{\mu - [1 + (\partial C_M/\partial\delta)/eC_{L_\delta}]\zeta} \tag{42}$$

If this formula indicates a low reversal speed, then an investigation of rolling moments at high speeds should be made. An indication of the manner in which the rolling moment drops off as the reversal speed is approached, curves of moment due to aileron and moment due to twist are shown in Fig. 4. This problem of re-

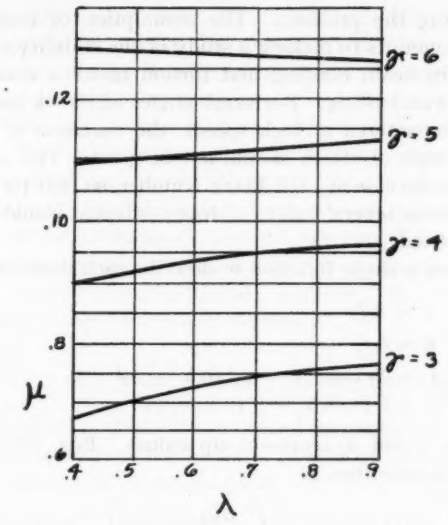

FIG. 7.

duction of rolling moments by twist is one that may be critical in design of high-speed fighters where maneuverability in roll is desired.

MIXED DEFORMATION AND INSTABILITY

Up to this point, only twist has been considered as important in influencing aerodynamic loading and instability. This is not always true, since wing bending deflection may be large enough to give drag forces appreciable moment about the elastic axis, thereby increasing the torsional moments as indicated in Fig. 6.

This problem of bending torsion instability has been treated by Viola,[11] but the solution is highly involved and does not lend itself to routine problems.

Aileron deflection may also affect the deformation of the wing, particularly if the aileron has a high degree of aerodynamic balance. This may be illustrated by a simple system similar to that used in the earlier part of this paper. Referring to Fig. 5 and writing the equation of equilibrium about the aileron hinge,

$$[(\partial c_h/\partial\alpha)(\alpha + \Delta\alpha) + (\partial c_h/\partial\beta)\beta]qSEc = K_a\beta$$

Solving for β

$$\beta = \frac{(\partial C_h/\partial\alpha)(\alpha_0 + \Delta\alpha)qsEc}{(\partial C_h/\partial\beta)qSEc - K_a} \tag{43}$$

When the denominator of this expression vanishes, aileron divergence occurs. It is seen that the denominator will vanish only when $dC_h/d_h\beta$ is positive or, in other words, when the control surface is overbalanced. Assuming that this does not occur, the influence of aileron deflection on the wing deformation may be determined. Eq. (43) may be written

$$\beta = \left[\frac{-\partial C_h/\partial\alpha}{\partial C_h/\partial\beta}\right]\left[\frac{(\alpha_0 + \Delta\alpha)}{1 - (q_{cr_a}/q)}\right] \tag{44}$$

Writing the equation for equilibrium of the wing about the elastic axis,

$$\frac{\partial C_L}{\partial\alpha}ce(\alpha_0 + \Delta\alpha)qS + ce\frac{\partial C_L}{\partial\beta}\beta qS + \frac{\partial C_M}{\partial\beta}\beta qSc = K\Delta\alpha \tag{45}$$

Substituting Eq. (44) into Eq. (45),

$$\Delta\alpha = \frac{-\dfrac{\partial C_L}{\partial\alpha}e\alpha_0 + \left(\dfrac{\partial C_L}{\partial\beta}e + \dfrac{\partial C_h}{\partial\beta}\right)\left(\dfrac{\dfrac{\partial C_h}{\partial\alpha}}{\dfrac{\partial C_h}{\partial\beta}}\right)\left(\dfrac{\alpha_0}{1 - \dfrac{q_{cr_a}}{q}}\right)}{\dfrac{\partial C_L}{\partial\alpha}e - \left(e\dfrac{\partial C_L}{\partial\beta} + \dfrac{\partial C_m}{\partial\beta}\right)\left(\dfrac{\dfrac{\partial C_h}{\partial\alpha}}{\dfrac{\partial C_h}{\partial\beta}}\right)\left(\dfrac{1}{1 - \dfrac{q_{cr_a}}{q}}\right) - \dfrac{K}{qsc}} \tag{46}$$

Divergence occurs when the denominator vanishes.

The second term in the denominator indicates the effect of the aileron. Since $\partial C_M/\partial\beta$ is usually greater than $\partial C_L/\partial\beta$ in absolute value and negative, the effect of the aileron is to lower the divergence speed. In fact, by analogy to Eq. (2) the effect of the aileron may be represented by an equivalent slope of the lift curve $(\partial C_L/\partial\alpha)'$.

The value of this equivalent slope is given by

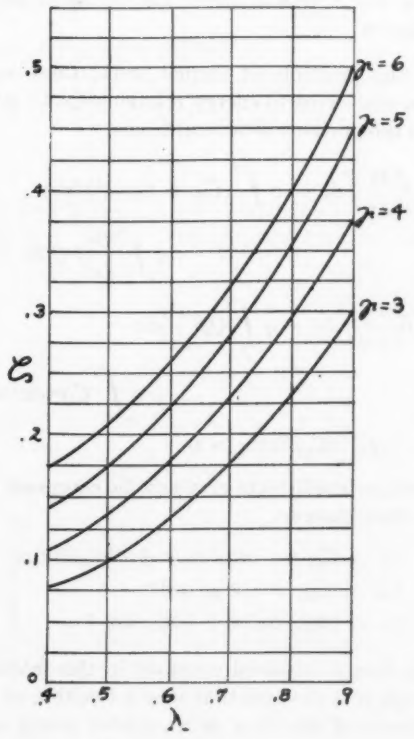

FIG. 8.

$$\left(\frac{\partial C_L}{\partial \alpha}\right)' = \frac{\partial C_L}{\partial \alpha} - \left(\frac{\partial C_L}{\partial \beta} + \frac{1}{e}\frac{\partial C_M}{\partial \beta}\right)\left(\frac{\partial C_h/\partial \alpha}{\partial C_h/\partial \beta}\right) \times \left(\frac{1}{1-(q_{cr_a}/q)}\right) \quad (47)$$

From this relationship, it may be seen that if q is close to q_{cr_a} the aileron effect is intensified.

To study the effects of bending and aileron deflection on the torsional deformation of an actual wing, the equations must be set up in differential form, since wing properties vary from station to station. The following equations are obtained:

$$\left.\begin{aligned} &\text{(Torsion)}\quad \frac{d}{dx}\left(GJ\frac{d\theta}{dx}\right) + q(C_M + C_L e)\bar{c}^2 + q\frac{d^2y}{dx^2}Q_x = 0 \\ &\text{(Bending)}\quad \frac{d^2}{dx^2}\left(EI\frac{d^2y}{dx^2}\right) - q\frac{d^2}{dx^2}(Q_x\theta) - qC_L c = 0 \\ &\text{(Aileron)}\quad K_a\beta + \int_{\gamma_1 l}^{\gamma_2 l} q\bar{E}c^2C_h = 0 \end{aligned}\right\} \quad (48)$$

where

K_a is the stiffness of the aileron control system
GJ is the torsional stiffness
EI is the bending stiffness
$\bar{E}$ is the aileron chord ratio
Q_x is the chordwise moment of the drag forces outboard of the section
$\gamma_1 l$ is the X coordinate of the inboard end of the aileron
$\gamma_2 l$ is the X coordinate of the outboard end of the aileron

Using the principle of virtual work, these equations may be converted to energy relationships to give, after partial integrations of several terms:

$$\left.\begin{aligned} &\int_0^l GJ\left(\frac{d\theta}{dx}\right)^2 dx - q\int_0^l (C_M + C_L e)c^2\theta dx + q\int_0^l \frac{d^2y}{dx^2}\theta\, Q_x dx = 0 \\ &\int_0^l EI\left(\frac{d^2y}{dx^2}\right)^2 dx - q\int_0^l Q_x\theta\frac{d^2y}{dx^2}dx - q\int_0^l C_L c y dx = 0 \\ &K_a\beta^2 + \int_{\gamma_1 l}^{\gamma_2 l}\beta C_h q\bar{E}c^2 dx = 0 \end{aligned}\right\} \quad (49)$$

The force coefficients may now be expressed in terms of the deformations.

$$\left.\begin{aligned} C_L &= C_{L_0} + (\partial C_L/\partial\alpha)\theta + (\partial C_L/\partial\beta)\beta \\ C_M &= C_{M_0} + (\partial C_M/\partial\beta)\beta \\ C_h &= (\partial C_h/\partial\alpha)\alpha + (\partial C_h/\partial\beta)\beta \end{aligned}\right\} \quad (50)$$

The drag is assumed constant in this investigation, although it is obvious that it is a function of θ and β. Treatment of the drag as a variable would make the differential equations nonlinear, thereby greatly complicating the problem. The assumption of constant drag amounts to making a study of the stability of the wing in beam bending and torsion under a constant chordwise loading. For small angles of attack such as are encountered at high speeds, the variation of drag with angle of attack should not be great. This might not be the case at high Mach Number, so that for such conditions several values of drag coefficient would have to be tried.

Using a single function to describe each deflection,

$$\begin{aligned} y &= h_t f_1 \\ \theta &= \theta_t f_2 \\ \beta &\begin{cases} = \beta_0 \text{ from } y = \gamma_1 l \text{ to } x = \gamma_2 l \\ = 0 \text{ from } x = 0 \text{ to } x = \gamma_1 l \end{cases} \end{aligned}$$

where h_t and β_t represent tip values. Eqs. (49) may now be rewritten as

$$\theta_t\left[\int_0^l GJ(f_2')^2 dx - q\int_0^l \frac{\partial C_L}{\partial\alpha}(f_2)^2 e dx\right] - q\beta_0 \times \int_{\gamma_1 l}^{\gamma_2 l}\left(\frac{\partial C_M}{\partial\beta} + e\frac{\partial C_L}{\partial\beta}\right)c^2 f_2 dx + qh_t\int_0^l f_1'' f_2 Q_x dx = q\int_0^l [C_{M_0} + C_{L_0}e]c^2 f_2 dx \quad (51)$$

$$-\theta_t q\left[\int_0^l Q_x f_1'' f_1 dx - \int_0^l \frac{\partial C_L}{\partial\alpha} c f_1 f_2 dx\right] - q\beta_0 \times \int_0^l \frac{\partial C_L}{\partial\beta} c f_1 dx + h_t\int_0^l EI(f_1'')^2 dx = q\int_0^l C_{L_0} c f_1 dx \quad (52)$$

$$\theta_t q\int_{\gamma_1 l}^{\gamma_2 l}\frac{\partial C_h}{\partial\alpha} f_2\bar{E}c^2 dx + \beta\left[K_a + \int_{\gamma_1 l}^{\gamma_2 l}\frac{\partial C_h}{\partial\beta}\bar{E}c^2 dx\right] = 0 \quad (53)$$

These equations may be written

$$\left.\begin{aligned} A\theta_t + B\beta_0 + Ch_t &= L \\ D\theta_t + E\beta_0 + Fh_t &= M \\ G\theta_t + H\beta_0 &= 0 \end{aligned}\right\} \quad (54)$$

Instability occurs when the determinant of the coefficients vanishes and θ_t, h_t, and β_0 may be found as in Eq. (22). For instability

$$\Delta = \begin{vmatrix} A & B & C \\ D & E & F \\ G & H & 0 \end{vmatrix} = 0 \quad (55)$$

This investigation of mixed instability should be made only when the simple torsional instability critical q is found to be low and where aileron aerodynamic balance and low bending stiffness make mixed instability likely. For wings of large dihedral, Eq. (51) is easily modified to account for the initial relative displacement of the sections.

It is obvious from this discussion of mixed instability that there are many possible modes of aero-elastic instability just as there are many possible modes of

flutter. One rough check for various instability speeds is to solve the flutter determinant[7] for $V/b\omega = 0$. This is not always entirely satisfactory. For instance, in the case of bending-torsion aileron deflection above, the flutter equations would not include the effects of drag. In considering whether flexibility of a particular structural component is likely to require consideration, a backlog of statistical data on past airplanes is the most valuable asset. General rules are difficult to state. If something looks doubtful a rough check is easily made. This is usually sufficient to indicate whether further analysis is necessary.

Effects of Flexibility on Dynamic Stability

Wing and tail flexibility may be detrimental to longitudinal stability of the airplane at high speeds. This will be dangerous in certain flight conditions. Pugsley[6] has already investigated the influences of wing flexibility, but the tail may be of equal importance. The notation employed will be that used by Diehl.[5] The influence of the tail on the X and Z derivatives will be neglected. Thus, Pugsley's expression for the X and Z derivatives may be used directly, with changes only in notation

$$X_u = -C_D - (V/2)(\partial C_D/\partial V) \tag{56}$$

$$X_w = +(C_L/2 - bC_L(\partial C_L/\partial \alpha) \tag{57}$$

where it is assumed that C_D may be satisfactorily expressed as $C_D = a + bC_L^2$; also

$$Z_u = -C_L - (V/2)(\partial C_L/\partial \alpha) \tag{58}$$

$$Z_w = -1/2(\partial C_L/\partial \alpha) \tag{59}$$

The moment derivatives are strongly influenced by the tail, and these are next derived:

$$M = C_M(\rho/2)SV^2C_m$$

and

$$C_M = C_{M_0} + \bar{X}C_L - (lC_{L_t}/C_m) \tag{60}$$

where $\bar{X}$ is the distance from the center of gravity to the wing aerodynamic center in terms of the mean chord C_m and l is the distance from the center of gravity to the tail.

$$m_u = \frac{\partial M/\partial V}{\rho SVl\eta} = \left[\bar{X}\frac{\partial C_L}{\partial V} - \frac{l}{C_m}\left(\frac{S_t}{S_w}\right)\frac{\partial C_{L_t}}{\partial V}\right]\frac{C_m}{l}\frac{V}{2\eta} \tag{61}$$

Similarly

$$m_w = \frac{1}{2\eta}\frac{C_m}{l}\left[\bar{X}\frac{\partial C_L}{\partial \alpha} - \frac{l}{C_m}\left(\frac{S_t}{S_w}\right)\frac{\partial C_{L_t}}{\partial \alpha}\right] \tag{62}$$

and

$$m_q = -\frac{K}{2}\left(\frac{l}{k_B}\right)^2\left(\frac{S_t}{S_w}\right)\left(\frac{\partial C_{L_t}}{\partial \alpha_t}\right)\eta_t \tag{63}$$

where

S_t = area of tail
S_w = area of wing
η = B/ml^2
B = moment of inertia of the airplane about the c.g.
k_B = radius of gyration of the airplane
K = a factor to allow for wing damping
η_t = tail efficiency factor
α = airplane angle of attack
α_t = tail angle of attack (referred to root section)
m = airplane mass

The changes in derivatives due to flexibility may be represented as increments added to the derivatives for a rigid airplane. Thus

$$\Delta X_u = -V(\partial C_L/\partial V) \tag{64}$$

$$\Delta X_w = -bC_L[(\partial C_L/\partial \alpha)_E - (\partial C_L/\partial \alpha)_R] \tag{65}$$

$$\Delta Z_u = -(V/2)(\partial C_L/\partial V) \tag{66}$$

$$\Delta Z_w = -1/2[(\partial C_L/\partial \alpha)_E - (\partial C_L/\partial \alpha)_R] \tag{67}$$

In considering the moment derivatives, the influence of the wing twist on tail down-wash must be considered. Thus

$$\alpha_t = \alpha[1 - (\partial \epsilon/\partial \alpha)] - \alpha_1(\partial \epsilon/\partial \alpha_1)$$

where α_1 is the wing angle of attack due to twist. The tip twist angle may be used as a reference value for α_1. Then

$$\partial \alpha_t/\partial \alpha = [1 - (\partial \epsilon/\partial \alpha)] - (\partial \alpha_1/\partial \alpha)(\partial \epsilon/\partial \alpha_1) \tag{68}$$

This may now be used to calculate Δm_w.

$$\partial C_{L_t}/\partial \alpha = (\partial C_L/\partial \alpha_t)(\partial \alpha_t/\partial \alpha)$$

$$= \frac{\partial C_{L_t}}{\partial \alpha_t}\left[\left(1 - \frac{\partial \epsilon}{\partial \alpha}\right) - \left(\frac{\partial \alpha_1}{\partial \alpha}\right)\left(\frac{\partial \epsilon}{\partial \alpha_1}\right)\right] \tag{69}$$

Then

$$m_u = \frac{1}{2\eta}\frac{C_m}{l}\left\{\bar{X}\frac{\partial C_L}{\partial \alpha} - \left(\frac{l}{C_m}\right)\frac{S_t}{S_w}\frac{\partial C_{L_t}}{\partial \alpha_t}\left[\left(1 - \frac{\partial \epsilon}{\partial \alpha}\right) - \left(\frac{\partial \alpha_1}{\partial \alpha}\right)\left(\frac{\partial \epsilon}{\partial \alpha_1}\right)\right]\right\}$$

also

$$(m_w)_R = \frac{1}{2\eta}\frac{C_m}{l}\left\{\bar{X}\left(\frac{\partial C_L}{\partial \alpha}\right)_R - \frac{l}{C_m}\frac{S_t}{S_w}\left(\frac{\partial C_{L_t}}{\partial \alpha_t}\right)_R\left(1 - \frac{\partial \epsilon}{\partial \alpha}\right)\right\}$$

$$\Delta m_w = \frac{1}{2\eta}\frac{C_m}{l}\left\{\bar{X}\,\Delta\left(\frac{\partial C_L}{\partial \alpha}\right) - \frac{l}{C_m}\frac{S_t}{S_w}\left(\frac{\partial C_{L_t}}{\partial \alpha}\right)_R\frac{\partial \alpha_1}{\partial \alpha}\frac{\partial \epsilon}{\partial \alpha_1} - \frac{l}{C_m}\frac{S_t}{S_w}\,\Delta\left(\frac{\partial C_{L_t}}{\partial \alpha_t}\right)\left[\left(1 - \frac{\partial \epsilon}{\partial \alpha}\right) - \frac{\partial \alpha_1}{\partial \alpha}\left(\frac{\partial \epsilon}{\partial \alpha}\right)\right]\right\} \tag{70}$$

where

$$\Delta(\partial C_L/\partial \alpha) = (\partial C_L/\partial \alpha)_E - (\partial C_L/\partial \alpha)_R$$

Further

$$\Delta m_u = \frac{C_m}{l}\frac{V}{2\eta}\left[\bar{X}\frac{\partial C_L}{\partial V} - \frac{l}{C_m}\frac{S_t}{S_w}\frac{\partial C_{L_t}}{\partial V}\right] \tag{71}$$

since m_u will normally be zero for a rigid wing, and

$$\Delta m_q = -\frac{K}{2}\left(\frac{l}{k_B}\right)^2 \frac{S_L}{S_u}\,\Delta\left(\frac{\partial C_{L_t}}{\partial \alpha_t}\right) \tag{72}$$

To evaluate $\Delta(\partial C_L/\partial\alpha)$ and $\partial C_L/\partial V$, consider the case of a wing or tail where the torsional deflection is given by a single term or

$$\theta = a_1 f_1$$

Then by Eq. (17)

$$a_1 = \frac{\int_0^l [C_{M_0} + (\partial C_L/\partial\alpha)\alpha\epsilon] f_1 c^2 dx}{\int_0^l GJ(f_1')^2 dx}\left[\frac{q}{[1-(q/q_{cr})]}\right] \tag{73}$$

The total lift coefficient for such an elastic wing or tail may be written

$$C_{L_E} = (\partial C_L/\partial\alpha)_R \alpha + (\partial C_1/\partial a_1) a_1 \tag{74}$$

Then

$$(\partial C_L/\partial\alpha)_E = (\partial C_L/\partial\alpha)_R + (\partial C_L/\partial a_1)(\partial a_1/\partial\alpha) \tag{75}$$

or using Eq. (73)

$$\Delta\left(\frac{\partial C_L}{\partial\alpha}\right) = \frac{\partial C_L}{\partial a_1}\left[\frac{(\partial C_L/\partial\alpha)_R \int_0^l \epsilon f_1 c^2 dx}{\int_0^l GJ(f_1')^2 dx}\right]\left[\frac{q}{1-(q/q_{cr})}\right] \tag{76}$$

$$\frac{\partial C_L}{\partial V} = \left(\frac{\partial C_L}{\partial a_1}\right)\left\{\frac{\int_0^l [C_{M_\alpha} + \dfrac{\partial C_L}{\partial\alpha}\epsilon\alpha] f_1 c^2 dx}{\int_0^l GJ(f_1')^2 dx}\right\} \times \left\{\frac{\rho V}{[1-(q/q_{cr})]^2}\right\} \tag{77}$$

The phugoid roots of the stability quartic are given approximately, according to Diehl, by

$$\lambda_1^2 + [D_1/C_1) - (B_1E_1/C_1^2)]\lambda_1 + (E_1/C_1) = 0 \tag{78}$$

where

$$\begin{aligned} B_1 &= -m_q - (X_u + Z_w) \\ C_1 &= m_q(X_u + Z_w) - (X_w Z_u - X_u Z_w) - \mu m_u \\ D_1 &= m_q(X_w Z_u - X_u Z_w) + \mu m_u\,[(C_L/2) - X_w] \\ E_1 &= \mu(C_L/2)(m_w Z_u - m_u Z_w) \end{aligned}$$

and where

$$\mu = m/\rho s l \tag{79}$$

The solution to Eq. (78) is

$$\lambda_1 = \frac{1}{2}\left(\frac{D_1C_1 - B_1E_1}{C_1^2}\right) \pm \sqrt{\left(\frac{D_1C_1 - B_1E_1}{2C_1^2}\right)^2 - \frac{E_1}{C_1}} \tag{80}$$

Pugsley[6] has concluded that the major effects of wing elasticity on stability may be traced through the change in E_1.

$$\Delta E = [(m_w)_R \Delta Z_u + (Z_u)_R \Delta m_w - (m_u)_R \Delta Z_w - (Z_w)_R \Delta m_u]\mu(C_L/2) \tag{81}$$

Terms involving $\Delta(\partial C_L/\partial\alpha)$ for wing or tail may change in magnitude but not in sign from $(\partial C_L/\partial\alpha)_R$. These terms are m_w, z_w, x_w, m_q. On the other hand, terms involving $\partial C_L/\partial V$ do not exist in the rigid case. These terms may be either positive or negative in sign depending on the initial torque on the surface. This may be seen from Eq. (77). A positive $\partial C_L/\partial V$ on the wing and a negative $\partial C_L/\partial V$ on the tail give conditions of increasing stability, while a negative value on the wing and a positive value on the tail give decreasing stability. ΔE may then undergo changes in sign due to the changes in m_u and z_u. From Eq. (86) it may be seen that if E_1 becomes negative, the roots of the stability equation may become real, indicating divergent instability. Eqs. (76) and (77) indicate that the magnitude of the flexibility corrections to the stability derivatives is dependent on proximity to q_{cr}. Thus, the correction may be minimized by stiff structures. $\partial C_L/\partial V$ for the wing is difficult to change by changing the initial torque, since this is fixed by the C_L required. However, wings of small C_{M_0} are desirable. $\partial C_L/\partial V$ for the tail may readily be made favorable by a nose down change in initial stabilizer setting. For flexible structures, a complete stability check, using derivatives corrected for flexibility as above, is probably necessary. It should be noted that large changes in trim with speed may be expected at high speed for flexible structure due to $\partial C_{L_t}/\partial V$.

Conclusion

Other changes in airplane characteristics not treated in this paper may be treated by the methods outlined herein. Obviously, loss of elevator control may result in a manner similar to loss of aileron control if the stabilizer is flexible. Also, deformations of the control surfaces may be important for flexible surfaces.

Aero-elastic effects are likely to be serious not only in high-speed airplanes but also in large heavy airplanes. For dimensional reasons it is difficult to maintain rigidity in large airplanes, even though strength may be adequate. Furthermore, the design load factors on large airplanes are lower than on small airplanes, so that the structures required for strength become relatively lighter. Such airplanes are then subject to changes in aerodynamic characteristics due to flexability. Since the present trends in design are toward higher speeds and larger airplanes, aero-elastic effect are likely to become increasingly important in the next few years.

References

[1] Pugsley, A. G., *Aerodynamic Characteristics of a Semi-Rigid Wing*, British R. & M. 1490, 1932.

[2] Duncan, W., and McMillan, C., *Reversal of Aileron Control Due to Wing Twist*, British R. & M. 1499, 1932.

[3] Cox, H., and Pugsley, A. G., *Theory of Loss of Lateral Control Due to Wing Twisting*, British R. & M. 1506, 1933.

[4] Pugsley, A. G., and Naylor, G., *The Divergence Speed of an Elastic Wing*, British R. & M. 1815, 1937.

(*Continued on page 117*)

A Simplified Analysis of Hollow Beams with Longitudinal Webs Subjected to Torsional Loads

ERYK KOSKO*
École Polytechnique de Montreal

ABSTRACT

The Maxwell-Mohr method, in general use in connection with statically indeterminate trusses, is applied here to the problem of the prismatic thin-walled beam with internal longitudinal webs, subjected to a constant torque. In comparison with other methods known to the author, the analysis outlined in the paper presents the advantage of involving fewer unknown quantities and of being easily adaptable to tabular work.

INTRODUCTION

THE DISTRIBUTION OF SHEAR STRESSES in a prismatic thin-walled multi-cell wing beam when subjected to a constant torque has been extensively studied in the past decade. The results of the theoretical analysis have been fairly well confirmed by experiment, at least for moderate loads which do not cause buckling of the thin-sheet walls of the section. An approximate treatment for larger loads is also possible under certain assumptions, which correspond to the diagonal-tension field theory. As far as the distribution of shear stresses is concerned, it is sufficient to assume a reduced modulus of elasticity or, better still, an effective wall thickness.

The assumptions generally made, and also underlying the present treatment, are the same as those on which the well-known Bredt-Batho formulas for torsion of a thin-walled tube are based. It seems, however, that in the case of a multi-cell beam the methods developed to date could still be simplified and the computation shortened without any loss in exactitude. These known methods will first be shortly discussed and the proposed method will then be presented.

Although no claim is made of bringing any fundamentally new relations, the author feels that his method will have an appeal to the engineer conversant with statically indeterminate structures. It is, in fact, but an adaptation of the widely used Maxwell-Mohr method.

REVIEW OF KNOWN METHODS

The usual way of approaching the problem, as developed by Atkin,[1] Duncan[2] and Kuhn,[3] and suggested with some modifications in textbooks[4, 5, 6] as a standard method, consists in considering the beam as composed of a number of "cells" some of which have common boundaries. A three-cell section will thus have two internal webs forming the common boundary between adjacent cells. Under a torsional load, a shear flow of constant intensity is developed in the perimeter of each cell; the actual shear flow in the common boundary of two cells is equal to the algebraic sum of the shear flows corresponding to those cells. The resultant of the shear flow developed in the perimeter of any cell is a torque equal to the double product of the corresponding shear flow by the cross-sectional area enclosed by the median line of the perimeter.

An equation of equilibrium expresses the applied external torque as balanced by the sum of the torsional couples developed by the individual cells. Further, an equation of deformation expressing the angle of twist per unit length of span in terms of the shear flow and of the elastic properties of the walls (thickness, length and modulus of rigidity) is written down for each cell. This angle of twist must, of course, be the same for all the cells and for the entire section, if, as assumed, there is no distortion of the cross-sectional shape. (Warping in longitudinal direction out of the cross-sectional plane is not considered here.) For a section consisting of n cells there are $n + 1$ unknowns, i.e., the n cell shear flows and the angle of twist; and as many equations, linear with respect to the unknowns, are available, thus making the problem determinate. Upon solving the equations the unknown shear flows can be expressed in terms of the applied torque.

Von Kármán and Christensen[7] proceed in a somewhat different way. They suppose first the angle of twist a known quantity and use only n equations of continuity for the n unknown shear flows. To express these in terms of the applied torque (which is the problem usually confronting the engineer) requires an additional computation, which amounts to the determination of the torsional stiffness of the beam. Although this additional work does not present any special difficulty it is felt that the procedure is less convenient than the more direct method presented here.

Successive approximations have been suggested by Baron[8, 9] as a means of solving the same problem. The procedure is similar to that developed by Hardy Cross for the analysis of flow in networks of conduits. It seems, however, that for a low degree of redundancy such as is the rule in aircraft structures, successive approximations do not present any distinct advantage

Received July 5, 1944.
* Assistant Professor of Aircraft Structures.

over the solution of the "exact" system of linear equations. Working out a sample problem given by Baron has actually shown that by the method outlined here the time necessary for the computation was considerably reduced.

Derivation of Formulas

Under the assumptions made, a simple tube under torsional load can be considered as a statically determinate structure; the stress distribution under an applied torque T is given by the equilibrium condition alone

$$2qA = T \qquad (1)$$

where q denotes the shear flow (or shear intensity per unit length of wall), and A the area enclosed by the median line of the tube wall.

An interior web can then be considered as a redundant member and the stress in this member can be determined as it is in other cases of statical indetermination, i.e., by consideration of the minimum strain energy, or by the Maxwell-Mohr method (which practically amounts to the same thing) of writing an equation of continuity for each of the points of application of redundant forces.

As is well known, the selection of the statically determinate included structure or basic system, as it is also called, is a matter of judgment. The most obvious choice would seem to be that of the outer perimeter of the shell, i.e., considering the interior webs as redundant members. The shear flow in the thus defined basic structure will be called "basic shear flow" and denoted by the subscript "0." Thus we have

$$q_0 = T/2A \qquad (2)$$

In many cases this basic shear flow is already a good approximation to the actual shear flow. The stresses in the interior webs being equal to differences between shear flows in adjacent cells will in most cases be small compared to the basic flow and may be considered as correction quantities expressed as fractions of the basic flow.

Let us take the case of two interior webs. The sign convention shall be as follows (Fig. 1). Looking upon the end of the beam, the shear flow in the external walls is considered as positive when directed counterclockwise (i.e., balancing a clockwise acting torque). Shear flow in an internal wall is positive when acting upwards. Portions of the external walls are denoted by a subscript corresponding to the cell the outer boundary of which they form. Interior webs are indicated by a double subscript referring to both neighboring cells.

"Removing" the redundant members means the same as effecting a longitudinal cut in each web (Fig. 2). Under the external torque T corresponding points like A and A' on the edges of the cut at the place X will be longitudinally displaced by a certain amount d_{X0}.

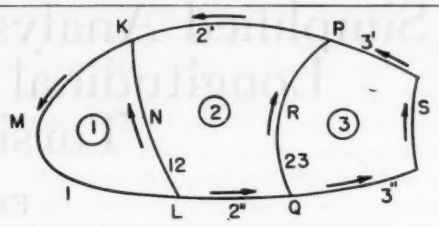

Fig. 1. Notations and sign convention.

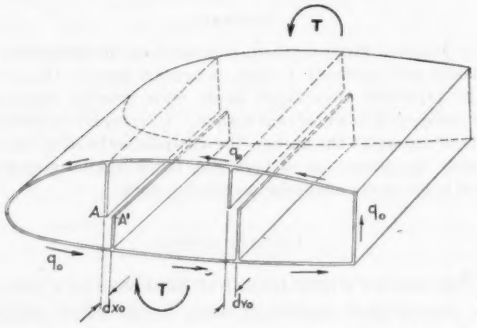

Fig. 2. Basic system under external torque.

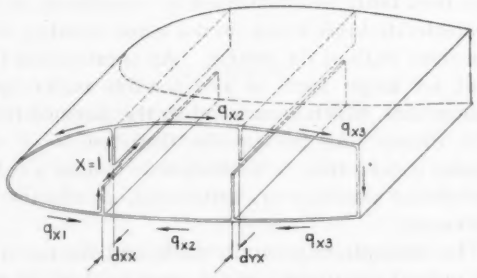

Fig. 3. Basic system under unit web shear force.

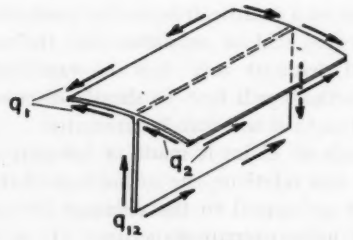

Fig. 4. Equilibrium at wall junction.

If the basic structure is now submitted to a statically indeterminate force X applied along the edges of the cut of the first web, the relative displacements of the cuts will be as shown in Fig. 3. By superposing the action of the external torque on the actions of the redundant forces X and Y of convenient magnitude, it is possible to obtain at each cut a resulting relative displacement equal to zero. This condition can be used to calculate the magnitudes of X and Y.

To keep a rectangular element of web in equilibrium, the longitudinal shear force per unit length X must also appear in the cross-sectional plane in the same direction on both sides of the cut. The shear configuration in the cross-sectional plane under an applied unit shear force $X = 1$ is then easily determined by means of a simple equilibrium consideration. It consists of a unit shear force $q_{12} = 1$ in the internal web, which at junction points K and L ramifies into two circuits, left (KML) and right ($KPSQL$) of the web. The hydrodynamic analogy may be used for better visualization. The longitudinal equilibrium of an isolated junction such as K (Fig. 4) in general requires

$$q_1 - q_2 = q_{12} \tag{3}$$

which in the present case reduces to

$$q_{X1} - q_{X2} = 1 \tag{4}$$

The subscript X is used to indicate that the shear flow in question is due to $X = 1$. At the junction P, since in the present case we have $q_{23} = 0$, we must have also $q_{X2} = q_{X3}$.

On the other hand, there being no external torque acting now on the basic structure, the torsional resultant of the "left" shear flow (around circuit "1") must be equal and opposite to that of the "right" shear flow (around circuits "2" and "3"), i.e.

$$2A_1q_{X1} + 2(A_2 + A_3)q_{X2} = 0 \tag{5}$$

A_1, A_2, A_3 denote the areas included in the perimeters of the corresponding cells; we have $A_1 + A_2 + A_3 = A$.

Solving Eqs. (4) and (5) we find

$$q_{X1} = (A_2 + A_3)/A \qquad q_{X2} = q_{X3} = -A_1/A \tag{6a}$$

Similarly, if a unit shear force $Y = 1$ is applied at the cut in the web "23," the shear configuration will consist of the web shear flow $q_{23} = 1$ and of two circuits

$$q_{Y1} = q_{Y2} = A_3/A \qquad q_{Y3} = -(A_1 + A_2)/A \tag{6b}$$

Supposing the magnitudes of the forces X and Y to be known, the resultant shear flow in any part of the section may be expressed as

$$q = Xq_X + Yq_Y + q_0 \tag{7}$$

For an element of thin wall having a length ds measured along the perimeter (the length in axial direction being taken equal to unity), the elastic energy of shear is expressed by

$$dW = \tau\gamma dst/2 = \tau^2 tds/2G$$

$\tau = q/t$ being the shear stress, G the modulus of rigidity and $\gamma = \tau/G$ the angle of shear deformation; this may be written

$$dW = (1/2G)(q^2/t)ds$$

The total work of the shear forces is equal to the integral extended over the whole section including outer perimeter and internal webs. As in each portion of the section between two junctions the shear flow remains constant (even if there is some change in wall thickness), the integral may be replaced by a sum

$$W = \frac{1}{2G}\sum_i \frac{L_i}{t_i} q_i^2 = \frac{1}{2G}\sum_i a_i q_i^2 \tag{8}$$

where the quantities

$$a_i = L_i/t_i \quad (i = 1, 2, 3, 12, 23) \tag{9}$$

are taken for each part of the section.

The condition equations of minimum shear strain energy take the form (assuming G = const. over the whole section)

$$\partial W/\partial X = 0 = \sum_i a_i q_i q_{Xi} \tag{10}$$

or, substituting for q_i its value from Eq. (7),

$$X\sum_i a_i q_{Xi}^2 + Y\sum_i a_i q_{Xi} q_{Yi} + \sum_i a_i l_{Xi} q_0 = 0 \tag{11}$$

which may be written

$$X\delta_{XX} + Y\delta_{XY} + \delta_{X0} = 0 \tag{12a}$$

A similar equation of condition for the displacement corresponding to the force Y can be written

$$X\delta_{YX} + Y\delta_{YY} + \delta_{Y0} = 0 \tag{12b}$$

The quantities δ_{XX}, δ_{X0}, etc., are respectively proportional to the relative displacements d_{XX}, d_{X0}, etc., such as shown in Fig. 2 and Fig. 3. The equations of elasticity, Eqs. (12a) and (12b), derived from the condition of minimum strain energy may thus be interpreted as equations of continuity at the cuts. For the sake of simplicity the quantities δ will be called "quantities of displacement." They are computed by the formulas

$$\left.\begin{aligned} \delta_{X0} &= \sum_i a_i q_{Xi} q_0 \qquad \delta_{Y0} = \sum_i a_i q_{Yi} q_0 \\ \delta_{XX} &= \sum_i a_i q_{Xi}^2 \qquad \delta_{YY} = \sum_i a_i q_{Yi}^2 \\ \delta_{XY} &= \delta_{YX} = \sum_i a_i q_{Xi} q_{Yi} \end{aligned}\right\} \tag{13}$$

These expressions are analogous to those encountered in the theory of redundant frames and could equally have been obtained by the method of "dummy unit loading." They are most conveniently computed in a tabular form (see example), and their values are then to be substituted into the equations of elasticity, Eqs. (12).

After solving these equations for X and Y, the resultant shear flow in each portion of the section is found by Eq. (7). In all these operations it is convenient to express all shear flows in terms of a unit basic shear flow $q_0 = 1$; the results have then to be multiplied by the appropriate value of q_0 as given by Eq. (2).

It is to be noted that in the presently discussed case of two internal webs there are only *two* simultaneous linear equations to be solved, as against *four* when the standard method is applied, or *three* by the Von Kármán-Christensen method (an additional computation

of the torsional rigidity being needed in the last case). In the general case of more than two interior webs the procedure is in principle the same as above outlined. There will be as many equations of elasticity to be solved as there are interior webs, which is always two less than in the standard solution by means of cell flows. In the case of n webs there will be in general $n(n + 3)/2$ different quantities of displacement to be computed and introduced as coefficients into the equations of elasticity. The most cumbersome part of the whole procedure which consists in the solution of the set of linear equations is thus considerably reduced and simplified.

The single-web (or double-cell) section is simply statically indeterminate; although the general method is also applicable in this case, the most expedient way of dealing with it appears to be the use of explicit formulas for all the shear flows involved. Such formulas are easily developed; they may also be found in the literature of the subject.[6]

The angle of twist now remains to be determined, although in many practical cases it is not required at all. Its calculation does not present any difficulties. Taking any of the closed circuits (which may be either the basic outer circuit or any of the partial circuits surrounding one or even more cells), the torsional angle per unit length of span is given by

$$\theta = (1/2GA_C)\sum_C aq \tag{14}$$

where the subscript C indicates the circuit in question, and where the summation has to be extended to all the walls of the chosen circuit. The torsional rigidity of the section is expressed by

$$C = T/G\theta \tag{15}$$

Substituting for θ its value from Eq. (14), we find

$$C = 2A_cT/\sum_C aq \tag{16}$$

This may be put in the form

$$C = 4AA_C/(\sum_C aq/q_0) \tag{17}$$

by use of Eq. (2). The ratios q/q_0 are independent of the torque; they are, in fact, constants of the section. Eqs. (14) to (17) afford an easy check of the whole computation, as the values of θ and of C should be independent of the choice of a particular closed circuit.

Example

In order that a comparison may be made with the standard method, the same section has been chosen as an illustration as that discussed by Kuhn.[3] Cols. 1 and 2 of Table 1 contain the data of the various portions of the section. The areas enclosed by the partial circuits are

$A_1 = 89.3$; $A_2 = 250$; $A_3 = 125$; total $A = 464.3$ sq.in.

Col. 3 gives the factors a_i calculated by Eq. (9). The next three columns indicate the distribution of shear flow in the basic system under unit basic shear flow and under unit web shear flows according to Eqs. (2), (6a) and (6b). The products of these quantities are then written in cols. 7 to 11; the summation of each of these columns yields one of the quantities of displacement δ (Eq. (13)). The equations of elasticity (12) can now be written

$$X736.6 + Y744.8 = 947q_0$$
$$X744.8 + Y3272.4 = 3145q_0$$

The solution is $X = 0.389q_0$ and $Y = 0.873q_0$.

After multiplying cols. 5 and 6 by these values, cols. 12 and 13 are obtained. The resultant shear flow (col. 14) is then found as indicated by Eq. (7) by adding the corresponding values from cols. 4, 12 and 13. The shear stresses for a unit torque (col. 15) are obtained by dividing the values of col. 14 by the wall thickness (col. 2) and by $2A = 928.6$. The values thus found agree very closely with those given by Kuhn.

To determine the angle of torsion let the outer circuit be taken. We have

$$\begin{aligned}\sum aq &= q_1a_1 + q_2a_2 + q_3a_3 \\ &= (1.549 \times 514.4 + 1.160 \times 1,875 + 0.287 \times 5,193)q_0 \\ &= 4,460q_0 = 4.80T\end{aligned}$$

The torsional rigidity of the section is then, by Eq. (17)

$$C = \frac{4A^2}{\sum_0 aq/q_0} = \frac{4 \times (464.3)^2}{4,460} = 193 \text{ in.}^4$$

Table 1

Member No.	1 L in.	2 t in.	3 a	4 Unit shear flow q_0	5 Unit shear flow q_X	6 Unit shear flow q_Y	7 aq_Xq_0	8 aq_Yq_0	9 aq_{X^2}	10 aq_{Y^2}	11 aq_Xq_Y	12 Xq_X	13 Yq_Y	14 q/q_0	15 τ/T
1	25.72	0.050	514.4	1.0	0.8077	0.2695	415	139	335	37.6	112.3	0.314	0.235	1.549	0.0333
2	25.0	0.040	1875	1.0	−0.1923	0.2695	− 362	506	69.6	136.5	−97.5	−0.075	0.235	1.160	0.03125
2′	25.0	0.020													0.0625
3	51.926	0.010	5193	1.0	−0.1923	−0.7305	−1000	−3790	192.3	2765	730	−0.075	−0.638	0.287	0.0311
12	10	0.060	166.7	0	1.0	0	0	0	166.7	0	0	0.389	0	0.389	0.0069
23	10	0.030	333.3	0	0	1.0	0	0	0	333.3	0	0	0.873	0.873	0.0313
Total							− 947	−3145	763.6	3272.4	744.8				

REFERENCES

[1] Atkin, E. H., *Torsion in Thin Cylinders*, Flight, October 30, 1931, Supplement, p. 76.

[2] Duncan, W. J., *The Torsion and Flexure of Cylinders and Tubes*, A.R.C. Reports and Memoranda, No. 1444, 1932.

[3] Kuhn, P., *The Initial Torsional Stiffness of Shells with Interior Webs*, N.A.C.A. T.N. No. 542, 1935.

[4] Timoshenko, S. P., *Strength of Materials*, 2nd Edition, Vol. 2, p. 280; D. Van Nostrand Company, Inc., New York, 1941.

[5] Niles, A. J., and Newell, J. S., *Airplane Structures*, 3rd Edition, Vol. II, par. 16:4; J. Wiley & Sons, New York, 1943.

[6] Bruhn, E. F., *Analysis and Design of Airplane Structures*, p. A5-3; John S. Swift, Cincinnati, 1943.

[7] von Kármán, Th., and Christensen, N. B., *Methods of Analysis for Torsion with Variable Twist*, Journal of the Aeronautical Sciences, Vol. 11, No. 2, pp. 112, 115, April, 1944.

[8] Baron, F. M., *Torsion of Multiconnected Thin-Walled Cylinders*, The American Society of Mechanical Engineers (Transactions), Vol. 64, Journal of Applied Mechanics, pp. A-72–A-74, June, 1942.

[9] Younger, J. E., *Mechanics of Aircraft Structures*, 2nd Edition pp. 188–193; McGraw-Hill Book Company, Inc., New York, 1942.

Letter to the Editor

Dear Sir:

The accuracy of the analysis demonstrated by Donald A. duPlantier (JOURNAL OF THE AERONAUTICAL SCIENCES, April, 1944) depends not only on the number of stations, as stated on page 141 of the paper, but much more on the method of calculating angular displacements and the corresponding centers of rotation, as may be seen in Problem 1—Unsymmetrical Ring, page 140. A continuity check shows the degree of accuracy:

Slope in member $AB = (+3.88 - 2.54) \times 10 - 3.75 \times 10$	$+ 13.4$	$- 37.5$
Slope in member $BC = (3.88 + 2.46) \times 10$	$+ 63.4$	
Slope in member $CD = (2.46 + 4.63) \times 20 - (75/8) \times 10$	$+141.8$	-187.5
Slope in member $DA = (4.63 - 2.54) \times 14.14$	$+ 29.55$	
	$+248.15$	-225.0

The positive and negative values should be equal.

For the elements 1 and 6 the angular displacements are: $\Delta W_1 = \Delta W_6 = 12.5$ and not zero as calculated by the author (because the ordinate of the moment diagram for the base structure at the center of elements 1 and 6 is equal to zero).

The correct values* are: $\Sigma \Delta W = 525$ (520); $C_x = 0.4301$ (0.429); $C_y = 0.0756$ (0.071); $I_x = (2000/3)(39 + 14\sqrt{2})/(4 + \sqrt{2}) = 7{,}240.0787$ (6,835); $I_y = (2000/3)(71 + 58\sqrt{2}/(4 + \sqrt{2}) = 18{,}842.3041$ (18,104); $I_{xy} = [2000/3(4 + \sqrt{2})^2](100 + 39\sqrt{2}) = 3{,}528.5955$(3,290). The corner moments result:

$M_A = -2.6928$ (-2.54), accuracy $+6$ per cent
$M_B = +3.7049$ (-3.88), accuracy -4.6 per cent
$M_C = +2.1926$ ($+2.46$), accuracy -11 per cent
$M_D = +4.3973$ ($+4.63$), accuracy -5 per cent

J. J. POLIVKA
Berkeley, Calif.

* The author's values are indicated in parentheses.

Vibrations of Composite Structures

H. SERBIN*

Fairchild Engine & Airplane Corporation

Introduction

It is primarily for reasons of expediency that the highly redundant structure that skeletonizes the airplane is regarded as the union of several simpler structures that are to a large extent independent of one another. The wing, the tail group, power plant, and so on are instances of such basic structures to which the airplane is reducible.

This simplification has generally proved to be satisfactory. However, when a closer analysis is required it becomes necessary to investigate the interrelation between the basic substructures.

Structural Interrelation

An example of structural interrelation exists in the practice of vibration isolation of engines. A widely adopted method for radial engines is to design the mountings so that the engine modes of translation and rotation about the centroid would be uncoupled. Then the frequencies of the power plant are to be reduced to below the range of forcing frequencies which occur in normal flight. In general, this is done for all frequencies except the fore and aft, which remains in the operating range where it will do little harm provided that it cannot be excited—or at least to a negligible degree—by the normal forcing impulses. On the other hand, if the structure supporting the engine ring is such that translation of the engine is coupled with pitching, then one can expect that rough engine operation will exist within the operating range—this despite the fact that the design procedure followed may have been perfectly satisfactory according to present-day practice.

Interrelations such as these are, of course, familiar to the engineer. But the difficulty of estimating these effects appears frequently to be formidable and time-consuming. This is especially so during a flight-test program when it may be desired to locate the source of undesirable vibrations. The "energy" methods that are now widely used and are, in fact, successful for simple continuous structures are cumbersome for composite structures. Frequently, they are improperly applied.

For the analysis of static loads on composite structures, a method is available—that of "Consistent Deformations" or "Minimum Energy of Deformation." The purpose of the present paper is to show how it may be applied to solve vibration problems. It will be seen that, although the underlying approach is the same, in application of the method the details will differ because of the *dynamic* nature of the problem.

Received May 19, 1944.

* Chief Aerodynamacist, Fairchild Aircraft Division.

Consistent Deformations

Consider an elastic structure S and assume it to be in static equilibrium under a certain loading L. By a series of cuts disconnect S into a set of substructures. Introduce at each cut the local stresses prevailing before the cut was made so that each substructure is in equilibrium. On both sides of the cut, the stresses will be of equal but opposite sign. According to Saint Venant's principle, a system of stresses at a cut may be replaced by a statically equivalent set of forces without affecting the distribution of internal stress at "large" distances. For instance, it is customary in the technical theory, when it is a case of transverse bending of beams, to choose the equivalent system that consists of a bending moment and a transverse shear. In a similar way, each set of stresses at a cut may be replaced. This is to be done on both sides of the cut in a completely antisymmetrical way, so that for every force P acting on one side of the cut there is a numerically equal but oppositely directed one acting on the other side.

Now use subscripts to denote the pairs of forces that have been introduced (Fig 1.):

P_j = each of the forces of pair j

Δ_j = structural displacement at the pair P_j in the direction of forces P_j due to the external loading L

δ_{ij} = structural displacement at the pair P_j due to the unit pair P_i

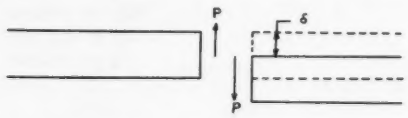

Fig. 1. Interaction forces and displacements.

Then the total relative displacement at j due to forces P_i and loading L is

$$\sum_i P_i \delta_{ij} + \Delta_j$$

where the summation is carried out over all pairs of forces. In order to preserve the continuity of the structure, the following *equation of continuity* must hold:

$$\sum_i P_i \delta_{ij} + \Delta_j = 0 \tag{1}$$

There are as many equations as there are pairs P_j, so that the equations will in general permit of a unique solution.

The exceptional case will occur if the determinant of the coefficients is zero.

$$|\delta_{ij}| = 0 \tag{2}$$

If this should be so, then the set of equations

$$\sum_i P_i \delta_{ij} = 0 \tag{3}$$

would permit of a solution for $P_1, P_2, \ldots, P_n$, which are not all zero. Then the internal deformation energy $\frac{1}{2}\Sigma P_i P_j \delta_{ij}$ would be zero, although the interaction forces would not be zero.

Thus, it can be seen that the characteristics of the composite structure are reducible to those of the simpler substructures by the use of the unit deflection elements δ_{ij}. A similar situation exists for certain dynamic loadings.

Harmonic Loadings

Suppose that the loading L to be applied consists of harmonic forces all of the same frequency ω. The assumption of static equilibrium is meaningless. Each of the applied forces can be expressed in the form $Qe^{i\omega t}$, where i is the pure imaginary unit and Q is a complex number indicating the modulus and phase of the exciting force. Introduce again a series of cuts and pairs of forces P_j. The forces P_j and the corresponding displacements will also be harmonic functions of frequency ω. Let

$\epsilon_{ij}e^{i\omega t}$ = displacement at j due to unit harmonic load $P_j = (1)(e^{i\omega t})$ at l

$\Delta_j e^{i\omega t}$ = displacement at j due to the external harmonic load L

Of course, definitions and equations such as these which involve complex numbers are to be interpreted as equalities only between the real parts. However, if an equation is valid for all values of t, the imaginary parts of both sides will be equal and the factor $e^{i\omega t}$ may be canceled out.

Applying this to the equation of continuity, one obtains

$$\sum_l P_l \epsilon_{lj} + \Delta_j = 0 \tag{4}$$

Again there are as many equations as unknowns P_l. When, in particular, all quantities Δ_j are zero, there will exist a nontrivial solution P, if and only if

$$|\epsilon_{ij}| = 0 \tag{4a}$$

This equation determines the natural frequencies of the composite system provided that the elements ϵ_{ij}, which are functions of ω^2, are known.

For small values of ω^2, *provided that the substructures affected can support the static loads* P, the value of ϵ_{ij} is approximated by

$$\epsilon_{ij} \sim \delta_{ij} \tag{5}$$

On the other hand, when the structure cannot support the static load P, the inertial forces must be considered instead. For instance, in the case in which one of the substructures is a mass concentrated at a point, then

$$\epsilon \sim -(1/m\omega^2) \tag{6}$$

A similar approximation for any free body can be made.

In general, ϵ_{ij} is a function of ω^2, which will be zero when an oscillating force of frequency ω_k applied at l will give a zero displacement at j and which will be infinite when ω^2 corresponds to a natural frequency Ω_k of a substructure affected by P_l. This, together with the preceding statements, suggests[1] the following forms for ϵ:

$$\epsilon_{ij} = \delta_{ij} \frac{[1 - (\omega^2/\omega_1^2)][1 - (\omega^2/\omega_2^2]}{[1 - (\omega^2/\Omega_1^2][1 - (\omega^2/\Omega_2^2)]\ldots.} \tag{5a}$$

$$\epsilon_{ij} = -\frac{1}{m\omega^2} \frac{[1 - (\omega^2/\omega_1^2)][1 - (\omega^2/\omega_2^2)]\ldots.}{[1 - (\omega^2/\Omega_1^2)][1 - (\omega^2/\Omega_2^2)]\ldots.} \tag{6a}$$

It must be understood that some of the natural frequencies ω_j or Ω_j may coincide so that several of the factors may be identical. In general, however, for simple continuous systems it will be assumed that apart from the zero frequencies the natural frequencies Ω_j will be distinct among themselves as will ω_j.

The function ϵ_{ij} or one that is proportional to it is referred to in the mathematical literature as the "resolvent kernel." For a mechanical system of a finite number n of degrees of freedom, it can be shown that ϵ is a rational function of ω^2 of degree $n - 1$ in the numerator and of degree n in the denominator. From this fact, knowing the number of frequencies which such a system can have, it follows that ϵ must have the form given in Eqs. (5a) or (6a).

In the case of the continuous systems such as occur in practice, these may be approximated by finite systems as closely as one desires. From this it follows that the functions ϵ take the form above also for continuous systems.

Examples

As a first example of a simple system but one with a wide application, consider a point mass m attached at a point 0 to an elastic structure, such as a beam, which is itself fastened to a rigid support (Fig. 2).

Let

ϵ' = displacement of the mass upward due to unit harmonic load upward

ϵ'' = displacement of the beam downward due to unit harmonic load downward

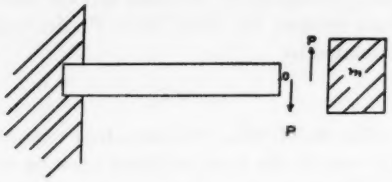

FIG. 2. Mass suspended on a beam.

δ = displacement of the beam per unit static force applied at 0

Then

$$\epsilon = \epsilon' + \epsilon''$$

$$\epsilon' = -(1/m\omega^2)$$

$$\epsilon'' = \delta \frac{[1 - (\omega^2/\omega_1^2)][1 - (\omega^2/\omega_2^2)] \ldots .}{[1 - (\omega^2/\Omega_1^2)][1 - (\omega^2/\Omega_2^2)] \ldots .}$$

Let

$$\omega_0^2 = 1/m\delta$$

The significance of $\omega_1, \omega_2, \ldots .$ is readily established. These are the natural frequencies of the beam when pinned at the point 0. The lowest of these is larger than the lowest natural frequencies Ω_1 of the beam vibrating freely. Therefore, for frequencies ω that are less than Ω_1, an approximation to ϵ'' is

$$\epsilon'' = \delta/[1 - (\omega^2/\Omega_1^2)]$$

The equation of continuity, Eq. (4a), becomes

$$\epsilon' + \epsilon'' = -(1/m\omega^2) + \delta/[1 - (\omega^2/\Omega_1^2)] = 0 \qquad (7)$$

This gives up on simplification the following equation:

$$1/\omega^2 = (1/\omega_0^2) + (1/\Omega_1^2) \qquad (8)$$

Eq. (8) yields the lowest natural frequency of the composite system. On the other hand, if it is desired to obtain higher frequencies, the approximation made above for ϵ'' is no longer valid. The solution of Eq. (7) can then be determined graphically (Fig. 3).

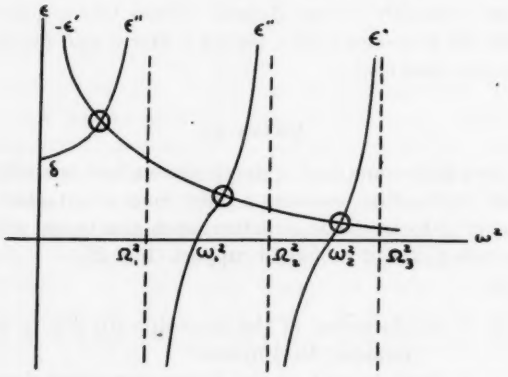

FIG. 3. Graphic solution of frequency equation.

In this way, a rapid evaluation of the effect of concentrated weights upon elastic structures can be made. For instance, the reduction of wing frequencies due to engine weights or gas loads may be readily determined. The effect of shock mounting of the power plant is easily ascertained.

One particular case may be cited. Two vibrators of different mass (Fig. 4) were mounted on the trailing edge of an irreversible tab, and the following data were recorded in the vibration tests:

Vibrator	Mass of Vibrator (Slugs)	Frequency ω (Rad. per Sec.)
#1	0.057	178
#2	0.096	144

The natural frequency Ω_1 of the tab was then obtained by solving the following two equations (see Eq. (8)) and the definition of ω_0^2 above):

$$1/178^2 = 0.057\delta + (1/\Omega_1^2)$$

$$1/144^2 = 0.096\delta + (1/\Omega_1^2)$$

The result was

$$\Omega_1 = 396 \text{ rad. per sec.} = 3{,}800 \text{ c.p.m.}$$

$$1/\delta = 2{,}290 \text{ lbs. per ft.} = 191 \text{ lbs. per in.}$$

The second result agreed well with the results of static deflection tests under low load.

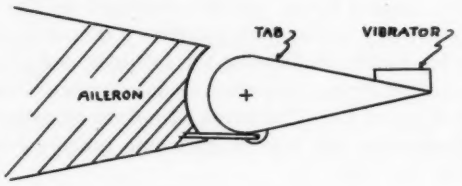

FIG. 4. Vibration of aileron tab.

Another example of interest occurs in the analysis of the double boom and tail system shown schematically in Fig. 5a. Assume that the tail is pin-connected to the boom. Other cases can be treated in a similar fashion, although with increased complexity. It is required to calculate the lower frequencies of the system involving bending perpendicular to the plane of Fig. 5a.

Write the relative displacement (Fig. 5b) of the boom relative to the tail in the form

$$\epsilon = \epsilon' + \epsilon''$$

where ϵ' = displacement of the boom and ϵ'' = displacement of the tail. In addition, let

k = stiffness of one boom at the tail attachment point

m = mass of the tail group

$\omega_0^2 = 2k/m$

ρ = radius of gyration of the tail group in rotation about its c.g. with reference to an axis in the fore-and-aft direction

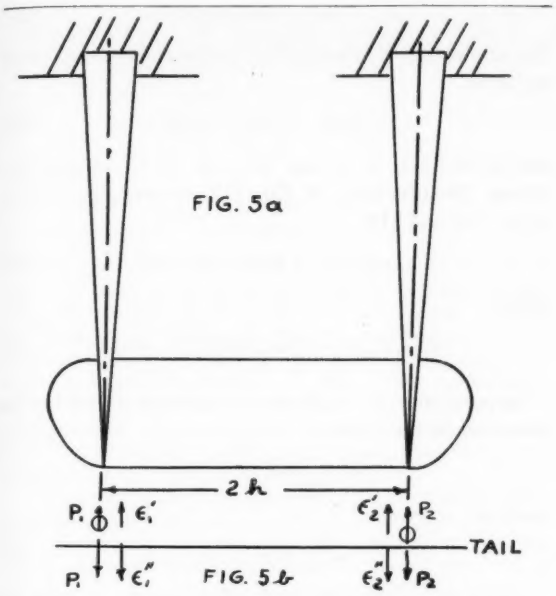

FIGS. 5a and 5b. Schematic diagram of double boom and tail system.

ω_b = lowest natural frequency of the boom in bending

Ω = lowest natural frequency of the horizontal tail in bending

Then in the terminology introduced above

$$\epsilon_{11}' = \epsilon_{22}' \sim 1/k[1 - (\omega^2/\omega_b^2)]$$

where only the first bending frequency of the boom is shown explicitly, the other terms being approximated by unity.

$$\epsilon_{12}' = \epsilon_{21}' = 0$$

Assume first that the horizontal tail is rigid. Then

$$\epsilon_{11}'' = \epsilon_{22}'' = -[1 + (h/\rho)^2]/m\omega^2$$
$$\epsilon_{12}'' = \epsilon_{21}'' = -[1 - (h/\rho)^2]/m\omega^2$$

The determinantal Eq. (4a) takes the form

$$0 = \begin{vmatrix} \epsilon_{11} & \epsilon_{21} \\ \epsilon_{12} & \epsilon_{22} \end{vmatrix} = \epsilon_{11}^2 - \epsilon_{21}^2$$

This gives

$$\epsilon_{11} = \pm\epsilon_{12} = \epsilon_{22} = \pm\epsilon_{21}$$

Substitution into Eq. (4) gives for the minus sign

$$P_1 - P_2 = 0 \qquad \text{(symmetrical boom-bending)}$$

and for the plus sign

$$P_1 + P_2 = 0 \qquad \text{(antisymmetrical boom-bending)}$$

Finally, substituting the expressions for ϵ_{ij} and simplifying the resulting equations,

$$1/\omega^2 = 1/\omega_b^2 + 1/\omega_0^2 \text{ (symmetrical bending)}$$

$$1/\omega^2 = 1/\omega_b^2 + 1/\omega_0^2(\rho/h)^2 \text{ (antisymmetrical bending)}$$

Now consider the modifications that are to be made for a nonrigid tail.

$$\epsilon_{11}'' = \epsilon_{22}'' = -\frac{1 + (h/\rho)^2}{m\omega^2} \frac{[1 - (\omega^2/\omega_1^2)] \ldots .}{[1 - (\omega^2/\Omega_1^2)] \ldots .}$$

$$\epsilon_{12}'' = \epsilon_{21}'' = -\frac{1 - (h/\rho)^2}{m\omega^2} \frac{[1 - (\omega^2/\tilde{\omega}_1^2)] \ldots .}{[1 - (\omega^2/\Omega_1^2)] \ldots .}$$

where

ω_1 = frequency of the tail when pinned only at one point of support

$\tilde{\omega}_1$ = frequency at which the deflection of the tail at one point of support is zero when the tail is vibrated at the other point of support

The restriction to small frequencies will now be made. The factors not shown explicitly can be replaced by unity. Proceeding as before, the equations $\epsilon_{11} = \pm\epsilon_{12}$ take the form upon simplification

$$\frac{1}{\omega^2} = \frac{1}{\omega_b^2} + \frac{1}{\omega_0^2} \frac{1 - (\omega^2/\Omega_1^2)}{1 - (\omega^2/\mu_2^2)} \qquad \text{(symmetrical bending)} \tag{9}$$

$$\frac{1}{\omega^2} = \frac{1}{\omega_b^2} + \frac{1}{\omega_0^2} \frac{1 - (\omega^2/\Omega_1^2)}{1 - (\omega^2/\mu_1^2)} \left(\frac{\rho}{h}\right)^2 \qquad \text{(unsymmetrical bending)}$$

The quantities μ_1^2 and μ_2^2 are defined by

$$\frac{1}{\mu_1^2} = \frac{(\rho/h)^2 + 1}{2\omega_1^2} - \frac{(\rho/h)^2 - 1}{2\tilde{\omega}_1^2}$$

$$\frac{1}{\mu_2^2} = \frac{(\rho/h)^2 + 1}{2\omega_1^2} + \frac{(\rho/h)^2 - 1}{2\tilde{\omega}_1^2}$$

The frequencies ω_1 and $\tilde{\omega}_1$ may be estimated according to the Rayleigh-Ritz method and ω determined from Eq. (9) either by algebraic or graphic means. By reference to Eq. (4) as shown above, the forces of interaction P for each ω can be determined up to a factor of proportionality. Finally, the analysis of the substructures, the tail and booms, under the loads P will furnish the mode corresponding to the natural frequency ω selected.

Forced Oscillations

The preceding discussion has been concerned primarily with the determination of the natural frequencies. It is clear that Eq. (4) may be used also for the calculation of forced oscillations.

Addendum

The reader who is familiar with the mathematical theory of integral equations[2] will see that the quantity ϵ is essentially the resolvent kernel.[3] To show this in some detail, as well as to obtain an interesting relation between the natural modes and frequencies, let us suppose that the basic equation governing the vibration of a structure can be put into the form

$$L[u] - \lambda\rho u = 0 \tag{10}$$

Here u represents the deflection of the system at some point, ρ represents the local density (always positive), and λ represents the square ω^2 of the frequency. The letter L signifies a linear operation as, for instance, in the theory of transverse oscillations of a beam where

$$L[u] \equiv (d^2/ds^2)[EI(d^2u/ds^2)] \tag{10a}$$

in which s represents a point on the beam.

Assume now that the structure is such that it can support any static load. Let s and t represent points of the structure and let

φ_i = natural mode of vibration (assumed normalized)

λ_i = square of the natural frequency ω_i corresponding to φ_i

k = influence function corresponding to $L[u]$

Then from the definition of φ_i and λ_i

$$L[\varphi_i] = \lambda_i\rho\varphi_i \tag{11}$$

and from the definition of k, the equation

$$L[u] = f \tag{12}$$

can be solved for u according to

$$u(s) = \int k(s, t)f(t)dt \tag{13}$$

Applying Eq. (13) to the inversion of Eq. (11),

$$\varphi_i(s) = \lambda_i \int k(s, t)\varphi_i(t)\rho(t)dt$$

Multiplying through by $\sqrt{\rho(s)}$ and rearranging the right side,

$$\sqrt{\rho(s)}\,\varphi_i(s) = \lambda_i \int \{\sqrt{\rho(s)\rho(t)}k(s, t)\}\sqrt{\rho(t)}\varphi_i(t)dt \tag{14}$$

From this, it follows that the symmetric kernel $\sqrt{\rho(s)\rho(t)}k(s, t)$ has the characteristic functions[2] $\sqrt{\rho(s)}\varphi_i(s)$. Moreover, it is clear that all characteristic functions will be so obtained. Now, since the functions φ_i have been normalized according to

$$\int [\sqrt{\rho(s)}\varphi_i(s)]^2 ds = \int \varphi_i^2(s)\rho(s)ds = 1 \tag{15}$$

it follows from Mercer's theorem that

$$\sqrt{\rho(s)\rho(t)}k(s, t) = \Sigma[\sqrt{\rho(s)\rho(t)}\varphi_i(s)\varphi_i(t)]/\lambda_i$$

Upon cancellation of the positive factor $\sqrt{\rho(s)\rho(t)}$,

$$k(s, t) = \Sigma\varphi_i(s)\varphi_i(t)/\lambda_i \tag{16}$$

Now apply the result to the equation defining a forced vibration

$$L[u] - \lambda\rho u = f \tag{17}$$

The modes and characteristic numbers of the associated equation

$$L[u] - \lambda\rho u = \lambda'\rho u \tag{18}$$

are given by $u = \varphi_i$ and $\lambda' = \lambda_i - \lambda$, respectively. Hence the inversion of Eq. (17) is now, paralleling Eqs. (13) and (16),

$$u(s) = \int K(s, t; \lambda)f(t)dt \tag{19}$$

where

$$K(s, t; \lambda) = \sum_i \varphi_i(s)\varphi_i(t)/(\lambda_i - \lambda) \tag{20}$$

In particular, if f is chosen to represent a unit forcing function at the point t,

$$u(s) = K(s, t; \lambda)$$

so that

$$\epsilon_{is} = K(s, t; \lambda) \tag{21}$$

Let t and s coincide and substitute for ϵ from Eq. (5a) and K from Eq. (20), letting $\lambda = \omega^2$, $\Lambda_n = \Omega_n^2$ and replacing λ_i in Eq. (20) by Λ_i to make the notation consistent.

$$\delta_{ss}\frac{\prod_n [1 - \prod (\lambda/\lambda_n)]}{\prod_n [1 - (\lambda/\Lambda_n)]} = \sum_n \frac{\varphi_n^2(s)}{\Lambda_n - \lambda} \tag{22}$$

The right side is the partial-fraction decomposition of the left. Comparing the mth term,

$$\varphi_m^2(s) = \delta_{ss}\frac{\Lambda_m \prod_n [1 - (\Lambda_m/\lambda_n)]}{\prod_{n \neq m} [1 - (\Lambda_m/\Lambda_n)]} \tag{23}$$

The product in the denominator is to be extended over all n different from m. Of course, λ_n is a function of s.

References

[1] Biot, M., *Coupled Oscillations of Aircraft Engine-Propeller Systems*, Journal of the Aeronautical Sciences, Vol. 7, No. 9, pp. 376–382, July, 1940. See also: Duncan, W. J., *Notes on Biot's Dynamic Modulus*, Journal of The Royal Aeronautical Society, Vol. 45, pp. 225–227, June, 1941.

[2] Courant and Hilbert, *Methoden der Mathematischen Physik*, Vol. 1, Chap. III; Interscience Publications, Inc., New York (Berlin, 1931).

[3] Saibel, Edward, *Vibration Frequencies of Continuous Beams*, Journal of the Aeronautical Sciences, Vol. 11, No. 1, pp. 88–90, January, 1944.

Airfoil Theory for Flows of Variable Velocity

RUFUS ISAACS*

United Aircraft Corporation

SUMMARY

In many cases of aircraft practice—notably that of the rotating wing—the lift surfaces are in air streams of variable velocity. There are two resulting effects that are excluded from a direct application of the usual airfoil formulas. One arises from the continuous wake of vortexes which are shed from the trailing edge with each change of circulation; the other, from the impulsive pressure because the air masses are accelerating. The purpose of this paper is to study this aerodynamic problem, taking into account these effects with a certain but sufficient degree of approximation.

The first section deals with the general problem of an airfoil at constant angle of attack but with a variable stream velocity. The main result is an integro-differential relation between the velocity and circulation which is true for general flows. It is given in two forms: the realistic, where the airfoil is assumed at some time to have started from rest; and the periodic, where the flow is periodic.

The second section is a complete solution to the important practical case: velocity = constant + sinusoidal variation.

In the third section the lift is calculated. In particular, an explicit formula is given for the case of the second section in the form of a Fourier series. The moment is not evaluated since the technique is similar.

Finally, the solution to a numerical example is given.

GENERAL THEORY

THE CIRCUMSTANCE to be covered will be that of an airfoil in a stream whose velocity is of variable magnitude but the angle of attack is constant. The case where the angle of attack is also varying—which is undeniably of importance in rotary wing aircraft—requires certain additions to the calculations which are not undertaken in the present paper. The procedure, however, is entirely similar.

In most of the existing treatments of this topic the objects of concern are first order effects that are useful for such questions as criteria of aerodynamic stability. In rotary wing aircraft, however, the variations of the stream velocity are certainly not of small order compared with the mean velocity.†

The two-dimensional approach for a helicopter problem leads to deviations from reality with respect to the position of the wake. But as most of the wake effects arise from that part of it near the airfoil, the errors should not be serious. This is especially true if the present results are regarded as corrections to the elementary two-dimensional theory or, better, a new theory of this type on which three-dimensional theories may later be based. An attempt to maintain the present level of detail for the actual wake—a sort of distorted helix—would involve hopeless complications.

The object of this section shall be to obtain the relationship between the stream velocity $w(t)$ and circulation $\Gamma(t)$ of an airfoil in a stream approaching from the left at the small but constant angle of attack α. The usual assumptions are made: two-dimensional flat plate airfoil; the continuous wake of trailing vortexes travel downstream with velocity w but remain in the plane of the plate; the Kutta condition is always satisfied.

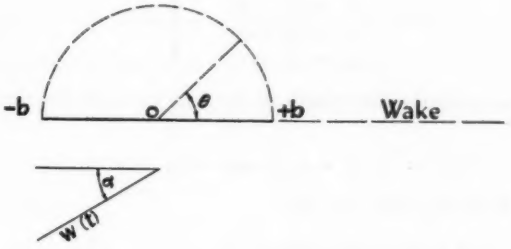

Instead of w it is convenient to work with $W(t)$ taken so that $W' = w$. In cartesian coordinates let the plate be: $-b \leqslant x \leqslant b, y = 0$. Then the upward vertical air velocity on the plate is

$$v = \alpha w + v_T(x, t) \tag{1}$$

where v_T is the velocity induced by the continuous sheet of trailing vortexes in the wake. As at time τ the plate shed a vortex of strength $-\Gamma'(\tau)d\tau$,

$$v_T = -\frac{1}{2\pi}\int_{-\infty}^{t} \frac{\Gamma'(\tau)d\tau}{(b - x) + (W(t) - W(\tau))} \tag{2}$$

It is advisable to erect a semicircle on the plate and use the angular coordinate θ: $x = b \cos\theta$. Then

$$v_T = -(1/2\pi b)\int_{-\infty}^{t} \Gamma'(\tau)d\tau/(a - \cos\theta) \tag{3}$$

where, for brevity,

$$a = 1 + (W(t) - W(\tau))/b \geqslant 1 \tag{4}$$

To expand Eq. (3) in a Fourier series, put

$$1/(a - \cos\theta) = (\gamma_0/2) + \Sigma\, \gamma_n \cos n\theta \tag{5}$$

Then, from an integral evaluation in Appendix I,

$$\gamma_n = 2(a - \sqrt{a^2 - 1})^n/\sqrt{a^2 - 1}$$

Presented at the Aerodynamics Session, Twelfth Annual Meeting, I.A.S., New York, January 25–27, 1944.

* Senior Analytical Engineer, Hamilton Standard Propellers Division.

† For stations sufficiently near the hub the variations are greater than the mean. This case involves reversed flow over an airfoil and is not amenable to existing methods.

and so, if the validity of termwise integration is assumed,

$$v_T = {}^1/_2 b_0(t) + \Sigma b_n(t) \cos n\theta \tag{6}$$

with

$$b_n = -\frac{1}{\pi b}\int_{-\infty}^{t} \Gamma'(\tau)\frac{(a - \sqrt{a^2 - 1})^n}{\sqrt{a^2 - 1}}d\tau \tag{7}$$

If the plate is considered as a bound vortex system of strength $\gamma(\theta, t)$, the downward velocity arising at the point of angular coordinate θ is, after integrating the vortex effect over the plate,

$$v_B = 1/2\pi\int_0^\pi [r(\phi, t) \sin \phi/(\cos\theta - \cos\phi)]d\phi \tag{8}$$

Putting

$$\gamma(\theta, t) \sin\theta = c_0(t) + \Sigma c_n(t) \cos n\theta$$

and

$$v_B = {}^1/_2 d_0(t) + \Sigma d_n(t) \cos n\theta$$

from Appendix I and a sequence of easy trigonometrical identities, it follows

$$\left.\begin{aligned} c_1 &= d_2 - d_0 \\ c_2 &= d_3 - d_1 \\ c_3 &= d_4 - d_2, \ldots \end{aligned}\right\} \tag{9}$$

The condition that there be no flow through the plate is

$$v = v_T + \alpha w = v_B$$

or from Eqs. (6) and (9)

$$\left.\begin{aligned} c_1 &= b_2 - b_0 - 2\alpha w \\ c_n &= b_{n+1} - b_{n-1} \ (n = 2, 3, 4, \ldots) \end{aligned}\right\} \tag{10}$$

The Kutta condition implies a finite γ at the trailing edge or

$$(c_0 + \Sigma c_n \cos n\theta)/\sin\theta$$

is finite for $\theta = 0$, which means

$$c_0 = -(c_1 + c_2 + \ldots) \tag{11}$$

From Eq. (10) and the fact that, as Fourier coefficients, $b_n \to 0$,

$$c_0 = 2\alpha w + b_0 + b_1 \tag{12}$$

Also

$$\Gamma(t) = \int_{-b}^{b} \gamma \, dx = b\int_0^\pi \gamma(\theta, t) \sin\theta d\theta = b\pi c_0$$

so that from Eqs. (12) and (7)

$$\Gamma = 2b\pi\alpha w - \int_{-\infty}^{t} \Gamma'(\tau)\frac{1 + a - \sqrt{a^2 - 1}}{\sqrt{a^2 - 1}}\,d\tau$$

$$= 2b\pi\alpha w - \int_{-\infty}^{t} \Gamma'(\tau)\left[\sqrt{\frac{a+1}{a-1}} - 1\right]d\tau$$

From the conservation of angular momentum

$$\Gamma(t) = \int_{-\infty}^{t} \Gamma'(\tau)d\tau \tag{13}$$

and so, using Eq. (4),

$$hW' = \int_{-\infty}^{t} \Gamma'(\tau)\sqrt{\frac{2b}{W(t) - W(\tau)} + 1}\,d\tau$$

$$= \int_0^\infty \Gamma'(t - \lambda)\sqrt{\frac{2b}{W(t) - W(t - \lambda)} + 1}\,d\lambda \tag{14}$$

where $h = 2b\pi\alpha = (2b)^1/_2 C_L)$. Eq. (14) is the sought relationship between velocity and circulation.

To bring Eq. (14) to a more manageable form, W can be used as independent variable instead of t. (W is steadily increasing because $w > 0$ by hypothesis.) Suppose Γ expressed in terms of W:

$$\Gamma = Q(W)$$

In the integral of Eq. (14) the new variable of integration X will be connected to λ by

$$X = W(t - \lambda)$$

whence $\Gamma(t - \lambda) = Q(X)$ and Eq. (14) becomes

$$hW'(t) = \int_{-\infty}^{W} Q'(X)\sqrt{[(2b)/(W - X)] + 1}\,dX$$

$$= \int_0^\infty Q'(W - \lambda)\sqrt{(2b/\lambda) + 1}\,d\lambda \tag{15}$$

If Q is given, Eq. (15) is a differential equation for W. If W is given, elimination of t from W' and W gives W' as a function of W, and Eq. (15) is an integral equation for the function Q.

The integral in Eq. (15) is of the form that appears in nonsteady airfoil problems with a uniform stream velocity.

If W is periodic, the integrals of both Eq. (14) and Eq. (15) diverge. The reason is the violation of Eq. (13). In this case we must use in place of Eq. (15)

$$hW' = Q(W) + \int_0^\infty Q'(W - \lambda)\left[\sqrt{\frac{2b}{\lambda} + 1} - 1\right]d\lambda \tag{16}$$

the integral now converging by Chartier's test (reference 3, page 78), and a similar replacement can be made for Eq. (14). The terms *realistic* and *periodic forms* will be used for these cases.

The Case of Rotary Wing Aircraft

Now will be studied the particular velocity

$$w = w_0(1 + \sigma \sin\omega t), \ |\sigma| < 1$$

or

$$W = w_0\left(t - \frac{\sigma}{\omega}\cos\omega t\right)$$

The solution Γ will then have period $2\pi/\omega$, and Q will be periodic. Thus, for some positive μ and a series of complex a_n,

$$Q(x) = \sum_{-\infty}^{\infty} a_n e^{in\mu x} \tag{17}$$

and as Q is to be real

$$a_{-n} = \bar{a}_n$$

Inserting this in Eq. (16),

$$W' = h^{-1}\sum a_n e^{in\mu W}\{1 + in\mu\int_0^\infty e^{-in\mu\lambda}[\sqrt{(2b/\lambda) + 1} - 1]d\lambda\}$$

$$= \sum A_n e^{in\mu W} \tag{18}$$

where

$$A_n = (a_n/h)R_n$$

and

$$R_0 = 1$$
$$R_n = \psi(nb\,\mu) \qquad (n = 1, 2, \ldots)$$

with

$$\psi(x) = 1 + i\int_0^\infty e^{-i\lambda}[\sqrt{(2x/\lambda) + 1} - 1]d\lambda \tag{19}$$

while from reality considerations

$$R_{-n} = \bar{R}_n$$

To make the right-hand side of Eq. (18), like the left, have period $2\pi/\omega$, μ is taken to be ω/w_0. Then $b\mu = b\omega/w_0 = k$, the reduced frequency. Eq. (18) becomes

$$w_0(1 + \sigma \sin\tau) = \sum A_n e^{in(\tau - \sigma\cos\tau)} \tag{20}$$

where for brevity $\tau = \omega t$. The problem is now to determine the A_n so as to make Eq. (20) an identity. To do this, note for any integer m

$$\int_0^{2\pi}(1 + \sigma\sin\tau)e^{im(\tau - \sigma\cos\tau)}d\tau = \int_{-\sigma}^{2\pi-\sigma} e^{im\lambda}d\lambda = \begin{cases} 0 (m \neq 0) \\ 2\pi (m = 0) \end{cases}$$

Then multiplying both sides of Eq. (20) by $(1 + \sigma\sin\tau)e^{-im(\tau-\sigma\cos\tau)}$ and integrating from 0 to 2π yields at once,

$$A_n = w_0/2\pi\int_0^{2\pi}(1 + \sigma\sin\tau)^2 e^{-in(\tau-\sigma\cos\tau)}\,d\tau$$

If $n \neq 0$, an integration by parts, gives

$$A_n = -\frac{i\sigma w_0}{2\pi n}\int_0^{2\pi}\cos\tau e^{-in(\tau-\sigma\cos\tau)}d\tau$$

$$= \frac{i^n\sigma w_0}{2n}[J_{n+1}(n\sigma) - J_{n-1}(n\sigma)] \tag{21}$$

(see reference 1, page 149), while

$$A_0 = w_0/2\pi\int_0^{2\pi}(1 + \sigma^2\sin^2\tau)d\tau = w_0[1 + (\sigma^2/2)] \tag{22}$$

Thus A_n is known, and, as the function ψ can be expressed in terms of Hankel functions, the aerodynamic problem for this case is completely solved.

Calculation of the Lift

From known aerodynamic theory, the lift L consists of two parts:

$$L = L_I + L_J$$

where L_J, the "Joukowsky" lift, equals $\rho w\Gamma$ and L_I, the "impulsive pressure" lift, equals

$$\rho\frac{d}{dt}\int_{-b}^{b}\gamma(x, t)(b - x)dx$$

The latter integral I is

$$I = b\Gamma - b^2\int_0^\pi \gamma(\phi, t)\sin\phi\cos\phi\,d\phi$$
$$= b\Gamma - b^2(\pi/2)c_1$$

whence, from Eqs. (10) and (7),

$$I = b\Gamma + \pi b^2\alpha w - b\int_{-\infty}^{t}\Gamma'(\tau)[a - \sqrt{a^2 - 1}]d\tau^* \tag{23}$$

Using Eq. (4) and the same type transformation as in passing from Eqs. (14) and (15)

$$I = bQ(W) + \pi b^2\alpha w - b\int_0^\infty Q'(W - \lambda)\times [1 + (\lambda/b) - \sqrt{[1 + (\lambda/b)]^2 - 1}]d\lambda^* \tag{24}$$

From Eq. (24) is obtained a general expression for the lift which is a companion to the general result of the first section. But the practical case of the second section will be considered, and in terms of Eq. (17)

$$I = \pi b^2\alpha w + b\sum a_n[1 - iS_n]e^{inkW/b} \tag{25}$$

where k, as before, is $b\omega/w_0$ and where

$$S_n = \xi(nk) \quad (n \neq 0)$$
$$S_0 = 0$$
$$\xi(x) = \int_0^\infty e^{-i\lambda}[1 + (\lambda/x) - \sqrt{[1 + (\lambda/x)]^2 - 1}]d\lambda$$

Then

$$L = \rho w\sum a_n[1 + nk(S_n + i)]e^{inkW/b} + \rho b^2\pi\alpha w' \tag{26}$$

In Eq. (26), if a_n is replaced by $A_n h/R_n$, the following function of nk is encountered:

$$[1 + nk(S_n + i)]/R_n = \begin{cases} 1 & (n = 0) \\ C(nk) & (n > 0) \end{cases}$$

where

$$C(x) = \{1 + x[\xi(x) + i]\}/\psi(x).$$

In Appendix II it is shown that $C(x)$ is the Theodorsen function[2] for $x > 0$:

$$C(x) = \frac{H_1^{(2)}(x)}{H_1^{(2)}(x) + iH_0^{(2)}(x)} = F(x) + iG(x) \tag{27}$$

whose values are known.† From reality considerations

$$C(-x) = \overline{C(x)}$$

For the flat plate airfoil

$$\pi\alpha = {}^1/_2 C_L$$

* This is in the periodic form. To bring Eq. (23) to the realistic form replace the first a in the bracket by its expression Eq (4). The first summand of the bracket is now 1, and when integrated it leads, by Eq. (13), to a term $-b\Gamma$, which cancels with the first term on the right in Eq. (23).

† Theodorsen's tabulation is incorrect for $x \leqslant 0.1$. A table computed by the author is given in Appendix III.

Put

$$L_0 = {}^1/_2 C_L \rho w_0^2 (2b)$$

i.e., the lift arising from w_0 alone. Then Eq. (26) can be written, using Eq. (22):

$$L = L_0\left[\left(1+\frac{\sigma^2}{2}\right)(1+\sigma\sin\tau)+\frac{\sigma k\cos\tau}{2}-\frac{i}{w_0}\frac{d}{d\tau}\sum_{n\neq 0}\frac{A_n C(nk)}{n}e^{in(\tau-\sigma\cos\tau)}\right] \quad (28)$$

It remains to arrange this result as a Fourier series. Setting the last term of the bracket equal to

$$\sigma\sum_1^\infty (l_m\cos m\tau + l_m'\sin m\tau)$$

there results

$$l_m + il_m' = -\frac{i}{\pi\sigma w_0}\sum_{n\neq 0}\frac{A_n C(nk)}{n}\int_0^{2\pi} e^{im\tau}\frac{d}{d\tau}e^{in(\tau-\sigma\cos\tau)}\,d\tau$$

$$= -m(-i)^m\sum_1^\infty \frac{J_{n+1}(n\sigma)-J_{n-1}(n\sigma)}{n^2}\times$$

$$[C(nk)J_{n+m}(n\sigma) - \overline{C(nk)}J_{n-m}(n\sigma)]$$

The second line follows from Eq. (25) and the same integral value of the Bessel functions as previously used.

Thus, finally,

$$L = L_0\left[\left(1+\frac{\sigma^2}{2}\right)+\sigma\left(l_1+\frac{k}{2}\right)\cos\omega t+\sigma\left(l_1'+1+\frac{\sigma^2}{2}\right)\times \sin\omega t+\sigma\sum_1^\infty (l_m\cos m\omega t + l_m'\sin m\omega t)\right] \quad (29)$$

where

$$l_m + il_m' = -m(-i)^m\sum_1^\infty\{F_n[J_{n+m}(n\sigma)-J_{n-m}(n\sigma)]+ iG_n(J_{n+m}(n\sigma)+J_{n-m}(n\sigma))\} \quad (30)$$

and

$$\left.\begin{matrix}F_n\\G_n\end{matrix}\right\} = \frac{J_{n+1}(n\sigma)-J_{n-1}(n\sigma)}{n^2}\left\{\begin{matrix}F(nk)\\G(nk)\end{matrix}\right. \quad (31)$$

In conclusion, the elementary lift is computed for comparison. This means the lift merely proportional to the square of the velocity, where the wake and impulsive pressures are neglected.

Calling it L_E,

$$L_E = L_0(1+\sigma\sin\omega t)^2 = L_0\left[\left(1+\frac{\sigma^2}{2}\right)+2\sigma\sin\omega t-\frac{\sigma^2}{2}\cos 2\omega t\right] \quad (32)$$

Note that the mean value is the same in the two cases.

References

[1] Jahnke and Emde, *Funktiontafeln mit formeln und kurven*, 3rd Edition (Leipzig, 1938); Dover Publication, Inc., New York 1944.

[2] Theodorsen, Theodore, *General Theory of Aerodynamic Instability and the Mechanism of Flutter*, N.A.C.A. Report No. 496, 1934.

[3] Whittaker, Edmond T., and Watson, G. N., *Course of Modern Analysis*, 4th Edition; The Macmillan Company, New York, 1928.

Appendix I

To evaluate certain Fourier coefficients, the integral evaluation is required:

$$\int_0^\pi \frac{\cos n\theta}{a-\cos\theta}d\theta = \begin{cases} -\dfrac{\pi\sin n\phi}{\sin\phi} & \text{if } -1<a<1 \text{ and } \cos\phi = a \\ \pi\dfrac{(a-\sqrt{a^2-1})^n}{\sqrt{a^2-1}} & \text{if } a>1 \end{cases}$$

This can be proved by taking

$$2i\int[z^n/(z^2-2az+1)]dz$$

around the unit circle in the z-plane and then putting $z = re^{i\theta}$. If $|a|<1$, the integrand will have two poles on the circle so that indentation is required. In fact, in this case the integral is improper and we obtain its Cauchy value. For $|a|>1$ there will be one pole within and one without the contour, and an evaluation of the residue gives the result.

Appendix II

Here will be shown

$$\frac{1+x[\xi(x)+i]}{\psi(x)} = \frac{H_1^{(2)}(x)}{H_1^{(2)}(x)+iH_0^{(2)}(x)} \quad (x>0) \quad (1)$$

The expression on the left is

$$\frac{1+ix+x^2\int_0^\infty e^{-itx}[1+t-\sqrt{t^2+2t}]dt}{1+ix\int_0^\infty e^{-itx}\left[\sqrt{\frac{2}{t}+1}-1\right]dt} \quad (2)$$

Hankel's integrals yield (reference 1, page 151) for $R[k]>0$

$$H_1^{(2)}(x) = k^{3/2}\frac{2}{\pi}e^{-i(x-3/4\pi)}x\int_0^\infty e^{-ktx}\sqrt{-ikt^2+2t}\,dt \quad (3)$$

$$H_0^{(2)}(x) = k^{1/2}\frac{2}{\pi}e^{-i[x-(\pi/4)]}\int_0^\infty e^{-ktx}\frac{dt}{\sqrt{-ikt^2+2t}} \quad (4)$$

When $k=i$, the integral of Eq. (4) converges. Further as $k\to i$ along, say, a horizontal line, it is easy to show that Eq. (4) is continuous, so that

$$H_0^{(2)}(x) = i\left(\frac{2}{\pi}\right)e^{-tx}\int^\infty e^{-itx}\frac{dt}{\sqrt{t^2+2t}} \quad (5)$$

Here the radical has a nonnegative value, which computation of a particular point shows is correct.

To treat Eq. (3): if $R[k] > 0$,

$$\int_0^\infty e^{-kxt}(1+t)dt = (1/kx) + (1/(kx)^2)$$

and so

$$\frac{1}{kx} + \frac{1}{(kx)^2} - \frac{1}{k^{3/2}x}\frac{\pi}{2}e^{i[x-(3\pi/4)]}H_1^{(2)}(x) = \int_0^\infty e^{-kxt}[1+t-\sqrt{-ikt^2+2t}]dt$$

The integral on the right now converges for $k = i$, and it is possible to show that it is a continuous function of k on a closed horizontal segment emanating to the right from i.

Thus, after verifying sign values by a particular case,

$$-\frac{i}{x} - \frac{1}{x^2} - \frac{i}{x}\frac{\pi}{2}e^{ix}H_1^{(2)}(x) = \int_0^\infty e^{-ixt}[1+t-\sqrt{t^2+2t}]dt \quad (6)$$

Another form is obtained by partial integration:

$$x\left(\frac{\pi}{2}\right)e^{ix}H_1^{(2)}(x) = x\int_0^\infty e^{-ixt}\left[1-\frac{t+1}{\sqrt{t^2+2t}}\right]dt + i \quad (7)$$

Substituting the values of the H from Eqs. (5), (6), and (7) in the right side of Eq. (1) gives our result.

Appendix III

Values of $C(x) = F + iG$ are as follows:

x	$F(x)$	$-G(x)$
0	1	0
0.02	0.963	0.0751
0.04	0.928	0.1140
0.06	0.892	0.1422
0.08	0.860	0.1601
0.1	0.831	0.1720
0.15	0.773	0.1870
0.2	0.728	0.1888
0.25	0.693	0.1857
0.3	0.665	0.1793
0.35	0.643	0.1722
0.4	0.624	0.1650

A Numerical Example

The following is typical of current heliocopter practice: $k = 0.0424$; $\sigma = 0.4$. Then

$$L/L_0 = 1.08 - 0.0376\cos\omega t + 0.770\sin\omega t - 0.0790\cos 2\omega t - 0.00697\sin 2\omega t - 0.00061\cos 3\omega t - 0.0050\sin 3\omega t - 0.00003\cos 4\omega t + 0.000042\sin 4\omega t + \ldots.$$

while

$$L_E/L_0 = 1.08 + 0.8\sin\omega t - 0.08\cos 2\omega t$$

so that for this case the effects herein considered are not large.

(*Continued from page 102*)

[5] Diehl, W., *Engineering Aerodynamics*, The Ronald Press Company, 1936.

[6] Pugsley, A. G., *Influence of Wing Elasticity on Longitudinal Stability*, British R. & M. 1548, 1933.

[7] Flax, A. H., *Three Dimensional Wing Flutter Analysis*, Journal of the Aeronautical Sciences, Vol. 10, No. 2, pp. 41–42, February, 1943.

[8] ANC-1 (1), *Spanwise Load Distribution*.

[9] Schrenk, O., *A Simplified Method of Spanwise Airload Distribution*, N.A.C.A. T.M. No. 948, 1940.

[10] von Kármán, Th., and Biot, M. A., *Mathematical Methods in Engineering;* McGraw-Hill Book Company, Inc., 1940.

[11] Viola, T., *New Methods of Calculation for the Determination of a Special Form of Instability of the Elastic Equilibrium of a Cantilever Wing*, Journal of The Royal Aeronautical Society, pp. 816–826, November, 1940.

[12] Reissner, H., *Neuere Probleme die Flugzeugstatick*, Z.F.M., 1926.

[13] Bliss, G. A., *Calculus of Variations*, The Carus Mathematical Monographs, 1925.

Calculated Gust Loads for Tailless Airplanes

RAYMOND F. ANDERSON*

Lockheed Aircraft Corporation

SUMMARY

Gust-load factors are calculated for tailless airplanes by a simplified method that includes directly the effect of the pitching motion. The calculations are made for a wide range of mass parameter (a quantity that includes both wing loading and chord), center of gravity position, and pitching radius of gyration. A linear gust with the maximum gust velocity at the critical distance of eight chord lengths is used. Although certain assumptions are made in order to simplify the calculations, it is shown that for a typical case the results agree with the results obtained by a rigorous solution.

The application of the results to tailless airplane design is illustrated by typical curves showing the variation of the limit load factor with wing loading for various values of center of gravity position and radius of gyration. It is found that the load factor is reduced by a forward movement of the center of gravity or by a reduction of the radius of gyration. For example, a representative case shows that, for a range of mass parameter from 5 to 30 (a variation of wing loading from 10 to 60 lbs. per sq.ft. for a 12-ft. chord), a movement of the center of gravity of 5 per cent chord forward of the aerodynamic center causes reductions of the limit load factor of 26, 11, and 3 per cent, for values of the ratio of the radius of gyration to the chord of 1/4, 1/2, and 1, respectively.

INTRODUCTION

ALTHOUGH CONSIDERABLE WORK has been done on the problem of the design gust loads for airplanes, little work has been done which applies specifically to tailless airplanes. Accordingly, it is the purpose of this paper to extend the work of representative previous papers[1, 2] by giving calculated gust-load factors for tailless airplanes with the effects of center of gravity position and pitching radius of gyration taken into account.

The paper differs from most previous ones in that the pitching motion (as affected by center of gravity position and radius of gyration) is taken into account, and, in addition, instead of assuming that the maximum load factor increment occurs at maximum gust velocity, one may calculate the distance to the maximum gust velocity and the corresponding load factor increment.

In the determination of the load factor increment the most important airplane variables are the mass parameter[2] (a factor dependent primarily upon wing loading and chord), center of gravity position, and radius of gyration. The calculations were accordingly made for the design range of these variables. In addition, a linear variation of gust velocity with distance is considered, with the maximum velocity at eight chord lengths, since this distance has been found in flight tests to be the most critical.

Received April 18, 1944.

* Aerodynamics Research Engineer.

NOTATIONS

A_s = growth of lift factor for an airfoil in a linear gust, at the distance s, $= \int_0^{s_2} C_{L_g}(s_2 - s)ds$

B_s = lift factor for an airfoil having vertical motion $= \int_0^{s_2} C_{L\alpha}(s_2 - s)sds$

C_s = lift factor for an airfoil with a changing angle of pitch $= \int_0^{s_2} C_{L\alpha}(s_2 - s)s^2ds$

c = chord

C_{L_g} = a factor giving the fraction of the final lift developed by an airfoil that penetrates a sharp edge gust

$C_{L\alpha}$ = a factor giving the fraction of the final lift developed by an airfoil subjected to a sudden angle of attack change

g = acceleration of gravity

k_y = radius of gyration in pitch

l = longitudinal distance from the center of gravity to the aerodynamic center (positive for the a.c. ahead of the c.g.)

m = lift curve slope, radian units

P = mass parameter $= 2W/\rho mSgc$

S = wing area

s = distance measured in wing chord lengths

s_1 = distance from beginning of gust to the maximum gust velocity

s_2 = distance at which a load factor increment is computed

s_3 = distance at which the load factor increment is a maximum

U = gust velocity

U_1 = maximum gust velocity

V = airplane velocity

W = airplane weight

Δn_S = load factor increment for a sharp edge gust with instantaneous lift increase assumed

Δn_0 = load factor increment for horizontal rectilinear translation

Δn_m = load factor increment for vertical motion

Δn_q = load factor increment resulting from pitching angular velocity

Δn_θ = load factor increment resulting from pitch angle change

Δn_T = total load factor increment

R = load factor increment ratio to Δn_S, subscripts same as above

METHOD OF CALCULATION

In the calculations the following usual assumptions are made: The structure is rigid, the airplane velocity is constant, and the airplane is in horizontal flight and meets a vertical gust. The linear two-dimensional gust used is represented in Fig. 1. Also shown is a cross section through the plane of symmetry of a wing of a tailless airplane. Three distances between the center of gravity and the aerodynamic center were used. Expressed as a ratio to the chord they were 0, −0.05, and −0.10. With the aerodynamic center assumed to be at the quarter-chord point, the center of gravity posi-

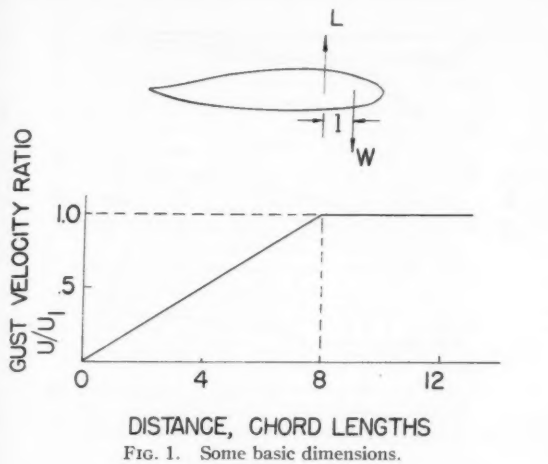

FIG. 1. Some basic dimensions.

tions would be 25, 20, and 15. A lift curve slope of 4.30 (radian units) was used, corresponding to an aspect ratio of approximately 6. The wing was assumed to have no taper and no sweepback. These assumptions were made to simplify the calculations, since variations of aspect ratio, taper ratio, and sweep should have only secondary effects. The radius of gyration was used in the form of a ratio to the chord, k_y/c, with values of approximately $^1/_4$, $^1/_2$, and 1, which should cover the design range.

When the load factor increment of an airplane entering a gust is calculated, it is convenient to separate the motion into its parts and to calculate the increment corresponding to each part. The total load factor increment may then be found by summation. The load factor increments arising from the following divisions of the motion will then be considered: horizontal rectilinear translation, rising or vertical motion, pitching angular velocity, and pitch angle change.

In the case of horizontal rectilinear translation it may be best to give first the load factor increment for the well-known case of the sharp edge gust. In this case the load factor increment is given by

$$\Delta n_S = \rho m S V U_1/2W \tag{1}$$

In this formula it is assumed that the lift coefficient reaches its full value at the instant the wing enters the gust. Actually, however, the full value is not reached until the wing has traveled several chord lengths, as shown by curves given in reference 3, Fig. 10. In that figure the lift coefficients are given as fractions of the final steady value and were based on reference 4. C_{L_g} represents the increase in lift coefficient for an airfoil with horizontal rectilinear translation entering a sharp edge gust, and C_{L_α} represents the increase in lift coefficient for an airfoil subjected to a sudden change of angle of attack (as in combined vertical and horizontal motion). Values of C_{L_g} and C_{L_α} for aspect ratio 6 will be used, because the values do not change rapidly in the usual range of aspect ratio. In what follows no attempt will be made to give the detailed mathematical development because of its length; the principal equations will simply be presented.

For horizontal rectilinear motion in a sharp edge gust Eq. (1) should be multiplied by C_{L_g} to take account of the noninstantaneous lift increase. For a linear gust, a factor A_s found by integration of the C_{L_g} values should be used. The term for the load factor increment resulting from horizontal motion is then

$$\Delta n_0 = (\rho m S V U_1/2W s_1) A_s \tag{2}$$

where

$$A_s = \int_0^{s_2} C_{L_g}(s_2 - s)\,ds \tag{3}$$

The parenthesis used here and in the following integrals indicates that C_{L_g} is a function of (at the distance) $s_2 - s$.

In the case of the vertical motion the load factor increment will depend on the total load factor increment curve. It is convenient and a reasonably close approximation to experimental results[2] to assume that the total load factor increment varies linearly with the distance in the gust and that it starts when the leading edge of the wing enters the gust. Accordingly, the total load factor increment is given by

$$\Delta n_T = (s/s_3)\,\Delta n_{T_{max.}}$$

Then the load factor increment resulting from the vertical motion may be written

$$\Delta n_m = -(\rho m S g c\,\Delta n_{T_{max.}}/2W s_3) B_s \tag{4}$$

where

$$B_s = \int_0^{s_2} C_{L_\alpha}(s_2 - s)s\,ds \tag{5}$$

The load factor increment arising from the pitching angular velocity may be expressed

$$\Delta n_q = -(\rho m S g c l^2\,\Delta n_{T_{max.}}/2W k_y^2 s_3) B_s \tag{6}$$

and the increment arising from the angle of pitch change may be expressed

$$\Delta n_\theta = (\rho m S g c^2 l\,\Delta n_{T_{max.}}/4W k_y^2 s_3) C_s \tag{7}$$

where

$$C_s = \int_0^{s_2} C_{L_\alpha}(s_2 - s)s^2\,ds \tag{8}$$

Of the four load factor increments, the principal one, Δn_0, will be observed to contain the airplane and gust velocities V and U_1. These values may be eliminated by expressing the load factor increments as a ratio to the value given by the sharp edge gust formula, Eq. (1). This ratio R will be given the proper subscript for each case—for example, the term for vertical motion will be $\Delta n_m/\Delta n_s = R_m$. The last three increments—Eqs. (4), (6), and (7)—will be seen to contain, in addition to the center of gravity position l and the radius of gyration k_y, a quantity $2W/\rho m S g c$. This is the mass

parameter P and will be observed to contain both the wing loading and chord.

With the substitution of P and with the c.g. location and radius of gyration given in terms of l/c and k_y/c, respectively, Eqs. (2), (4), (6), and (7) may be written

$$R_0 = A_3/s_1 \tag{9}$$

$$R_m = -(B_3/Ps_3)R_{Tmax.} = -k_m R_{Tmax.} \tag{10}$$

$$R_q = -\left(\frac{l^2}{c^2}\right)\left(\frac{c^2}{k_y{}^2}\right)\left(\frac{1}{P}\right)\left(\frac{B_3}{s_3}\right)R_{Tmax.} = -k_q R_{Tmax.} \tag{11}$$

$$R_\theta = \left(\frac{l}{c}\right)\left(\frac{c^2}{k_y{}^2}\right)\left(\frac{1}{2P}\right)\left(\frac{C_3}{s_3}\right)R_{Tmax.} = -k_\theta R_{Tmax.} \tag{12}$$

The total load factor increment ratio R_T is given by the sum of the four preceding terms, and its maximum value, which is the one of interest for an airplane design, may be expressed as

$$R_{Tmax.} = R_0/(1 + k_m + k_q + k_\theta) \tag{13}$$

The maximum value of R_T may be found by assuming that it may occur successively at several values of s near the distance to maximum gust velocity. If the values so calculated from Eq. (13) are plotted against s, the actual value of $R_{Tmax.}$ and the corresponding value s_3 may be found. The maximum load factor increment ratio and the distance s_3 were calculated for the values of the variables previously given and for a wide range of the mass parameter.

Results and Discussion

Values of the maximum load factor increment ratio are plotted against mass parameter on Fig. 2. To relate the results to a familiar quantity, scales of wing loading for various chords are also given. Sea-level density and a lift slope of 4.30 (radian units) were used. It will be observed that $R_{Tmax.}$ is decreased as the radius of gyration is reduced and as the center of gravity is moved forward. This is because of the increasing effect of downward pitch. The load factor increment and, of course, the design load factor will also be reduced. It will also be observed that the effect of the center of gravity position increases as the radius of gyration is reduced. The same trends may be observed from Fig. 3, where $R_{Tmax.}$ has been plotted against center of gravity position.

In order to check the accuracy of the relatively easy method of calculation used here, some results calculated by this method have been compared with results[5] that were obtained by a rigorous mathematical method using operational calculus. The comparison is given in Fig. 4, and it will be observed that agreement is good for most of the range of center of gravity position. Where results obtained by the present method depart appreciably, they are in a direction that would make the load factor conservative.

The distance at which the maximum load factor increment occurred is plotted against mass parameter

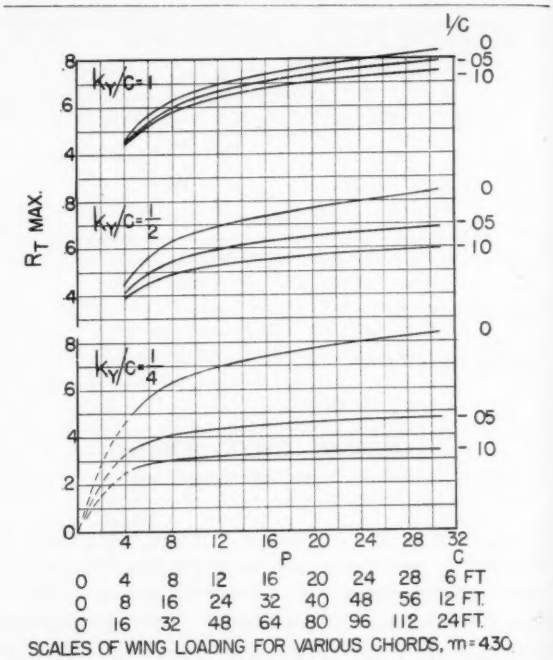

Fig. 2. Variation of load factor increment ratio with mass parameter.

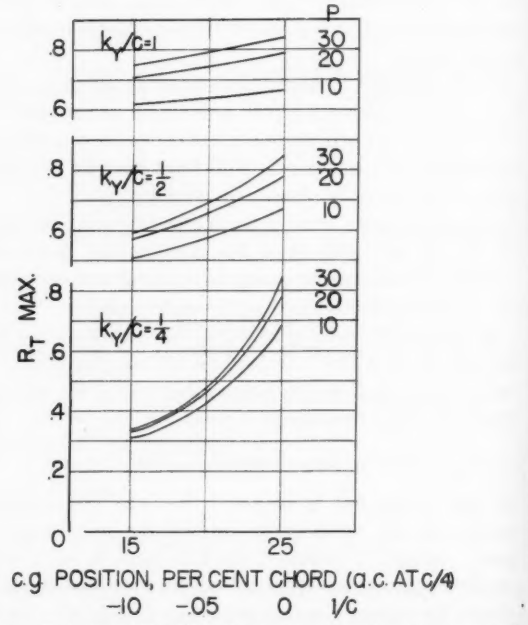

Fig. 3. Variation of load factor increment ratio with center of gravity position.

in Fig. 5. It will be observed that the distance tends to decrease as the radius of gyration decreases and as the center of gravity moves forward. This is an effect of the pitching motion. The calculations indicate that, if the radius of gyration were sufficiently small and the center of gravity sufficiently far forward, the maximum

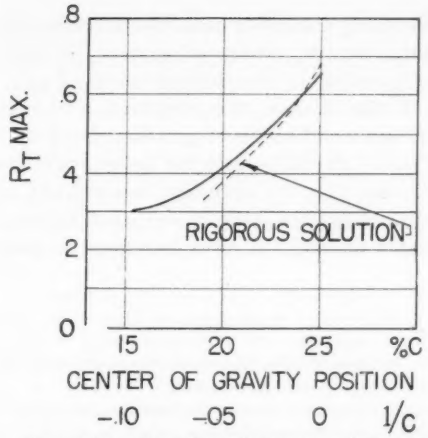

FIG. 4. Comparison of results with rigorous solution ($P = 10.75$, $m = 4.65$, $k_y/c = 1/4$).

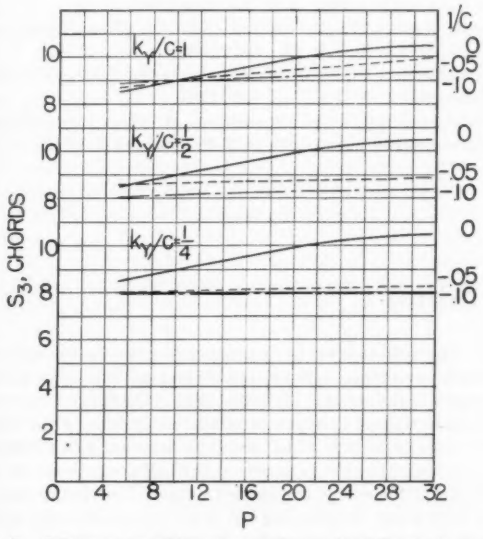

FIG. 5. Distance at which the maximum load factor increment occurs.

load factor increment would actually be obtained before the maximum gust velocity is reached.

To show the relation of the results to data commonly used, the values of Fig. 2 were converted to an effective gust factor. The effective gust factor K, previously used in most design work,[6] was based on calculated values of load factor increment ratio and upon flight measurements of the Boeing 247 airplane. This airplane had a wing loading of 16 lbs. per sq.ft. and a chord of 11 ft. which corresponds to a value of P of 8.8 (approximately). Therefore, K, of reference 6, should pass through 1.0 at this value of the mass parameter as shown on Fig. 6. This value of K was specified for use with an effective gust velocity of 30 ft. per sec. The latest gust or alleviation factor cannot be given because it is contained in a confidential publication.

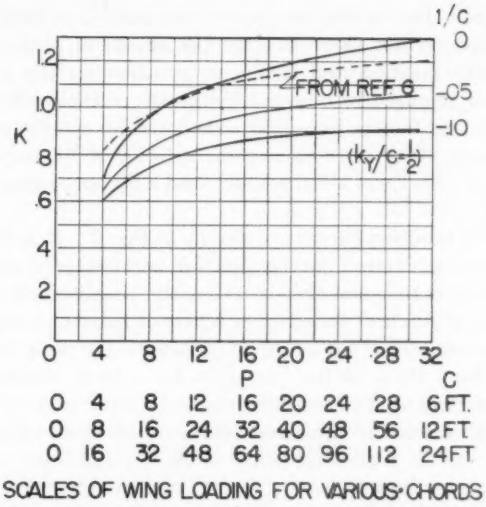
K
FROM REF 6
$(k_y/c=\frac{1}{2})$
1/C
P
C
0 4 8 12 16 20 24 28 6FT.
0 8 16 24 32 40 48 56 12FT.
0 16 32 48 64 80 96 112 24FT.
SCALES OF WING LOADING FOR VARIOUS CHORDS

FIG. 6. Influence of center of gravity position on effective gust factor.

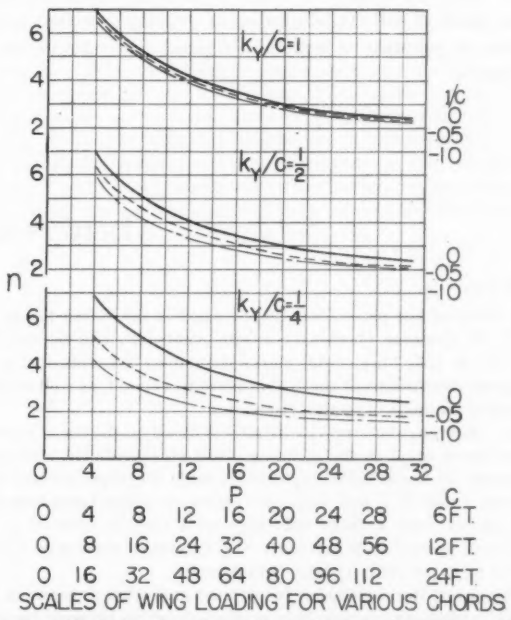

FIG. 7. Effect of radius of gyration and center of gravity position on limit load factor ($m = 4.30$, $V = 300$ m.p.h.).

The factor given in reference 6 and plotted in Fig. 6 will, however, be just as suitable for comparative purposes. The remaining values in Fig. 6 were obtained from Fig. 2, using the representative value of $k_y/c = 1/2$. An effective gust factor K was obtained by multiplying the values of Fig. 2 by a factor that would make the curve for the center of gravity at 25 per cent pass through 1.0 when $P = 8.8$. Fig. 6 illustrates the effect of center of gravity position on K for $k_y/c = 1/2$. The effect for other values of k_y/c may be inferred from Fig. 2. Also, if desired, values of K may be obtained by multiplying $R_{Tmax.}$ by 1.54.

The values of effective gust factor derived as just described do not show directly the effects of center of gravity position and radius of gyration on the load factor required in design. To illustrate these effects, limit load factors have been calculated for specific conditions. They were an airplane velocity of 300 m.p.h., a gust velocity of 30 ft. per sec., and a lift curve slope of 4.30.

The resulting curves are shown in Fig. 7. It will be seen that center of gravity position and radius of gyration show the same trends as on the previous curves. As an example of the effect of center of gravity position, for a range of P from 5 to 30 (a variation of wing loading from 10 to 60 lbs. per sq.ft. for a 12-ft. chord), a movement of the center of gravity to 5 per cent of the chord forward of the aerodynamic center causes reductions of the limit load factor of 26, 11, and 3 per cent for k_y/c values of $^1/_4$, $^1/_2$, and 1, respectively. Similar results would have been obtained if the latest "alleviation factor" and the corresponding gust velocity had been used. Further, it may be anticipated that the same kind of effects of center of gravity position and radius of gyration would be obtained for conventional airplanes.

The preceding discussion indicates the desirability of taking into account center of gravity position and radius of gyration in the determination of gust load factors. If this is done, the combination of center of gravity position and radius of gyration giving the highest load factor should be used for design. Conversely, it is indicated that the optimum combination of forward center of gravity position and small radius of gyration should be sought in order to reduce the gust-load factor.

References

[1] Rhode, Richard V., *Gust Loads on Airplanes*, SAE Journal, Vol. 40, No. 3, pp. 81–88, March, 1937.

[2] Donely, Philip, *An Experimental Investigation of the Normal Acceleration of an Airplane Model in a Gust*, N.A.C.A. T.N. No. 706, p. 11, 1939.

[3] Donely, Philip, Pierce, Harold B., and Pepoon, Philip W., *Measurement and Analysis of the Motion of a Canard Airplane Model in Gusts*, N.A.C.A. T.N. No. 758, 1940.

[4] Jones, Robert T., *The Unsteady Lift of a Wing of Finite Aspect Ratio*, N.A.C.A. T.R. No. 681, 1940.

[5] Jones, Robert T., *Notes on the Stability and Control of Tailless Airplanes*, N.A.C.A. T.N. No. 837, 1941.

[6] Civil Aeronautics Administration, *Airplane Airworthiness*, Civil Aeronautical Manual 04, p. .2–2, February 1, 1941.

Letters to the Editor

Dear Sir:

A study of the paper "Bending Strength in the Plastic Range," by F. P. Cozzone (JOURNAL OF THE AERONAUTICAL SCIENCES, Vol. 10, p. 137, May, 1943) shows that many experimental and theoretic conclusions of the author must be revised, as well as the practical methods of analysis indicated:

(1) Rectangular stress distributions based on the use of a constant stress equal to the ultimate stress give predicted ultimate moments in much better agreement with the experimental results of Tables 2, 3, and 4 than the elaborate method proposed by the author: the average difference with tests is reduced to 3 per cent, instead of 9 per cent; the maximum difference is reduced to 19 per cent, instead of 44 per cent.

Moreover, the correlation (as defined in statistics) between K and the ultimate moment is negative; the ratio between results of experiments and those of the rectangular theory increases when K increases, while the trapezoidal theory predicts the opposite. Those conclusions have been found by the writer by calculating the ultimate moments: M_r (rectangular theory), M_t (author's trapezoidal theory) by the expressions (C_f correction factor, Eq. (6)):

$$M_r = 2Q_m F_{tu}'; \quad M_t = (Mc/I)_u (I/c) : C_f$$

and comparing them with the results of the 40 tests indicated by the author. Such results lead to a revision and simplification of all the methods of analysis proposed; the use of graphs is unnecessary, and, for simple bending, the margin of safety is: M.S. $= 2Q_m F_{tu}' : M - 1$.

The fact that the trapezoidal theory does not represent experimental data is probably explained by the "necking" of the outer fibers of a bent piece, which allows the inner fibers to reach the ultimate stress, thus giving a nearly rectangular distribution.

(2) The definition of the quantity $2Q_m$ given by the author is valid only for sections symmetric with respect to the axis parallel to the axis of the couple. Actually, $2Q_m$ is the sum of the static moments in respect to any axis parallel to the axis of the couple of two *equal* areas into which the total area must be divided in such a manner that the centroids of the half areas be on the perpendicular to the axis of the applied couple. For that reason, for angles with a thin outstanding leg, or for tee sections, the author finds $K > 2$ (asymptotic value 3), while actually $K \leq 1.8$ (asymptotic value 1.5). Also, for I and channel sections in Table 4, several values of K are greater than 1.5, in contradiction with Table 1. The formula $2Q_m = 0.85\sqrt{IA_t}$ is inadequate, even for an approximate analysis; the numerical coefficient may have any value between 0 and 1; generally it is greater than 0.6, as can be ascertained by considering an I section successively bent in the principal directions. The average value proposed may lead to errors up to 25 per cent.

(3) The correct definition of $2Q_m$ applies as well to complex bending and shows that the interaction formula $R_{bx}^2 + R_{by}^2 = 1$, exact for an elliptic section, gives fairly good results for other sections: for a square section the error is smaller than 6 per cent. On the contrary, the straight-line interaction formula, proposed by the author gives, for those two cases, errors up to 29 and 25 per cent, respectively, and must be rejected.

For unsymmetric sections, there is no relationship between the principal directions conventionally defined and the "principal directions" for rectangular distribution and the neutral axis for rectangular distribution does not necessarily pass through the centroid.

When the material has different ultimate stresses in tension and in compression, the two areas in tension and compression are

not equal and their ratio is the reciprocal of the ratio of the ultimate stresses.

(4) For combined bending and axial stress, the total area must be divided in two areas, such as: (a) the centroids of the two areas must be in line with the point of application of the load. (b) The static moments of the two areas (concentrated at their centroids) with respect to the point of application of the load must be equal. The ultimate load is equal to the difference of the areas multiplied by the ultimate stress. In order to simplify the designer's work, charts can be made for various sections, giving ultimate loads in function of the location of the resultant.

For a rectangular section, and a load along a principal axis, the interaction formula is $R_a^2 + R_b = 1$; that formula is true within 2 per cent for a circular section. For those conditions, the straight-line formula gives errors up to 25 per cent.

When the ultimate stresses in tension and compression are different, the ratio of the static moments must be the reciprocal of the ratio of the corresponding ultimate stresses. The ultimate load is equal to the difference of the products of the areas by the corresponding ultimate stresses.

(5) Relations derived for shear are incorrect, since it is assumed that the existence of shear has no influence on the stress-strain curve, although it is obvious that the values F_{tu}, F_{tp} are decreased in presence of shear. Moreover, as shear distribution varies from section to section, there are axial stresses perpendicular to the principal stresses, which precludes any exact analysis. Also, shear is nonuniform through the width of thick sections for which the theory is specially adapted. Finally, as the rectangular distribution seems closer to actual results than the trapezoidal distribution, the latter cannot be used as a basis for shear distribution. For those reasons, only a fictitious average shear stress can be defined, which can be combined with the bending stress by means of conventional interaction formulas.

(6) The method proposed to take crippling into consideration is a return to methods of elasticity and defines the ultimate load on a structure by the strain corresponding to the ultimate load on the weakest part of the structure. For a web with stiffeners, the ultimate load on the system would thus be determined by the buckling strength of the web, which is unacceptable.

(7) The value of the correction factor C_f in the case of rectangular distribution is $C_f = F_{tu} : F_{tu}'$, replacing Eq. (6).

LEON BESKIN
Consolidated Vultee Aircraft Corporation

Dear Sir:

Reference is made to the article by Donald A. duPlantier, Chief of Structures, Consolidated Vultee Aircraft Corporation, which appeared in the April issue of the JOURNAL OF THE AERONAUTICAL SCIENCES, entitled "Analysis of Fuselage Rings by the Column Analogy."

Although there are many methods of applying the principles of continuity for the solution of redundant forces in closed frames or rings, the writer agrees with the author that the column analogy method appears to have certain advantages, especially if one axis of the ring is an axis of symmetry, as is usually encountered in aeronautical design. However, the writer believes that the use of the elastic center and its application, with reference to problem 2, would have been more enlightening.

On page 148 of the article, Table 3, the section properties of the analogous column (i.e., elastic area properties) with its elastic center location have been calculated. (See Fig. 1 herewith.)

The ring section has been made statically determinate by cutting the ring just to the left of stringer No. 1, page 147, Fig. 7. With the cantilever static moment curve as the load on the analogous column, the redundant forces required to keep the section in

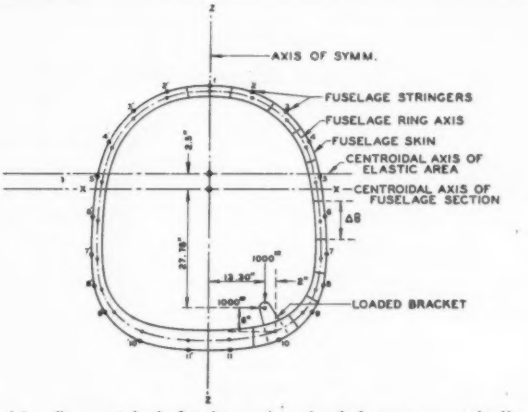

FIG. 1. Symmetrical fuselage ring loaded unsymmetrically showing location of centroid of elastic area.

equilibrium, and acting at the elastic center (since the true continuity of the ring has been altered), have been calculated on page 149, Table 4. These have been determined by the use of the general flexure formula for an eccentrically loaded column.

Relative to the elastic center, the sense of the indeterminate moment is known, since moments producing compression on the inner face of the ring (counterclockwise) have been assumed as positive (page 147, Sign Convention (3)). Since the indeterminate moment as calculated has a plus sign before it (page 149, Table 4, column 6 divided by column 2), the moment is in a counterclockwise direction at the elastic center. The magnitudes of the H and V forces are also known but their direction unknown.

Consider the cut ring with the known moment and forces acting at the elastic center. (See Fig. 2 herewith.)

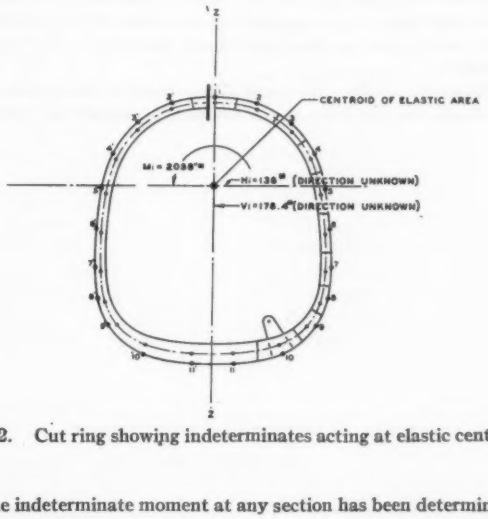

FIG. 2. Cut ring showing indeterminates acting at elastic center.

The indeterminate moment at any section has been determined by the equation

$$\frac{W}{A} + \frac{M_x}{I_x}(Z) + \frac{M_z}{I_z}(X) \text{ (page 138, Eq. (2))}$$

Therefore $M_i^n = 2{,}050 - 138(Z) + 178.4(X)$.

For station No. 1

$$M_i^1 = 2{,}058 - 138\,(21) + 179.4\,(0)$$
$$= 2{,}058 - 2{,}898$$
$$= -840 \text{ in-lb clockwise}$$

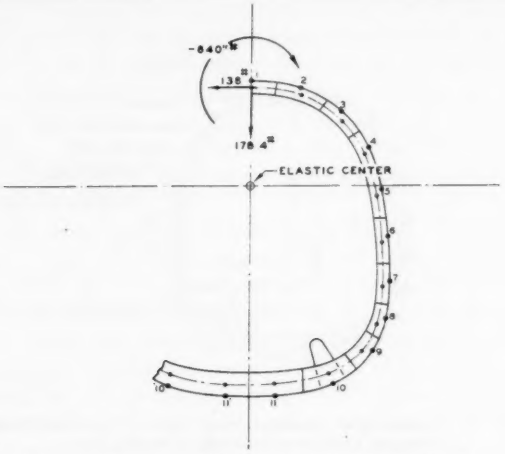

FIG. 3. Showing indeterminates acting at station 1.

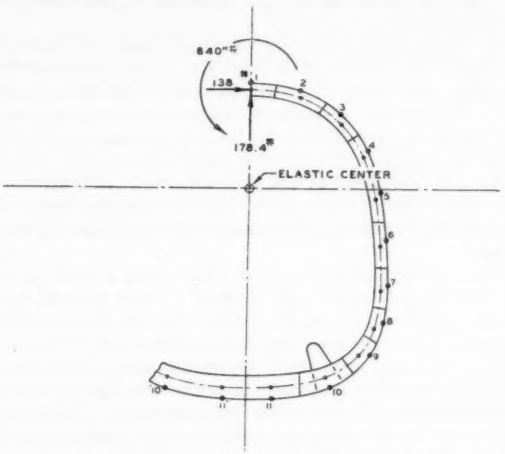

FIG. 4. Showing true sense of indeterminates at station 1.

From the above it is seen that to obtain a clockwise moment at station No. 1, the H force must act in a clockwise direction (←) at the elastic center.

For station No. 2

$$M_1^2 = 2{,}058 - 138\,(19.5) + 178.4\,(9.2)$$
$$= 2{,}058 - 2{,}691 + 1{,}641$$
$$= 1008 \circlearrowleft \text{ counterclockwise}$$

Likewise from the above, it is seen that to obtain a counterclockwise moment at station 2, the V force must act in a counterclockwise direction (↓) at the elastic center.

With the sense of the forces determined, we have the following, acting at station 1, the cut section. (See Fig. 3 herewith.)

Since these are the indeterminate forces necessary for equilibrium, and acting on the ring at station 1, the true forces are of equal magnitude but of opposite sense because of the cantilever beam assumption for the determinate structure. (See Fig. 4 herewith.)

The author employs the use of a force polygon for determining the shears and end loads at the sections considered once the unknown forces have been determined. The component of the resultant forces parallel to, and acting at, the section considered determines the end load on the section. The component of the resultant force perpendicular to, and acting at, the section considered determines the shear at the section. It is believed that this method is much simpler, since the large scale drawing is already available for this purpose, having been required to obtain previous information for the analysis.

REFERENCES

[1] Cross, H., and Morgan, N. D., *Continuous Frames of Reinforced Concrete*, p. 46; John Wiley & Sons, Inc., New York, 1932.

[2] Bruhn, E. F., *Airplane Structural Design*, page A9-1; John S. Swift Co., Cincinnati, Ohio, 1942.

JOSEPH F. BARBA
Structures Engineer
Installation Development Department
Pratt & Whitney Aircraft Division
United Aircraft Corporation

EDITORIAL AND PROFESSIONAL ACTIVITIES COMMITTEE

HUGH L. DRYDEN, *Chairman*

Aerodynamics
William Bollay
Kenneth S. M. Davidson
Walter S. Diehl
Hugh L. Dryden
R. Paul Harrington
P. E. Hemke
Eastman N. Jacobs
Th. von Kármán
Alexander Klemin
W. B. Klemperer
Otto C. Koppen
A. M. Kuethe
John G. Lee
John R. Markham
Clark B. Millikan
Richard von Mises
Shatswell Ober
W. Bailey Oswald
Manfred Rauscher
Elliott G. Reid
H. J. E. Reid
Hans Reissner
Benjamin F. Ruffner
G. B. Schubauer
Abe Silverstein
R. H. Smith
Th. Theodorsen
M. J. Thompson
Starr Truscott
Michael Watter
K. D. Wood

Air Transport
Ralph S. Damon
Charles Froesch
Melvin N. Gough
J. A. Herlihy
William Littlewood
A. A. Priester
Paul E. Richter
N. F. Scudder

Aircraft Design
Karl Arnstein
Rex B. Beisel
B. C. Boulton
C. P. Burgess
C. H. Chatfield
J. W. Crowley, Jr.
R. C. Gazley
Leroy R. Grumman
Hall L. Hibbard
A. L. Klein
Otto C. Koppen
I. M. Laddon
John G. Lee
C. J. McCarthy
William H. Miller
R. H. Prewitt
Igor I. Sikorsky
E. A. Stalker
Th. Troller
Starr Truscott
R. H. Upson
Fred E. Weick
Robert J. Woods
T. P. Wright

Aircraft Production
John L. Atwood
W. E. Beall
Carl de Ganahl
W. K. Ebel
Fredric Flader
Hall L. Hibbard
Guy A. Luburg
C. J. McCarthy
A. E. Raymond
W. T. Schwendler
Harry A. Sutton
John Tjaarda
Robert J. Woods
T. P. Wright

Radio
C. S. Draper
Lloyd Espenschied
C. G. Fick
Lewis M. Hull
Haraden Pratt
F. X. Rettenmeyer

Physiologic Problems
H. G. Armstrong
Louis H. Bauer
David B. Dill
Eugene Du Bois
W. Randolph Lovelace, II
Ross A. McFarland
A. D. Tuttle

Power Plants and Propellers
M. A. Biot
George W. Brady
Frank W. Caldwell
Ivan H. Driggs
Louis H. Enos
David Gregg
L. S. Hobbs
Albert R. Jacobs
E. E. Johnson
H. M. McCoy
W. C. Nelson
Arthur Nutt
Shatswell Ober
Elliott G. Reid
Hans Reissner
David R. Shoults
C. Fayette Taylor
E. S. Taylor
Th. Theodorsen
A. V. Willgoos
D. H. Wood

Structures and Materials
M. A. Biot
W. B. Bleakney
C. P. Burgess
E. W. Conlon
George W. DeBell
A. V. de Forest
L. H. Donnell
L. G. Dunn
Richard C. Gazley
W. C. Geer
E. C. Hartmann
J. P. Den Hartog
N. J. Hoff
Zay Jeffries
Th. von Kármán
W. B. Klemperer
E. E. Lundquist
C. J. McCarthy
C. F. Nagel, Jr.
J. S. Newell
Alfred S. Niles
Thomas D. Perry
W. Ramberg
E. Reissner
F. R. Shanley
H. W. Sibert
S. Timoshenko
H. S. Tsien
L. B. Tuckerman
George Tweney
J. A. Wise
J. E. Younger

Meteorology
C. F. Brooks
Karl O. Lange
D. M. Little
E. J. Minser
Sverre Petterssen
F. W. Reichelderfer
A. F. Spilhaus
P. V. H. Weems
H. C. Willett

Education
R. Paul Harrington
C. S. Jones
Alexander Klemin
Clark B. Millikan
W. C. Nelson
George B. Pegram
Richard H. Smith
Ben D. Wood

Fuels and Oils
D. P. Barnard
A. L. Beall
J. H. Doolittle
Graham Edgar
Luis de Florez
R. T. Goodwin
Raymond Haskell
S. D. Heron
A. M. Rothrock

Instruments
P. R. Bassett
W. G. Brombacher
Charles H. Colvin
C. S. Draper
Lucien L. Friez
Walter McKay
W. A. Reichel
C. F. Savage
A. F. Spilhaus
S. J. Zand

I.A.S. REPRESENTATIVES TO OTHER ORGANIZATIONS

Aeronautical Chamber of Commerce of America—CHARLES MARCUS
American Association for the Advancement of Science—J. C. HUNSAKER
American Institute of Mining & Metallurgical Engineers—A. V. DE FOREST
American Society of Mechanical Engineers—JOHN E. YOUNGER
American Standards Association—P. R. BASSETT
Greater New York Safety Council—WILLIAM LITTLEWOOD
Daniel Guggenheim Medal Board of Award—CHARLES H. COLVIN, RALPH S. DAMON, LESTER D. GARDNER
Institute of Radio Engineers—L. M. HULL
Manufacturers Aircraft Association—J. T. HARTSON
National Aeronautic Association—WILLIAM R. ENYART
National Safety Council—JEROME LEDERER
National Research Council Engineering Division—FRANK W. CALDWELL
New York Museum of Science and Industry—LESTER D. GARDNER
Society of Automotive Engineers—EDWARD P. WARNER

Services of the Aeronautical Archives of the Institute of the Aeronautical Sciences

The services of the Aeronautical Archives are available to all members of the Institute, to Corporate Members, to advertisers in the Aeronautical Engineering Review and, under usual library limitations, to the public. Four specialized services are available.

The Paul Kollsman Library

This lending library service makes available, *without charge*, the latest and more important aeronautical books.

As far as the facilities permit, any person in the United States over 18 years of age who can furnish references which certify to his or her responsibility may become a member of the library.

Members may request the loan of any aeronautical or technical book they wish to borrow. Through an exchange agreement with the Engineering Societies Library, any book on general engineering may be borrowed from its great collection of over 160,000 volumes.

A photostating service is available at usual library rates.

Applications for membership in the library and further information will be sent on request.

The Burden Reference Library

This reference library contains over 14,000 aeronautical books, magazines, pamphlets, photographs, reports, and clippings gathered from world-wide sources and is one of the most complete aeronautical libraries in the world. Material from this library is not available for loan but may be used for reference purposes at the Aeronautical Archives.

The Pacific Aeronautical Library

6715 Hollywood Boulevard
Hollywood, California

Established in cooperation with the aircraft companies the library serves. The leading aircraft companies in or near Los Angeles participate in its support and operation.

This service library for aeronautical research is available to the public for reading privileges. Source material includes aerodynamic and structural research reports, as well as books on drafting, production methods, history, and allied sciences. It furnishes books, periodicals, and pamphlet material to the participating aircraft companies to supplement their engineering libraries.

The Aeronautical Archives Technical Information Service

This service has experienced personnel under the supervision of trained aeronautical engineers to compile any information desired. The services range from listing specialized reference books to the preparation of exhaustive bibliographies, digesting of reports, and general surveys of any aeronautical subject. Some of the available services are:

Bibliographies on any aeronautical subject.
Reports on any aeronautical subject.
Digests of aeronautical books, papers, periodicals, and references.
Translations.
Engineering investigations of special aeronautical subjects.
Biographies of individuals engaged in aeronautics.
Photostats of any aeronautical or general engineering material.
Microfilms made on special order.
Photographs made from the Institute's photographic collection.
Drawings and tracings made.

In addition to the services mentioned any commission which comes within the scope of the Service will be accepted. Special arrangements may be made for work requiring several weeks or months.

Translators are available for accurate transcriptions of all foreign language data. Translations are carefully edited by trained engineers.

Reproductions of any material in the Aeronautical Archives of the Institute may be ordered at standard photostat rates.

INSTITUTE OF THE AERONAUTICAL SCIENCES
1505 RCA BUILDING WEST
30 ROCKEFELLER PLAZA, NEW YORK 20, N. Y.